

Redox regulation of photosynthetic carbon metabolism in leaves of *Arabidopsis thaliana*

Dissertation

zur Erlangung des Doktorgrades der Naturwissenschaften

an der Fakultät für Biologie

der Ludwig-Maximilians-Universität München



vorgelegt von

Ina Thormählen

München, 23. Dezember 2014

Erstgutachter: Prof. Dr. Peter Geigenberger

Zweitgutachter: Prof. Dr. Ute C. Vothknecht

Datum der Abgabe: 23.12.2014

Datum der mündlichen Prüfung: 11.03.2015

Eidesstattliche Erklärung

Ich versichere hiermit an Eides statt, dass die vorgelegte Dissertation von mir selbstständig und ohne unerlaubte Hilfe angefertigt wurde. Des Weiteren erkläre ich, dass ich nicht anderweitig ohne Erfolg versucht habe, eine Dissertation einzureichen oder mich der Doktorprüfung zu unterziehen. Die folgende Dissertation liegt weder ganz, noch in wesentlichen Teilen einer anderen Prüfungskommission vor.

München, 19.12.2014

Ina Thormählen

Statutory declaration

I declare that I have authored this thesis independently, that I have not used other than the declared (re)sources. As well I declare, that I have not submitted a dissertation without success and not passed the oral exam. The present dissertation (neither the entire dissertation nor parts) has not been presented to another examination board.

Munich, 19.12.2014

Ina Thormählen

Contents

Abbreviations	1
Articles originating from this thesis with declaration of contribution	2
Summary	5
Zusammenfassung	7
Introduction	9
The photosynthetic electron distribution in autotrophic tissues of plants	9
The Trx-based redox regulatory system in chloroplasts	14
The photosynthetic end product synthesis of starch in plant leaves	16
Objectives of the thesis	20
Results	22
Chapter 1 - Inactivation of thioredoxin <i>f1</i> leads to decreased light activation of ADP-glucose pyrophosphorylase and altered diurnal starch turnover in leaves of <i>Arabidopsis</i> plants	22
Chapter 2 – Interaction between thioredoxin <i>f1</i> and NADPH-dependent thioredoxin reductase C regulates photosynthetic metabolism and plant growth	39
Chapter 3 – Disruption of both chloroplastic and cytosolic FBPases genes results in dwarf phenotype and important starch and metabolite changes in <i>Arabidopsis thaliana</i>	114
Chapter 4 - <i>Arabidopsis tic62 trol</i> mutant lacking thylakoid-bound ferredoxin-NADP ⁺ oxidoreductase shows distinct metabolic phenotype	168
Discussion	192
Trx <i>f1</i> and NTRC participate cooperatively in regulating carbon assimilation	192
Trx <i>f1</i> and NTRC participate cooperatively in regulating starch metabolism	193
Trx <i>f1</i> and NTRC are critical for the NADP redox poise in <i>Arabidopsis</i> leaves	195
Trx <i>f1</i> and NTRC are involved in the plant growth acclimation to varying light conditions	198
Physical interaction of Trx <i>f1</i> and NTRC <i>in vivo</i> underpin their cooperative regulation of photosynthetic carbon metabolism	199
References	201
Curriculum vitae	212
Acknowledgement	215

Abbreviations

AGPase	ADP-glucose pyrophosphorylase
APL	AGPase large subunit
APS	AGPase small subunit
CBC	Calvin-Benson cycle
F1,6BP	Fructose 1,6-bisphosphate
FBPase	Fructose 1,6-bisphosphatase
Fdx	Ferredoxin
FNR	Ferredoxin NADP reductase
F6P	Fructose 6-phosphate
FTR	Ferredoxin thioredoxin reductase
G6PDH	Glucose 6-phosphate dehydrogenase
NADP-MDH	NADPH-dependent malate dehydrogenase
NTR	NADPH-dependent thioredoxin reductase
NTRC	NADPH-dependent thioredoxin reductase C
OPPP	Oxidative pentose phosphate pathway
3PGA	3-phosphoglycerate
PS	Photosystem
RBP	Ribulose 1,5-bisphosphate
ROS	Reactive oxygen species
Tic62	62-kDa subunit of translocon of inner chloroplast membrane
TROL	Thylakoid rhodanese-like protein
Trx	Thioredoxin

Articles originating from this thesis with declaration of contribution

Chapter 1

Ina Thormählen, Joachim Ruber, Edda von Roepenack-Lahaye, Sven Matthias Ehrlich, Vincent Massot, Christine Hümmer, Justyna Tezycka, Emmanuelle Issakidis-Bourguet, Peter Geigenberger (2013) Inactivation of thioredoxin f1 leads to decreased light activation of ADP-glucose pyrophosphorylase and altered diurnal starch turnover in leaves of *Arabidopsis* plants. *Plant Cell Environ.* 36(1):16-29.

I.T. and P.G. designed and developed the study. I.T. performed the experiments of the chlorophyll fluorescence measurement, the western blot procedure for APS1 monomerisation (diurnal leaves, illuminated chloroplasts, sugar infiltrated leaves), and the photometric determination of starch, sucrose, 3PGA, hexose and triose phosphates. J.R. and C.H. contributed to the experiments for APS1 monomerisation of diurnal leaves, and S.M.E. of illuminated chloroplasts. E.v.R.-L. performed the GC-MS analysis, and J.T. the *in vitro* analysis of APS1 reducing efficiencies of thioredoxins. E.I.-B. and V.M. performed and analysed the experiments of the molecular characterization of the mutants. The other data were analysed by I.T., J.R., E.v.R.-L., J.T and P.G., and the manuscript was written by I.T., E.I.-B. and P.G.

Chapter 2

Ina Thormählen, Tobias Meitzel, Julia Groysman, Alexandra Bianca Öchsner, Edda von Roepenack-Lahaye, Belén Naranjo, Francisco Javier Cejudo, Peter Geigenberger (2014) Interaction between thioredoxin f1 and NADPH-dependent thioredoxin reductase C regulates photosynthetic metabolism and plant growth. *Manuscript submitted (Plant Cell)*.

I.T., T.M. and P.G. designed and developed the study. I.T. performed the experiments of the molecular and growth phenotype characterization of the mutants, the gas exchange and chlorophyll fluorescence measurements, the measurements of the diurnal FBPase and NADP-MDH activity, the diurnal APS1 monomerisation, and the photometric determination of NAD(P), starch, sucrose, 3PGA, hexose and triose phosphates. T.M. performed the BiFC and GUS expression analysis. J.G. determined the ATP, ADP and chlorophyll content, the transient

light activation of FBPase, and contributed to the experiments of NADP-MDH activity and NAD(P) content. A.B.Ö. performed the western blots of photosynthetic electron transport-related proteins, E.v.R.-L. the GC-MS analysis. B.N. and F.J.C. performed and analysed the FBPase redox shift assay. The other data were analysed by I.T., T.M., J.G., A.B.Ö., E.v.R.-L. and P.G., and the manuscript was written by I.T., T.M., F.J.C. and P.G.

Chapter 3

José A. Rojas-González, Mauricio Soto-Súarez, Ángel García-Díaz, María C. Romero-Puertas, Luisa M. Sandalio, Ángel Mérida, Ina Thormählen, Peter Geigenberger, Antonio J. Serrato, Mariam Sahrawy (2014) Disruption of both chloroplastic and cytosolic FBPases genes results in dwarf phenotype and important starch and metabolite changes in *Arabidopsis thaliana*. *Manuscript submitted, first revision (revision-major) (J Exp Bot)*.

J.A.R.-G., A.J.S. and M.S. designed and developed the study. M.S.-S. performed the genomic characterization of the mutants. A.G.-D. contributed with a technical support of all this study and obtained the FBPase-complementation constructions. J.A.R.-G., M.C.R. and L.M.S. performed the oxidative metabolism assays of the mutants. A.M. analyzed the data related to the starch content of the mutants. I.T. and P.G. performed and analysed the photometric measurements of 3PGA, hexose and triose phosphate contents, and analysed the GC-MS analysis. The manuscript was written by M.S., A.J.S. and J.A.R.-G. Each author contributed actively with critical reading of the manuscript.

Chapter 4

Minna Lintala, Natalie Schuck, Ina Thormählen, Andreas Jungfer, Katrin L. Weber, Andreas P.M. Weber, Peter Geigenberger, Jürgen Soll, Bettina Böltner, Paula Mulo (2014) *Arabidopsis tic62 trol* mutant lacking thylakoid-bound ferredoxin-NADP⁺ oxidoreductase shows distinct metabolic phenotype. *Mol Plant*. 7(1):45-57.

J.S., B.B. and P.M. designed and developed the study. M.L. performed pigment analyses, BN PAGE, immuno blots and photosynthetic measurements. N.S. generated the double mutant and analysed the plants. A.J. performed protein purification and Bioacore analyses. I.T. and P.G. performed and analysed the experiments of NAD(P) and starch contents, of NADP-ICDH,

ARTICLES ORIGINATING FROM THIS THESIS WITH DECLARATION OF CONTRIBUTION

G6PDH and NADP-MDH activities, and of APS1 monomerization. K.L.W. and A.P.W. performed and analysed the GC-MS experiment. The other data were analysed by M.L., J.S., B.B. and P.M., and the manuscript was written by P.M. and B.B.

Munich, 19.12. 2014

Peter Geigenberger

Ina Thormählen

Summary

The redox regulation of metabolic processes in plants is characterized by the involvement of oxidoreductases. Two distinct systems exist in chloroplasts of autotrophic tissues based on the thiol-disulfide exchange of redox-active cysteins to modify target enzyme conformations and activities: the ferredoxin-dependent thioredoxin (Trx) system and the NADPH-dependent thioredoxin reductase C (NTRC) system. Trxs become exclusively reduced by the ferredoxin thioredoxin reductase depending on the photosynthetic electron flux. The reducing power for NTRC, which contains a NADPH-dependent thioredoxin reductase and a thioredoxin domain in a single polypeptide, is provided by NADPH *via* the ferredoxin NADP reductase (FNR) or the oxidative pentose phosphate pathway, the latter operating also in darkness. Previous *in vitro* studies revealed specific functions of the different plastidial Trx isoforms, however, little is known on their *in vivo* relevance. In the present work, a reverse genetic approach was used to investigate the function of Trx *f* and NTRC in *Arabidopsis thaliana* plants. Compared to wild-type, *Arabidopsis* T-DNA insertion lines with a deficiency in Trx *f* showed no significant changes in photosynthesis and growth despite the proposed exclusive role of Trx *f* in regulating the Calvin-Benson cycle enzyme fructose 1,6-bisphosphatase (FBPase). In contrast to this, T-DNA insertion lines with a combined deficiency of Trx *f* and NTRC showed strongly impaired growth and light acclimation capacity, accompanied by diminished photosynthetic electron transport rates, and elevated ratios of the primary light reaction products ATP/ADP and NADPH/NADP⁺, compared to wild-type and the single mutants. Despite the increase in energy and reducing equivalents, the combined deficiency of Trx *f* and NTRC led to strongly impaired CO₂ assimilation rates. In line with this, the light-dependent redox activation of the FBPase was almost completely abolished leading to an accumulation of its substrate fructose 1,6-bisphosphate. *Arabidopsis* mutant lines lacking the redox-sensitive plastidial FBPase isoform showed a similar growth and metabolic phenotype to the *trxf1 ntrc* mutants, confirming that an inhibition of this enzyme has dramatic effects on carbon assimilation and growth. In addition to the strong impairment of the Calvin-Benson cycle, the synthesis of starch as an end product of carbon fixation was almost completely abolished in the *trxf1 ntrc* plants, while there was a less strong effect in the single mutants. In response to varying light conditions the changes in growth, carbon assimilation and starch accumulation were additively increased in the *trxf1 ntrc* plants compared to the single mutants suggesting a cooperative redox regulatory function of Trx *f* and NTRC in photosynthetic metabolism. A direct interaction between Trx *f* and NTRC

SUMMARY

was observed *in vivo* by bimolecular fluorescence complementation assays. Finally, *Arabidopsis* mutants with a disturbed binding of FNR to chloroplast membranes were investigated. While the NADPH/NADP⁺ redox state was decreased, no significant effects on photosynthesis and growth were observed in these mutants, compared to wild-type plants. This underpins the flexibility of the redox regulatory system in photosynthetic metabolism of higher plants, compensating the perturbation of one of its components.

Zusammenfassung

Die Redoxregulation metabolischer Prozesse in Pflanzen ist durch die Beteiligung von Oxidoreduktasen charakterisiert. In Chloroplasten autotropher Gewebe existieren zwei unterschiedliche Systeme, die auf dem Austausch von Thiol-Disulfiden redoxaktiver Cysteine basieren, um die Konformation und Aktivität von Zielenzymen zu modifizieren: das System Ferredoxin-abhängiger Thioredoxine (Trx) und das System der NADPH-abhängigen Thioredoxin-Reductase-C (NTRC). Trx werden abhängig vom photosynthetischen Elektronenfluss ausschließlich durch die Ferredoxin-Thioredoxin-Reductase reduziert. Die Reduktionskraft für NTRC, die eine NADPH-abhängige Thioredoxin-Reduktase-Domäne und eine Thioredoxin-Domäne in einem einzelnen Polypeptid enthält, wird durch NADPH über die Ferredoxin-NADP-Reduktase (FNR) oder den oxidativen Pentosephosphate-Weg, der auch im Dunkeln operiert, bereitgestellt. Vorangegangene *in vitro*-Studien ergaben spezifische Funktionen der verschiedenen plastidären Trx-Isoformen, allerdings ist nur wenig über die Relevanz *in vivo* bekannt. In der vorliegenden Arbeit wurde ein Ansatz der reversen Genetik genutzt, um die Funktion von Trx *f* und NTRC in *Arabidopsis thaliana*-Pflanzen zu untersuchen. Im Vergleich zum Wildtyp zeigten *Arabidopsis*-T-DNA-Insertionslinien mit einem Mangel an Trx *f* keine signifikanten Veränderungen in der Photosynthese und im Wachstum, obwohl für Trx *f* vermutet wird, eine exklusive Rolle in der Regulation des Calvin-Benson-Zyklus-Enzyms Fruktose-1,6-bisphosphatase (FBPase) zu spielen. Im Gegensatz dazu zeigten T-DNA-Insertionslinien mit einem kombinierten Mangel an Trx *f* und NTRC im Vergleich zum Wildtyp und den Einzelmutanten ein stark gehemmtes Wachstum und Lichtanpassungsvermögen, das von verringerten photosynthetischen Elektronentransportraten und erhöhten Verhältnissen der primären Lichtreaktionsprodukten ATP/ADP und NADPH/NADP⁺ begleitet wurde. Trotz erhöhter Energie- und Reduktionsäquivalenten, führte der kombinierte Mangel an Trx *f* und NTRC zu stark beeinträchtigten CO₂-Assimulationsraten. Dementsprechend war die lichtabhängige Redoxaktivierung der FBPase fast vollständig aufgehoben und führte zu einer Akkumulation des Substrates Fruktose-1,6-bisphosphat. *Arabidopsis*-Mutantenlinien, denen die redox-sensitive plastidäre FBPase-Isoform fehlte, zeigten einen ähnlichen Wachstums- und Stoffwechselphänotyp wie die *trxf1 ntrc*-Mutanten und verdeutlichten, dass eine Hemmung des Enzyms dramatische Effekte auf die Kohlenstoffassimilation und das Wachstum hat. Zusätzlich zu der starken Beeinträchtigung des Calvin-Benson-Zyklus, war die Synthese von Stärke als ein Endprodukt der

ZUSAMMENFASSUNG

Kohlenstofffixierung in den *trxf1 ntrc*-Pflanzen fast vollständig aufgehoben, während der Effekt in den Einzelmutanten weniger ausgeprägt war. In Antwort auf variierende Lichtbedingungen nahmen die Veränderungen im Wachstum, der Kohlenstoffassimilation und der Stärkeakkumulation in den *trxf1 ntrc*-Pflanzen im Vergleich zu den Einzelmutanten additiv zu, was auf eine kooperative Funktion von Trx f und NTRC in der Redoxregulation des photosynthetischen Stoffwechsel schließen lässt. Eine direkte Interaktion zwischen Trx f und NTRC wurde *in vivo* durch Bimolekulare Fluoreszenzkomplementations-Ansätze beobachtet. Abschließend wurden *Arabidopsis*-Pflanzen untersucht, in denen die FNR-Bindung an die Chloroplastenmembranen gestört war. Während der NADPH/NADP⁺-Redoxstatus verringert war, wurden keine signifikanten Effekte auf die Photosynthese und das Wachstum in diesen Mutanten im Vergleich zum Wildtyp beobachtet. Das unterstreicht die Flexibilität des redoxregulatorischen Systems im photosynthetischen Stoffwechsel höherer Pflanzen, da die Störung einer Komponente ausgeglichen werden kann.

Introduction

Plants depend on the ability to adapt to changing environmental conditions, due to their sessile and autotrophic lifestyle. The essential and ubiquitous process in plant life is the oxygenic photosynthesis, which enables the conversion of the light energy to chemical energy for the production of sugars as carbon source for growth and development. Since environmental factors, such as light, are fluctuating in nature, the plant developed highly flexible and complex regulatory systems to balance and optimise metabolic processes for survival.

The photosynthetic electron distribution in autotrophic tissues of plants

The photosynthetic electron transport uses the light energy to produce chemical energy and reducing power for downstream metabolic processes in plants (Geigenberger and Fernie 2014). This process operates in chloroplasts of autotrophic tissues such as leaves. The linear electron flux involves the serial action of different proteins located at the thylakoid membranes, generating trans-thylakoid proton gradients for ATP synthesis *via* the CF_0F_1 ATPase, and transferring reducing power to final electron acceptors such as $NADP^+$ for the production of NADPH. The absorption of the light energy by the photosystem (PS) II enables the transfer of electrons, provided by the cleavage of water to protons and oxygen, *via* the electron carriers plastoquinone, the cytochrom b₆f complex and plastocyanin to the PS I complex (see Figure 1). Finally, the mobile electron acceptor ferredoxin (Fdx) becomes reduced at the stromal side of PS I, and acts as key player, channeling the redox power to different pathways (Scheibe and Dietz 2011). Fdx directly donates electrons to assimilatory processes of the sulphur and nitrogen metabolism, or other stromal processes such as chlorophyll, phytochrome and fatty acid biosynthesis (Hanke and Mulo 2013). Additionally, Fdx distributes electrons to the ferredoxin NADP reductase system (FNR) system for the production of NADPH, and to the ferredoxin thioredoxin reductase (FTR) system for redox regulatory processes. The cyclic electron transport is able to redirect reduced Fdx from the stroma to the electron transport chain at the thylakoid membranes by the involvement of the proton-gradient-regulation-5/proton-gradient-regulation-like protein 1 or the NADH-dehydrogenase-like complex (Johnson 2011). These processes support the formation of the trans-thylakoid proton gradient through the proton-pumping plastoquinone pool, whereas the electron distribution by Fdx to other pathways such

INTRODUCTION

as the FNR system is diminished (Foyer et al. 2012). Consequently, this leads to a higher ATP/NADPH ratio, which is important especially if the demand on NADPH in downstream metabolism is lower in relation to ATP. For situations of limited electron acceptors at the stromal side of PS I, the plant evolves reactive oxygen species (ROS) at the PS I complex by the transfer of electrons to oxygen, which subsequently leads to a decreased electron pressure to the electron acceptors (Noctor et al. 2014, Geigenberger and Fernie 2014). ROS, such as H_2O_2 , are involved in signalling functions, however, if H_2O_2 accumulate, it acts as harmful molecule with a strong oxidising power.

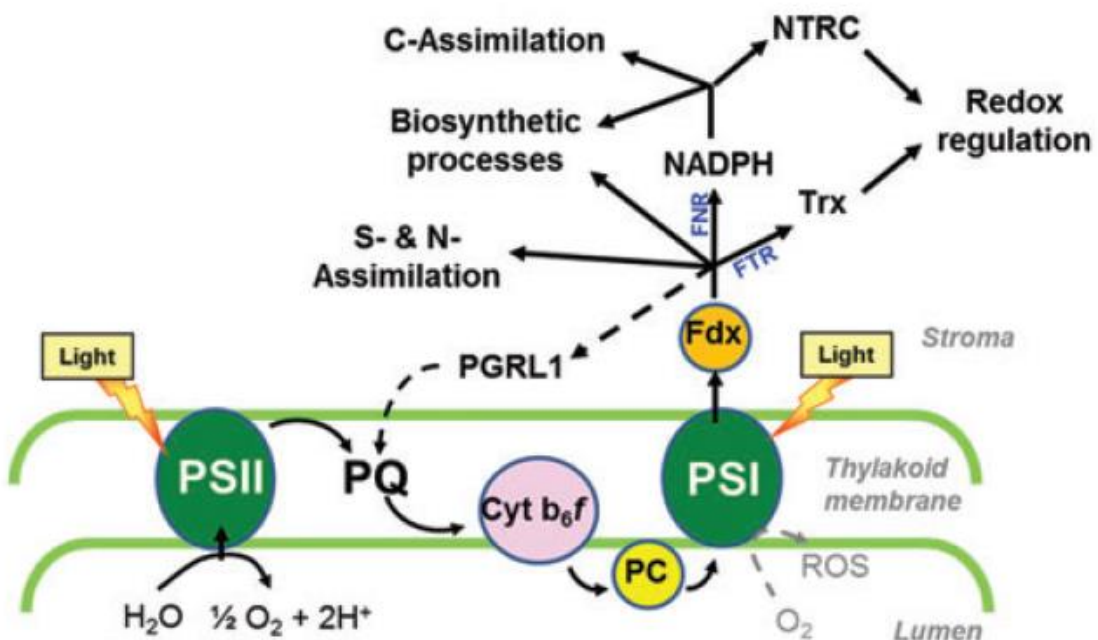


Figure 1 (taken from Geigenberger and Fernie 2014): The photosynthetic electron transport chain in chloroplasts is initiated by the cleavage of water to oxygen and protons in the thylakoid lumen for the provision of electrons. The electron transfer at the thylakoid membrane is mediated by the light absorption of the photosystems II (PSII) and I (PSI), which serially act with the help of the electron carriers plastoquinone (PQ), the cytochrome b_6f complex (Cyt b_6f) and plastocyanin (PC). The stromal electron acceptor ferredoxin (Fdx) distributes the redox power to the S- and N-assimilation, to biosynthetic processes, or to the ferredoxin thioredoxin reductase (FTR) system, involving the reduction of thioredoxins (Trx) for redox regulatory processes. Additionally, Fdx donates electrons to the ferredoxin NADP reductase (FNR) system, which produces NADPH for the C-assimilation, other biosynthesis processes, and for the NADPH-dependent thioredoxin reductase C (NTRC) as redox regulatory component. As indicated with black-dotted lines, the cyclic electron flow enables the reintroduction of electrons from Fdx to the PQ pool by the involvement of other protein complexes such as the proton-gradient-regulation-5/proton-gradient-regulation-like protein 1 (PGRL1). Alternatively, PSI is able to photoreduce oxygen to reactive oxygen species (ROS).

INTRODUCTION

Under optimal growth conditions, Fdx channels the main flux of reducing equivalents to the FNR system, which enables the formation of NADPH by the reduction of NADP⁺ (Meyer et al. 2012, Michelet et al. 2013). In leaves of *Arabidopsis*, two FNR isoforms (LFNR1 and LFNR2) are known, which mainly exist soluble in the chloroplast stroma or attached to the thylakoid membranes (Hanke et al. 2005, Lintala et al. 2007). Several FNR-binding partners have been suggested, however, the 62-kDa subunit of translocon of inner chloroplast membrane (Tic62) and the thylakoid rhodanese-like protein (TROL) are the most promising ones, sharing a characteristic FNR-binding domain (Benz et al. 2010). Tic62 is able to shuttle between the membrane and the stroma dependent on the redox status of the plastid (Stengel et al. 2008). Low NADPH/NADP⁺ ratios induce a strong attachment to the membrane, while a high ratio increases the solubility of Tic62. Contrarily, TROL is an intrinsic thylakoid protein (Juric et al. 2009). The interaction of FNR with the anchor-proteins Tic62 and TROL is favoured by an acidic pH, while the binding decreases at alkaline pH, occurring during the day in the stroma due to the proton-pumping action of the photosynthetic light reaction (Benz et al. 2009, Alte et al. 2010). It is suggested that Tic62 and TROL might have chaperone functions especially during the night since the FNR stability is diminished in low pH environments (Benz et al. 2010).

The main part of the NADPH, produced by the FNR system, is used in the Calvin-Benson cycle (CBC) for the CO₂ fixation and subsequent formation of carbon assimilates (see Figure 2; Michelet et al. 2013, Geigenberger and Fernie 2014). The CBC is divided in three stages, which are called the carboxylation, the reduction and regeneration phase. The carboxylation of Ribulose 1,5-bisphosphate (RBP) is mediated by the ribulose 1,5-bisphosphate carboxylase/oxygenase, and produces 3-phosphoglycerate (3PGA). The reduction of 3PGA consumes ATP and NADPH due to the enzymatic reactions of the phosphoglycerate kinase and the NADPH-dependent glyceraldehyde 3-phosphate dehydrogenase, respectively. The third phase includes several enzymatic steps, such as the ATP-dependent reaction of the phosphoribulokinase, which finally leads to the regeneration of RBP. In addition to this, various other metabolic processes in chloroplasts are dependent on the reductant NADPH, such as fatty acid and chlorophyll biosynthesis. Additionally, the NADPH is used by the NADPH-dependent thioredoxin reductase C (NTRC) for redox regulatory processes (Cejudo et al. 2012). NTRC consists of a NADPH-dependent thioredoxin reductase (NTR) domain and a thioredoxin (Trx) domain in a single polypeptide, and shows oxidoreductase activity with its redox-active cysteins in the catalytic centre. NADPH is used as reducing power for the NTR domain, which transfers

INTRODUCTION

the electrons to the Trx domain to modify the redox state of thiol-disulfides in target proteins. In situations of excess NADPH in the stroma, the plant is able to recycle NADP⁺ as electron acceptor for PS I by the malate valve (Scheibe and Dietz 2011). The plastidial NADPH-dependent malate dehydrogenase (NADP-MDH) converts stromal NADPH and oxaloacetate to malate and NADP⁺. The activity is increased at elevated NADPH/NADP⁺ ratios and *vice versa*, and the posttranslational redox-activation strictly light-dependent, which both enables the plant to maintain the redox poise in chloroplasts during the day. In addition to the recycling of NADP⁺ by the NADP-MDH, the malate valve involves the followed export of malate outside of the chloroplast in a counterexchange with oxaloacetate. The cytosolic malate pool can fulfil different functions, such as the provision of NADH after the re-conversion to oxaloacetate for nitrate reduction, the generation of ATP after the transport to the mitochondria, the support of photorespiration, or the storage of malate in the vacuole (Scheibe et al. 2005).

Beside the Fdx-dependent electron distributions mentioned above, the photosynthetic electron flux delivers also the FTR system with reducing power (Hanke and Mulo 2013). Fdx transfers its electrons to the FTR for the light-dependent reduction of Trx. Trxs are ubiquitous proteins, acting as oxidoreductases with redox-active cysteins in their catalytic centre to modify thiol-disulfides of target enzymes, which finally lead to changes in enzyme conformation and activities (Schürmann and Buchanan 2008, Meyer et al. 2012). Originally, they were identified in plants, mediating the activation of CBC enzymes. Indeed, four CBC enzymes are subjected to a direct redox activation by Trxs (see Figure 2; Michelet et al. 2013). The NADPH-dependent glyceraldehyde 3-phosphate dehydrogenase from the reduction phase provides triose phosphates for the running CBC, but as well as for the sucrose synthesis in the cytosol, and three enzymes from the regeneration phase are redox-activated by Trxs, namely phosphoribulokinase, sedoheptulose 1,7-bisphosphatase, and the fructose 1,6-bisphosphatase (FBPase). The latter enzyme dephosphorylates fructose 1,6-bisphosphate (F1,6BP) to Fructose 6-phosphate (F6P), which is used for the regeneration of RBP in the CBC, but serves additionally as important precursor for starch synthesis and the oxidative pentose phosphate pathway (OPPP) in the chloroplast (Geigenberger and Fernie 2014). In *Arabidopsis* two plastidial FBPase isoforms (cFBP1 and cFBP2) are known (Serrato et al. 2009). cFBP1 has an approximately 6-fold higher affinity to the substrate F1,6BP than cFBP2, and is strictly redox-activated by the plastidial Trx *f* isoform, while cFBP2 is redox-insensitive (Serrato et al. 2009, Michelet et al. 2013). Finally, the FTR system and the subsequent reduction of Trxs complete the Fdx-dependent electron distribution in chloroplasts. This enables a light-dependent

INTRODUCTION

coordination of produced energy and reducing equivalents with the redox-activated carbon assimilation process and related metabolic pathways.

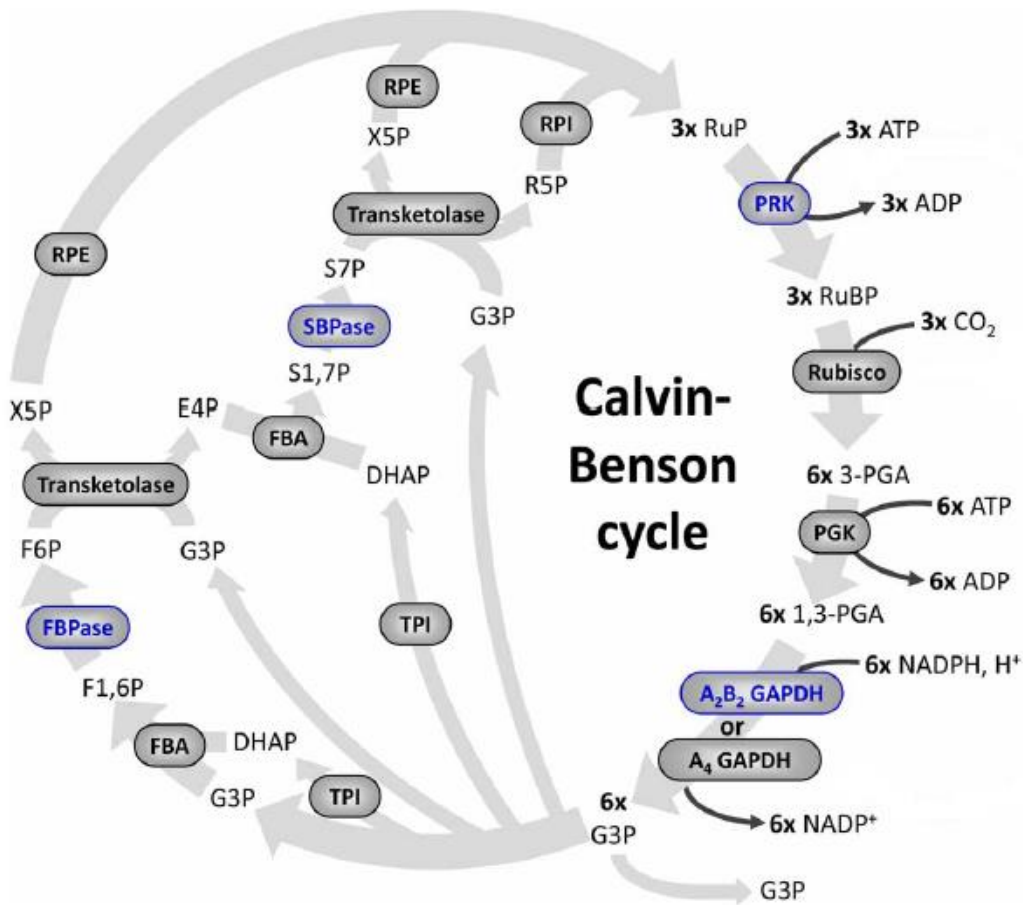
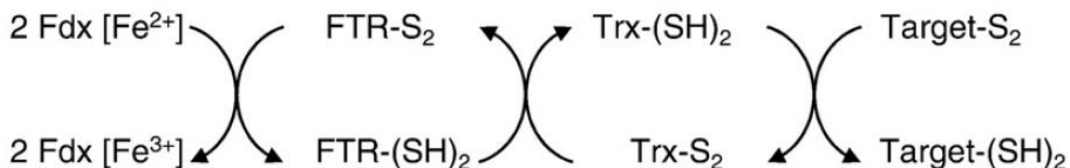


Figure 2 (taken and modified from Michelet et al. 2013): The Calvin Benson cycle in chloroplasts enables the fixation of carbon by the Rubisco reaction for the production of carbon assimilates as important precursors for downstream metabolism. The fixation of one CO_2 molecule needs three ATP and two NADPH, mainly provided by the photosynthetic light reaction, and one molecule of RuBP. Eleven enzymes are involved in the complete cycle, and four of them are subjected to a direct redox activation by thioredoxins, which are indicated with blue letters. Enzymes: FBA, fructose 1,6-bisphosphate aldolase; FBPase, fructose 1,6-bisphosphatase; GAPDH, glyceraldehydes 3-phosphate dehydrogenase; PGK, phosphoglycerate kinase; PRK, phosphoribulokinase; SBPase, sedoheptulose 1,7-bisphosphatase; TK, transketolase; TPI, triose phosphate isomerase; RPE, ribulose 5-phosphate 3-epimerase; RPI, ribose 5-phosphate isomerase; Rubisco, ribulose 1,5-bisphosphate carboxylase/oxygenase. Metabolites: DHAP, dihydroxyacetone phosphate; E4P, erythrose 4-phosphate; F1,6P, fructose 1,6-bisphosphate; F6P, fructose 6-phosphate; G3P, glyceraldehydes 3-phosphate; 1,3-PGA, 1,3-bisphosphoglycerate; 3-PGA, 3-phosphoglycerate; R5P, ribulose 5-phosphate; RuBP, ribulose 1,5-bisphosphate; RuP, ribulose 5-phosphate; S1,7P, sedoheptulose 1,7-bisphosphate; S7P, sedoheptulose 7-phosphate; X5P, xylulose 5-phosphate.

The Trx-based redox regulatory system in chloroplasts

Since their discovery in plants, 39 putative Trxs were identified in *Arabidopsis* (Belin et al. 2014). The typical Trxs with the catalytic motif WCXPC and a molecular weight of approximately 12 kDa are phylogenetically separated to seven different subtypes, named Trx *f*, *m*, *x*, *y*, *z*, *h* and *o* (Schürmann and Buchanan 2008, Meyer et al. 2012). The 10 isoforms Trx *f1-2*, *m1-4*, *x*, *y1-2* and *z* are localized to the plastids, while the isoforms of Trxs *h* and *o* are mainly localized to the cytosol and mitochondria, respectively. In contrast to the Fdx-dependent reduction of plastidial Trx by the FTR, the Trx isoforms present in other compartments of plant cells are dependent on the reducing power of NADPH (see Figure 3; Montrichard et al. 2009). The electron transfer from NADPH to the extraplastidial Trxs in *Arabidopsis* is catalysed by the two NTR isoforms NTRA and NTRB, which are mainly present in the cytosol and mitochondria, respectively (Reichheld et al. 2005).

Ferredoxin-thioredoxin system



NADP-thioredoxin system

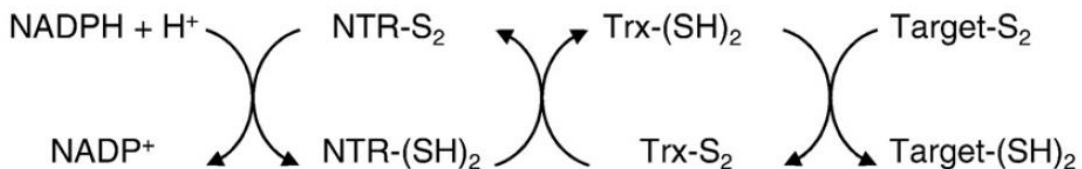


Figure 3 (taken from Montrichard et al. 2009): The thiol disulfide exchange in the ferredoxin-thioredoxin system of plastids is dependent on the sequential electron transfer between ferredoxin (Fdx), ferredoxin thioredoxin reductase (FTR), thioredoxins (Trx) and target proteins. The NADP-thioredoxin system operates in other compartments of plant cells, using NADPH as reducing power for the reduction of the NADPH-dependent thioredoxin reductase (NTR), Trxs, and finally the target proteins.

INTRODUCTION

The redox regulatory functions of the plastidial Trxs are widespread and still under investigation, but several biochemical studies revealed specificities for the regulation of target enzymes (Meyer et al. 2012). Trxs *f* and *m* regulate predominantly primary metabolism in chloroplasts, like CBC enzyme activities (Collin et al. 2003, Michelet et al. 2013), starch synthesis (Ballicora 2000, Geigenberger et al. 2005) and degradation (Mikkelsen et al. 2005, Valerio et al. 2011, Seung et al. 2013, Silver et al. 2013), NADPH production by the glucose 6-phosphate dehydrogenase (G6PDH) in the OPPP (Nee et al. 2009) and export by the malate valve *via* NADP-MDH (Collin et al. 2003), the synthesis of fatty acids (Sasaki et al. 1997), amino acids (Lichter and Häberlein et al. 1998, Choi et al. 1999, Motohashi et al. 2001) and chlorophyll (Ikegami et al. 2007, Luo et al. 2012), in most cases Trx *f* being more efficient than Trx *m*. Trxs *x*, *y* and *z* mainly serve as reducing substrates for enzymes such as thiol-peroxidases or methionine sulfoxide reductases under oxidative stress conditions (Collin et al. 2003, Collin et al. 2004, Chibani et al. 2011, Bohrer et al. 2012). Little is known about the *in vivo* relevance of plastidial Trxs, however, in the last five years the findings increased by reverse genetic approaches with *Arabidopsis* plants, lacking specific Trx isoforms. Studies revealed a redundant function of Trx *m1*, *m2* and *m4* in the biogenesis of the PS II complex (Wang et al. 2013), an involvement of Trx *m3* in meristem development (Benitez-Alfonso et al. 2009), of Trx *m4* in the down regulation of cyclic electron transport at PS I (Courteille et al. 2013), of Trx *y2* in the repair of oxidised proteins by methionine sulfoxide reductases (Laugier et al. 2013), and evidences indicate an influence of Trx *z* to the chloroplast gene expression and development (Arsova et al. 2010).

An alternative plastidial redox system exists beside the Fdx Trx system (see Figure 4; Cejudo et al. 2012). About 10 years ago, the NTRC was identified as an atypical NTR enzyme, consisting of a NTR and an additional Trx domain in a single polypeptide, contrarily to the other two known NTR isoforms of *Arabidopsis* (Serrato et al. 2004, Cejudo et al. 2012). For the reduction of the catalytic cysteins in the Trx domain of NTRC, NADPH is used, which is not only provided during the day by photosynthesis, but also during the night by the OPPP. This includes the possibility that NTRC regulates redox processes additionally in the dark independent of the photosynthetic electron transport chain (Perez-Ruiz et al. 2006). *Arabidopsis* mutants with a deficiency in NTRC protein show retarded growth and pale green leaves (Serrato et al. 2004). Investigations with the *ntrc* mutants revealed redox-regulatory functions of NTRC in the oxidative stress response influencing the redox state of 2-Cys peroxiredoxins (Perez-Ruiz et al. 2006, Kirchsteiger et al. 2009, Pulido et al. 2010), in the starch synthesis modifying the

INTRODUCTION

activation state of ADP-glucose pyrophosphorylase (AGPase) (Michalska et al. 2009, Lepistö et al. 2013), and in the chlorophyll biosynthesis process (Richter et al. 2013, Perez-Ruiz et al. 2014). Further preliminary evidences suggest additional functions of NTRC in the aromatic amino acid synthesis and chloroplast biogenesis (Nikkanen and Rintamäki 2014).

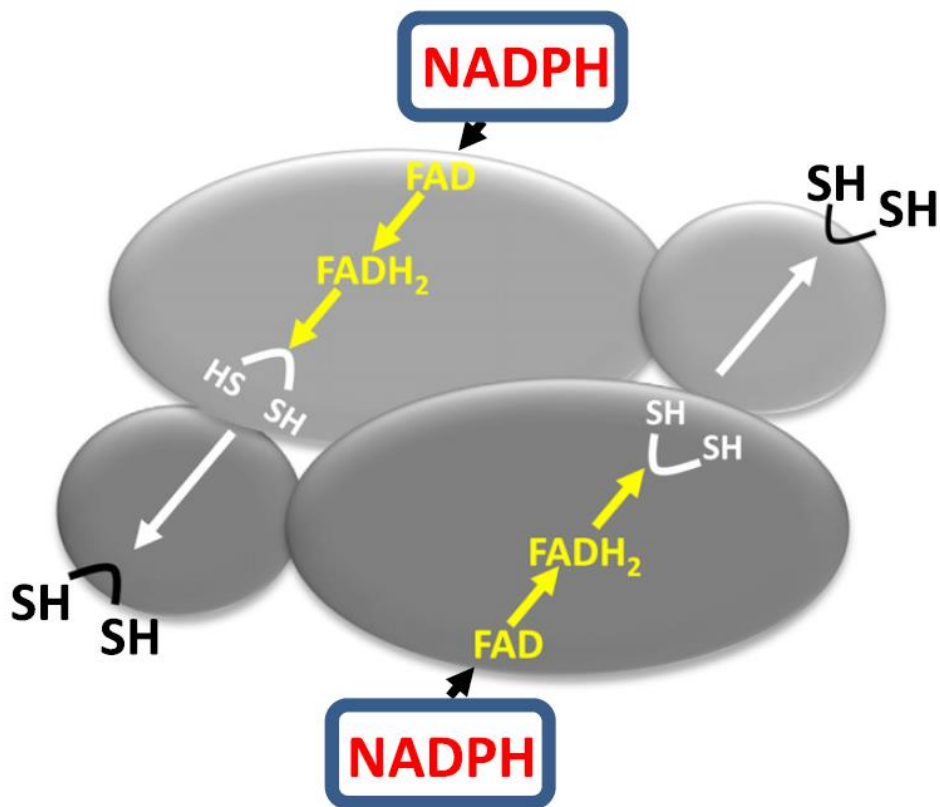


Figure 4 (taken from Cejudo et al. 2012): The proposed catalytic conformation of the NADPH-dependent thioredoxin reductase C (NTRC) has a homodimeric structure. Each subunit consists of a NADPH-dependent thioredoxin reductase (NTR) and a thioredoxin (Trx) domain in a single polypeptide, while the electron transfer is directed in an intersubunit way. NADPH reduces the cofactor FAD and leads to the cleavage of a disulfide bridge in the catalytic site of the NTR domain. The NTR domain is then reducing the cysteine residues of the Trx domain belonging to the other NTRC subunit to enable the redox-dependent modification of target enzymes.

The photosynthetic end product synthesis of starch in plant leaves

The two main end products of photosynthesis are starch and sucrose, which provide the plant with carbon as primary source for growth (Geigenberger and Fernie 2014). While sucrose is synthesized in the cytosol for further metabolism and export to sink tissues, the accumulation of starch is located to the chloroplasts of higher plants (see Figure 5; Zeeman et al. 2007). The

flux of carbon assimilates from the CBC into starch and sucrose has to be balanced to avoid feedback inhibition effects on photosynthesis by elevated sugar levels (Stitt et al. 2010). The CBC provides triose phosphates, which are used for sucrose synthesis in the cytosol. If sucrose accumulates, the synthesis is inhibited, and subsequently the transport of triose-phosphates from the chloroplast to the cytosol diminishes. Finally, the carbon assimilates rise in the stroma, and the starch synthesis is facilitated. Dependent on current carbon necessities for metabolism and growth, the plant is able to balance the photosynthetic end product synthesis between starch and sucrose during the day.

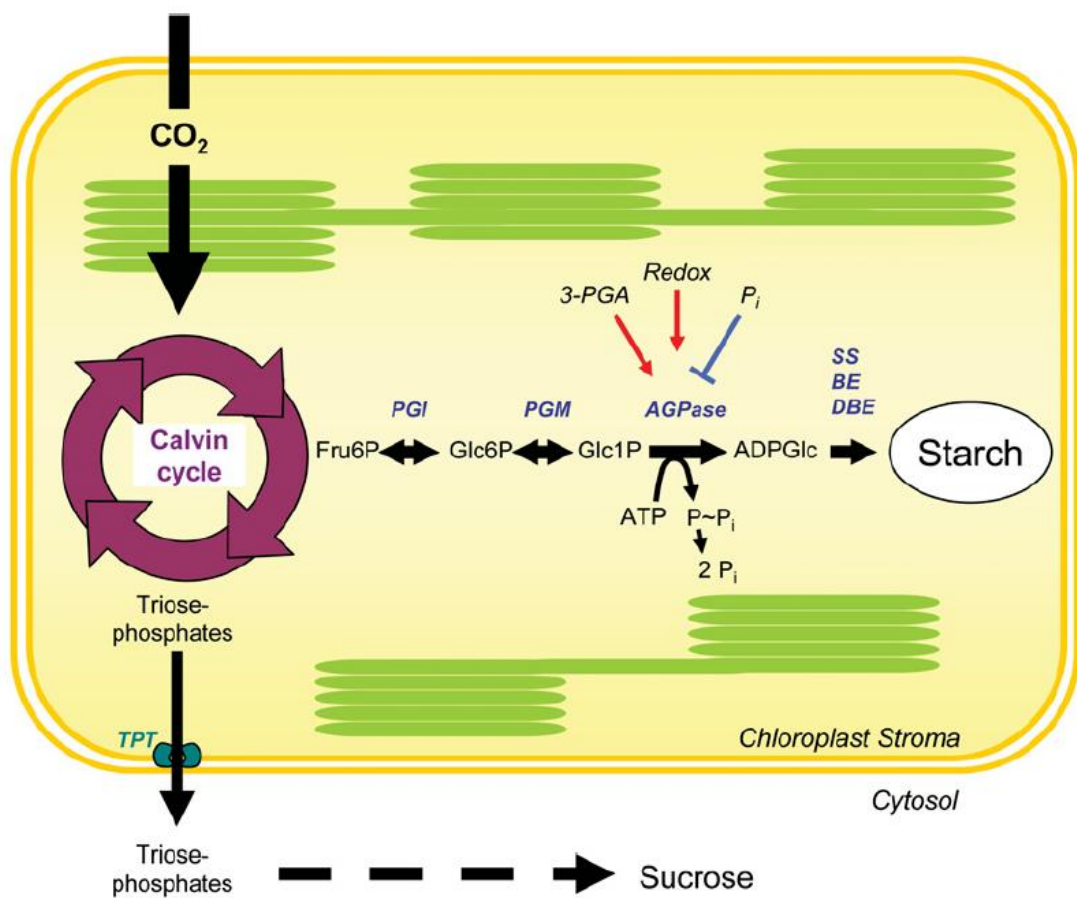


Figure 5 (Reproduced with permission, from Zeeman SC, Smith SM, Smith AM, 2007, Biochemical Journal, **401**, 13-28. © the Biochemical Society.): The Calvin-Benson cycle in chloroplasts of dicotyledonous plants assimilates carbon, and subsequently provides intermediates for the biosynthesis of the two main end products of photosynthesis, namely sucrose and starch. Triose phosphates are transported to the cytosol *via* the TPT for sucrose synthesis. Fru6P is the precursor for the starch synthesis, and converted to Glc1P by two enzymatic steps, involving the sequential action of PGI and PGM. Afterwards, the AGPase uses Glc1P and ATP to produce ADPGlc, which acts as glycosyl donor for the subsequent enzymatic formation of the starch granule. The AGPase controls the flux of the starch synthesis pathway, while being subjected to several regulatory events such as the allosteric inhibition

INTRODUCTION

by P_i or activation by 3-PGA, and the posttranslational modification by redox processes. Enzymes: AGPase, ADP-glucose pyrophosphorylase; BE, branching enzyme; DBE, de-branching enzyme; PGI, phosphoglucoisomerase; PGM, phosphoglucomutase; SS, starch synthase; TPT, triose phosphate/phosphate translocator. Metabolites: ADPGlc, ADP-glucose; Fru6P, fructose 6-phosphate; Glc1P, glucose 1-phosphate; Glc6P, glucose 6-phosphate; 3-PGA, 3-phospho glycerate; P_i , inorganic phosphate.

Starch is the major carbohydrate store for many plants in a wide range of tissues (Zeeman et al. 2007). The typical insoluble, semi-crystalline structure of starch granules is obtained by two different glucan polymers, named amylose and amylopectin. Amylose consists of α -1,4-linked glucose monomers, while amylopectin shows a branched structure with additional α -1,6-linked glucosyl chains. The transient synthesis of starch occurs in most cases during the day in chloroplasts of leaves (Geigenberger 2011). Genetic approaches with starchless mutants showed that transient starch is essential for plant survival, if the night exceeds 12 h (Stitt et al. 2010). During the night when photosynthesis is inactive the transient starch is degraded for maintaining metabolism and growth (Stitt and Zeeman 2012). It is essential that the transient starch accumulation and degradation is regulated to react to environmental changes like fluctuating light conditions and to avoid exhausted reserves at night. The pathway of starch synthesis starts with F6P, produced in the CBC, which is converted to glucose 1-phosphate by two enzymatic steps, involving the sequential action of phosphoglucoisomerase and phosphoglucomutase (see Figure 5). The AGPase converts glucose 1-phosphate and ATP to ADP-glucose and pyrophosphate, while ADP-glucose acts as glucosyl donor for the elongation of glucan chains, and the subsequent formation of starch granules (Geigenberger and Fernie 2014). Flux control analyses revealed that the AGPase catalyses a near rate-determining step of the starch synthesis pathway (Neuhaus and Stitt 1990, Stitt et al. 2010). The holoenzyme of AGPase has a heterotetrameric structure and consists of two large APL (51 kDa) and two small APS (50 kDa) subunits, both fulfilling regulatory and catalytic functions for adjusting the activity (Cross et al. 2004, Ventriglia et al. 2008, Geigenberger 2011).

The AGPase is highly regulated at several levels of control (Hädrich et al. 2012). The expression of the genes coding for the AGPase subunits (APL1-4 and APS1-2) is influenced by the nutritional status of the plant. At elevated nitrogen or phosphate levels AGPase genes are less expressed (Scheible et al. 1997, Nielsen et al. 1998), however, an increased carbon supply induces a higher expression (Müller-Röber et al. 1990, Sokolov et al. 1998, Crevillen 2005). The allosteric regulation by 3PGA stimulates the activity of AGPase, while P_i inhibits the activity (Ghosh and Preiss 1966, Sowokinos and Preiss 1982). A further posttranslational

INTRODUCTION

mechanism for the adjustment of AGPase activity is the redox modification of conserved cysteins in the catalytic small subunit APS1, representing the predominant catalytic isoform in leaves (Geigenberger et al. 2011). An intermolecular disulfide bridge between conserved cysteins of the two small subunits is cleaved under reducing conditions, leading to an increased activity of AGPase (see Figure 6). The mechanism was first observed with recombinant potato tuber protein (Fu et al. 1998), and *in vitro* assays showed that the stromal oxidoreductases Trx *f* and *m* influence the activity of AGPase, changing the thiol-disulfide state of the APS1 protein (Ballicora et al. 2000, Geigenberger et al. 2005). Reduction of the conserved cysteins in the APS1 proteins cause altered kinetic properties of the enzyme, leading to higher substrate affinities, higher sensitivities to the allosteric activator 3PGA, and this correlates with higher starch levels in leaves (Fu et al. 1998, Ballicora et al. 2000, Hendriks et al. 2003). The redox-activating mechanism was confirmed *in vivo* with heterotrophic (Tiessen et al. 2002) and autotrophic (Hendriks et al. 2003) plant material from potato, pea and *Arabidopsis*. Studies with transgenic *Arabidopsis* plants, containing constantly redox-activated AGPase enzyme, confirmed that the redox regulation of AGPase contributes significantly to the accumulation of starch (Hädrich et al. 2012). Leaf material of *Arabidopsis* and other dicotyledonous species shows a strong dependency between APS1 monomerisation and light as external factor (Hendriks et al. 2003, Michalska et al. 2009). Additionally, sugar incubation in the dark changed the redox state of the small subunit, which has an additive effect on the light-dependent redox activation. As confirmed later the sugar-dependent activation of starch synthesis is mediated by the redox-regulatory NTRC protein (Michalska et al. 2009). The *Arabidopsis* T-DNA insertion line *ntrc* with a deficiency in NTRC protein showed a decreased APS1 monomerisation in illuminated and in darkened sugar-incubated leaves. It is suggested that NTRC acts during the day, using photosynthetically produced NADPH as reducing power to redox-activate starch synthesis, whereas elevated sugar level induce the NADPH production throughout the activity of OPPP enzymes. The latter mechanism might function during day and night.

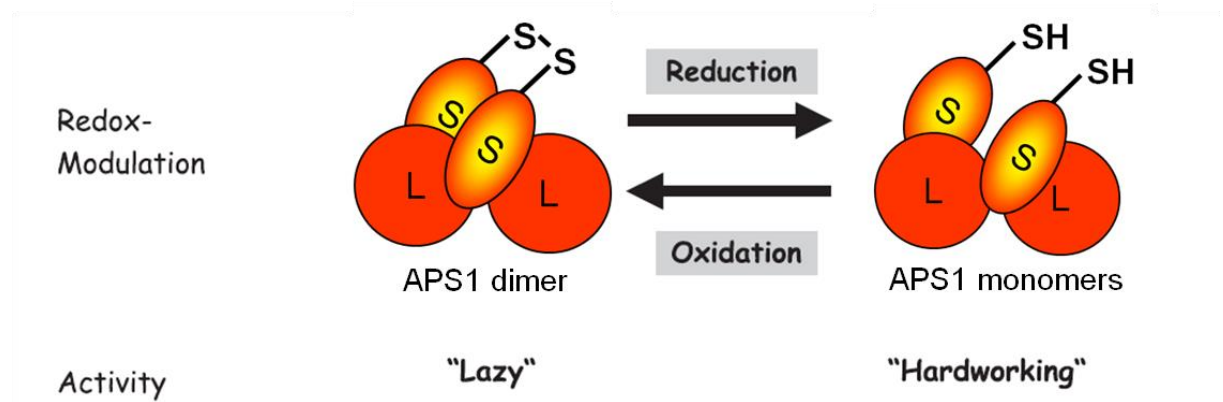


Figure 6 (taken and modified from Geigenberger et al. 2005): The redox modulation of the ADP-glucose pyrophosphorylase (AGPase) is accompanied by changes in the conformation and the activity of the enzyme. The AGPase acts as heterotetramer and consists of two large (APL) and two small (APS) subunits. The major isoform of the small subunit is the APS1 protein, which contains a conserved cysteine, and forms in the oxidised state an intermolecular disulfide bridge with the second APS1 protein of the holoenzyme. Under reducing conditions this APS1 dimer is cleaved to two APS1 monomers, and enables an increased activity of the AGPase.

Objectives of the thesis

In the 1970s, the redox regulatory function of Trxs was discovered as connection between light and photosynthesis-related enzymatic processes (Buchanan et al. 2012). In the last 40 years the knowledge about the influence of the redox network in chloroplasts increased, but still information is lacking about the specificities and interrelations of the redox regulatory proteins, especially *in vivo*. Recent investigations *in planta* observed redox regulatory functions of NTRC in the detoxification of ROS, the synthesis of starch, and in the chlorophyll biosynthesis. Biochemical studies revealed functions of Trx *f* in the primary metabolism of chloroplasts, e.g. the redox activation of the AGPase as key enzyme of starch synthesis, or the exclusive redox activation of Calvin-Benson cycle enzymes, such as the FBPase, while nothing was known about the *in vivo* relevance. To find out, whether Trx *f* also plays a role in promoting the starch synthesis in leaves, the present work analysed two independent *Arabidopsis* T-DNA-Insertion lines with a deficiency in Trx *f* (Chapter 1). To reveal the relevance of Trx *f* and NTRC for photosynthetic processes and carbon metabolism in *Arabidopsis* leaves, T-DNA insertion lines lacking both redox regulatory proteins were used to study the impact on photosynthetic electron transport, CBC activity, end product synthesis of starch and related metabolic pathways (Chapter 2). To compare the effects on photosynthetic carbon assimilation and growth, *Arabidopsis* plants lacking the main plastidial FBPase as exclusive Trx *f* target enzyme were

INTRODUCTION

investigated (Chapter 3). To obtain insights in upstream processes as the photosynthetic electron transport machinery, *Arabidopsis* mutant lines with deficiencies in the FNR anchor proteins TIC62 and TROL were analyzed (Chapter 4).

RESULTS

Results

Chapter 1 - Inactivation of thioredoxin *f1* leads to decreased light activation of ADP-glucose pyrophosphorylase and altered diurnal starch turnover in leaves of *Arabidopsis* plants

Ina Thormählen, Joachim Ruber, Edda von Roepenack-Lahaye, Sven Matthias Ehrlich, Vincent Massot, Christine Hümmer, Justyna Tezycka, Emmanuelle Issakidis-Bourguet, Peter Geigenberger (2013) Inactivation of thioredoxin *f1* leads to decreased light activation of ADP-glucose pyrophosphorylase and altered diurnal starch turnover in leaves of *Arabidopsis* plants. *Plant Cell Environ.* 36(1):16-29.

Inactivation of thioredoxin *f1* leads to decreased light activation of ADP-glucose pyrophosphorylase and altered diurnal starch turnover in leaves of *Arabidopsis* plants

INA THORMÄHLEN¹, JOACHIM RUBER¹, EDDA VON ROEPENACK-LAHAYE², SVEN-MATTHIAS EHRLICH¹, VINCENT MASSOT³, CHRISTINE HÜMMER¹, JUSTYNA TEZYCKA¹, EMMANUELLE ISSAKIDIS-BOURGUET³ & PETER GEIGENBERGER¹

¹Plant Metabolism Group and ²Mass-Spectrometry Group, Ludwig-Maximilians-Universität München, Department Biologie I, 82152 Martinsried, Germany and ³Institut de Biologie des Plantes, UMR 8618 CNRS/Univ. Paris-Sud, 91405, Orsay Cedex, France

ABSTRACT

Chloroplast thioredoxin *f* (Trx *f*) is an important regulator of primary metabolic enzymes. However, genetic evidence for its physiological importance is largely lacking. To test the functional significance of Trx *f* *in vivo*, *Arabidopsis* mutants with insertions in the *trx f1* gene were studied, showing a drastic decrease in Trx *f* leaf content. Knockout of Trx *f1* led to strong attenuation in reductive light activation of ADP-glucose pyrophosphorylase (AGPase), the key enzyme of starch synthesis, in leaves during the day and in isolated chloroplasts, while sucrose-dependent redox activation of AGPase in darkened leaves was not affected. The decrease in light-activation of AGPase in leaves was accompanied by a decrease in starch accumulation, an increase in sucrose levels and a decrease in starch-to-sucrose ratio. Analysis of metabolite levels at the end of day shows that inhibition of starch synthesis was unlikely due to shortage of substrates or changes in allosteric effectors. Metabolite profiling by gas chromatography–mass spectrometry pinpoints only a small number of metabolites affected, including sugars, organic acids and ethanolamine. Interestingly, metabolite data indicate carbon shortage in *trx f1* mutant leaves at the end of night. Overall, results provide *in planta* evidence for the role played by Trx *f* in the light activation of AGPase and photosynthetic carbon partitioning in plants.

Key-words: carbon partitioning; light signalling; redox regulation.

INTRODUCTION

Regulation of protein function by a change in thiol redox state has gained prominence as a universal concept throughout biology (Buchanan & Balmer 2005). It was discovered in chloroplasts more than 40 years ago, providing a

Correspondence: P. Geigenberger. *Fax:* +49 89 218074599; *e-mail:* geigenberger@bio.lmu.de

mechanism for the regulation of photosynthesis in response to environmental changes in light–dark conditions (Buchanan 1980). Illumination promotes the reduction of ferredoxin (Fdx), which, in turn, leads to the sequential reduction of ferredoxin : thioredoxin reductase (FTR) and a family of thioredoxins (Trxs). Trxs then reduce disulfide bonds in selected target enzymes, some of them being involved in the Calvin–Benson cycle, ATP synthesis or NADPH export from the chloroplast. Most Trx target proteins are reductively activated in the light and deactivated in the dark, when the Trx system is re-oxidized (Schürmann & Buchanan 2008).

Although well characterized in photosynthesis, relatively little is known about the role of this concept in regulating other metabolic processes in plants. Several years ago, it was shown that thioredoxins regulate ADP-glucose pyrophosphorylase (AGPase), a key enzyme of starch biosynthesis in plastids (Fu *et al.* 1998; Ballicora *et al.* 2000; Geigenberger, Kolbe & Tiessen 2005; Geigenberger 2011). AGPase is rapidly activated upon illumination by reduction of an intermolecular disulfide bond between the Cys residues joining the two small subunits (APS1) of this heterotetrameric enzyme (Hendriks *et al.* 2003; Kolbe *et al.* 2005). Using transgenic *Arabidopsis* plants expressing a mutated AGPase where the regulatory Cys-81 of APS1 has been replaced by Ser, genetic evidence has been provided that redox regulation of AGPase contributes significantly to photosynthetic starch turnover during the light/dark cycle in leaves (Hädrich *et al.* 2012). In addition to light, redox activation of AGPase is also promoted by sugars, in illuminated as well as darkened leaves and in non-photosynthetic tissues (Tiessen *et al.* 2002; Hendriks *et al.* 2003; Kolbe *et al.* 2005). In recent proteomic studies, a large number of further potential Trx targets have been identified, distributed in various metabolic processes, different cellular organelles and diverse tissues (Montrichard *et al.* 2009). Although these targets still have to be confirmed at the biochemical level, this suggests that Trxs have a more general role in metabolic regulation than initially expected.

The *Arabidopsis* genome contains a family of Trxs, including 20 different isoforms grouped in seven types (Meyer, Reichheld & Vignols 2005; Lemaire *et al.* 2007; Arsova *et al.* 2010). Trxs *f*, *m*, *x*, *y* and *z* are located in the chloroplast, Trx *o* in mitochondria and Trx *h* in the cytosol and mitochondria. The chloroplast Trxs can be further subdivided into two *f*-type (Trxs *f*1, 2), four *m*-type (Trxs *m*1-4), one *x*-type (Trx *x*), two *y*-type (Trx *y*1-2) and one *z*-type (Trx *z*) isoforms. *In vitro* studies using purified proteins show that Trx *f* and *m* regulate various enzymes mainly involved in primary metabolism, while *x*-, *y*- and *z*-types serve as reducing substrates for antioxidant enzymes such as peroxiredoxins, indicating their role in oxidative stress responses (Collin *et al.* 2003, 2004; Chibani *et al.* 2011). However, little is known about the *in vivo* importance and specificity of these different Trxs isoforms *in planta*. Studies of *Arabidopsis* knockout mutants revealed a role of Trx *m*3 in meristem development (Benitez-Alfonso *et al.* 2009) and of Trx *z* in chloroplast gene expression and development (Arsova *et al.* 2010). Intriguingly, reverse genetic studies on the roles of *f*- and *m*-type Trxs in primary metabolism are largely lacking.

In addition to these classical Trx forms which are freely linked to photoreduced Fdx, plants contain an unusual plastid-localized NADP-thioredoxin reductase c (NTRC) containing both an NADP-thioredoxin reductase (NTR) and a Trx domain on a single polypeptide (Serrato *et al.* 2004). This bimodular enzyme conjugates both NTR and Trx activities to efficiently regulate chloroplast target enzymes such as 2-Cys peroxiredoxins (Pérez-Ruiz *et al.* 2006) or AGPase (Michalska *et al.* 2009) using NADPH as reducing power. Consistently, NTRC has been found to play a role in both detoxification of hydrogen peroxide (Pérez-Ruiz *et al.* 2006) and regulation of starch synthesis (Michalska *et al.* 2009). However, the relative importance of free Trxs, compared to NTRC in regulating these processes has not been fully investigated yet.

In this report, the role of Trx *f* in regulating AGPase and starch synthesis has been investigated by using both biochemical and genetic approaches. Analyses of *Arabidopsis* knockout mutants show that a decrease in Trx *f* leads to a decrease in redox activation of AGPase and starch accumulation in the light, while sucrose-dependent redox activation of AGPase in the dark remains unaffected. Metabolite profiling by gas chromatography-mass spectrometry (GC-MS) was used to pinpoint more global metabolic changes in response to a decrease in Trx *f* level. Results provide direct biochemical and genetic evidence for the role played by Trx *f* in regulating photosynthetic carbon partitioning in plants.

MATERIALS AND METHODS

Plant material and growth conditions

Two *Arabidopsis thaliana* *trx f1* T-DNA insertion lines (*trx f1.1*, SALK_128365 and *trx f1.2*, SALK_063799; Alonso *et al.* 2003) and their in parallel segregated

respective wild types (WT.1 and WT.2) were grown on potting soil (Stender, Germany) in a growing chamber with an 8 h day of 160 μmol photons $\text{m}^{-2} \text{s}^{-1}$, 20 °C/ 16 °C, and 60%/75% humidity (day/night). Every experiment was done with 5-week-old plants. Harvested leaves (fully expanded, not shaded) were put directly into liquid nitrogen, and stored at -80 °C until use. For extractions, the leaves were pulverized with liquid nitrogen to a fine powder using a mixer mill (MM 400, Retsch GmbH, Haan, Germany).

In vitro assays with purified recombinant proteins

In vitro assays with purified recombinant APS1, Trxs and NTRC proteins were performed as previously described in Michalska *et al.* (2009). The proteins were assayed at 10 μM concentrations in buffer solution containing 50 mM HEPES (pH 7.8), 3 mM MgCl₂, 1 mM ATP, and 1 mM 3-phosphoglycerate (3-PGA) for the time intervals indicated in the figures. Purified recombinant APS1 (Michalska *et al.* 2009), NTRC (Pérez-Ruiz *et al.* 2006) and Trxs *f1*, *m1*, *x* and *y1* proteins (Collin *et al.* 2003, 2004) were produced as previously described. In the assays with Trxs, 0.5 mM dithiothreitol (DTT) was included. In the assays with NTRC, DTT was replaced by 300 μM NADPH.

Molecular characterization of the knockout lines

Transcripts levels were estimated by semi-quantitative RT-PCR experiments using gene-specific primer pairs: ACGACGACGTTGTGTTCTAAAG and CTTCTT GACAACCTTGTATCC for Trx *f1* (At3g02730), AGC TATCGGAGAAGTACCAGGAC and CTTCAATGGC TGCAAGTAAGTCT for Trx *f2* (At5g16400) and GAT GCAATCTCTCATTCCGATAG and AGAGCTTGAT TTGCGAAATACC for PP2A (At1g13320, a constitutively expressed protein phosphatase) genes. PCR products were fractionated on agarose gel, and visualized by ethidium bromide staining. Detection of Trx *f* in wild-type and mutant plants was done by Western blot analysis on 50 μg of leaf soluble proteins using antibodies raised against pea Trx *f* (Hodges *et al.* 1994) recognizing *Arabidopsis* Trx *f1* and Trx *f2* recombinant proteins with comparable efficiencies.

Chlorophyll fluorescence analysis

For the *in vivo* chlorophyll a fluorescence measurement and the calculation of standard photosynthesis parameters of PSII a Dual-PAM fluorometer (Dual-PAM 100, Walz GmbH, Effeltrich, Germany) was used according to Pesaresi *et al.* (2009). Whole plants were dark adapted for 10 min to determine the dark fluorescence yield (F_0). Then one fully expanded leaf was exposed to a single red pulse (5000 μmol photons $\text{m}^{-2} \text{s}^{-1}$, 800 ms) to determine the maximal fluorescence yield (F_m) and the ratio (F_m/F_0)

$F_m = F_v/F_m$. The exposure time of the actinic red light ($166 \mu\text{mol photons m}^{-2} \text{s}^{-1}$) was 10 min for driving electron transport. Afterwards, a second pulse was applied to measure the maximum fluorescence yield under illumination and the steady-state fluorescence. Values for the effective PSII (Φ_{PSII}) and non-photochemical (Φ_{NO} and Φ_{NPO}) quantum yields were calculated according to Genty, Briantais & Baker (1989) and Kramer *et al.* (2004). For each genotype, 5–6 individual plants were measured in independent experiments.

Immunoblotting of APS1

The trichloroacetic acid (TCA) extraction of frozen pulverized leaf material and the immunoblotting procedure for visualization of APS1 monomerization was done as described by Hendriks *et al.* (2003). Signal intensities were analysed by the free software ImageJ version 1.45d (<http://rsbweb.nih.gov/ij/>).

Starch and sucrose measurements

The determination of starch and sucrose was done according to Hendriks *et al.* (2003). Twenty milligrams of pulverized leaf material was extracted three times with $250 \mu\text{L}$ ethanol (twice with 80% EtOH, once with 50% EtOH). After the addition of the first $250 \mu\text{L}$ ethanol, the samples were heated for 30 min at 90°C . The supernatants were collected in separate tubes, and the next extraction volume was added to the pellets for repeating the procedure. The combined supernatants of the ethanol extracts were used for the enzymatic sucrose determination described by Jones, Outlaw & Lowry (1977). $30\text{--}50 \mu\text{L}$ sample was mixed with $200 \mu\text{L}$ 50 mM HEPES/KOH (pH 7), 5 mM MgCl_2 , 0.8 mM NADP, 1.7 mM ATP and G6PDH (0.7 U mL^{-1}). While the stepwise addition of $2 \mu\text{L}$ hexokinase (HK) (250 U mL^{-1}), $2 \mu\text{L}$ PGI (580 U mL^{-1}) and $4 \mu\text{L}$ Invertase ($33\text{--}280 \text{ U mL}^{-1}$) the NADPH production was determined photometrically at 340 nm. For starch determination, the pellets of the ethanol extraction were dried at 30°C for 40 min with a vacuum concentrator (Concentrator Plus, Eppendorf AG, Hamburg, Germany), resuspended in $400 \mu\text{L}$ 0.1 M NaOH, incubated at 95°C with 1400 rpm shaking for 1 h (Thermomixer comfort, Eppendorf AG) and neutralized with a HCl/sodium-acetate mixture (0.5 M HCl + 0.1 M acetate/NaOH, pH 4.9). $40 \mu\text{L}$ of the supernatant was digested overnight at 37°C with $110 \mu\text{L}$ amyloglucosidase (3 U mL^{-1}), α -amylase (4 U mL^{-1}) and 50 mM acetate/NaOH (pH 4.9). $30\text{--}50 \mu\text{L}$ of the digested supernatant was mixed with $160 \mu\text{L}$ 0.1 M HEPES/3 mM MgCl_2 (pH 7), 3 mM ATP, 1.4 mM NADP and G6PDH (3.4 U mL^{-1}). To assess the glucose content photometrically, $1 \mu\text{L}$ HK (450 U mL^{-1}) was added. The determination of NADPH at 340 nm was done with the Anthos reader HT-3 (Anthos Mikrosysteme GmbH, Krefeld, Germany). Every individual plant sample was measured with at least two analytical replicates.

Measurement of hexose-phosphates, triose-phosphates and 3-PGA

The extraction of harvested leaves and the measurement of hexose-phosphates, triose-phosphates and 3-PGA were done as described by Häusler, Fischer & Flügge (2000) with following modifications. Fifty milligrams of frozen pulverized leaf material was extracted with 0.7 mL 1 M ice-cooled perchloric acid and incubated on ice for 15 min. The pH of the supernatant was modified to 6–7 with 5 M K_2CO_3 , and after removal of the precipitated KClO_4 , 8–10 mg activated charcoal was added. The levels of hexose-phosphates and triose-phosphates were measured enzymatically (reactions of NAD(P)H formation) via NAD(P)H fluorescence using the Safire² microplate reader (Tecan GmbH, Crailsheim, Germany) and the Magellan software version 6.2 (Tecan GmbH). The 3-PGA levels were also measured enzymatically, but in the absorption measuring mode at 340 nm using the Anthos reader HT-3 (Anthos Mikrosysteme GmbH). Every individual plant sample was measured with at least two analytical replicates.

GC–MS analysis of polar primary compounds

For each genotype, 50 mg of frozen pulverized plant material, harvested at the end of day (8 h light), was extracted with $360 \mu\text{L}$ of pre-cooled (-20°C) methanol (containing $50 \mu\text{g mL}^{-1}$ ribitol, Sigma, St Louis, MO, USA), $200 \mu\text{L}$ CHCl_3 and $400 \mu\text{L}$ H_2O . All solvents used for extraction and the GC–MS system were of MS quality (Carl Roth GmbH, Karlsruhe, Germany). Essentially, the preparation of the polar fraction was performed as described previously by Erban *et al.* (2007). For methoxyamination $10 \mu\text{L}$ of methoxyamine hydrochloride (dissolved at 20 mg mL^{-1} in pyridine, Sigma) was added to a dried $20 \mu\text{L}$ aliquot of the hydrophilic fraction and agitated for 90 min at 40°C . Subsequently, the persilylation mixture containing $15 \mu\text{L}$ BSTFA (Supelco) and $5 \mu\text{L}$ retention index standard [n-alkanes (Sigma): $0.5 \mu\text{g mL}^{-1}$ C10; $0.5 \mu\text{g mL}^{-1}$ C12; $1.0 \mu\text{g mL}^{-1}$ C15; $1.5 \mu\text{g mL}^{-1}$ C19; $1.5 \mu\text{g mL}^{-1}$ C22; 1.2 g mL^{-1} C28; $4.0 \mu\text{g mL}^{-1}$ C32] was included in the derivatization process followed by an additional 45 min agitation interval at the previous temperature. The instrumental gas chromatography time-of-flight mass spectrometry (GC–TOF–MS) profiling analysis was basically performed as reported in the literature (Erban *et al.* 2007) using a VF-5 ms column (30×0.25 (0.25) + 10 m guard column, Agilent Technologies, Palo Alto, CA, USA) and a lower final oven temperature (320°C) due to column specifications. The analysing GC–MS system (Pegasus HT, Leco Instrumente, Mönchengladbach, Germany; 7890A, Agilent Technologies) was equipped with a multipurpose sampler (MPS, Gerstel, Linthicum, MD, USA) and a cooled GC inlet (starting temperature 68°C , ramp rate 12°C s^{-1} , end temperature 275°C ; Cis4, Gerstel). A sample volume of $1 \mu\text{L}$ was injected in split less mode. Automated data pre-processing and annotation of peak identity was carried out by using the TagFinder, including the spectra and retention

time index collection of the Golm Metabolome Database (Luedemann *et al.* 2008; Hummel *et al.* 2010) as well as the vendor software (ChromaTOF, Leco Instrumente). The process was manually supervised. The baseline correction was 0.5 and spectra conversion and threshold signal to noise was set to 50. Quantitative analysis of cluster intensities was automatically performed using the ProfileBuilder algorithm implemented in the TagFinder. Tag intensities were normalized to the maximum sample value and averaged over the whole cluster. For the internal standardization of variations, peak heights of mass (m/z) fragments were normalized using the amount of ribitol as internal standard. Values of genotypes were averaged (three biological replicates with three analytical replicates for each individual plant material) to calculate fold changes (mutant to WT).

Light incubation of isolated chloroplasts

Chloroplasts from *Arabidopsis* leaves were purified and incubated as described by Seigneurin-Berny *et al.* (2008) with following modifications. Ten-gram leaves of pooled rosettes, harvested after an extended night of 20 h, were homogenized by three bursts of 2–3 s each at high speed (Waring blender, Snijders Scientific, Tilburg, the Netherlands) in 100 mL of cold homogenization buffer [0.4 M sorbitol, 20 mM tricine/KOH pH 8.4, 10 mM ethylenediaminetetraacetic acid (EDTA) pH 8.0, 10 mM NaHCO₃, 0.15% bovine serum albumin]. The homogenate was rapidly filtered through two layers of miracloth and centrifuged for 6 min at 500 g (Eppendorf Centrifuge 5810R). To the pellet 0.4 mL 1x resuspension buffer (0.4 M sorbitol, 20 mM HEPES/KOH pH 7.6, 2.5 mM EDTA, 5 mM MgCl₂, 10 mM NaHCO₃, 0.15% bovine serum albumin) was added. Percoll gradients with resuspended crude chloroplasts were centrifuged at 3200 g for 20 min with diminished acceleration and the brake off. Percoll gradients were performed by mixing different volumes of cold Percoll (Sigma-Aldrich) and cold 5x resuspension buffer followed by depositing one layer (80% Percoll) below the other (40% Percoll). Diluted intact chloroplasts were centrifuged for 2 min at 3200 g including deceleration and afterwards solubilized in 1 mL reaction medium (0.4 M sorbitol, 20 mM HEPES/KOH pH 7.6, 2.5 mM EDTA, 0.5 mM MgCl₂, 10 mM NaHCO₃, 0.15% bovine serum albumin, 300 U mL⁻¹ catalase, 100 μM KH₂PO₄, 500 μM PGA). Chloroplasts of both genotypes were illuminated in parallel at 18 °C for 0, 1, 3 and 5 min using the beam of a slide projector. Intactness of chloroplasts, chlorophyll content and APS1 monomerization was determined as previously described by Hendriks *et al.* (2003). Signal intensities of the APS1 immunodetection were analysed by the free software ImageJ version 1.45d. Every replicate of both genotypes represents one independent illumination experiment from different plant set ups.

Sucrose feeding of leaves in the dark

Leaves sampled at the end of the night were put directly into liquid nitrogen (t_0) or infiltrated with 100 mM sucrose

or sorbitol in 2 mM 2-(N-morpholino) ethane sulfonic acid (MES) buffer (pH 6.5) by applying a vacuum of –200 mbar for 1 min and subsequent incubation in the same solution for further 5 h in the dark at room temperature and with moderate shaking. After the incubation, the leaves were shortly dried with a tissue and then quickly frozen with liquid nitrogen. Every replicate for the t_0 , sorbitol or sucrose samples included three fully expanded leaves of three independent plant individuals. The APS1 immunodetection and quantification was done as described above.

Statistical analysis

The statistical data analyses were done with Microsoft Office Excel 2007 (*t*-test) and SYSTAT SigmaPlot 11 [two-way analysis of variance (ANOVA), Tukey test].

RESULTS

Trx f1 has a higher efficiency to monomerize the small subunit of AGPase compared to Trxs m1, x and y1 *in vitro*

Thioredoxins comprise a small gene family in plants (Lemaire *et al.* 2007). To investigate the efficiency of different plastidial Trxs to redox-activate AGPase, 10 μM of purified recombinant Trxs f1, m1, x and y1 from *Arabidopsis* were incubated for different time intervals with purified recombinant AGPase small subunit (APS1) in the presence of 0.5 mM DTT. Redox activation of APS1 was monitored in non-reducing sodium dodecyl sulphate (SDS) gels, where the oxidized less-active form of APS1 migrates as a 100 kDa dimer that, upon reduction, gets activated and converted to a 50 kDa monomer. Figure 1a shows that the purified Trxs converted APS1 from dimer to monomer with different efficiencies. Trx f1 showed the highest efficiency, with 50% monomerization of APS1 being achieved after ($t_{0.5}$) 7 min of incubation, followed by Trx m1 with a $t_{0.5}$ value of 9 min. In comparison, Trxs x and y1 were rather inefficient, yielding only 22 and 30% monomerization of APS1 after 30 min, respectively. In control incubations containing 0.5 mM DTT without Trxs, APS1 remained a dimer. In the same experiment, purified recombinant NTRC (10 μM) was incubated with APS1 in the presence of 300 μM NADPH, for comparison. The $t_{0.5}$ value obtained for NTRC (8 min) was similar to Trx f1 (Fig. 1b).

Arabidopsis knockout mutants defective in Trx f1 show a strong decrease in Trx f protein levels in leaves, with no effect on photosynthetic parameters and growth

The *in vitro* results described above suggest Trx f1 to be the most efficient Trx isoform in activating AGPase. To test its functional significance *in vivo*, we characterized the metabolic phenotype of two *Arabidopsis* *trx f1* T-DNA Insertion lines (*trx f1.1*, SALK_128365 and *trx f1.2*, SALK_063799; see Fig. 2a) in comparison with their isogenic respective

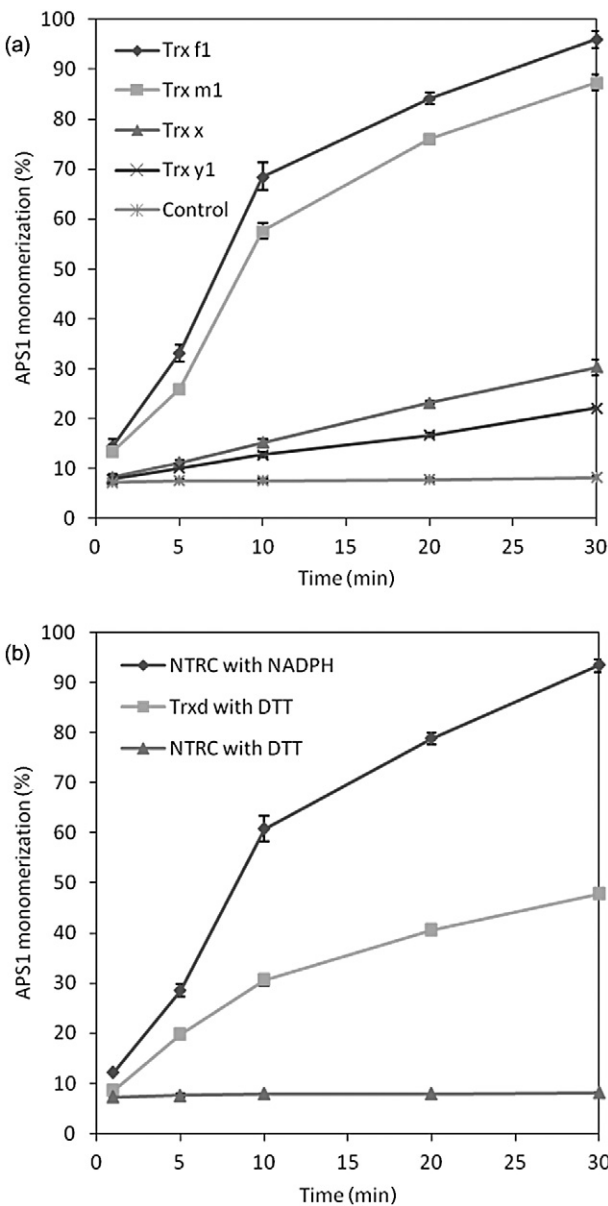


Figure 1. Efficiencies of different thioredoxin (Trx) isoforms (a) and NADP-thioredoxin reductase c (NTRC) (b) to reduce APS1 *in vitro*. 10 μ M recombinant purified Trxs f1, m1, x or y1 or NTRC proteins were incubated together with 10 μ M APS1 protein for different time intervals, before reduction of APS1 was determined as percent monomerization in non-reducing sodium dodecyl sulphate (SDS) gels. Incubation with Trxs was performed in assays including 0.5 mM DTT, while in incubations with NTRC, DTT was replaced by 300 μ M NADPH. In control incubations, 0.5 mM DTT was included without Trx. Results are means \pm SE, $n = 3$. Trxd, Trx domain of NTRC.

wild types (WT.1 and WT.2) segregated from their parent heterozygous plants. In both lines, mRNA expression levels of Trx f1 were strongly decreased to detection limit (Fig. 2b), while the levels of the other plastidial Trxs, including Trx f2, were not significantly altered (data not shown). Trx f protein levels were analysed by Western blots and were found to be drastically decreased down to

approximately 4% of wild-type level in both mutant lines (after scanning and correction for background), indicating that in *Arabidopsis* leaves Trx f1 protein corresponds to the major form (approximately 96%) of f-type Trx (Fig. 2c).

Despite the strong decrease in Trx f protein level, in optimal growth conditions, there was no visible effect on the phenotype of the *trx f1.1* and *trx f1.2* mutant lines (data not shown). To investigate a possible effect on photosynthetic parameters, chlorophyll fluorescence was measured by pulse-amplitude modulation (PAM) fluorimetry in leaves of the two knockout lines, compared to wild type (Fig. 3a,b). As revealed by light dependencies of photosynthesis, there were no changes in maximal (F_v/F_m) and effective quantum yield of PS II (Φ_{PSII}), indicating that the lack of Trx f1 affected neither PS II functionality nor photosynthetic electron transport rates. In addition, quantum yields of regulated (Φ_{NPQ}) and non-regulated (Φ_{NO}) energy dissipation remained unaltered by the mutation. This shows that

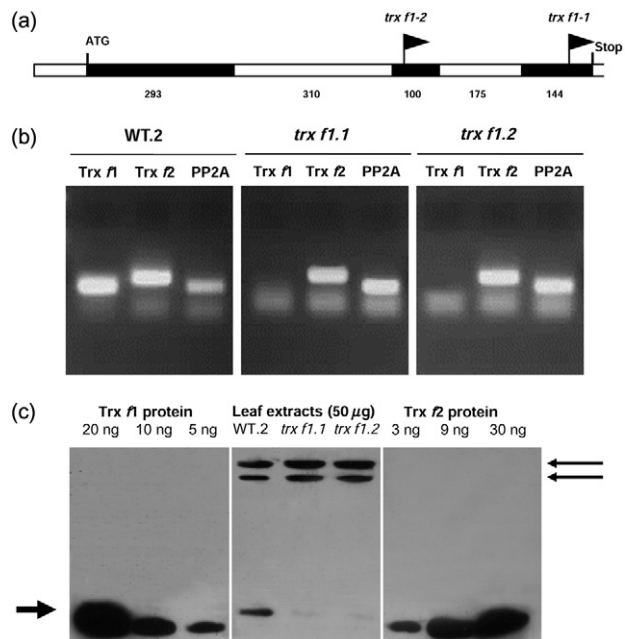


Figure 2. Molecular characterization of the Trx f1 knockout lines. (a) Schematic representation of the *trx f1* locus. The intron-exon structure of the *trx f1* gene and sizes (in base pairs) are shown. T-DNA insertion site in *trx f1.1* and *trx f1.2* mutants is positioned by a flag. (b) Comparison of Trx f transcripts in *trx f1.1* and *trx f1.2* mutants and isogenic wild-type WT.2 plants. Transcript levels of Trx f1, Trx f2 and PP2A (constitutively expressed gene) were analysed by semi-quantitative PCR. (c) Detection of Trx f proteins in isogenic wild-type and in mutant plants. Western blot analysis of leaf proteins along with varying amounts of *Arabidopsis* Trx f1 and Trx f2 purified proteins was made using antibodies raised against pea Trx f (Hodges *et al.* 1994). High-molecular weight non-specific signals (thin arrows on the right side) always observed when using these antibodies on *Arabidopsis* leaf extracts allowed verification of a constant protein loading between lanes. The signal corresponding to *Arabidopsis* Trx f protein(s) is indicated on the left by a thick arrow.

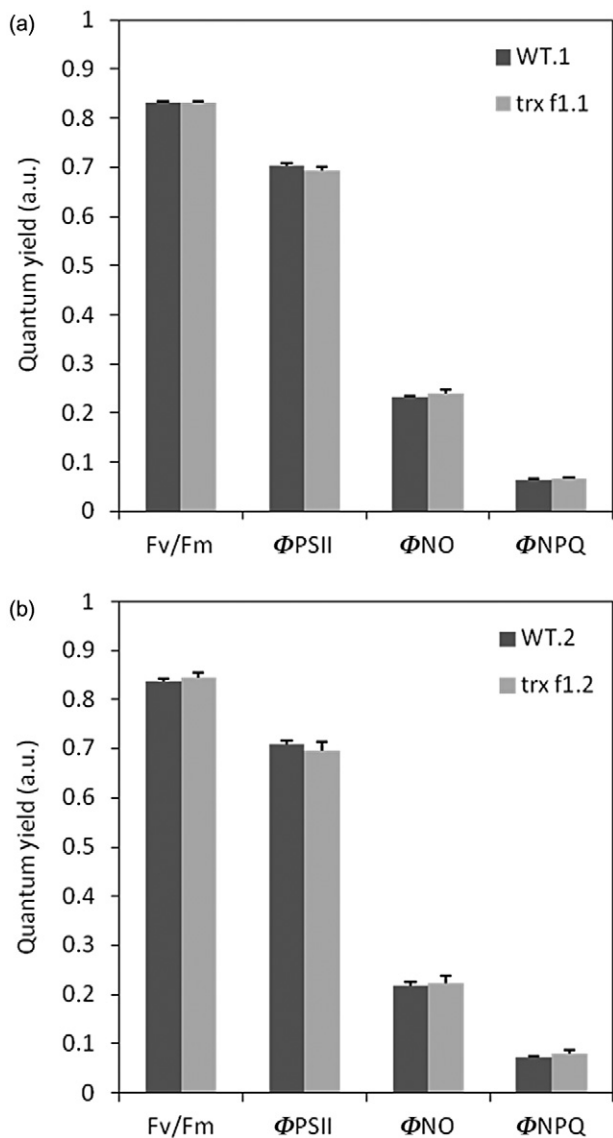


Figure 3. PAM measurements in *Arabidopsis* leaves of the Trx f1 knockout lines *trx f1.1* (a) and *trx f1.2* (b) compared to the respective wild types. The plants were dark adapted for 10 min, before exposure to a red-light saturation pulse ($5000 \mu\text{mol m}^{-2} \text{s}^{-1}$ for 0.8 s) of single leaves. Afterwards the maximal chlorophyll a fluorescence was quenched by electron transport with an actinic red light of $166 \mu\text{mol photons m}^{-2} \text{s}^{-1}$. Within 10 min, the steady state was reached and another saturation pulse was given. In the end, the maximal PSII (F_v/F_m), the effective PSII (Φ_{PSII}), the non-regulated energy dissipation (Φ_{NO}) and the regulated energy dissipation (Φ_{NPQ}) quantum yields were calculated. Results are means \pm SE, $n = 15$ for line *trx f1.1* and $n = 6$ for line *trx f1.2*.

knocking out Trx f1 did not affect photosynthetic parameters.

Knockout of Trx f1 leads to decreased redox activation of AGPase in leaves during the day

To investigate the physiological relevance of the redox activation of AGPase by Trx f1 demonstrated *in vitro*, leaves of

trx f1.1 (Fig. 4a) and *trx f1.2* (Fig. 4b) mutant lines and their segregating wild types were sampled at different time points during the diurnal cycle to analyse the reduction state of the regulatory small subunit dimer of the enzyme by non-reducing sodium dodecyl sulphate–polyacrylamide gel electrophoresis (SDS–PAGE). As shown in Fig. 4, leaves of wild-type plants reveal a strong increase in the monomerization of APS1 during the day, while APS1 was almost completely dimerized in the dark, confirming results from earlier studies (see Hendriks *et al.* 2003). Compared to the segregating wild types, both Trx f1 knockout lines showed a similar dimerization degree of APS1 in the dark, while the conversion of APS1 dimer to monomer in response to light was clearly delayed and reached only about 50% of wild-type APS1 monomerization at the end of the day (Fig. 4; Supporting Information Table S1).

Knockout of Trx f1 leads to a decrease in the starch-to-sucrose ratio in leaves during the day

The above results demonstrate that knockout of Trx f1 dampens diurnal changes in redox activation of AGPase in leaves. To investigate whether this leads to changes in starch metabolism, we analysed diurnal changes in leaf starch and sucrose content. In the wild type, starch levels increased towards the middle and the end of the day by a factor of 3–10 (Fig. 5a,d), while sucrose increased already after 1 h in the light (1.5–2-fold) and stayed at a high and constant level until the end of the day (Fig. 5b,e). Compared to wild type, both Trx f1 knockout lines (*trx f1.1* and *trx f1.2*) showed a significant decrease in starch accumulation by up to 22%

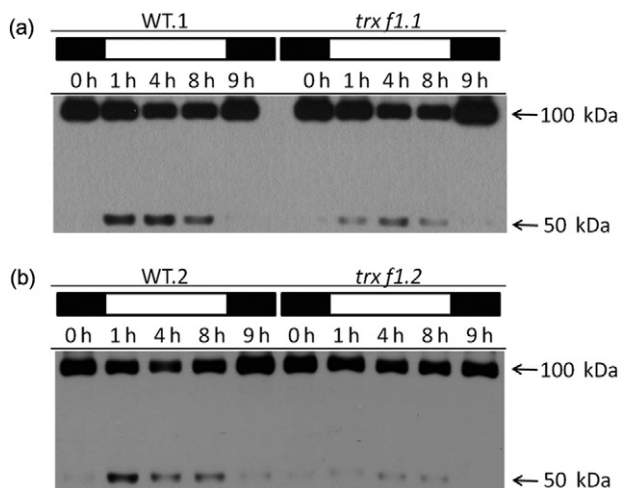


Figure 4. Diurnal changes in APS1 monomerization in *Arabidopsis* leaves of the Trx f1 knockout lines *trx f1.1* (a) and *trx f1.2* (b) compared to the respective wild types. Leaf samples were taken at different time points during the diurnal cycle, extracted with 16% TCA in diethylether, separated on a non-reducing 10% sodium dodecyl sulphate–polyacrylamide gel electrophoresis (SDS–PAGE) gel and then immuno-decorated by specific APS1 antibodies. The horizontal bars represent the dark (black) and light (white) periods at given time points.

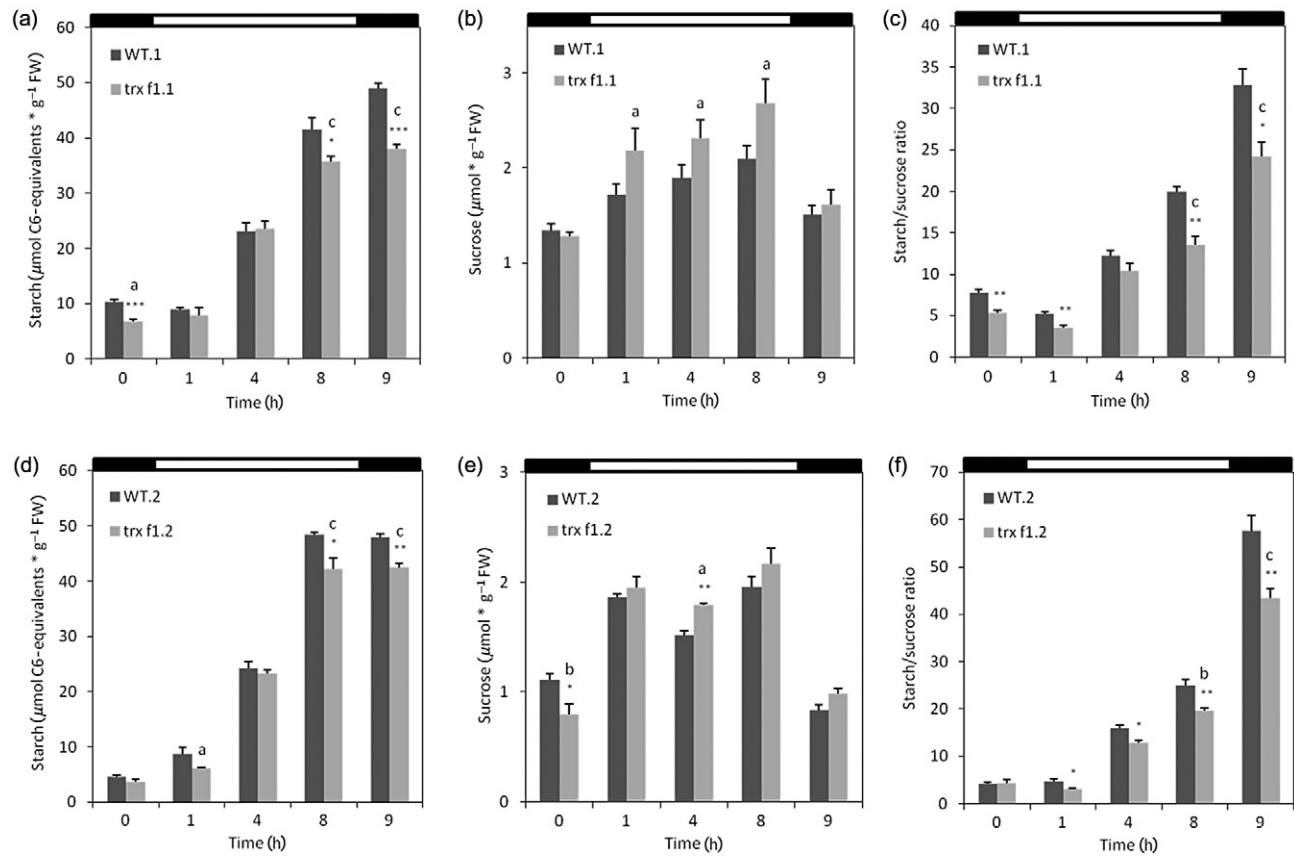


Figure 5. Diurnal changes of starch (a and e), sucrose (b and e) and starch/sucrose ratio (c and f) in *Arabidopsis* leaves of Trx f1 knockout lines *trx f1.1* (a-c) and *trx f1.2* (e-f) compared to the respective wild types. Leaf samples were taken at different time points during the diurnal cycle and extracted to measure the levels of sucrose and starch. Results are means \pm SE, $n = 4$. * $P \leq 0.05$, ** $P \leq 0.01$, *** $P \leq 0.001$ (student *t*-test); a: $P \leq 0.05$, b: $P \leq 0.01$, c: $P \leq 0.001$ [two-way analysis of variance (ANOVA), Tukey test]. The horizontal bars represent the dark (black) and light (white) periods at given time points.

towards the end of the day, while there were significant decreases in only one of the two mutant lines at the end of the night and 1 h into the light period (Fig. 5a,d). In contrast to this, sucrose levels increased up to 22% throughout the day, which was significant for all time points in the light in *trx f1.1* (using the two-way ANOVA test) and only for the 4 h light time point in the *trx f1.2* mutant (using, both, *t*-test and two-way ANOVA test; Fig. 5b,e). During the diurnal time course, the starch/sucrose ratio decreased in both Trx knockout lines by a factor of up to 1.7, compared to their respective isogenic wild type (Fig. 5c,f, significant for all time points, except 4 h light in *trx f1.1* and end of night in *trx f1.2*). This shows that knockout of Trx f1 alters the ratio between sucrose and starch in favour of sucrose.

Effect of Trx f1 knockout on leaf metabolite levels

To investigate whether knockout of Trx f1 leads to changes in metabolite levels involved in the pathways of sucrose and starch metabolism, levels of hexose-phosphates and triose-phosphates were analysed in both mutant lines compared to isogenic wild types (Table 1). In leaves sampled at the end

of the day, Trx f1 knockout did not affect the levels of hexose-phosphates, while triose-phosphates such as glyceraldehyde phosphate and dihydroxyacetone phosphate (DHAP) were slightly increased, indicating that the inhibition of starch synthesis is unlikely due to a shortage of substrates. This contrasts with the situation at the end of the night, where Trx f1 knockout led to a decrease in hexose-phosphate and triose-phosphate levels, indicative of a shortage of nocturnal carbon supply by starch degradation (significant for fructose-6-phosphate and DHAP in *trx f1.1*). We also analysed the level of 3-PGA, which is an exquisite allosteric effector of AGPase (Preiss 1988). There were no changes in 3-PGA levels between wild type and mutants, indicating that inhibition of AGPase is unlikely due to changes in the levels of its allosteric effectors (see also below).

Metabolite profiling by GC-TOF MS was employed to investigate whether there are more global effects of a lack of Trx f1 on metabolism. Table 2 shows changes in leaf metabolite levels at the end of the day in both mutant lines relative to the wild type. Only eight metabolites were pinpointed to be significantly different from the wild type in both mutant lines: fructose, ribose, trehalose and shikimate

Table 1. Diurnal changes in hexose-phosphates (Glc6P, Fru6P and Glc1P), triose-phosphates (GAP, DHAP) and 3-phosphoglycerate (3-PGA) levels in *Arabidopsis* leaves of both *Trx f1* knockout lines (*trx f1.1* and *trx f1.2*) compared to the respective wild types. Leaf samples were taken at the end of the night and at the end of the day (8 h light) and extracted with perchloric acid to measure metabolite levels using enzymatic test systems. Results are given in nmol per gFW and means \pm SE ($n = 4$). Values that are significantly different from the wild type according to the student *t*-test are indicated in bold (P value ≤ 0.05)

Metabolites	End of night				End of day			
	WT1	<i>trx f1.1</i>	WT2	<i>trx f1.2</i>	WT1	<i>trx f1.1</i>	WT2	<i>trx f1.2</i>
Glucose 6-phosphate	165.7 \pm 19.2	143.1 \pm 20.1	223.9 \pm 22.1	206.0 \pm 19.8	194.0 \pm 27.4	173.1 \pm 23.6	243.1 \pm 21.6	250.8 \pm 18.5
Fructose 6-phosphate	71.7 \pm 1.4	60.1 \pm 3.8	46.7 \pm 8.9	35.4 \pm 10.9	145.2 \pm 5.2	161.3 \pm 8.7	118.3 \pm 6.7	109.3 \pm 8.0
Glucose 1-phosphate	27.2 \pm 9.6	31.0 \pm 7.1	29.3 \pm 2.8	15.3 \pm 3.6	27.8 \pm 3.3	28.4 \pm 5.7	23.6 \pm 2.2	25.0 \pm 0.5
Glyceraldehyde 3-phosphate	1.7 \pm 0.04	1.7 \pm 0.3	1.6 \pm 0.1	1.2 \pm 0.2	6.8 \pm 0.6	9.2 \pm 0.9	7.8 \pm 0.4	9.5 \pm 0.7
Dihydroxyacetone phosphate	44.7 \pm 1.7	33.5 \pm 2.6	46.7 \pm 5.0	37.0 \pm 1.7	71.5 \pm 3.9	70.8 \pm 1.9	59.8 \pm 2.3	68.9 \pm 4.5
3-Phosphoglyceric acid	179.8 \pm 35.2	202.4 \pm 16.4	265.4 \pm 8.4	253.3 \pm 5.8	400.0 \pm 18.9	394.8 \pm 20.8	379.0 \pm 10.1	361.2 \pm 35.5

were found to be increased, while citrate, 2-methyl-malate, glycerate and ethanolamine were decreased. The following metabolites also showed changes relative to the wild type, but were significantly different only in one of the two mutant lines. Glucose, galactose, rhamnose, xylose, phosphoenolpyruvate, threonate, trans-3-caffeo-yl-quinate, 2-oxo-gulonate, 4-aminobutanoate, asparagine, isoleucine and proline were increased, while 2-oxo-glutarate, fumarate, malate, succinate and maltitol were decreased.

Knockout of *Trx f1* inhibits light activation of AGPase in isolated chloroplasts, while having no effect on sucrose-induced redox activation of AGPase in leaves in the dark

Earlier studies showed that AGPase can be redox activated by both light and sucrose-dependent signals (Hendriks *et al.* 2003; Kolbe *et al.* 2005). To investigate whether *Trx f1* is involved in light-dependent reduction of AGPase, we analysed the responses in isolated chloroplasts that were transiently illuminated for 1, 3 and 5 min. In the wild type, monomerization of APS1 was low in the dark and increased significantly by up to sixfold after 3 and 5 min of illumination (Fig. 6a), confirming earlier studies (Hendriks *et al.* 2003). This effect was strongly attenuated in the *Trx f1* knockout line, reaching only a slight and non-significant increase in APS1 monomerization after 5 min of illumination (Fig. 6a), indicating a major role played by *Trx f1* in the light activation of AGPase.

To investigate whether *Trx f1* is involved in sucrose-dependent redox activation of AGPase, mutant and wild-type leaves were harvested at the end of the night and infiltrated either with 100 mM sucrose or sorbitol as control in the dark. In confirmation to earlier studies, sucrose supply led to a significant sevenfold increase in the monomerization of APS1 in the wild type (Fig. 6b; Supporting Information Fig. S1). A similar increase was observed in the mutant, indicating that *Trx f1* plays no substantial role in the nocturnal reduction of AGPase in response to sugars.

DISCUSSION

Starch is the major storage carbohydrate in higher plants. It has been identified as an important integrator in the regulation of plant growth to cope with continual changes in carbon availability in response to environmental alterations in light, day length, temperature, water supply and CO₂ concentrations affecting photosynthesis (Sulpice *et al.* 2009). In photosynthesizing leaves, starch accumulates during the day and is remobilized at night to support continued sucrose export and growth in the dark (Caspar, Huber & Somerville 1986; Geiger & Servaites 1994; Weise, van Wijk & Sharkey 2011). This requires a tight regulation of the pathways of starch synthesis and degradation in response to light as environmental and sucrose as internal stimuli (Kötting *et al.* 2010; Geigenberger 2011). In this

Table 2. Changes in *Arabidopsis* leaf metabolite levels at the end of the day (8 h light) in both Trx f1 knockout lines (*trx f1.1* and *trx f1.2*) relative to the respective wild types. Metabolite profiling was performed using GC-TOF-MS analysis. Results are means \pm SD ($n = 9$). Values that are significantly different from the wild type according to the student *t*-test are indicated in bold (*P* value ≤ 0.05)

Metabolites	WT.1	<i>trx f1.1</i>	<i>P</i> value	WT.2	<i>trx f1.2</i>	<i>P</i> value
Sugars						
Fructose	1.00 \pm 0.16	2.11 \pm 0.93	0.007	1.00 \pm 0.24	2.10 \pm 0.74	0.001
Fucose	1.00 \pm 0.14	1.03 \pm 0.16	0.709	1.00 \pm 0.31	1.07 \pm 0.34	0.654
Galactose	1.00 \pm 0.08	1.16 \pm 0.20	0.047	1.00 \pm 0.09	1.02 \pm 0.14	0.712
Glucose	1.00 \pm 0.09	1.58 \pm 0.68	0.033	1.00 \pm 0.18	0.91 \pm 0.16	0.285
Isomaltose	1.00 \pm 0.58	0.83 \pm 0.58	0.549	1.00 \pm 0.92	0.90 \pm 0.82	0.801
Maltose	1.00 \pm 0.16	1.05 \pm 0.11	0.484	1.00 \pm 0.16	0.95 \pm 0.27	0.613
Mannose	1.00 \pm 0.18	1.17 \pm 0.30	0.149	1.00 \pm 0.16	1.14 \pm 0.15	0.077
Psicose	1.00 \pm 0.05	1.06 \pm 0.08	0.077	1.00 \pm 0.10	1.03 \pm 0.11	0.519
Raffinose	1.00 \pm 0.43	1.16 \pm 0.30	0.365	1.00 \pm 0.57	0.76 \pm 0.43	0.342
Rhamnose	1.00 \pm 0.16	1.35 \pm 0.27	0.004	1.00 \pm 0.37	1.04 \pm 0.32	0.807
Ribose	1.00 \pm 0.11	1.12 \pm 0.07	0.016	1.00 \pm 0.06	1.13 \pm 0.08	0.002
Trehalose	1.00 \pm 0.12	1.14 \pm 0.14	0.043	1.00 \pm 0.13	1.41 \pm 0.36	0.010
Xylose	1.00 \pm 0.17	1.29 \pm 0.11	<0.001	1.00 \pm 0.06	0.94 \pm 0.10	0.128
Phosphate ester						
Fructose-6-phosphate	1.00 \pm 0.28	1.21 \pm 0.44	0.246	1.00 \pm 0.91	0.99 \pm 0.96	0.978
Glucose-6-phosphate	1.00 \pm 0.30	1.08 \pm 0.42	0.659	1.00 \pm 0.72	0.96 \pm 0.86	0.913
Glycerol-3-phosphate	1.00 \pm 0.20	1.10 \pm 0.31	0.438	1.00 \pm 0.26	0.94 \pm 0.37	0.689
Phosphoenolpyruvate	1.00 \pm 0.14	1.28 \pm 0.27	0.015	1.00 \pm 0.36	1.00 \pm 0.40	0.988
Organic acids						
Aconitate	1.00 \pm 0.09	1.15 \pm 0.20	0.058	1.00 \pm 0.40	0.93 \pm 0.27	0.648
Benzoate	1.00 \pm 0.20	0.95 \pm 0.22	0.618	1.00 \pm 0.18	0.94 \pm 0.17	0.468
Caffeate (cis)	1.00 \pm 0.30	1.18 \pm 0.27	0.198	1.00 \pm 0.24	1.22 \pm 0.47	0.237
3-caffeyl-quinate (cis)	1.00 \pm 0.18	1.17 \pm 0.22	0.102	1.00 \pm 0.19	1.15 \pm 0.33	0.242
3-caffeyl-quinate (trans)	1.00 \pm 0.17	1.30 \pm 0.32	0.023	1.00 \pm 0.42	1.21 \pm 0.45	0.314
Citrate	1.00 \pm 0.11	0.77 \pm 0.14	0.002	1.00 \pm 0.18	0.53 \pm 0.19	<0.001
Fumarate	1.00 \pm 0.08	1.11 \pm 0.15	0.072	1.00 \pm 0.12	0.79 \pm 0.13	0.002
Galactonate	1.00 \pm 0.21	1.14 \pm 0.12	0.096	1.00 \pm 0.14	1.01 \pm 0.15	0.920
Glycerate	1.00 \pm 0.02	0.55 \pm 0.06	<0.001	1.00 \pm 0.13	0.73 \pm 0.12	<0.001
Gulonate	1.00 \pm 0.15	1.18 \pm 0.35	0.207	1.00 \pm 0.43	0.83 \pm 0.07	0.384
Malate	1.00 \pm 0.08	1.01 \pm 0.12	0.818	1.00 \pm 0.04	0.80 \pm 0.13	0.002
Maleate	1.00 \pm 0.30	1.01 \pm 0.34	0.946	1.00 \pm 0.56	0.84 \pm 0.51	0.537
2-methyl-malate	1.00 \pm 0.09	0.89 \pm 0.10	0.026	1.00 \pm 0.06	0.87 \pm 0.13	0.016
2-oxo-glutarate	1.00 \pm 0.24	1.09 \pm 0.30	0.516	1.00 \pm 0.14	0.73 \pm 0.15	0.001
2-oxo-gulonate	1.00 \pm 0.19	1.23 \pm 0.25	0.045	1.00 \pm 0.18	0.90 \pm 0.12	0.183
Pyruvate	1.00 \pm 0.18	0.89 \pm 0.13	0.155	1.00 \pm 0.12	0.99 \pm 0.09	0.913
Quinate	1.00 \pm 0.45	1.01 \pm 0.46	0.969	1.00 \pm 0.69	0.73 \pm 0.20	0.294
Shikimate	1.00 \pm 0.18	1.39 \pm 0.06	<0.001	1.00 \pm 0.10	1.13 \pm 0.13	0.029
Succinate	1.00 \pm 0.08	0.99 \pm 0.12	0.821	1.00 \pm 0.18	0.73 \pm 0.10	0.001
Sinapate (cis)	1.00 \pm 0.14	0.91 \pm 0.21	0.322	1.00 \pm 0.52	0.77 \pm 0.42	0.334
Sinapate (trans)	1.00 \pm 0.16	0.79 \pm 0.26	0.074	1.00 \pm 0.57	0.73 \pm 0.48	0.327
Threonate	1.00 \pm 0.05	1.13 \pm 0.13	0.021	1.00 \pm 0.30	0.91 \pm 0.17	0.436
Amino acids						
Alanine	1.00 \pm 0.32	1.05 \pm 0.20	0.706	1.00 \pm 0.41	1.12 \pm 0.33	0.522
β -alanine	1.00 \pm 0.39	1.30 \pm 0.34	0.097	1.00 \pm 0.38	1.09 \pm 0.29	0.563
Aspartate	1.00 \pm 0.87	1.22 \pm 0.57	0.535	1.00 \pm 0.57	0.63 \pm 0.28	0.101
Asparagine	1.00 \pm 0.15	1.25 \pm 0.25	0.021	1.00 \pm 0.29	0.92 \pm 0.33	0.597
Glycine	1.00 \pm 0.22	2.38 \pm 0.28	<0.001	1.00 \pm 0.13	0.81 \pm 0.16	0.014
4-hydroxy-proline (cis)	1.00 \pm 0.19	1.01 \pm 0.18	0.936	1.00 \pm 0.15	1.14 \pm 0.42	0.378
4-hydroxy-proline (trans)	1.00 \pm 0.13	1.13 \pm 0.27	0.224	1.00 \pm 0.17	0.98 \pm 0.24	0.873
Methionine	1.00 \pm 0.72	0.93 \pm 0.45	0.805	1.00 \pm 1.01	0.50 \pm 0.26	0.212
Isoleucine	1.00 \pm 0.48	1.46 \pm 0.37	0.035	1.00 \pm 0.61	1.34 \pm 0.75	0.311
Proline	1.00 \pm 0.70	2.04 \pm 0.86	0.012	1.00 \pm 0.70	0.68 \pm 0.36	0.263
Pyroglutamate	1.00 \pm 0.45	1.98 \pm 1.28	0.071	1.00 \pm 0.70	1.22 \pm 0.83	0.554
Serine	1.00 \pm 0.52	0.84 \pm 0.43	0.505	1.00 \pm 0.45	0.81 \pm 0.45	0.398
Threonine	1.00 \pm 0.45	1.48 \pm 0.85	0.157	1.00 \pm 0.53	0.80 \pm 0.44	0.418
Valine	1.00 \pm 0.32	1.28 \pm 0.26	0.055	1.00 \pm 0.49	1.19 \pm 0.41	0.404
Sugar alcohols						
Erythritol	1.00 \pm 0.25	0.90 \pm 0.24	0.397	1.00 \pm 0.28	0.89 \pm 0.24	0.391
Glycerol	1.00 \pm 0.06	0.88 \pm 0.19	0.118	1.00 \pm 0.11	0.92 \pm 0.13	0.207
Mannitol	1.00 \pm 0.23	1.05 \pm 0.38	0.757	1.00 \pm 0.20	0.91 \pm 0.28	0.516
Maltitol	1.00 \pm 0.50	0.98 \pm 0.62	0.945	1.00 \pm 0.50	0.50 \pm 0.23	0.021
Sorbitol	1.00 \pm 0.18	1.12 \pm 0.29	0.341	1.00 \pm 0.22	1.26 \pm 0.35	0.128
Others						
4-amino-butanoate	1.00 \pm 0.10	1.30 \pm 0.19	0.001	1.00 \pm 0.15	0.88 \pm 0.22	0.215
Ascorbate	1.00 \pm 0.62	2.54 \pm 1.98	0.051	1.00 \pm 1.08	0.42 \pm 0.12	0.146
Dehydroascorbate	1.00 \pm 0.47	1.01 \pm 0.49	0.962	1.00 \pm 0.76	0.69 \pm 0.20	0.271
Ethanolamine	1.00 \pm 0.65	0.38 \pm 0.09	0.020	1.00 \pm 0.52	0.38 \pm 0.09	0.007
Phosphate	1.00 \pm 0.20	1.01 \pm 0.20	0.943	1.00 \pm 0.27	0.91 \pm 0.23	0.459
Putrescine	1.00 \pm 0.82	1.06 \pm 1.05	0.889	1.00 \pm 0.78	1.01 \pm 0.72	0.977

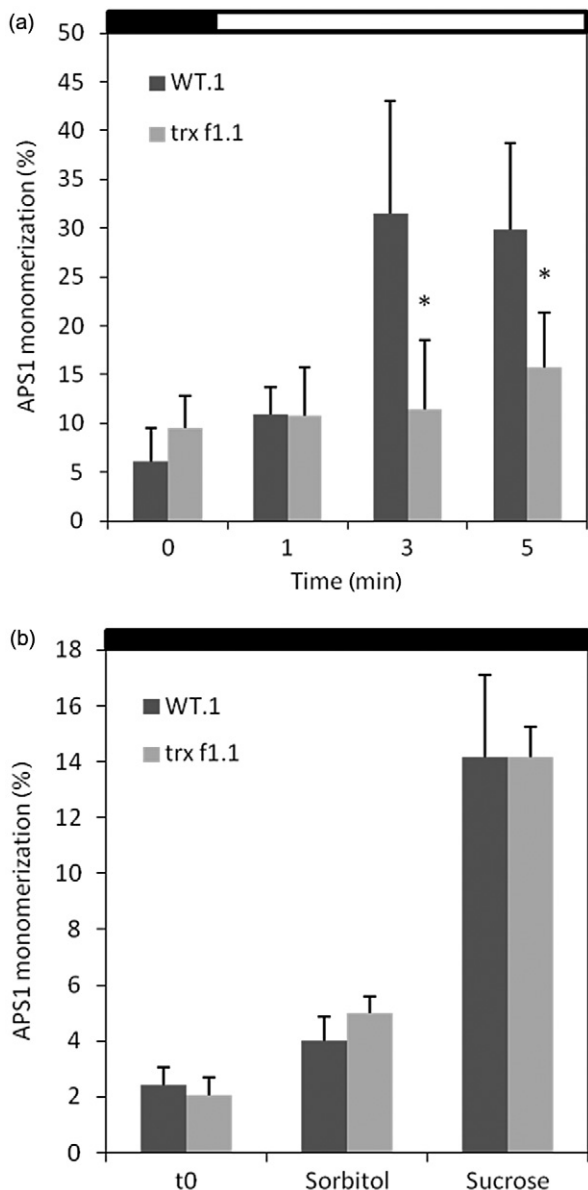


Figure 6. Effect of Trx f1 knockout (line *trx f1.1*) on (a) light-dependent redox activation of ADP-glucose pyrophosphorylase (AGPase) in isolated chloroplasts, and (b) sucrose-dependent redox activation of AGPase in leaves in the dark. The conversion of the 100 kDa to the 50 kDa form of APS1 was analysed using Western blots, which were scanned and the intensity of the protein bands corrected for background. (a) Isolated chloroplasts of *Arabidopsis* leaves were light incubated for 0, 1, 3 and 5 min. Results are means \pm SE, $n = 4$ –6 separate experiments with different batches of plants. * $P \leq 0.05$ (paired *t*-test). Chloroplasts were prepared from leaves harvested at the end of the night and were kept in the dark during the preparation procedure. The chloroplast preparations from wild type and mutant plants were illuminated simultaneously in parallel incubations. (b) For the sucrose-dependent effect on APS1 monomerization, *Arabidopsis* leaves were harvested at the end of night (t_0), and incubated with sucrose or sorbitol (100 mM) for 5 h in the dark. Results are means \pm SE, $n = 4$ separate experiments. The horizontal bars represent dark (black) and light (white) periods at given time points.

work, the role of Trx f in redox activation of the key enzyme of starch synthesis, AGPase, was analysed using biochemical and genetic approaches. Results provide *in vivo* evidence for the role played by Trx f to redox activate AGPase and diurnal starch synthesis in leaves in response to light, but not to sucrose signals.

Genetic evidence for a role of Trx f as light signal but not as a sucrose signal leading to redox activation of AGPase

Chloroplasts contain different Trx isoforms as well as NTRC as an alternate redox system conjugating Trx and NTR on the same polypeptide (Dietz & Pfannschmidt 2011). Using recombinant purified proteins, we could show that Trx f1 is redox activating AGPase more efficiently than other plastidial Trxs, such as Trx m1, x and y1 (Fig. 1a). The time to achieve 50% reduction of APS1 ($t_{0.5}$) was 7 min for Trx f1 and 9 min for Trx m1, indicating that Trx m1 is less efficient than Trx f1. This confirms previous studies, showing that Trx m has a twofold lower affinity for AGPase than Trx f (Ballicora *et al.* 2000). Trxs x and y1 were much less efficient than Trx f1 and m1, leading only to a 22–30% reduction of APS1 after 30 min. It is therefore highly unlikely that Trxs x and y will play a substantial physiological role in the reduction of AGPase. This confirms previous studies indicating that these types of Trxs serve as reducing substrates for antioxidant enzymes, rather than enzymes involved in primary metabolism (Collin *et al.* 2003, 2004). The $t_{0.5}$ values also show that Trx f1 is of similar efficiency as NTRC as a redox regulator for AGPase (compare Fig. 1a,b). This confirms previous studies showing that Trx f (4.6 μ M) and NTRC (2.8 μ M) have similar $S_{0.5}$ values to achieve half-maximal reduction of AGPase as a substrate (Ballicora *et al.* 2000; Michalska *et al.* 2009).

To test the functional significance of Trx f1 as a redox regulator of AGPase *in vivo*, Trx f1 knockout *Arabidopsis* plants were analysed showing a strong decrease in Trx f protein levels (Fig. 2). AGPase has previously been reported to be activated in response to light and sucrose in *Arabidopsis* leaves (Hendriks *et al.* 2003). In the present study, Trx f1 knockout led to a strong attenuation of the light activation of AGPase, both, in isolated chloroplasts (Fig. 6a) and intact leaves (Fig. 4). In the latter case, light activation of AGPase was inhibited even in the presence of elevated internal sugar levels (Fig. 5; Table 2). This shows that Trx f1 plays an important role as a light signal, providing reducing equivalents for light-dependent activation of AGPase in leaves independently of sucrose. In confirmation to this, Trx f1 knockout did not affect sucrose-dependent redox activation of AGPase in leaves in the dark, showing that this type of Trx is unlikely to be involved in the nocturnal activation of AGPase by sugars (Fig. 6b; Supporting Information Fig. S1). Under these conditions, redox is transferred to AGPase independently of the Fdx/Trx system via NTRC by using metabolically derived NADPH most likely from the oxidative pentose phosphate pathway (Michalska

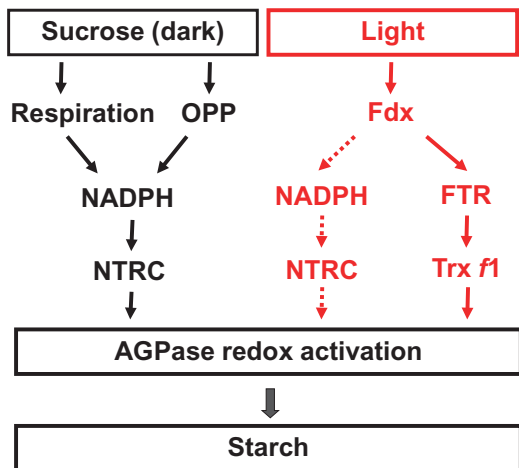


Figure 7. Working model of the different reduction pathways of AGPase. Trx f1 is involved in light activation, but not in sucrose-dependent activation of AGPase (see Fig. 6). NTRC may partially complement Trx f1 in light activation of AGPase by using photoreduced NADPH, while it is crucial for sucrose-dependent reduction of AGPase in the dark by using metabolically generated NADPH most likely from the oxidative pentose phosphate pathway (Michalska *et al.* 2009) or from respiratory processes in mitochondria (Centeno *et al.* 2011).

et al. 2009) or from respiratory processes in mitochondria (Centeno *et al.* 2011).

Knockout of Trx f1 led to a 35–70% attenuation of redox activation of AGPase in leaves during the day, but not to a complete inhibition (Fig. 4; Supporting Information Table S1). This indicates compensation by other Trx isoforms or NTRC as alternate redox system. NTRC may complement Trx f1 in light-activation of AGPase by using photoreduced NADPH, although this has not been clearly demonstrated yet. Moreover, sugar levels, including sucrose and trehalose, were increased in the *trxf1.1* and *trxf1.2* mutants (Fig. 5 and Table 2), which may have led to a compensatory increase in redox activation of AGPase by stimulating NTRC (Michalska *et al.* 2009) or trehalose-6-phosphate (Tre6P) related pathways (Kolbe *et al.* 2005). Both, NTRC and Tre6P have been found to significantly affect redox regulation of AGPase and starch synthesis in *Arabidopsis* leaves (Kolbe *et al.* 2005; Michalska *et al.* 2009). A working model of the different reduction pathways of AGPase is presented in Fig. 7. More work is required to investigate how the different reduction pathways of AGPase are regulated and coordinated.

Trx f1 contributes significantly to regulate diurnal starch turnover in plants

Knockout of Trx f1 led to a 22% decrease in starch accumulation, to a 22% increase in sucrose levels and to a 1.7-fold decrease in the starch/sucrose ratio in leaves during the day (Fig. 5). This shows that Trx f1 contributes significantly to regulate diurnal starch turnover in plants. The changes in starch metabolism are most likely due to Trx f1 affecting

redox activation of AGPase, which was observed *in vitro* (Fig. 1) as well as *in vivo* (Figs 4 & 6). This is consistent with recent studies, demonstrating the importance of the redox regulatory cysteine (Hädrich *et al.* 2012) and the kinetic properties (Obana *et al.* 2006) of AGPase in regulating diurnal starch turnover in *Arabidopsis* leaves.

As shown in Figs 4 and 5, the decrease in APS1 monomerization state preceded the decrease in starch accumulation and correlated with the decrease in the starch/sucrose ratio in leaves during the day. The time delay between the change in APS1 monomerization and the change in starch accumulation is most probably due to the different time frames by which these parameters respond during the diurnal cycle. While changes in monomerization of APS1 occur within a time frame of minutes after illumination (Figs 4 & 6), changes in starch accumulation require several hours to develop (Fig. 5). Moreover, starch accumulation in leaves is also affected by other factors than redox regulation of AGPase. Firstly, net starch accumulation could be determined by synthesis as well as degradation pathways operating at the same time, although this is not very likely (see Kötting *et al.* 2010). Secondly, besides AGPase, several other enzymes involved in the pathway of starch synthesis and degradation have been pinpointed to be redox regulated, including starch branching enzyme, glucan water dikinase, beta-amylase and phosphoglucan phosphatase (Kötting *et al.* 2010). It remains to be determined, whether these enzymes are also affected during the light–dark cycle or in Trx f1 knockout mutants. Thirdly, starch synthesis is also regulated by changes in metabolite levels, including the substrates (hexose-phosphates) and allosteric effectors (3-PGA, inorganic phosphate) of AGPase (Preiss 1988). It is however unlikely that the decrease in starch synthesis in response to a lack of Trx f1 is due to changes in metabolite levels. There were no changes in photosynthetic parameters (Fig. 3), while the levels of hexose-phosphates (Tables 1 and 2) and triose-phosphates (Table 1) as photosynthetic products and substrates for starch synthesis remained constant or increased during the day. Moreover, there were no substantial changes in the levels of 3-PGA (Table 1) and inorganic phosphate (Table 2) representing the allosteric activator and inhibitor of AGPase, respectively. This makes it very unlikely that the changes in starch synthesis are due to allosteric regulation of AGPase by changes in metabolite levels.

In the Trx f1 mutant lines, the decrease in AGPase redox activation was much larger (up to 70%) compared to the adjacent decrease in starch accumulation (up to 22%), indicating a flux-control coefficient of approximately 0.3. This is in confirmation to previous reports on flux-control coefficients of AGPase for starch synthesis in *Arabidopsis* leaves yielding values around 0.3 under similar light conditions as used in the present study (Neuhaus & Stitt 1990). It shows that AGPase is co-regulating starch synthesis while control is being shared between several enzymes constituting the pathway.

Compared to wild type, the diurnal increase in sucrose level in the mutant is most probably a consequence of the

inhibition of starch synthesis. A similar scenario has been observed in previous studies with *aps1* *Arabidopsis* mutants (Sun, Okita & Edwards 1999) and transgenic potato tubers with decreased expression of *aps1* (Müller-Röber, Sonnewald & Willmitzer 1992) where inhibition of starch synthesis led to a compensatory increase in sucrose levels. Alternatively, lack of *Trx f1* could have led to an inhibition of sucrose export, which may explain the relatively rapid increase in sucrose accumulation already 1 h after illumination. Only little is known concerning the effect of Trxs on carbon transport rates. Previous studies in potato tuber tissue (Tiessen *et al.* 2002) and *Arabidopsis* leaves (Kolbe *et al.* 2006) indicate that DTT-dependent activation of Trxs leads to an inhibition rather than a stimulation of sucrose transport functions.

Trx f1 does not affect photosynthetic parameters and growth but might provide an interesting strategy to manipulate metabolic pathways in plants

At the end of the night, lack of *Trx f1* led to a decrease in residual starch levels (Fig. 5) and in the levels of metabolites deriving from starch degradation, such as hexose-phosphates and triose-phosphates (Table 1), sucrose (Fig. 5) and maltose (data not shown), indicating decreased nocturnal carbon availability in the mutants. However, these changes were clearly not large enough to affect overall plant growth, as it is otherwise known from mutants completely lacking starch (Caspar *et al.* 1986).

Lack of *Trx f1* also did not affect photosynthetic parameters (Fig. 3), although *Trx f* protein level decreased by more than 90% in the two knockout lines (Fig. 2). This is unexpected due to the crucial role of *Trx f* in the light regulation of photosynthesis proposed in many studies. Clearly, the remaining *Trx f* protein level based on *Trx f2* expression or the remaining other types of Trxs were still sufficient for an effective regulation of photosynthesis, while starch synthesis was already impaired under these conditions. The reason for this is not clear, but it may be due to the different affinities of Trxs to their individual target proteins. This interpretation is supported by previous studies showing that the concentration of *Trx f* leading to half-maximal activation of AGPase (4.6 μ M; Ballicora *et al.* 2000) is much higher than the concentration leading to half-maximal activation of the Calvin–Benson cycle enzyme fructose-1,6-bisphosphatase (FBPase; 0.9 μ M, see Mora-Garcia, Rodriguez-Suarez & Wolosiuk 1998). Any decrease in *Trx f* will therefore affect AGPase much more strongly than FBPase, especially since the concentrations of Trxs in chloroplasts have been found to be several magnitudes lower than the concentrations of the corresponding target proteins (König, Muthuramalingam & Dietz 2012). *Trx f* may be already limiting for light activation of AGPase under the prevailing conditions in the wild type. In leaves, the concentration of *Trx f* has been reported to be increased in response to a variety of signals, including light (Carrasco *et al.* 1992), circadian rhythms (Barajas

et al. 2011), thiol status and sugars (Barajas *et al.* 2012), most of them are also positively linked to starch synthesis (Geigenberger 2011). Transgenic approaches to overexpress *Trx f1* could therefore provide an interesting strategy to improve starch synthesis in plants, especially since other enzymes in the pathway of starch synthesis have been found to be regulated by Trxs in addition to AGPase (Kötting *et al.* 2010).

The metabolite profiling data in Table 2 indicate that genetic manipulation of *Trx f1* might also affect other pathways in plants. In this respect, the strong effect of *Trx f1* knockout on ethanolamine levels is very interesting. Ethanolamine plays a major role in phospholipid biosynthesis and has been identified as an important part of the metabolic signature predicting plant biomass (Meyer *et al.* 2007). Investigating the role of *Trx f* in regulating lipid biosynthesis will be an interesting avenue of future research.

ACKNOWLEDGMENTS

This work was supported by funding from the Deutsche Forschungsgemeinschaft (grants Ge 878/5-1 and 8-1). The Deutsche Forschungsgemeinschaft also partly funded the GC-TOF-MS machine used in this study (grant INST 86/1254-1 to P.G.). Scientific exchange between Munich and Orsay was supported by funds of the Bayerisch-Französisches Hochschulzentrum (grant FK-27/10 to P.G., I.T and E.I.) We are grateful to Dario Leister (LMU Munich) for providing facilities for PAM analysis.

REFERENCES

- Alonso J.M., Stepanova A.N., Leisse T.J., *et al.* (2003) Genome-wide insertional mutagenesis of *Arabidopsis thaliana*. *Science* **301**, 653–657.
- Arsova B., Hoja U., Wimmelbacher M., Greiner E., Üstün S., Melzer M., Petersen K., Lein W. & Börnke F. (2010) Plastidial thioredoxin z interacts with two fructokinase-like proteins in a thiol-dependent manner: Evidence for an essential role in chloroplast development in *Arabidopsis* and *Nicotiana benthamiana*. *The Plant Cell* **22**, 1498–1515.
- Ballicora M.A., Frueauf J.B., Fu Y., Schürmann P. & Preiss J. (2000) Activation of the potato tuber ADP glucose pyrophosphorylase by thioredoxin. *Journal of Biological Chemistry* **275**, 1315–1320.
- Barajas J.D., Serrato A., Cazalí R., Reichheld J.P., Meyer Y., Chueca A. & Sahrawy M. (2011) Circadian regulation of the pea chloroplastic f and m1 thioredoxins through the interaction of the CCA1 transcription factor to an evening element. *Journal of Experimental Botany* **62**, 2039–2051.
- Barajas J.D., Tezycka J., Travaglia C.N., Serrato A.J., Chueca A., Thormählen I., Geigenberger P. & Sahrawy M. (2012) Expression of the chloroplast thioredoxins f and m is linked to short-term changes in the sugar and thiol status in leaves of *Pisum sativum*. *Journal of Experimental Botany* (in press).
- Benítez-Alfonso Y., Cilia M., San Roman A., Thomas C., Maule A., Hearn S. & Jackson D. (2009) Control of *Arabidopsis* meristem development by thioredoxin-dependent regulation of intercellular transport. *Proceedings of the National Academy of Sciences of the United States of America* **106**, 3615–3620.
- Buchanan B.B. (1980) Role of light in the regulation of chloroplast enzymes. *Annual Review of Plant Physiology* **31**, 341–374.

Buchanan B.B. & Balmer Y. (2005) Redox regulation: a broadening horizon. *Annual Review of Plant Biology* **56**, 187–220.

Carrasco J.L., Chueca A., Sahrawy M., Hermoso R., Lázaro J.J. & López Gorgé J. (1992) Role of light in the *in vivo* and *in vitro* synthesis of spinach thioredoxin f. *Physiologia Plantarum* **84**, 236–242.

Caspar T., Huber S.C. & Somerville C. (1986) Alterations in growth, photosynthesis and respiration in a starch deficient mutant of *Arabidopsis thaliana* (L.) Heynh deficient in chloroplast phosphoglucomutase activity. *Plant Physiology* **79**, 11–17.

Centeno D.C., Osorio S., Nunes-Nesi A., et al. (2011) On the crucial role of malate in transitory starch metabolism, ripening, total soluble solid content at harvest and post-harvest softening in tomato fruit. *The Plant Cell* **23**, 162–184.

Chibani K., Tarrago L., Schurmann P., Jacquot J.P. & Rouhier N. (2011) Biochemical properties of poplar thioredoxin z. *FEBS Letters* **585**, 1077–1081.

Collin V., Issakidis-Bourguet E., Marchand C., Hirasawa M., Lancelin J.M., Knaff D.B. & Migniac-Maslow M. (2003) The *Arabidopsis* plastidial thioredoxins: new functions and new insights into specificity. *Journal of Biological Chemistry* **278**, 23747–23752.

Collin V., Lamkemeyer P., Migniac-Maslow M., Hirsawa M., Knaff D.B., Dietz K.-J. & Issakidis-Bourguet E. (2004) Characterisation of plastidial thioredoxins from *Arabidopsis* belonging to the new y-type. *Plant Physiology* **136**, 4088–4095.

Dietz K.-J. & Pfannschmidt T. (2011) Novel regulators in photosynthetic redox control of plant metabolism and gene expression. *Plant Physiology* **155**, 1477–1485.

Erban A., Schauer N., Fernie A.R. & Kopka J. (2007) Non-supervised construction and application of mass spectral and retention time index libraries from time-of-flight gas chromatography-mass spectrometry metabolite profiles. *Methods in Molecular Biology* **358**, 19–38.

Fu Y., Ballicora M.A., Leykam J.F. & Preiss J. (1998) Mechanism of reductive activation of potato tuber ADP-glucose pyrophosphorylase. *Journal of Biological Chemistry* **273**, 25045–25052.

Geigenberger P. (2011) Regulation of starch biosynthesis in response to a fluctuating environment. *Plant Physiology* **155**, 1566–1577.

Geigenberger P., Kolbe A. & Tiessen A. (2005) Redox-regulation of carbon storage and partitioning in response to light and sugars. *Journal of Experimental Botany* **56**, 1469–1479.

Geiger D.R. & Servaites J.C. (1994) Diurnal regulation of photosynthetic carbon metabolism in C3 plants. *Annual Review of Plant Physiology and Plant Molecular Biology* **45**, 235–256.

Genty B., Briantais J.-M. & Baker N.R. (1989) The relationship between the quantum yield of photosynthetic electron transport and quenching of chlorophyll fluorescence. *Biochimica et Biophysica Acta* **990**, 87–92.

Hädrich N., Hendriks J.H.M., Kötting O., Arrivault S., Feil R., Zeeman S.C., Gibon Y., Schulze W.X., Stitt M. & Lunn J.E. (2012) Mutagenesis of cysteine 81 prevents dimerization of the APS1 subunit of ADP-glucose pyrophosphorylase and alters diurnal starch turnover in *Arabidopsis thaliana* leaves. *Plant Journal* **70**, 231–242.

Häusler R.E., Fischer K.L. & Flügge U.I. (2000) Determination of low abundant metabolites in plant extracts by NAD(P)H fluorescence with a microtiter plate reader. *Analytical Biochemistry* **281**, 1–8.

Hendriks J.H.M., Kolbe A., Gibon Y., Stitt M. & Geigenberger P. (2003) ADP-glucose pyrophosphorylase is activated by post-translational redox-modification in response to light and to sugars in leaves of *Arabidopsis* and other plant species. *Plant Physiology* **133**, 838–849.

Hodges M., Migniac-Maslow M., Decottignies P., Jacquot J.P., Stein M., Lepiniec L., Crétin C. & Gadal P. (1994) Purification and characterization of pea thioredoxin f expressed in *Escherichia coli*. *Plant Molecular Biology* **26**, 225–234.

Hummel J., Strehmel N., Selbig J., Walther D. & Kopka J. (2010) Decision tree supported substructure prediction of metabolites from GC-MS profiles. *Metabolomics* **6**, 322–333.

Jones M.G.K., Outlaw W.H. & Lowry O.H. (1977) Enzymic assay of 10^{-7} to 10^{-14} moles of sucrose in plant tissues. *Plant Physiology* **60**, 379–383.

Kolbe A., Tiessen A., Schluepman H., Paul M., Ulrich S. & Geigenberger P. (2005) Trehalose 6-phosphate regulates starch synthesis via posttranslational redox regulation of ADP-glucose pyrophosphorylase. *Proceedings of the National Academy of Sciences of the United States of America* **102**, 11118–11123.

Kolbe A., Oliver S.N., Fernie A.R., Stitt M., van Dongen J.T. & Geigenberger P. (2006) Combined transcript and metabolite profiling of *Arabidopsis* leaves reveals fundamental effects of the thiol-disulfide status on plant metabolism. *Plant Physiology* **141**, 412–422.

König J., Muthuramalingam M. & Dietz K.-J. (2012) Mechanisms and dynamics in the thiol/disulphide redox regulatory network: transmitters, sensors and targets. *Current Opinion in Plant Biology* **15**, 261–268.

Kötting O., Kossmann J., Zeeman S.C. & Lloyd J.R. (2010) Regulation of starch metabolism: the age of enlightenment? *Current Opinion in Plant Biology* **13**, 321–329.

Kramer D.M., Johnson G., Kiarats O. & Edwards G.E. (2004) New fluorescence parameters for the determination of Q_A redox state and excitation energy fluxes. *Photosynthesis Research* **79**, 209–218.

Lemaire S.D., Michelet L., Zaffagnini M., Massot V. & Issakidis-Bourguet E. (2007) Thioredoxins in chloroplasts. *Current Genetics* **51**, 343–365.

Luedemann A., Strassburg K., Erban A. & Kopka J. (2008) Tag-Finder for the quantitative analysis of gas chromatography-mass spectrometry (GC-MS)-based metabolite profiling experiments. *Bioinformatics* **24**, 732–737.

Meyer Y., Reichheld J.P. & Vignols F. (2005) Thioredoxins in *Arabidopsis* and other plants. *Photosynthesis Research* **86**, 419–433.

Meyer R.C., Steinath M., Liseck J., et al. (2007) The metabolic signature related to high plant growth rate in *Arabidopsis thaliana*. *Proceedings of the National Academy of Sciences of the USA* **104**, 4759–4764.

Michalska J., Zauber H., Buchanan B.B., Cejudo F.J. & Geigenberger P. (2009) NTRC links built-in thioredoxin to light and sucrose in regulating starch synthesis in chloroplasts and amyloplasts. *Proceedings of the National Academy of Sciences of the United States of America* **106**, 9908–9913.

Montrichard F., Alkhalfioui F., Yano H., Vensel W.H., Hurkman W.J. & Buchanan B.B. (2009) Thioredoxin targets in plants: the first 30 years. *Journal of Proteomics* **72**, 452–474.

Mora-Garcia S., Rodriguez-Suarez R. & Wolosiuk R.A. (1998) Role of electrostatic interactions on the affinity of thioredoxin for target proteins. *Journal of Biological Chemistry* **273**, 16273–16280.

Müller-Röber B., Sonnewald U. & Willmitzer L. (1992) Antisense inhibition of the ADP-glucose pyrophosphorylase in transgenic potato leads to sugar storing tubers and influences tuber formation and expression of tuber storage protein genes. *EMBO Journal* **11**, 1229–1238.

Neuhaus H.E. & Stitt M. (1990) Control analysis of photosynthate partitioning: impact of reduced activity of ADP glucose pyrophosphorylase and plastid phosphoglucomutase on the fluxes to

starch and sucrose in *Arabidopsis thaliana* L. Heynh. *Planta* **182**, 445–454.

Obana Y., Omoto D., Kato C., *et al.* (2006) Enhanced turnover of transitory starch by expression of up-regulated ADP-glucose pyrophosphorylases in *Arabidopsis thaliana*. *Plant Science* **170**, 1–11.

Pérez-Ruiz J.M., Spínola M.C., Kirchsteiger K., Moreno J., Sahrawy M. & Cejudo F.J. (2006) Rice NTRC is a high-efficiency redox system for chloroplast protection against oxidative damage. *The Plant Cell* **18**, 2356–2368.

Pesaresi P., Hertle A., Pribil M., *et al.* (2009) *Arabidopsis* STN7 kinase provides a link between short- and long-term photosynthetic acclimation. *The Plant Cell* **21**, 2402–2423.

Preiss J. (1988) Biosynthesis of starch and its regulation. In *The Biochemistry of Plants* (ed. J. Preiss), pp. 181–254. Academic Press, San Diego, CA.

Schürmann P. & Buchanan B.B. (2008) The ferredoxin/thioredoxin system of oxygenic photosynthesis. *Antioxidants & Redox Signaling* **10**, 1235–1273.

Seigneurin-Berny D., Salvi D., Dorne A.-J., Joyard J. & Rolland N. (2008) Percoll-purified and photosynthetically active chloroplasts from *Arabidopsis thaliana* leaves. *Plant Physiology and Biochemistry* **46**, 951–955.

Serrato A.J., Perez-Ruiz J.M., Spínola M.C. & Cejudo F.J. (2004) A novel NADPH thioredoxinreductase, localized in the chloroplast, which deficiency causes hypersensitivity to abiotic stress in *Arabidopsis thaliana*. *Journal of Biological Chemistry* **279**, 43821–43827.

Sulpice R., Pyl E-T., Ishihara H., *et al.* (2009) Starch as a major integrator in the regulation of plant growth. *Proceedings of the National Academy of Sciences of the United States of America* **106**, 10348–10353.

Sun J., Okita T.W. & Edwards G.E. (1999) Modification of carbon partitioning, photosynthetic capacity, and O₂ sensitivity in *Arabidopsis* plants with low ADP-glucose pyrophosphorylase activity. *Plant Physiology* **119**, 267–276.

Tiessen A., Hendriks J.H.M., Stitt M., Branscheid A., Gibon Y., Farre E.M. & Geigenberger P. (2002) Starch synthesis in potato tubers is regulated by post-translational redox modification of ADP-glucose pyrophosphorylase: a novel regulatory mechanism linking starch synthesis to the sucrose supply. *The Plant Cell* **14**, 2191–2213.

Weise S.E., van Wijk K.J. & Sharkey T.D. (2011) The role of transitory starch in C-3, CAM, and C-4 metabolism and opportunities for engineering leaf starch accumulation. *Journal Experimental Botany* **62**, 3109–3118.

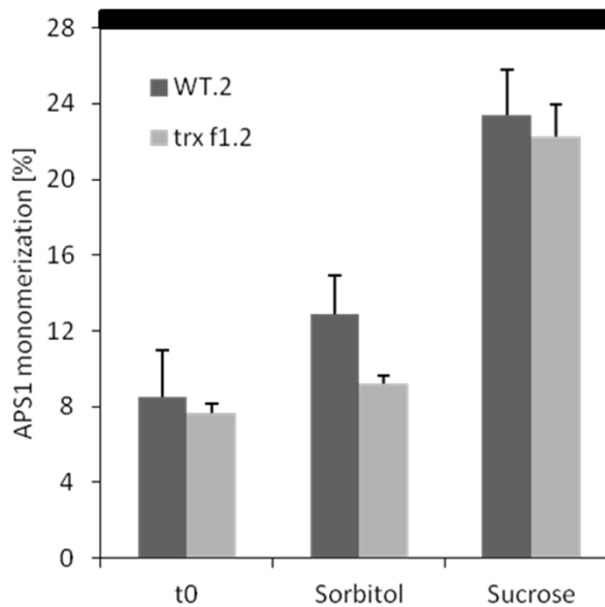
Received 3 November 2011; received in revised form 18 May 2012; accepted for publication 22 May 2012

SUPPORTING INFORMATION

Additional Supporting Information may be found in the online version of this article:

Figure S1. Effect of Trx f1 knockout (line *trx f1.2*) on sucrose-dependent redox activation of AGPase in leaves in the dark. For the sucrose-dependent effect on APS1 monomerization, *Arabidopsis* leaves were harvested at the end of night (t0), and incubated with sucrose or sorbitol (100 mM) for 5 h in the dark. Results are means ± SE (*n* = 4).

Table S1. Effect of light on the conversion of the 100 kDa to the 50 kDa form of APS1 in leaves of the Trx f1 *Arabidopsis* knockout lines (*trx f1.1* and *trx f1.2*), compared to the respective segregating wild-types. The Western blots from Fig. 4 were scanned, and the intensity of the protein bands corrected for background.



Supplemental Figure S1:

Effect of *Trx f1* knockout (line *trx f1.2*) on sucrose-dependent redox activation of AGPase in leaves in the dark. For the sucrose-dependent effect on APS1 monomerization, *Arabidopsis* leaves were harvested at the end of night (t0), and incubated with sucrose or sorbitol (100 mM) for 5 h in the dark. Results are means \pm SE (n = 4).

Supplemental Table S1: Effect of light on the conversion of the 100 kDa to the 50 kDa form of APS1 in leaves of the *Trx f1* *Arabidopsis* knockout lines (*trx f1.1* and *trx f1.2*), compared to the respective segregating wild-types. The western blots from Fig. 4 were scanned, and the intensity of the protein bands corrected for background. Data are given as monomerization of APS1 in %.

Time [h]	WT.1	<i>trx f1.1</i>	WT.2	<i>trx f1.2</i>
0	1.2	0.6	7.3	6.9
1	25.5	8.0	37.0	10.7
4	30.9	19.8	31.9	17.2
8	21.0	11.3	28.3	15.5
9	2.5	1.5	10.5	4.3

RESULTS

Chapter 2 – Interaction between thioredoxin *f1* and NADPH-dependent thioredoxin reductase C regulates photosynthetic metabolism and plant growth

Ina Thormählen, Tobias Meitzel, Julia Groysman, Alexandra Bianca Öchsner, Edda von Roepenack-Lahaye, Belén Naranjo, Francisco Javier Cejudo, Peter Geigenberger (2014) Interaction between thioredoxin *f1* and NADPH-dependent thioredoxin reductase C regulates photosynthetic metabolism and plant growth. *Manuscript submitted (Plant Cell)*.

Interaction between thioredoxin *f1* and NADPH-dependent thioredoxin reductase C regulates photosynthetic metabolism and plant growth

Ina Thormählen^a, Tobias Meitzel^b, Julia Groysman^a, Alexandra Bianca Öchsner^a, Edda von Roepenack-Lahaye^a, Belén Naranjo^c, Francisco J. Cejudo^c and Peter Geigenberger^{a1}

^a Ludwig-Maximilians-Universität München, Department Biologie I, Grosshaderner Str. 2-4, 82152 Martinsried, Germany

^b Leibniz-Institut für Pflanzengenetik und Kulturpflanzenforschung (IPK), D-06466 Gatersleben, Germany

^c Instituto de Bioquímica Vegetal y Fotosíntesis, University of Seville and CSIC, Avda Américo Vespucio 49, 41092-Sevilla, Spain

Running Title:

Cooperative interaction of Trx *f* and NTRC

Page calculator estimate: 20 pages

Footnotes:

¹Address correspondence to:

E-mail: geigenberger@bio.lmu.de; Tel: +49 (0)89 218074710

The author responsible for distribution of materials integral to the findings presented in this article in accordance with the policy described in the Instructions for Authors (www.plantcell.org) is: Peter Geigenberger (geigenberger@bio.lmu.de).

ABSTRACT

Two different thiol-redox-systems exist in plant chloroplasts, the ferredoxin-thioredoxin system, which depends of ferredoxin reduced by the photosynthetic electron-transport chain and, thus, of light, and the NADPH-dependent thioredoxin reductase C (NTRC) system, which relies on NADPH and thus may be operative also during the night. Previous in-vitro studies led to the view that both systems act independently in the chloroplast stroma. We now report that there is a previously unrecognized cooperative interaction of thioredoxin-*f1* and NTRC in regulating photosynthetic metabolism and growth. In *Arabidopsis* mutants, combined but not single deficiencies of thioredoxin-*f1* and NTRC led to severe growth inhibition and perturbed light acclimation, accompanied by strong impairments of Calvin-Benson-cycle activity and starch accumulation. Light-activation of key-enzymes of these pathways, fructose-1,6-bisphosphatase and ADP-glucose pyrophosphorylase, was almost completely abolished. The subsequent increase in NADPH/NADP⁺ and ATP/ADP ratios led to increased light-vulnerability of photosystem I core-proteins. In a biochemical approach, bimolecular-fluorescence-complementation assays were performed showing physical interaction between thioredoxin-*f1* and NTRC at the protein level in-vivo. Results provide genetic and biochemical evidence that the different stromal thiol-redox-systems interact at the level of thioredoxin-*f1* and NTRC to coordinately participate in the regulation of Calvin-Benson-cycle, starch metabolism and growth in response to varying light conditions.

INTRODUCTION

Reversible disulfide-bond formation between two cysteine residues regulates structure and function of many proteins in diverse organisms (Cook and Hogg, 2013). Thiol-disulfide exchange is controlled by thioredoxins (Trx), which are small proteins containing a redox-active disulfide group in their active site (Holmgren, 1985; Baumann and Juttner, 2002). The latter can be reduced to a dithiol by Trx reductases using NADPH or ferredoxin (Fdx) as electron donors. Due to their low redox potential, reduced Trxs are able to reductively cleave disulfide-bonds in many target proteins and, thus, modulate their functions.

Plants contain the most versatile Trx system found in all organisms with respect to the multiplicity of different isoforms and reduction systems (Buchanan and Balmer, 2005; Nikkanen and Rintamäki, 2014). The *Arabidopsis* genome contains a complex family of Trxs, including up to 20 different isoforms grouped into seven subfamilies (Schuermann and Buchanan, 2008; Dietz and Pfannschmidt, 2011). Trxs *f1-2*, *m1-4*, *x*, *y1-2* and *z* are located exclusively in the chloroplast, Trx *o* exclusively in the mitochondria, while the six Trx *h* representatives are distributed between the cytosol, nucleus, endoplasmic reticulum (ER), and mitochondria (Meyer et al., 2012). The different Trxs can be reduced by two different redox systems, dependent on Fdx and Fdx-Trx reductase (FTR) in the chloroplast or NADPH and NADPH-Trx reductase (NTRA and NTRB) in other cell compartments (Buchanan and Balmer, 2005). More recently, a third type of NADPH-Trx reductase (NTRC) has been identified which forms a separate Trx system in the chloroplast (Serrato et al., 2004; Perez-Ruiz et al., 2006). NTRC is a bimodular enzyme containing both an NTR and Trx domain on a single polypeptide (Serrato et al., 2004). Its catalytic unit is a homodimer, transferring electrons from NTR to Trx domains via inter-subunit pathways (Pérez-Ruiz and Cejudo, 2009). In vitro studies suggest that NTRC is a Trx with its own Trx reductase, since it has not been shown to interact with other free Trxs (Perez-Ruiz et al., 2006; Bohrer et al., 2012). This is in contrast to experiments on transgenic *Arabidopsis* lines overexpressing NTRC with an inactive Trx domain, indicating a possible interaction of NTRC with other chloroplast Trx systems (Toivola et al., 2013). Therefore, the possible interaction of NTRC and other plastidial Trxs remains an open question.

In chloroplasts, Trxs are reduced via FTR in a light-dependent manner, using photosynthetic electrons provided by Fdx. The Fdx-Trx system with Trxs *f* and *m* was originally discovered as a mechanism for the regulation of the Calvin-Benson cycle, ATP synthesis and NADPH export in response to light-dark changes (Buchanan et al., 1979; Buchanan, 1980). In numerous biochemical studies performed in-vitro, the roles of Trxs *f* and *m* were extended to the regulation of many other chloroplast enzymes involved in various pathways of primary metabolism (Buchanan and Balmer, 2005; Meyer et al., 2012). Experiments with purified proteins revealed differences in biochemical specificities to different types of Trxs. Enzymes of the Calvin-Benson cycle were found to be exclusively regulated by *f*-type Trxs (Collin et al., 2003a; Michelet et al., 2013), while key-enzymes involved in related pathways such as starch synthesis (Fu et al., 1998; Ballicora et al., 2000; Geigenberger et al., 2005; Thormahlen et al., 2013), starch degradation (Mikkelsen et al., 2005; Valerio et al., 2011; Seung et al., 2013; Silver et al., 2013), fatty acid synthesis (Sasaki et al., 1997), amino acid synthesis (Lichter and Häberlein, 1998; Choi et al., 1999; Balmer et al., 2003), chlorophyll synthesis (Ikegamie et al. 2007; Luo et al. 2012), NADPH export (Collin et al., 2003; Scheibe, 2004) and oxidative pentose-phosphate pathway (OPPP, Nee et al. 2009) were found to be regulated by both Trxs *f* and *m*, with *f*-being in most cases more effective than *m*-type. Other plastidial isoforms belonging to the *x*- and *y*-types were found to mainly serve as reducing substrates for antioxidant enzymes such as peroxiredoxins, thiol-peroxidases and methionine sulfoxide reductases, indicating their role in oxidative stress responses (Collin et al., 2003a; Collin et al., 2004; Meyer et al., 2012). The biochemical properties of Trx *z* are largely unresolved. While this new type of Trx has been identified to be part of the plastid-encoded RNA polymerase indicating a role in transcriptional regulation (Arsova et al., 2010), it has also been found to support the activity of several plastidial antioxidant enzymes, indicating a role in stress responses (Chibani et al., 2011).

While most of the results mentioned above are based on biochemical studies, little is known about the in-vivo relevance and specificity of the different chloroplast Trxs isoforms in planta. Recent progress in this area was made by using reverse genetic

studies, including *Arabidopsis* mutants and transgenic plants. Intriguingly, these genetic studies revealed specific roles of *m*-type Trxs in regulating photosynthetic electron transport and developmental processes, rather than its expected roles in primary metabolism. *Arabidopsis* lines under-expressing Trxs *m1*, *m2* and *m4* were defective in the biogenesis of photosystem II (Wang et al., 2013), single mutants with deletions in Trx *m4* were affected in alternative photosynthetic electron transport pathways (Courteille et al., 2013), while deletions in Trx *m3* affected meristem development (Benitez-Alfonso et al., 2009). In addition to this, *Arabidopsis* mutants with deletions in Trx *f1* leading to a more than 97% decrease in Trx *f* protein level showed alterations in diurnal starch accumulation, rather than any changes in photosynthetic parameters and growth (Thormahlen et al., 2013). This is surprising, given the exclusive regulation of individual steps of the carbon fixation cycle by Trx *f1* in-vitro (Collin et al., 2003a; Michelet et al., 2013).

Compared to the Fdx-Trx system, relatively little is known on the more recently identified chloroplast NADPH-NTRC system, which uses NADPH as a source of electrons, provided by FNR in the light or the OPPP in the dark. So far only a few targets have been identified to be regulated by NTRC, with 2-Cys peroxiredoxins (2-Cys Prxs) involved in H₂O₂-detoxification (Perez-Ruiz et al., 2006), ADPGlc pyrophosphorylase (AGPase) the key enzyme of starch biosynthesis (Michalska et al., 2009; Lepisto et al., 2013) and enzymes of chlorophyll biosynthesis (Richter et al., 2013; Perez-Ruiz et al., 2014) being the most elaborated ones. Regulation of these processes by NTRC was confirmed in planta by analyzing an insertional knockout mutant of NTRC, revealing (i) an attenuation of redox-activation of AGPase and starch accumulation (Michalska et al., 2009; Lepisto et al., 2013), (ii) decreased chlorophyll levels and impaired redox status of GluTR1 and CHLM activities (Richter et al., 2013) and CHLI subunit of the Mg-chelatase complex (Perez-Ruiz et al., 2014), and (iii) increased levels of hydrogen peroxide and lipid peroxidation (Perez-Ruiz et al., 2006). While the first two effects were observed in plants growing in a normal diurnal cycle, the third one was only observed under conditions of prolonged darkness followed by illumination. In addition to the NADPH-NTRC system, 2-Cys Prx and AGPase have also been found to be regulated by the Fdx-Trx system with Trx *x* (Konig et al., 2002) and Trx *f1* (Thormahlen et al., 2013), respectively.

However, little is known on the interrelation of both chloroplast redox systems in regulating these targets.

In this report, the interrelation between Trx *f1* and NTRC in regulating plant metabolism and growth was investigated by using genetic and biochemical approaches. Analysis of an *Arabidopsis* *trxf1 ntrc* double mutant shows that combined inactivation of Trx *f1* and NTRC leads to a strong inhibition of photosynthesis and related metabolic activities resulting in a severe limitation of growth, while these responses were not or only weakly expressed in the single mutants. Synergistic effects of Trx *f1* and NTRC were specifically found in relation to enzymes of the Calvin-Benson cycle and starch metabolism. Moreover, bimolecular fluorescence complementation (BiFC) assays were performed showing that Trx *f1* and NTRC are physically interacting at the protein level *in vivo*. Results provide direct evidence for a previously unknown cooperative interaction of Trx *f1* and NTRC in regulating photosynthetic metabolism and growth.

RESULTS

Combined inactivation of Trx *f1* and NTRC leads to a severe growth phenotype

To analyze the interrelation between Trx *f1* and NTRC in regulating growth and metabolism of *Arabidopsis* plants, the well-characterized *trxf1* (SALK_128365; (Thormahlen et al., 2013) and *ntrc* (SALK_012208; (Serrato et al., 2004; Pérez-Ruiz et al., 2006) T-DNA insertion lines were crossed to generate a *trxf1 ntrc* double mutant. A homozygous *trxf1 ntrc* line was identified, where T-DNA insertions were present in both genomic alleles (Fig. 1A), while protein content (Fig. 1B) of both Trx *f1* and NTRC were strongly decreased to detection limit. In comparison to this, expression of NTRC and Trx *f1* was still detectable in the *trxf1* and *ntrc* single mutants, respectively, although Trx *f1* protein levels (Fig. 1B) were found to be slightly lower in the *ntrc* background than in the wild-type. In the Western blots of Fig. 1B, a Trx *f* antibody was used that gives similar signals with Trx *f1* and Trx *f2* (Thormahlen et al., 2013), indicating that Trx *f1* is the major Trx *f* isoform in *Arabidopsis*.

As previously reported, *trxf1* (Thormahlen et al., 2013) and *ntrc* single mutants (Perez-Ruiz et al., 2006; Lepisto et al., 2013) showed no or moderate growth phenotypes, respectively, when grown in a 8 h photoperiod at 160 $\mu\text{mol m}^{-2} \text{s}^{-1}$ light intensity (Fig. 2B). In contrast to this, growth of the *trxf1 ntrc* double mutant was very severely perturbed, when compared to the wild-type or the single mutants (Fig. 2B). The rosette fresh-weights of the *trxf1 ntrc* double mutant decreased to below 2% of wild-type level, while those of the *ntrc* mutant decreased to 25% and those of the *trxf1* mutant remained unaltered (Fig. 2H). Despite this very strong growth defect, *trxf1 ntrc* mutant plants were viable and produced seeds under these conditions (Fig. 2G). Interestingly, the extent of the growth phenotypes differed depending on the length of the photoperiod and the light intensity (Figs. 2 A-F). When the length of the photoperiod was decreased from 8 to 4 h light, rosette fresh-weights decreased significantly to 80% and 15% of wild-type level in the *trxf* and *ntrc* single mutants, respectively, and to levels below the detection limit in the *trxf1 ntrc* double mutant (Fig. 2H). Conversely, an increase in the length of the photoperiod from 8 to 24 h led to a partial relieve in the growth retardation of both the *ntrc* and the *trxf1 ntrc* mutant. In the *ntrc* mutant, rosette fresh-weights increased from 25 to 50% of wild-type level in 16 h and 24 h, compared to 8 h photoperiods (Fig. 2H), in agreement with previous studies (Lepisto et al., 2009). The *trxf1 ntrc* double mutant showed no significant change in fresh-weight when the photoperiod was increased from 8 h to 16 h light, but there was an increase from 1 to 3% of wild-type level when the photoperiod was increased from 16 h to 24 h light (Fig. 2H). Also a change in the light intensity at 8 h-photoperiod affected the growth phenotype of the mutants. When the light intensity was decreased from 160 $\mu\text{mol m}^{-2} \text{s}^{-1}$ to 30 $\mu\text{mol m}^{-2} \text{s}^{-1}$, the rosette fresh weights dropped significantly to 75 and 35% of wild-type level in the *trxf1* and *ntrc* mutants, respectively, and to levels below the detection limit in the *trxf1 ntrc* double mutant (Fig. 2H). When the light intensity was increased from 160 to 950 $\mu\text{mol m}^{-2} \text{s}^{-1}$, rosette fresh-weights dropped severely in the *trxf1 ntrc* mutant, moderately in the *ntrc* mutant, while no effect was observed in the *trxf1* mutant, compared to wild-type (Fig. 2H). Overall, the results show that knockout of Trx f1 leads to a severe growth inhibition in the *ntrc*, but not in the wild-type background, suggesting a synergistic interaction of both redox systems.

Combined deficiency of Trx f1 and NTRC leads to a strong impairment of photosynthesis

To investigate whether the severe growth phenotype of the *trxf1 ntrc* mutant is due to an effect on photosynthesis, CO₂ assimilation rates were measured in leaves of the different genotypes grown in an 8 h photoperiod at 160 $\mu\text{mol m}^{-2} \text{s}^{-1}$ light intensity using an open gas-exchange system. The light response-curves at ambient CO₂ are shown in Fig. 3A. At light intensities between 150 and 1000 μE , CO₂ fixation rates were strongly decreased in the *trxf1 ntrc* mutant relative to the wild-type, the decrease being light intensity-dependent: 6-fold at 150, 2.5-fold at 200-300, 2-fold at 400-600, and 1.5-fold at 800-1000 $\mu\text{mol m}^{-2} \text{s}^{-1}$. At light intensities between 50-100 $\mu\text{mol m}^{-2} \text{s}^{-1}$, CO₂ assimilation rates were below the respiration rate in the double mutant, but not in the wild-type, the light compensation point switching from 20 μE in the wild-type to 120 μE in the double mutant. In the dark, CO₂ release rates were 4-fold higher in the double mutant compared to wild-type. In contrast to the double mutant, the single mutants showed no or only slight changes in CO₂ assimilation rates compared to wild-type. Deletion of Trx f1 led to a slight tendency of CO₂-assimilation rates to increase at higher light intensities, although this was not statistically significant. Deletion of NTRC led to a slight decrease in CO₂-assimilation rates at all light intensities, which was statistically significant at 50 and 200 μE using the student *t*-test (Suppl. Table S1) and for all light intensities using the two-way Anova test (Fig. 3A), confirming previous studies (Lepisto et al., 2009). Overall, the results show that inactivation of Trx f1 led to a strong decrease in CO₂ fixation rates in the *ntrc*, but not in the wild-type background, lending further support to the proposal of a synergistic cooperation of both systems to regulate the CO₂ fixation rate.

In Fig. 3B, leaf transpiration rates are shown across different light intensities and genotypes. Compared to wild-type, there was a strong (up to 8-fold) increase in transpiration rates in the *trxf1 ntrc* mutant, while the single mutants behaved like the wild-type at all light conditions tested. Similar results were observed for stomal conductance (data not shown) and intercellular CO₂ concentration (Fig. 3C), both parameters being strongly increased in the double mutant relative to the wild-type. These results show that the lower rate of CO₂ fixation caused by the combined

deficiency of Trx *f1* and NTRC is not due to a restriction in CO₂ uptake rates or a decrease in internal CO₂ concentrations, but most likely to a direct inhibition of the CO₂-fixation cycle.

To investigate whether the inhibition of CO₂-assimilation is accompanied by changes in photosynthetic light reactions, chlorophyll fluorescence parameters were measured by pulse-amplitude modulation (PAM) fluorimetry. A significant decrease of maximal (F_v/F_m) and effective quantum yield of PS II (Φ_{PSII}) was observed in the double mutant relative to the single mutants or the wild-type (Figs. 4A and 4B), indicating that the combined deficiency of Trx *f1* and NTRC led to a strong impairment of PSII functionality and photosynthetic electron transport rates. Correspondingly, quantum yields of regulated (Φ_{NPQ}) and non-regulated (Φ_{NO}) energy dissipation (Fig. 4B) were strongly increased in the double mutant. Similar to previous studies (Lepisto et al., 2009; Thormahlen et al., 2013), no changes in chlorophyll fluorescence parameters were found in the *trxf1* mutant, while the *ntrc* mutant revealed moderate but significant changes in Φ_{PSII} and Φ_{NPQ} , relative to the wild-type (Fig. 4B).

We further investigated whether impaired photosynthetic light reactions were accompanied by decreased abundance of proteins involved in photosynthetic electron transport (Fig. 5). Western blot analyses showed that combined deficiency of Trx *f1* and NTRC led to a strong decrease in proteins of the PSI complex (PsaA and PsaB) down to approx. 25% of wild-type level and to more moderate decreases in proteins of PSII (PsbD), cytochrome b6-f (PetC), light-harvesting (Lhca1 and Lhcb1) and ATPase complexes (Atp β). In comparison to this, the *trxf1* and *ntrc* single mutants were only weakly affected. Chlorophyll content remained unaltered in the *trxf1* mutant, but was significantly decreased down to 56 and 45% of wild-type level in the *ntrc* single and *trxf1 ntrc* double mutant, respectively (Suppl. Fig. S1). This confirms previous studies showing chlorophyll levels to be decreased by 50% in the *ntrc* mutant relative to the wild-type (Perez-Ruiz et al., 2006; Lepisto et al., 2009), while a combined deficiency of Trx *f1* and NTRC only led to minor additional effects (Suppl. Fig. S1).

Combined deficiency of Trx f1 and NTRC affects NADP reduction and adenylate energy states

The Calvin–Benson cycle uses most of the ATP and NADPH delivered by the photosynthetic light reactions (Michelet et al., 2013). To investigate the relationship between photosynthetic activity and the function of the Calvin-Benson cycle, the levels of NAD(P)H, NAD(P)⁺, ATP and ADP were analyzed in leaves of wild-type and the different redox mutants (Fig. 6). In wild-type plants, the sum of NADPH and NADP⁺ increased at the end of the day relative to the end of the night (Fig. 6A), while the NADPH/NADP⁺ ratio decreased (Fig 6B). Similar results have been observed in previous studies (Liu et al., 2008; Beeler et al., 2014; Lintala et al., 2014), indicating that light regulates NAD(P)H biosynthesis as well as NADPH/NADP⁺ ratios. The light-induced decrease in the NADPH/NADP⁺ ratio is probably attributable to the Calvin-Benson cycle being activated under these conditions. In the *trxf1 ntrc* mutant, the diurnal changes in the sum of NADPH and NADP⁺ levels were strongly attenuated (Fig. 6A), while there was a clear increase in the NADPH/NADP⁺ ratio at the end of the day (3-fold) and at the end of the night (2-fold), compared to wild-type (Fig. 6B). No changes were observed in the *trxf1* mutant while in the *ntrc* mutant the NADPH/NADP⁺ ratio was slightly but significantly increased (Figs. 6A and 6B). The wild-type also showed diurnal changes in the sum of NADH and NAD⁺ (Fig. 6C) and in the NADH/NAD⁺ ratio (Fig. 6D), with the former decreasing and the latter increasing towards the end of the day. In the *trxf1 ntrc* mutant, the sum of NADH and NAD⁺ was further decreased, while the NADH/NAD⁺ ratio further increased, compared to wild-type.

In the wild-type, the diurnal changes in NADP redox state were accompanied by corresponding changes in adenylate energy state, with ATP/ADP ratios being decreased at the end of the day as compared to the end of the night (Fig. 6F). This is most probably attributable to light-activation of the Calvin-Benson cycle and other ATP-consuming biosynthetic processes. In the *trxf1 ntrc* mutant, diurnal changes in both adenylate levels (Fig. 6E) and ATP/ADP ratios (Fig. 6F) were opposite to the wild-type, being increased during the day relative to the night, while the *trxf1* and *ntrc* single mutants were largely similar to wild-type (Figs. 6E and 6F).

Overall these results show that a combined deficiency of Trx *f1* and NTRC causes major alterations in both NADPH/NADP⁺ and ATP/ADP ratios during the day, indicating that the primary cause for the strong impairment of photosynthesis is an inhibition of the Calvin-Benson cycle rather than the light reactions.

Combined deficiency of Trx *f1* and NTRC impairs redox-activation of fructose-1,6-bisphosphatase

The above described results show that the combined deficiency of Trx *f1* and NTRC causes impairment of photosynthetic parameters, the diurnal oscillation of energy availability and carbon fixation rate. We then analyzed whether this could be due to direct effects on enzymes of the Calvin-Benson cycle or NADPH export from the chloroplast. To this end we focused on FBPase and NADP-MDH, representing key-regulatory steps of these processes and classical targets of Trx *f* and Trx *m*, respectively (Zimmermann et al., 1976). FBPase is known to be subject to exquisite light-activation via the Fdx-Trx *f* system, leading to reduction of an intra-molecular disulfide that promotes activation of the enzyme. To analyze the effect of a combined deletion of NTRC and Trx *f1* on redox regulation of FBPase, the redox status of the chloroplast enzyme was analyzed *in vivo* by labeling of thiol groups with the alkylating agent MM-PEG₂₄, which adds 1.5 kDa per thiol, thus causing a switch of the electrophoretic mobility of the reduced form of the enzyme as compared to the oxidized form. In the wild-type, FBPase protein was completely oxidized at the end of the night, while more than 50% of the protein was in the reduced state at the end of the day (Fig. 7A), confirming light-induced reduction of its intra-molecular disulfide *in vivo*. This response was strongly modified in the redox mutants. At the end of the day, the ratio of reduced to oxidized FBPase protein was substantially decreased in *trxf1* and *ntrc* single mutants relative to the wild-type, while there was an even stronger decrease in the double mutant (Fig. 7A). No changes were observed between the genotypes at the end of the night. Results from four independent experiments were quantified and are summarized in Fig. 7B, showing that the ratio of reduced to oxidized FBPase protein decreased significantly by 40% in *trxf1*, 20% in *ntrc* and 70% in *trxf1 ntrc* mutants relative to the wild-type, indicating an additive effect in the double mutant. Finally, it was noticed that the content of chloroplast FBPase protein in the double mutant was slightly decreased as compared with the

wild type or single mutants (Fig. 7A) suggesting minor effects on FBPase protein turnover in addition to post-translational thiol-disulfide modulation.

We then investigated whether a deficiency in *Trx f1* and NTRC also affects FBPase enzyme activity. In leaves of the wild-type, FBPase activity was very low at the end of the night and increased 20-fold towards the end of the day (Fig. 7C), confirming previous studies (Chiadmi et al., 1999). This response was strongly attenuated in the redox mutants. At the end of the day, FBPase activity was progressively decreased down to 40, 80 and 7% of wild-type level in *trxf1*, *ntrc* and *trxf1 ntrc* mutants, respectively, while there were no significant changes between these genotypes at the end of the night. In the double mutant, no significant changes between nocturnal and day-time FBPase activity were observed, indicating that diurnal activation of FBPase has been abolished. The data also show a correlation between FBPase activity and FBPase redox-state across different genotypes and day-night conditions (compare Figs. 7B and 7C), confirming the major role of thiol-disulfide modulation in regulating FBPase enzyme activity in-vivo. To investigate transient light-activation of FBPase in a detailed time course, FBPase activity was analyzed in leaves 0, 2, 5, 10, 20 and 30 min after illumination. As shown in Fig. 7D, light led to a rapid increase in FBPase activity, reaching half-maximal activity within 1 min after the start of illumination in the wild-type. Compared to wild-type, the increase in FBPase activity was significantly delayed by approx. 50% in *trxf1* and *ntrc* single mutants, reaching half-maximal activities 5 and 10 min after the start of illumination, respectively. Between 10 and 30 min, FBPase activity showed no further increase or increased only slightly, with *trxf1* and *ntrc* mutants both saturating at approx. 50% of wild-type level. Intriguingly, combined deficiency of *Trx f1* and NTRC led to a complete loss in light-activation of FBPase, with the double mutant showing no significant increase in FBPase activity upon illumination. When FBPase activity was measured in the presence of 10 mM DTT in the assay medium to fully reduce the regulatory disulfide of the enzyme, no significant changes were detected in the different genotypes and light conditions, except a slight decrease of the maximal FBPase activity in the *trxf1 ntrc* mutant compared to wild-type and single mutants (Fig. 7E). The ratio between the activities in the two assay conditions (minus DTT versus plus DTT) is shown as a calculated redox-activation state in Fig. 7F. The changes in the redox-activation state followed similar curves as the initial activities measured without DTT (compare Figs. 7D and

7F). The results show that knockout of *Trx f1* led to a decreased efficiency in light activation of FBPase which is in-line with earlier studies showing that chloroplast FBPase is redox-activated by *f*-type Trx in vitro (Collin et al., 2003). However, deletion of *Trx f1* only led to a 50% inhibition in FBPase activation, which is similar to the degree of inhibition in the *ntrc* mutant, indicating that neither of these redox systems has an exclusive role in the redox-regulation of FBPase in-vivo. Moreover, the almost complete loss of light-dependent activation of FBPase in the *trxf1 ntrc* mutant strongly suggests the synergistic effect of Trx *f* and NTRC in FBPase redox regulation.

For comparative purposes, we also measured the activity of NADP-dependent malate dehydrogenase (MDH), a chloroplast enzyme involved in the export of NADPH to the cytosol, which is known to be primarily regulated by *m*-type Trxs (Scheibe, 2004). In the wild-type, NADP-MDH activity was higher at the end of the day compared to the end of the night (Fig. 8A), confirming previous studies on the light-activation of this enzyme in the chloroplast stroma (Scheibe, 2004). Interestingly, this response was promoted rather than inhibited in the redox mutants. Compared to wild-type, *trxf1*, *ntrc* and *trxf1 ntrc* mutants showed increased activation of NADP-MDH during the day, while there were no substantial changes observed in the night. When NADP-MDH activity was measured in the presence of 10 mM DTT in the assay medium to fully reduce the regulatory disulfide of the enzyme, no substantial changes were detected across the different genotypes and light conditions (Fig. 8B). The ratio between the activities in the two assay conditions (minus DTT versus plus DTT) is shown as a calculated redox-activation state (Fig. 8D). It followed a similar curve as the initial activities measured without DTT (compare Figs. 7D and 7F). Increased activation of NADP-MDH is probably due to increased chloroplast NADPH/NADP⁺ ratios (Fig. 6), which promote NADP-MDH redox-activation by acting on the redox-potential of its regulatory disulfide (Faske et al., 1995).

Combined deficiency of *Trx f1* and NTRC leads to decreased starch accumulation and redox-activation of ADPGlc pyrophosphorylase

Following with our purpose of determining the function of *Trx f1* and NTRC in redox regulation of different carbon metabolic pathways, we investigated the effect of the

combined deficiency of *Trx f1* and *NTRC* on the synthesis of photosynthetic end products, starch and sucrose. Wild-type leaves showed characteristic diurnal changes of starch (Fig. 9A) and sucrose levels (Fig. 9B), which increased by 3- and 2-fold, respectively, towards the end of the day. These diurnal changes were attenuated in the redox-mutants. At the end of the day, *trxf1*, *ntrc* and *trxf1 ntrc* mutants showed a progressive decrease in starch accumulation down to 80, 65 and 25% of wild-type levels, respectively (Fig. 9A), confirming previous studies showing attenuation of starch accumulation in *trxf1* (Thormahlen et al., 2013) and *ntrc* single mutants (Michalska et al., 2009; Lepisto et al., 2013). The decrease in day-time starch content was additive in the double mutant (Fig. 9A), dropping to levels below those of the wild-type at the end of the night. At any time, the starch content in the double mutant did not exceed nocturnal wild-type levels. At the end of the night, *trxf1*, *ntrc* and *trxf1 ntrc* mutants showed a further progressive decrease in the remaining starch content, reaching 35, 25 and less than 10% of the nocturnal wild-type level, respectively (Fig. 9A), showing that starch reserves were exhausted in the double mutant. The *trxf1 ntrc* mutant showed decreased accumulation of sucrose, which at a lower level was also affected in the *ntrc* mutant but not in the *trxf1* mutant (Fig. 9B). All mutants under analysis showed a decrease of the starch/sucrose ratio relative to the wild-type, the decrease being more pronounced in the *trxf1 ntrc* double mutant with 55% at the end of the day and 80% at the end of the night (Fig. 9C).

AGPase is a key-enzyme of starch synthesis, which is rapidly activated upon illumination by reduction of an intermolecular disulfide bond between the Cys-81 residues joining the two small subunits (APS1) of this heterotetrameric enzyme (Hendriks et al., 2003; Kolbe et al., 2005). To investigate whether the inhibition of starch synthesis in the different genotypes is due to decreased redox-activation of AGPase, monomerisation of APS1 was analyzed in leaves harvested at the end of the night and at the end of the day. As seen in previous studies (Hendriks et al., 2003), wild-type leaves revealed a strong increase in the monomerization of APS1 during the day, while APS1 was almost completely dimerized in the night (Fig. 9D). Compared to wild-type, light-dependent monomerisation of APS1 was attenuated in the *trxf1* and *ntrc* single mutants (Fig. 9D), confirming results from earlier studies (Michalska et al., 2009; Thormahlen et al., 2013). Compared to the single mutants, there was an additional attenuation of APS1 monomerisation in the *trxf1 ntrc* double

mutant (Fig. 9D), indicating Trx *f1* and NTRC to act additively on the reduction of APS1 in vivo.

Combined deficiency of Trx *f1* and NTRC causes deep effects on metabolite levels

The above data clearly indicate the combined action of Trx *f* and NTRC on redox regulation of different aspects of carbon metabolism. The impairment of the regulation of the Calvin-Benson cycle and attendant starch synthesis in the mutants under investigation is expected to provoke changes of in-vivo metabolite levels indicative of regulatory steps in these pathways. In wild-type plants, the levels of 3-phosphoglycerate (3PGA) (Fig. 10A), fructose-1,6-bisphosphate (FBP) (Fig. 10B) and fructose-6-phosphate (F6P) (Fig. 10C) showed strong diurnal alterations, higher levels being observed at the end of the day, which is in-line with the changes in Calvin-Benson cycle activity. These diurnal changes in metabolite levels were differentially modified in the *trxf1 ntrc* mutant. Compared to wild-type, the day-time increase in the level of 3PGA, the first fixation product of Rubisco, was attenuated by 75% in the *trxf1 ntrc* mutant, while there were no changes in the *trxf1*, and only a smaller decrease (by 35%) in the *ntrc* mutant (Fig. 10A). In contrast to this, the day-time levels of FBP, the substrate of FBPase, were significantly increased by 50, 125 and 75% in *trxf1*, *ntrc* and *trxf1 ntrc* mutants, respectively (Fig. 10B), while those of F6P, the product of FBPase, were only slightly increased in *trxf1* and *ntrc* single mutants, or even decreased in the *trxf1 ntrc* double mutant, compared to wild-type (Fig. 10C). Concerning the ratio between product and substrate of FBPase (F6P/FBP), there was a significant and progressive decrease down to 80, 55 and 45% of wild-type level in *trxf1*, *ntrc* and *trxf1 ntrc* mutants, respectively (Fig. 10D), indicating a progressive inhibition of plastidial FBPase in vivo and confirming the decrease in FBPase activity and reduction state (Fig. 7). Compared to wild-type, glucose-1-phosphate (G1P), the substrate of AGPase, remained unchanged or increased slightly in the different genotypes, indicating that the inhibition of starch synthesis was unlikely to be due to a shortage of this substrate (Fig. 10F). At the end of the night, the levels of 3PGA (Fig. 10A) and hexose-phosphates (Figs. 10C, E, F) all showed a progressive decrease in *trxf1*, *ntrc* and *trxf1 ntrc* mutants relative to the wild-type, with the decrease being specifically pronounced in the *trxf1 ntrc* double

mutant. This is consistent with a progressive shortage of carbon in these mutants. Nocturnal levels of FBP were below the detection limit in all genotypes (Fig. 10B).

To gain a more in-depth insight into the global effects of Trx f1 and NTRC on redox regulation of metabolism, GC-MS based metabolite profiling was performed. Suppl. Table S4 and Fig. 11A show significant changes in leaf metabolite levels at the end of the day in *trxf1*, *ntrc* and *trxf1 ntrc* mutants, relative to the wild-type. In the *trxf1 ntrc* mutant, sugars like glucose and raffinose decreased by a factor of 2, while the levels of maltose and ribose were 3-times and the level of trehalose 2-times increased. Similar or less strongly expressed changes in sugar levels were observed in the *ntrc* mutant, while sugar levels remained rather unchanged or increased slightly in the *trxf1* mutant. Several organic acids showed a significant decrease in both *ntrc* and *trxf1 ntrc* mutants, such as citrate, fumarate, glycerate, 2-oxoglutarate, shikimate, succinate and threonate, while malate decreased only in the double mutant. The decrease in glycerate (3-fold), suggests possible effects on photorespiration. In contrast to this, organic acid levels were largely unchanged or showed only slight alterations in the *trxf1* mutant. Also amino acids showed large and significant alterations in the *trxf1 ntrc* mutant. With the exception of glycine and serine which were both 2-fold decreased, most other amino acids were increased in the double mutant, this is the case of alanine (1.4-fold), aspartate (1.8-fold), asparagine (2-fold), isoleucine (2.3-fold), leucine (2-fold), methionine (1.4-fold), phenylalanine (6.7-fold), proline (7.2-fold), valine (2.2-fold). Amino acids remained unchanged or showed only slight changes in the *trxf1* and *ntrc* single mutants, with the exception of glycine and serine, which both decreased by a similar degree in the *ntrc* single and *ntrc trxf1* double mutants. The decrease in glycine and serine is consistent with NTRC having effects on photorespiration. This confirms previous studies, indicating increased photorespiration in the *ntrc* mutant (Lepisto et al., 2009). Other metabolites showed a more pronounced or differential behavior in the double mutant compared to the single mutants. In the *trxf1 ntrc* mutant, there were significant increases in erythritol (7.4-fold), glycerol (1.4-fold), mannitol (8-fold), 4-amino-butanoate (5-fold), putrescine (2-fold) and uracil (3.4-fold), while myo-inositol was decreased (2.4-fold), compared to wild-type. The strong increase in ascorbate which was observed in the *trxf1* and *ntrc* single mutants was strongly attenuated in the double mutant.

Metabolite levels were also determined at the end of the night where sugars derive from the degradation of starch reserves (Suppl. Table S5 and Fig. 11B). Compared to wild-type, *trxf1*, *ntrc* and *trxf1 ntrc* mutants showed a further progressive decrease in the levels of various sugars, with the double mutant revealing a specifically strong decrease in maltose (down to 19% of wild-type level) and sucrose (46% of wild-type level) consistent with an increased shortage of carbon under these conditions. There were significant decreases in the levels of various organic acids, which in most cases were more severe in the double mutant, compared to the single mutants, specifically fumarate, glycerate, pyruvate, shikimate and succinate. Large and significant alterations were observed in the levels of various amino acids, which increased in the double mutant, compared to wild-type or the single mutants. While glycine decreased, there were increases in the levels of alanine (3-fold), arginine (7.5-fold), asparagine (43.7-fold), glutamate (1.9-fold), isoleucine (4-fold), leucine (3.3-fold), lysine (10.2-fold), phenylalanine (10.3-fold), proline (2.4-fold), serine (2.3-fold), threonine (2-fold) and valine (2.6-fold). The 1.5-fold decrease in shikimate, while phenylalanine levels were more than 10-fold increased, indicates aromatic amino acid synthesis and related pathways to be strongly perturbed by the combined deficiency of Trx *f1* and NTRC. An accumulation of aromatic amino acid levels was also found in the *ntrc* mutant in previous studies, where it was suggested to be due to a decrease in phenol or auxin synthesis (Lepisto et al., 2009). In the double mutant, there were also changes in other selected metabolites: erythritol, glycerol, mannitol, sorbitol, P_i, putrescine, spermidine and uracil increased, while myo-inositol decreased relative to the wild-type (Suppl. Table S5).

In vivo BiFC assays provide direct evidence of Trx *f1* and NTRC interaction in vivo

To further investigate the interrelation between Trx *f1* and NTRC, we analyzed a possible physical interaction between both proteins using the in vivo BiFC assay (Fig. 12). To do this, *Nicotiana benthamiana* leaves were coinfiltrated with *Agrobacterium tumefaciens* cells carrying gene fusion constructs that encode Trx *f1* or NTRC combined at their C-termini with either the N- or C-terminal part of the Venus protein, which is a yellow fluorescent protein (YFP) derivate. When Trx *f1* was fused with the Venus N-terminal part and NTRC with the Venus C-terminal part, a strong fluorescent

signal was observed in chloroplasts, which was identified as a YFP signal by Lambda scanning of its fluorescence spectrum (data not shown). A similar signal was observed when *Trx f1* was combined with the Venus C-terminal part and NTRC with the Venus N-terminal part. This indicates that *Trx f1* and NTRC interact with each other in planta. Cotransformation of NTRC fused to the N-terminal part of the Venus protein with NTRC fused to the C-terminal part of the Venus protein served as a positive control (Fig. 12), which is in-line with previous studies (Richter et al., 2013). As observed previously, there is an association of NTRC to dimeric and oligomeric structures in higher plants (Perez-Ruiz et al., 2009; Wulff et al., 2011). Interestingly, YFP signals were also observed when *Trx f1* combined with the Venus C-terminal part was cotransformed with *Trx f1* combined with the Venus N-terminal part, indicating dimerization of *Trx f1* in planta. This confirms previous studies showing that *Trx f* exists in an oligomeric state in *Arabidopsis* plants (Sanz-Barrio et al., 2012). No YFP signal was observed when *Trx f1* and NTRC - combined with either the Venus N- or C-terminal part - were expressed separately as negative controls.

GUS analysis of *Trx f1* expression (Suppl. Figure S2) reveals a pattern similar to NTRC expression in *Arabidopsis* plants (Kirchsteiger et al., 2012). This indicates that *Trx f1* and NTRC are both active in the same tissues, highlighting the biological relevance of their interaction.

DISCUSSION

Two different thiol redox-systems exist in plant chloroplasts, the Fdx-Trx, which is dependent of Fdx reduced by the photosynthetic electron transport chain and, thus, of light, and the NADPH-NTRC system, which relies on NADPH and thus may be operative also during the night. Previous in-vitro studies led to the view that both systems may act independently in the chloroplast stroma, however, the possibility remains that both systems might act cooperatively. In the present work we have tested this possibility by a combination of genetic and biochemical approaches. Results provide evidence that both redox systems interact at the level of *Trx f1* and NTRC and coordinately participate in the regulation of photosynthetic carbon metabolism and growth in response to changes in light conditions.

Trx *f1* and NTRC coordinately participate in redox regulation of the Calvin-Benson cycle in response to light

Our results show that single knockouts of Trx *f1* or NTRC cause no or only slight impairment of photosynthesis (Fig. 3 and 4), respectively, confirming previous studies (Lepisto et al., 2009; Thormahlen et al., 2013). Interestingly, the combined deficiency of both thiol redox-regulators led to a more severe inhibition of photosynthetic CO₂-assimilation (Fig. 3) and electron transport rates (Fig. 4) than in both single knockouts. This was accompanied by an increase in both the NADPH/NADP⁺ and ATP/ADP ratios (Fig. 6), indicating that the primary cause for the strong impairment of photosynthesis is an inhibition of the Calvin-Benson cycle rather than the light reactions. Direct measurements of FBPase, a key enzyme of the Calvin-Benson cycle, confirm this interpretation (Fig. 7). Light activation of FBPase was attenuated by up to 50% in the Trx *f1* and NTRC single mutants, while it was almost completely abolished in the double mutant (Fig. 7). A similar picture emerged when the redox-state of the regulatory disulfide of chloroplast FBPase was directly analyzed using gel-shift assays in vivo (Fig. 7). The sensitivity of the FBPase protein per se towards redox-regulation was however not altered, since addition of DTT led to a strong activation of the enzyme in extracts from the double mutant in-vitro (compare Figs. 7D and 7E). This shows that a combined knockout of Trx *f1* and NTRC leads to deregulation of FBPase by disturbing the light signal leading to its redox-activation. This ultimately leads to a decrease in Calvin-Benson cycle activity (Fig. 3) and growth (Fig. 2), which is in-line with earlier studies on transgenic plants (Koßmann et al., 1994) or mutants (Livingston et al., 2010) showing that a decrease in chloroplast FBPase activity below 36% of wild-type level affects photosynthetic CO₂ assimilation and growth. Inhibition of FBPase is also indicated at the metabolite level, since it is accompanied by a decrease in F6P/FBP metabolite ratios in-vivo (Fig. 10D). In contrast to the strong effect on FBPase, combined knockout of Trx *f1* and NTRC did not lead to any inhibition in the redox-activation of NADP-MDH (Fig. 8), demonstrating the specificity of the effects.

In textbooks, Trx *f* is proposed to act as the exclusive thiol redox-regulator of FBPase and other enzymes of the Calvin-Benson cycle, a scenario which is mainly based on in-vitro studies performed during the last 40 years. Our in-vivo studies show that this

paradigm has to be revised. First, a decrease in Trx *f* protein level by more than 97% in the single mutant (Thormahlen et al., 2013) (Fig. 1B) only partly affects light-activation of FBPase by 40-50% (Fig. 7), while it does not affect photosynthesis (Fig. 4), Calvin-Benson cycle activity (Fig. 3) or growth (Fig. 2). This indicates that Trx *f* is either redundant or so far in excess that a strong decrease in its level still allows a sufficient regulation of the Calvin-Benson cycle. The latter however is unlikely given that in the wild-type high levels of Trx *f* are not sufficient to fully reduce chloroplast FBPase in the light (Fig. 7A and 7B). The small residual activity of Trx *f2* - approx. 1-3% of total wild-type Trx *f* protein level (Thormahlen et al., 2013) – remaining in the *trxf1* mutant will therefore not be high enough to provide sufficient activation of the Calvin-Benson cycle in the light. Secondly, our results provide evidence for an unexpected role of NTRC in the regulation of the Calvin-Benson cycle. Knockout of NTRC in the wild-type background led to an up to 50% attenuation in thiol-based light activation of FBPase, while there was a nearly complete attenuation when NTRC knockout was performed in the *trxf1* mutant background (Fig. 7). There is the possibility that NTRC may directly transfer electrons from NADPH to FBPase to directly activate the enzyme. This however would require sensitive regulation of NTRC activity to prevent activation of FBPase and the Calvin-Benson cycle also in the night. Alternatively, NTRC may act as an activator of Trx *f*, either by allosteric effects or by direct electron transfer. While physical interaction between Trx *f1* and NTRC has been shown *in vivo* (Fig. 12), more detailed studies are needed to investigate this phenomenon *in vitro*.

Trx *f1* and NTRC are also involved in light acclimation of photosystem I

Impaired photosynthetic light reactions in the *trxf1 ntrc* mutant were most likely a consequence of the inhibition of the Calvin-Benson cycle and the subsequent increase in NADPH/NADP⁺ ratios. Combined knockout of Trx *f1* and NTRC led to a strong decrease in the abundance of PSI core proteins (Fig. 5), which was most likely due to an inhibition of electron transfer at the acceptor side of PSI, leading to its over-reduction. As shown by previous studies, PSI is very sensitive to excess electrons delivered from PSII due to its limited capacity of regeneration by protein turnover (Suorsa et al., 2012; Tikkanen and Aro, 2014). The moderate decrease in the abundance of PSII core proteins (Fig. 5) and in chlorophyll levels (Suppl. Fig. S1) is

most likely part of an adaptive response to relieve the electron pressure on PSI and to protect PSI from photo-damage (Grieco et al., 2012; Suorsa et al., 2012; Tikkanen et al., 2014). The decreased ability of the *trxf1 ntrc* mutant to adapt to high-light conditions (Fig. 2F) provides further evidence for a role of Trx f1 and NTRC in light-acclimation of PSI. Proteins involved in cyclic electron transport around PSI may also be part of an adaptive response to preserve PSI, although their specific functions remain to be clarified (Livingston et al., 2010; Suorsa et al., 2012; Hertle et al., 2013). Interestingly, an Arabidopsis mutant deficient in chloroplast FBPase showed impaired linear electron transport and increased cyclic electron flow (Livingston et al., 2010). More studies are needed to resolve the roles of the stromal redox-regulators Trx f1 and NTRC in the regulatory network of plant thylakoid energy transduction.

Alternatively, our data could indicate more specific effects of Trx f1 and NTRC on chloroplast protein synthesis. It has been shown in previous studies that light plays a crucial role in regulating chloroplast protein translation, which most likely involves the Fdx-Trx system as one of the underlying signaling pathways (Pfannschmidt and Liere, 2005). More recently, a role of NTRC was proposed to regulate translation of the D2 protein of PSII by thiol-disulfide modulation of chloroplast translation factors in *Chlamydomonas reinhardtii* (Schwarz et al., 2012). However, in-vivo evidence to support this conclusion is lacking at the moment.

Trx f1 and NTRC act additively in redox-regulation of starch metabolism

The results of the present study confirm previous studies in showing that single knockouts of Trx f1 or NTRC lead to partial inhibition of AGPase redox-activation (Michalska et al., 2009; Thormahlen et al., 2013) and starch synthesis (Michalska et al., 2009; Lepisto et al., 2013; Thormahlen et al., 2013) in Arabidopsis plants. However, they also extend previous studies in showing that Trx f1 and NTRC act additively in redox-regulation of AGPase and starch synthesis (Fig. 9). The additive effect on the APS1 reduction state is probably attributable to Trx f1 and NTRC being both able to reduce APS1 with similar efficiencies, as observed by in-vitro studies (Thormahlen et al., 2013). The additive effect on starch accumulation is partly due to redox-regulation of AGPase and the concomitant regulation of the Calvin-Benson cycle. Interestingly, combined deficiency of Trx f1 and NTRC led to a strong increase

in the level of the starch degradation product maltose in the light (Fig. 11A and Table 1). This may indicate that in addition to their effect on starch synthesis, Trx *f1* and NTRC coordinately participate in the diurnal regulation of starch degradation. This is in-line to previous studies reporting that several enzymes in the pathway of starch degradation are subject to thiol redox-regulation in vitro (Valerio et al., 2011; Glaring et al., 2012). Specifically, a plastid-targeted beta-amylase has been shown to be regulated by both Trx *f1* and NTRC in vitro (Valerio et al., 2011). It remains to be determined whether a similar mechanism is operational in-vivo.

Combined deletion of Trx *f1* and NTRC resulted in a strong decrease in the levels of nearly all sugars, sugar phosphates and organic acids, while the levels of most amino acids increased (see Suppl. Tables S4 and S5, and Fig. 11). These changes were specifically pronounced at the end of the night, when the carbon reserves of the double mutant were almost completely exhausted. Under these conditions, the strong increase in the levels of nearly all amino acids could indicate that protein degradation has been stimulated to mobilize additional carbon reserves. Alternatively, low sugar levels may have led to an increase in amino acid levels to prevent osmotic imbalances in the tissue (Fernie et al., 2002; Faix et al., 2012).

Trx *f1* and NTRC coordinately participate in the acclimation of plant growth to varying light conditions

In the *trxf1 ntrc* mutant, deregulation of the Calvin-Benson cycle and starch metabolism led to strong effects in plant growth (Fig. 2). The combined deficiency of Trx *f1* and NTRC specifically affected growth acclimation to varying light conditions, leading to severely impaired acclimation of plant growth to a decrease in the length of the photoperiod or changes in light intensities (Fig. 2H). The ability to acclimate to a 4 h photoperiod or to low light ($30 \mu\text{mol photons m}^{-2} \text{ s}^{-1}$) was almost completely lost, as well as the ability to acclimate to high-light conditions ($950 \mu\text{mol m}^{-2} \text{ s}^{-1}$). Impaired photoperiod acclimation recovered only partly in continuous light, indicating that deregulation of starch synthesis (Fig. 9A) only partly contributes to the vulnerability of the double mutant to decreased photoperiods. The strong decrease in CO_2 assimilation rates and the resultant carbon depletion will be additional factors contributing to impaired growth acclimation to short days in the double mutant (Figs.

3 and 11). Deregulation of photosynthesis is also the most likely reason for the decreased ability to acclimate to low light, while the decreased ability to acclimate to high light is most likely attributable to the increased sensitivity of PSI to photo-damage in the double mutant (see Fig. 5 and discussion above). The strong depletion in soluble sugars prevailing in the double mutant (Fig. 11) may have contributed to the decrease in its ability for high-light acclimation, compared to wild-type. As shown in previous studies, soluble sugars act as signals in the high-light response of *Arabidopsis* plants, while high-light acclimation is impaired when soluble sugar levels are decreased (Schmitz et al., 2014).

Vulnerability in the acclimation of plant growth to a decrease in the length of the photoperiod or changes in light intensities (Fig. 2H) was less strongly expressed in the *trxf1* and *ntrc* single mutants, compared to the double mutant. Single deficiency of *Trx f1* led to partly impaired acclimation of plant growth to extreme light conditions, such as 4h-photoperiods or very low light intensities ($30 \text{ } \mu\text{mol photons m}^{-2} \text{ s}^{-1}$). Single deficiency of NTRC led to a partly impaired acclimation of plant growth to a decrease in the length of the photoperiod below 16h. This is most likely attributable to knockout of NTRC leading to an inhibition of starch accumulation (Fig. 9A), confirming earlier studies (Lepisto et al., 2009). However, growth did not fully recover to wild-type levels in continuous light (Fig. 2H), implying that other factors besides the deregulation of starch synthesis contribute to the growth phenotype of the *ntrc* mutant. As shown in Figs. 3 and 11, NTRC knockout leads to a slight attenuation of CO_2 assimilation and decreased carbon availability. Overall these results provide in-planta evidence that stromal redox regulation at the levels of *Trx f1* and NTRC is essential for acclimation of plant growth to varying light conditions.

Trx f1 and NTRC are interactive in vivo

The analyses here reported of the *Arabidopsis* mutant with combined inactivation of *Trx f1* and NTRC provide genetic evidence for a cooperative synergistic role of *Trx f1* and NTRC in regulating photosynthetic metabolism and growth, thus suggesting their functional interaction in vivo (Figs. 1-11). Results from BiFC assays provide direct evidence for physical interaction between *Trx f1* and NTRC at the protein level in-vivo (Fig. 12). Our results are in-line with recent studies, showing that complementation of

the *ntrc* mutant with the full-length *NTRC* gene containing an active NTR but an inactive Trx domain, or vice versa, recovered wild-type chloroplast phenotype, indicating that NTRC is capable of interacting with other chloroplast Trx systems to compensate a loss in activity of one of its domains in vivo (Toivola et al., 2013). NTRC from different plant species is characterized by a homo-dimeric structure which is important for its catalytic activity (Perez-Ruiz et al., 2009; Bernal-Bayard et al., 2012; Lee et al., 2012; Toivola et al., 2013). According to the proposed reaction model, electrons are transferred from the NTR domain of one subunit to the Trx domain of the second subunit, which subsequently reacts with target proteins (Pérez-Ruiz and Cejudo, 2009; Lee et al., 2012). Reduction of the Trx domain is proposed to be accompanied by conformational alterations in the NTRC dimer, leading to exposition of the NTR active site which may promote the interaction of this domain and free Trxs (Bernal-Bayard et al., 2012; Toivola et al., 2013). Supplementation of the Trx domain in the NTRC homo-dimer model by different types of free Trxs indicated that Trx *f* is the most likely partner to interact with NTRC (Toivola et al., 2013). Our BiFC results provide direct evidence in favor of this model by showing physical interaction between NTRC and Trx *f1* in vivo (Fig. 12), while our results with the *trxf1 ntrc* double mutant indicate interaction between Trx *f1* and NTRC to be of functional importance. This is consistent with recent studies, showing that overexpression of Trx *f* (Sanz-Barrio et al., 2013) and NTRC (Toivola et al., 2013) cause an unexpected increase in plant growth and biomass yield, which supports the view of a synergistic interaction between both thiol redox-regulators (Toivola et al., 2013). Interestingly, interactive effects between NTRC and free Trxs have not been observed in in-vitro studies (Pérez-Ruiz et al., 2006; Bohrer et al., 2012). This could be due to NTRC forming oligomeric structures under these conditions (Wulff et al., 2011) which may prevent its interaction with free Trxs in vitro (Toivola et al., 2013).

METHODS

Plant material and growth conditions

Arabidopsis thaliana T-DNA insertion lines *trx f1* (SALK_128365) (Thormahlen et al., 2013), *ntrc* (SALK_012208) (Perez-Ruiz et al., 2006), the double mutant *trxf1 ntrc*, generated by cross breeding, and the respective Col-0 wild-types were grown for five

weeks on potting soil (Stender, Germany) in a growth chamber with 8 h photoperiod, 160 μmol photons $\text{m}^{-2} \text{ s}^{-1}$, 20°C/16°C, and 60%/75% humidity (day/night), if not indicated otherwise in the figure legends. For rosette fresh-weight determination, plants were grown for the first week under the conditions indicated above, before they were transferred to 16 h or 24 h photoperiods for additional 3 weeks or to 4 h photoperiod, 30 or 950 μmol photons $\text{m}^{-2} \text{ s}^{-1}$ for additional 4 weeks using a growth chamber at 21°C. For all metabolite, DNA or protein extractions, leaves were shock-frozen directly into liquid nitrogen, and subsequently homogenized to a fine powder using a liquid nitrogen-cooled ball mill (MM 400, Retsch GmbH, Haan, Germany).

Selection and molecular characterization of the knockout lines

The *trxf1 ntrc* mutant was selected after crossing the well-characterized homozygous parental lines carrying T-DNA insertions in *Trx f1* (Thormahlen et al., 2013) and *NTRC* genes (Perez-Ruiz et al., 2006). The selection of a homozygous line with insertion in both alleles was performed by PCR analyses of genomic DNA using gene-specific primers for the *trx f1* (At3g02730; 5`-TGTCAAGTGGTCAGGTGAC-3` and 5`-AGAACCCATCCAACACACTTG-3`) and *ntrc* (At2g41680; 5`-TATTGAGCAACACCAAGGGAC-3` and 5`-CATAATTCCAGCTGCTTCAGC-3`) genes or oligonucleotides of the T-DNA (5`-ATTTGCCGATTCGGAAC-3`). PCR products were fractionated on 1 % agarose gels, and visualized by ethidium bromide staining. Detection of *Trx f* and *NTRC* proteins was done by Western blot analysis (Laemmli, 1970) using antibodies raised against pea *Trx f* (Hodges et al., 1994) and rice *NTRC* (Serrato et al., 2004). To do this, frozen leaf powder was extracted with 2-fold Laemmli buffer (Laemmli, 1970) including 20 mM DTT instead of β -mercaptoethanol. After shaking the extract for 3 min with 90°C, each lane of the polyacrylamide gels was loaded with sample corresponding to 1 mg fresh weight for each genotype. The pea *Trx-f* antibody used in these experiments has been found in previous studies to recognize *Arabidopsis Trx f1* and *Trx f2* recombinant proteins with comparable efficiencies (Thormahlen et al., 2013).

Gas exchange measurements

Photosynthesis-related gas exchange parameters were determined on 4 to 5 week old plants with the portable GFS-3000 system (Heinz Walz GmbH, Effeltrich, Germany). The control unit 3000-C with the measuring head 3010-S was used by adapting the cuvette to *Arabidopsis* Chamber 3010-A. The conditions within the cuvette were 22°C, 60% relative humidity and ambient CO₂ concentrations, while the impeller speed was set to 7, and the flow rate to 750 µmol s⁻¹. The monitoring of the light curve was started with darkened rosettes. When the CO₂ and H₂O system parameters were stabilized, the light was switched on and changed in the following order: 50, 100, 150, 200, 300, 400, 600, 800, 1000 µmol m⁻² s⁻¹. The parameters of CO₂ assimilation rate, transpiration rate and intercellular CO₂ mole fraction were calculated by the software GFS-Win V3.50b (Heinz Walz GmbH, Effeltrich, Germany).

Chlorophyll fluorescence analysis

For the *in vivo* chlorophyll a fluorescence measurement and the calculation of standard photosynthesis parameters of PSII, a Dual PAM fluorometer (Dual-PAM 100, Walz GmbH, Effeltrich, Germany) was used as described previously (Thormahlen et al., 2013).

Analysis of Chlorophyll content

The chlorophyll level was determined photometrically as described in (Scheibe and Stitt, 1988). Leaf extracts were diluted in methanol and the light absorption was measured at 665 nm (Chl a) and 652 nm (Chl b) with an UV/VIS spectrophotometer (Ultrospec 3100 pro, GE Healthcare Europe GmbH, Freiburg, Germany).

Enzyme-coupled analysis of metabolite levels by spectrophotometry

Extraction and analysis of the pyridine nucleotides NAD, NADP, NADH and NADPH were performed as described previously (Lintala et al., 2014). The final detection mix for NAD(H) contained 100 mM Tricine/KOH (pH 9), 4 mM EDTA, 500 mM EtOH, 0.1 mM phenazine ethosulfate (PES), 0.6 mM methylthiazolyldiphenyl-tetrazolium bromide (MTT), 6 U ml⁻¹ alcohol dehydrogenase (ADH). For NADP(H) the final mix

consisted of 100 mM Tricine/KOH (pH 9), 4 mM EDTA, 3 mM glucose 6-phosphate, 0.1 mM PES, 0.6 mM MTT, 6 U ml⁻¹ G6PDH. The extraction of ATP and ADP was performed according to previous studies (Jelitto et al., 1992). In brief, 50 mg frozen leaf powder was extracted with ice-cold 16% TCA (w/v), 5 mM EGTA by vortexing 1 h at 4°C. After centrifugation for 10 min at 4°C with 20,000 g, the supernatant was shortly mixed with 4 ml ice-cold, water-saturated diethyl ether (DEE) and centrifuged again with 3,200 g at 4°C for 5 min. The upper ether phase was discarded to repeat the washing step. The pH adjustment of the remaining water phase was done with 5 M KOH, 1 M triethanolamine or 1 M HCl until a pH of 6-7 was reached. The remaining DEE in the extract evaporated under the hood for 1 h on ice. Directly after the extraction, ATP and ADP levels were measured enzymatically as described previously (Stitt et al., 1989), with the exception that the change in NAD(P)H levels was measured by fluorescence spectroscopy in 96-well micro plates at 360 nm with a FilterMax F5 Multi-Mode Microplate reader (Molecular Devices, Sunnyvale, USA). Starch and sucrose were measured photometrically by NADPH absorption, hexose phosphates, FBP, triose phosphates and 3PGA by NAD(P)H fluorescence as described previously (Thormahlen et al., 2013). Each individual plant sample was measured with at least 2 analytical replicates.

GC-MS analysis of polar primary metabolites

GC-TOFMS-based analysis of primary metabolites was performed exactly as described previously (Thormahlen et al., 2013). For each biological replicate three analytical replicates were measured. To visualize the metabolite changes within an overview, we used the open source software VANTED version 2.1.0 (<http://wanted.ipk-gatersleben.de/>).

Immunodetection of photosynthesis and starch related proteins

Proteins involved in photosynthetic electron transport (PsaA, PsaB, PsbA, PsbD, Lhca1, Lhcb1, PetC, Atpβ), Rubisco (RbcL) and actin were detected by Western blotting using specific antibodies (Agrisera, Vännäs, Sweden) according to company instructions. Frozen leaf powder was extracted with 2-fold Laemmli buffer (Laemmli, 1970) including 20 mM DTT instead of β-mercaptoethanol. After shaking the extract

for 3 min with 90°C, each lane of the polyacrylamide gels was loaded with sample corresponding to 1 mg fresh weight (100%) for each genotype. Immunoblotting of APS1, detection and quantification of ECL signals were performed as described previously (Thormahlen et al., 2013).

FBPase gel-shift assays

For FBPase gel-shift assays proteins from leaves of wild-type and mutant plants, harvested at the end of the night (EN) or the day (ED), were extracted in the presence of 10% (v/v) trichloroacetic acid (TCA) and protein thiols were alkylated with 10 mM MM(PEG)₂₄. For the Western blot analysis, samples were subjected to SDS-PAGE (9.5% polyacrylamide) under non-reducing conditions, transferred onto nitrocellulose membranes and probed with an anti-FBPase antibody kindly provided by Mariam Sahrawy (Estación Experimental del Zaidín, CSIC, Granada, Spain). Quantification of the protein band intensities was done by using the open source software ImageJ version 1.49g (<http://imagej.nih.gov/ij/>).

Enzyme activity measurements

The activity of plastidial FBPase was determined as described in a previous study (Holaday et al., 1992). In short, 20 mg frozen leaf powder was extracted with 1 ml extraction buffer (10 mM MgCl₂, 1 mM EDTA, 0.05 % (v/v) Triton X-100, 100 mM Tris (pH 8, HCl), 1 mM fructose 1,6-bisphosphate) by mixing for about 4 min, followed by a centrifugation step for 5 min at 18.000g at 4°C. 10 µl of the supernatant was added to 190 µl assay mixture in the well of 96-well microplate. The final assay contained 10 mM MgCl₂, 1 mM EDTA, 0.05 % Triton X-100, 100 mM Tris (pH8, HCl), 0.5 mM NADP⁺, 2 units ml⁻¹ G6PDH and 4 units ml⁻¹ PGI. For the maximal activity measurement, 10 mM DTT was included. To start the reaction, FBP (0.1 mM for initial activity and 4 mM for the maximal activity) was added, while NADPH formation was measured spectro-photometrical at 340 nm using a micro-plate reader (HT-3, Anthos Mikrosysteme GmbH, Krefeld, Germany). The activity of NADP-malate dehydrogenase was measured as described previously (Lintala et al., 2014). Every individual plant sample was measured with at least 2 analytical replicates.

Bimolecular fluorescence complementation (BiFC) assays

For BiFC-based protein-protein interaction studies of NTRC and Trx *f1* the entire coding region of each gene was amplified from Arabidopsis (Col-0) cDNA by PCR using the following primer pairs (NTRC-fwd 5'-CACCATGGCTGCGTCTCCAAGATAGGCATCGGTAT-3'/NTRC-rev 5'-TTTATTGGCCTCAATGAATTCTCGTACTCTT-3` and Trxf1-fwd 5'-CACCATGCCTCTTCTCCGTCTTCTCCTCGCC-3/TRXf1-rev 5'-TCCGGAAGCAGCAGACTTCGCTGTTCAATCGC-3'). The PCR products were inserted into the pENTR-D/TOPO (Invitrogen) entry vector and were checked by sequencing. The resulting entry clones were subsequently recombined by using L/R-Clonase (Invitrogen) into a modified GATEWAY-BiFC-vector set (Gehl et al., 2009) based on the pBAR binary vector backbone (Zakharov et al., 2004). Both NTRC and Trx *f1* cDNAs were inserted into the vector pBAR-VYNE and the complementary vector pBAR-VYCE in order to generate gene fusions with either the N-terminal or the C-terminal sub-fragment of the yellow fluorescent protein (Venus), respectively. Each binary vector construct was separately transformed into *Agrobacterium tumefaciens* strain EHA105 for subsequent transient transformation of leaves of 4 week-old *Nicotiana benthamiana* grown in soil under greenhouse conditions (Gehl et al., 2009). The BiFC induced fluorescence of YFP was monitored by Zeiss LSM 780 confocal laser scanning microscope 48 h after co-infiltration of different BiFC-partner into tobacco leaves. BiFC-signals, chlorophyll autofluorescence and bright field images were scanned sequentially in channel mode to prevent any crosstalk between fluorescence channels. The lambda mode was used to confirm the spectral signature of the fluorophores.

Promoter-GUS analysis

An 875 bp fragment of the *Trx f1* gene promoter was amplified from Arabidopsis (Col-0) DNA by standard PCR method using a Phusion DNA polymerase (Thermo Scientific) and the following primer pair (Tf1prom-fwd 5'-TACTGCAGGCGGTGGAGTACGATTAGGACAAAGAA-3'/Tf1prom-rev 5'-TAGTCGACTGTTGAGGAATTCAACAGAGAGACGAT-3'). The PCR product was restricted with *Pst*I and *Sal*I (Thermo Scientific) and cloned into the pBAR binary

vector (Zakharov et al., 2004) containing the GUS-reporter expression cassette. The construct was transformed into cells of the *Escherichia coli* DH5 α strain for amplification and subsequent sequencing of the plasmids. Purified plasmids were used for *Agrobacterium tumefaciens* mediated transformation of *Arabidopsis thaliana* (Col-0) via the floral dip method (Clough and Bent, 1998). Transformed plants were selected for homozygosity and assayed for GUS activity as described previously (Jefferson et al., 1987). GUS stained specimens were bleached in 70% (v/v) ethanol and either directly analyzed by stereomicroscopy (Zeiss Stereo Lumar.V12) or samples were cleared by mounting in Hoyer's solution (100 g chloral hydrate, 5 ml glycerol in 30 ml water). Cleared specimens were imaged by differential interference contrast microscopy (Zeiss Axio Imager.M2).

Statistical Analysis

The statistical data analyses were done with Microsoft office Excel 2007 (*t*-test) and SYSTAT Sigma Plot 11 (two way analysis of variance, Tukey's multiple comparison test). The student *t*-test was done as a two-tailed test assuming unequal or equal variance depending on the data (checked by performing a F-test in the beginning). If the paired *t*-test was used, because of experimental procedures, it is indicated in the figure legends.

ACKNOWLEDGEMENTS

This work was supported by funding from the Deutsche Forschungsgemeinschaft (grants Ge 878/5-2, Ge 878/8-1 and INST 86/1254-1 to P.G.). Work in F.J.C.'s lab was supported by grant BIO2010-15430 of the Spanish Ministry of Science and Innovation. Scientific exchange between Munich and Seville was supported by funds of a German-Spanish interaction program (grant AIB2010DE-00291 to P.G. and F. J.C.). We are grateful to Anne Orwat (LMU Munich) for excellent technical assistance, Ana Luz Rodriguez Muslera (LMU Munich) for performing preliminary work, Dario Leister (LMU Munich) for providing facilities for PAM analysis and a set of antibodies to analyze photosynthetic proteins, Jürgen Soll (LMU Munich) for providing facilities for gas exchange measurement, and to Emmanuelle Issakidis-

Bourguet (University Paris-Orsay, France) and Mariam Sahrawy (CSIC, Spain) for providing anti-Trx *f* and anti-FBPase antibodies, respectively.

AUTHOR CONTRIBUTIONS

I.T., T.M. and P.G. designed research. I.T., T.M, J.G. A.B.Ö., E.v.R.-L., B.N. and F.J.C. performed research. I.T., T.M, J.G. A.B.Ö., E.v.R.-L., B.N., F.J.C. and P.G. analyzed data. I.T., T.M., F.J.C. and P.G. wrote the article.

FIGURE LEGENDS

Figure 1: Molecular characterization of *trxf1*, *ntrc* and *trxf1 ntrc* Arabidopsis mutants compared to wild-type. **(A)** Genotyping by PCR analysis with different primer combinations (wild-type or insertion) for the identification of T-DNA insertions in *Trx f1* and *NTRC* genes. **(B)** Detection of Trx f and NTRC proteins using Western blot analysis. Representative Western blots are shown of measurements, which were performed in leaves of 5-week old plants grown in an 8h-day with 160 μ mol photons $m^{-2} s^{-1}$ light regime harvested 4 h into the light period. Rubisco protein level is shown as control.

Figure 2: Growth analysis of wild-type, *trxf1*, *ntrc* and *trxf1 ntrc* Arabidopsis mutants across different light conditions. **(A)**, **(B)**, **(E)** and **(F)** correspond to 5 week-old plants, while **(C)** and **(D)** correspond to 4 week-old plants, and **(G)** to 7 week-old plants. In the first week, plants - except **(G)** - were grown in an 8 h-day and 160 μ E regime before they were transferred for additional 3-4 weeks to the conditions indicated below: **(A)** 4 h-day and 160 μ E, **(B)** 8 h-day and 160 μ E, **(C)** 16 h-day and 160 μ E, **(D)** 24 h-day and 160 μ E, **(E)** 8 h-day and 30 μ E, **(F)** 8 h-day and 950 μ E, and **(G)** 16 h-day in greenhouse. In **(H)**, rosette fresh-weights of plants corresponding to the conditions shown in **(A)** to **(F)** are given as percent of wild-type levels in the respective conditions. Results are the mean \pm SE, $n = 30-86$ (wild-type), 15-44 (*trxf1*), 5-44 (*ntrc*) or 70-111 (*trxf1 ntrc*) different plants. All values are significantly different from wild-type according to the student *t*-test ($P < 0.05$), except the *trxf1* mutant in 8 h-, 16 h- and 24 h-day regimes at 160 μ E and in 950 μ E. μ E = μ mol photons $m^{-2} s^{-1}$; n.d. = not detectable (fresh-weight values were below the detection limit)

Figure 3: Changes in gas-exchange parameters in leaves of *trxf1*, *ntrc* and *trxf1 ntrc* Arabidopsis mutants compared to wild-type. **(A)** CO_2 assimilation rate, **(B)** transpiration rate, and **(C)** intercellular CO_2 concentration were measured at different light intensities in leaves from plants growing in an 8 h photoperiod with 160 μ mol photons $m^{-2} s^{-1}$. Results are the mean \pm SE, $n = 10$ (wild-type) or 5 (mutants) different plant replicates. *: $P < 0.05$, **: $P < 0.01$, ***: $P < 0.001$ (according to two-way analysis of variance [Anova]), Tukey test); PAR = photosynthetic active radiation

Figure 4: Changes in chlorophyll fluorescence parameters in leaves of *trxf1*, *ntrc* and *trxf1 ntrc* Arabidopsis mutants compared to wild-type. Plants growing in an 8 h photoperiod with 160 $\mu\text{mol photons m}^{-2} \text{ s}^{-1}$ were dark adapted for 10 min, before exposure of a far red light saturation pulse (5,000 $\mu\text{mol m}^{-2} \text{ s}^{-1}$ for 0.8 s) to single leaves. Afterwards the maximal chlorophyll a fluorescence was quenched by electron transport with an actinic red light of 166 $\mu\text{mol photons m}^{-2} \text{ s}^{-1}$. Within 10 min the steady state was reached and another saturation pulse was given. In the end, **(A)** the maximal PSII (F_v/F_m), and **(B)** the effective PSII (Φ_{PSII}), the non-regulated energy dissipation (Φ_{NO}) and the regulated energy dissipation (Φ_{NPQ}) quantum yields were calculated. Results are means \pm SE, $n=11$ different plants.

*: $P<0.05$, **: $P<0.01$, ***: $P<0.001$ (according to student *t*-test); a. u. = arbitrary unit

Figure 5: Changes in the levels of proteins involved in photosynthetic electron transport and ATP synthesis in leaves of *trxf1*, *ntrc* and *trxf1 ntrc* Arabidopsis mutants compared to wild-type. PsaA, PsaB, PsbA, PsbD, PetC, Lhca1, Lhcb1 and Atp β proteins were detected using specific antibodies. Representative Western blots are shown from 5-week old plants growing in an 8h-day with 160 $\mu\text{mol photons m}^{-2} \text{ s}^{-1}$ light regime harvested 4 h into the light period. Actin protein level is shown as control.

Figure 6: Changes in nucleotide levels in leaves of *trxf1*, *ntrc* and *trxf1 ntrc* Arabidopsis mutants compared to wild-type. **(A)** Sum of NADPH and NADP, **(B)** NADPH/NADP ratio, **(C)** sum of NADH and NAD, **(D)** NADH/NAD ratio, **(E)** sum of ATP and ADP, and **(F)** ATP/ADP ratio were measured in leaves harvested at the end of day and end of night. Results are means \pm SE, $n=20-30$ (wild-type) or 10-15 (mutants) different plant replicates. Plants were grown in an 8 h photoperiod with 160 $\mu\text{mol photons m}^{-2} \text{ s}^{-1}$. *: $P<0.05$, **: $P<0.01$, ***: $P<0.001$, according to student **(A)** to **(D)** or paired **(E)** to **(F)** *t*-test

Figure 7: Light-dependent redox activation of fructose-1,6-bisphosphatase (FBPase) in leaves of *trxf1*, *ntrc* and *trxf1 ntrc* Arabidopsis mutants compared to wild-type. **(A)** and **(B)** show the thiol-disulfide reduction state of chloroplast FBPase in leaves harvested at the end of night (EN) and end of day (ED) analyzed by using gel-shift

assays: **(A)** Representative gel-shift blot using an antibody specific for chloroplast FBPase, and **(B)** calculated ratio of reduced to oxidized FBPase. **(C)** Corresponding initial enzyme activity of FBPase (assay without DTT) in leaves harvested at the end of night (EN) and end of day (ED). **(D)** to **(F)** Transient light activation of FBPase during a detailed time course. At the end of the night (0 min), plants were illuminated for different time-periods (2, 5, 10, 20 and 30 min) to measure FBPase activity using different assay conditions: **(D)** Initial activity without DTT additions in the assay, **(E)** maximal activity with 10 mM DTT included in the assay, and **(F)** redox-activation state (initial/maximal activity*100). Results are means \pm SE, $n = 8$ (wild-type) or 4 (mutants) different plant replicates **(B)**, $n = 20$ (wild-type) or 10 (mutants) different plant replicates **(C)**, and $n = 8$ (wild-type) or 4 (mutants) different plant replicates **(D)** to **(F)**. All plants were grown in an 8 h photoperiod with 160 μmol photons $\text{m}^{-2} \text{s}^{-1}$. *: $P < 0.05$, **: $P < 0.01$, ***: $P < 0.001$, according to paired t-test **(B)** and **(C)** or two-way analysis of variance [Anova] Tukey test **(D)** to **(F)**

Figure 8: Light-dependent redox activation of NADP-dependent malate dehydrogenase (MDH) in leaves of *trxf1*, *ntrc* and *trxf1 ntrc* *Arabidopsis* mutants compared to wild-type. **(A)** Initial activity without DTT additions in the assay, **(B)** maximal activity with 10 mM DTT included in the assay, **(C)** redox-activation state (initial/maximal activity*100). Leaves were sampled at the end of night and end of day. Results are means \pm SE, $n = 24$ (wild-type) or 12 (mutants) different plant replicates. Plants were grown in an 8 h photoperiod with 160 μmol photons $\text{m}^{-2} \text{s}^{-1}$. *: $P < 0.05$, **: $P < 0.01$, ***: $P < 0.001$ (according to student t-test)

Figure 9: Changes in the accumulation of starch and sucrose and in the thiol-disulfide reduction state of ADP-glucose pyrophosphorylase (AGPase) in leaves of *trxf1*, *ntrc* and *trxf1 ntrc* *Arabidopsis* mutants compared to wild-type. **(A)** Starch level, **(B)** sucrose level, **(C)** starch/sucrose ratio, and **(D)** APS1 monomerisation (representative Western-blot) were measured in leaves sampled at the end of night (EN) and end of day (ED). Results for **(A)** to **(C)** are means \pm SE, $n = 8$ (wild-type) or 4 (mutants) different plant replicates growing in an 8 h photoperiod with 160 μmol photons $\text{m}^{-2} \text{s}^{-1}$. *: $P < 0.05$, **: $P < 0.01$, ***: $P < 0.001$ (according to student t-test); APS1 = small subunit of AGPase

Figure 10: Changes in the in-vivo levels of phosphorylated intermediates in leaves of *trxf1*, *ntrc* and *trxf1 ntrc* *Arabidopsis* mutants compared to wild-type. **(A)** 3-phosphoglycerate (3PGA) level, **(B)** fructose-1,6-bisphosphate (FBP) level, **(C)** fructose-6-phosphate (F6P) level, **(D)** F6P/FBP ratio, **(E)** glucose-6-phosphate (G6P) level, and **(F)** glucose-1-phosphate (G1P) level were measured in leaves sampled at the end of the night and end of the day. Results are means \pm SE, $n=30$ (wild-type) or 15 (mutants) different plant replicates growing in an 8 h photoperiod with 160 μmol photons $\text{m}^{-2} \text{s}^{-1}$. *: $P<0.05$, **: $P<0.01$, ***: $P<0.001$ (according to student *t*-test); n.d. = not detectable (values were below the detection limit)

Figure 11: Overview of changes in metabolite profiles from leaves of *trxf1*, *ntrc* and *trxf1 ntrc* *Arabidopsis* mutants compared to wild-type. Results from leaves sampled at the end of day **(A)** and end of night **(B)** are visualized using Wanted diagrams. Metabolite levels which are significantly different from wild-type according to the student *t*-test ($P<0.05$) are indicated in blue (increase) or red (decrease) color, while black color indicates no significant difference from wild-type. The order of the squares from left to right is *trxf1*, *ntrc* and *trxf1 ntrc* mutants being in first, second and third position, respectively. Data are taken from Supplemental Tables S4 – S7.

Figure 12: Visualization of protein-protein interactions of NTRC and Trx f1 in *Nicotiana benthamiana* chloroplasts by the BiFC assay. Confocal microscopy picture series present transiently transformed leaf mesophyll cells expressing combinations of the fusion proteins as indicated. Single pictures represent from left to right images of the yellow YFP fluorescence representing the BiFC-signal, the red autofluorescence of chlorophyll, the merge of both fluorescence signals illustrating the overlay of chlorophyll fluorescence and the BiFC-signal, and the bright field channel. No YFP-specific fluorescence signal was detectable in cells expressing fusion proteins separately (negative controls). Pictures were monitored in the channel mode with identical microscope settings. Bars = 10 μm

SUPPLEMENTAL FIGURES

Suppl. Figure S1: Changes in chlorophyll content in leaves of *trxf1*, *ntrc* and *trxf1 ntrc* *Arabidopsis* mutants compared to wild-type. Results are the mean \pm SE, $n=24$

(wild-type) or 12 (mutants) different plant replicates growing in an 8 h photoperiod with 160 μmol photons m^{-2} s^{-1} . *: $P<0.05$, **: $P<0.01$, ***: $P<0.001$ (according to student *t*-test)

Suppl. Figure S2: Histochemical localization of GUS expression in *Arabidopsis* plants transformed with a Trx1_{pro} -GUS reporter gene. GUS staining of 10-day-old seedlings grown in a 16 h photoperiod (**A**) to (**D**), and of 6-week-old plants having flowered and begun to set seed (**E**) to (**I**). GUS staining is shown in emerging leaves (**A**) and (**B**), roots (**C**), hypocotyl (**D**), siliques petiol (**E**), siliques (**F**), flower (**G**), sepal (**H**) and stigma (**I**). No GUS staining was observed in trichomes (**B**). The following microscopic techniques were used: (**A**), (**E**) and (**F**) Stereomicroscopy, (**B**), (**C**), (**D**), (**G**), (**H**) and (**I**) differential interference contrast microscopy, and (**G**) and (**H**) single image merge. Bars = 1000 μm in (**A**), (**E**), (**F**), (**G**) and (**H**), and 100 μm in (**B**), (**C**), (**D**) and (**I**).

SUPPLEMENTAL TABLES

Suppl. Table S1: Statistical analysis for rosette fresh weights of *trxf1*, *ntrc* and *trxf1 ntrc* *Arabidopsis* mutants growing in different light conditions, compared to wild-type. Values are based on the data presented in Figure 2H. Significantly different values from wild-type according to the student *t*-test are indicated in bold ($P<0.05$). n.d. = not detectable.

Suppl. Table S2: Statistical analysis for gas exchange parameters of *trxf1*, *ntrc* and *trxf1 ntrc* *Arabidopsis* mutants dependent on different light intensities, compared to wild-type. Values are based on the data presented in Figure 3. Significantly different values from wild-type according to the student *t*-test ($P<0.05$) are indicated in bold. PAR = photosynthetic active radiation.

Suppl. Table S3: Statistical analysis for the time course of fructose-1,6-bisphosphatase light activation in leaves of *trxf1*, *ntrc* and *trxf1 ntrc* *Arabidopsis* mutants, compared to wild-type. Values are based on the data presented in Figure 7D-F. Significantly different values from wild-type according to the student *t*-test ($P<0.05$) are indicated in bold.

Suppl. Table S4: Changes in GC-MS based metabolite profiles in leaves of *trxf1*, *ntrc* and *trxf1 ntrc* *Arabidopsis* mutants compared to wild-type. Leaves were sampled at the end of the day. Results are means \pm SD, $n = 12$. Values which are significantly different from wild-type according to the student t-test ($P < 0.05$) are indicated in bold (see also Figure 11A).

Suppl. Table S5: Changes in GC-MS based metabolite profiles in leaves of *trxf1*, *ntrc* and *trxf1 ntrc* *Arabidopsis* mutants compared to wild-type. Leaves were sampled at the end of the night. Results are means \pm SD, $n = 12$. Values which are significantly different from wild-type according to the student t-test ($P < 0.05$) are indicated in bold (see also Figure 11B).

Suppl. Table S6: Changes in the levels of phosphorylated intermediates and starch in leaves of *trxf1*, *ntrc* and *trxf1 ntrc* *Arabidopsis* mutants compared to wild-type, based on spectrophotometric measurements. Leaves were sampled at the end of the day. Results are normalized to wild-type level and represent means \pm SE, $n = 8-30$ (wild-type) or 4-15 (mutants). Values which are significantly different from wild-type according to the student t-test ($P < 0.05$) are indicated in bold (see Figure 11A).

Suppl. Table S7: Changes in the levels of phosphorylated intermediates and starch in leaves of *trxf1*, *ntrc* and *trxf1 ntrc* *Arabidopsis* mutants compared to wild-type, based on spectrophotometric measurements. Leaves were sampled at the end of the night. Results are normalized to wild-type level and represent means \pm SE, $n = 8-30$ (wild-type) or 4-15 (mutants). Values which are significantly different from wild-type according to the student t-test ($P < 0.05$) are indicated in bold (see also Figure 11B). n.d. = not detectable.

REFERENCES

Arsova, B., Hoja, U., Wimmelbacher, M., Greiner, E., Ustun, S., Melzer, M., Petersen, K., Lein, W., and Boernke, F. (2010). Plastidial Thioredoxin z Interacts with Two Fructokinase-Like Proteins in a Thiol-Dependent Manner: Evidence for an Essential Role in Chloroplast Development in Arabidopsis and Nicotiana benthamiana. *Plant Cell* **22**, 1498-1515.

Ballicora, M.A., Frueauf, J.B., Fu, Y., Schürmann, P., and Preiss, J. (2000). Activation of the Potato Tuber ADP-glucose Pyrophosphorylase by Thioredoxin. *J Biol Chem* **275**, 1315-1320.

Balmer, Y., Koller, A., del Val, G., Manieri, W., Schürmann, P., and Buchanan, B.B. (2003). Proteomics gives insight into the regulatory function of chloroplast thioredoxins. *Proceedings of the National Academy of Sciences* **100**, 370-375.

Baumann, U., and Juttner, J. (2002). Plant thioredoxins: the multiplicity conundrum. *Cellular and Molecular Life Sciences* **59**, 1042-1057.

Beeler, S., Liu, H.-C., Stadler, M., Schreier, T., Eicke, S., Lue, W.-L., Truernit, E., Zeeman, S.C., Chen, J., and Kötting, O. (2014). Plastidial NAD-Dependent Malate Dehydrogenase Is Critical for Embryo Development and Heterotrophic Metabolism in Arabidopsis. *Plant Physiol* **164**, 1175-1190.

Benitez-Alfonso, Y., Cilia, M., Roman, A.S., Thomas, C., Maule, A., Hearn, S., and Jackson, D. (2009). Control of Arabidopsis meristem development by thioredoxin-dependent regulation of intercellular transport. *P Natl Acad Sci USA* **106**, 3615-3620.

Bernal-Bayard, P., Hervas, M., Cejudo, F.J., and Navarro, J.A. (2012). Electron Transfer Pathways and Dynamics of Chloroplast NADPH-dependent Thioredoxin Reductase C (NTRC). *J Biol Chem* **287**, 33865-33872.

Bohrer, A.-S., Massot, V., Innocenti, G., Reichheld, J.-P., Issakidis-Bourguet, E., and Vanacker, H. (2012). New insights into the reduction systems of plastidial thioredoxins point out the unique properties of thioredoxin z from Arabidopsis. *J Exp Bot* **63**, 6315-6323.

Buchanan, B.B. (1980). Role of Light in the Regulation of Chloroplast Enzymes. *Annual Review of Plant Physiology* **31**, 341-374.

Buchanan, B.B., and Balmer, Y. (2005). Redox regulation: a broadening horizon. *Annual review of plant biology* **56**, 187-220.

Buchanan, B.B., Wolosiuk, R.A., and Schürmann, P. (1979). Thioredoxin and enzyme regulation. *Trends in Biochemical Sciences* **4**, 93-96.

Chiadmi, M., Navaza, A., Miginiac-Maslow, M., Jacquot, J.P., and Cherfils, J. (1999). Redox signalling in the chloroplast: structure of oxidized pea fructose-1,6-bisphosphate phosphatase. *The EMBO journal* **18**, 6809-6815.

Chibani, K., Tarrago, L., Schuermann, P., Jacquot, J.-P., and Rouhier, N. (2011). Biochemical properties of poplar thioredoxin z. *Febs Letters* **585**, 1077-1081.

Choi, Y.A., Kim, S.G., and Kwon, Y.M. (1999). The plastidic glutamine synthetase activity is directly modulated by means of redox change at two unique cysteine residues. *Plant Science* **149**, 175-182.

Clough, S.J., and Bent, A.F. (1998). Floral dip: a simplified method for Agrobacterium-mediated transformation of Arabidopsis thaliana. *Plant J* **16**, 735-743.

Collin, V., Issakidis-Bourguet, E., Marchand, C., Hirasawa, M., Lancelin, J.M., Knaff, D.B., and Miginiac-Maslow, M. (2003). The Arabidopsis plastidial

thioredoxins - New functions and new insights into specificity. *J Biol Chem* **278**, 23747-23752.

Collin, V., Lamkemeyer, P., Miginiac-Maslow, M., Hirasawa, M., Knaff, D.B., Dietz, K.-J., and Issakidis-Bourguet, E. (2004). Characterization of Plastidial Thioredoxins from *Arabidopsis* Belonging to the New γ -Type. *Plant Physiol* **136**, 4088-4095.

Cook, K.M., and Hogg, P.J. (2013). Post-translational control of protein function by disulfide bond cleavage. *Antioxid Redox Signal* **18**, 1987-2015.

Courteille, A., Vesa, S., Sanz-Barrio, R., Cazale, A.-C., Becuwe-Linka, N., Farran, I., Havaux, M., Rey, P., and Rumeau, D. (2013). Thioredoxin m4 Controls Photosynthetic Alternative Electron Pathways in *Arabidopsis*. *Plant Physiol* **161**, 508-520.

Dietz, K.-J., and Pfannschmidt, T. (2011). Novel Regulators in Photosynthetic Redox Control of Plant Metabolism and Gene Expression. *Plant Physiol* **155**, 1477-1485.

Faix, B., Radchuk, V., Nerlich, A., Hummer, C., Radchuk, R., Emery, R.J., Keller, H., Gotz, K.P., Weschke, W., Geigenberger, P., and Weber, H. (2012). Barley grains, deficient in cytosolic small subunit of ADP-glucose pyrophosphorylase, reveal coordinate adjustment of C:N metabolism mediated by an overlapping metabolic-hormonal control. *Plant J* **69**, 1077-1093.

Faske, M., Holtgrefe, S., Ocheretina, O., Meister, M., Backhausen, J.E., and Scheibe, R. (1995). Redox equilibria between the regulatory thiols of light/dark-modulated chloroplast enzymes and dithiothreitol: fine-tuning by metabolites. *Biochimica et biophysica acta* **1247**, 135-142.

Fernie, A.R., Tiessen, A., Stitt, M., Willmitzer, L., and Geigenberger, P. (2002). Altered metabolic fluxes result from shifts in metabolite levels in sucrose phosphorylase-expressing potato tubers. *Plant, Cell & Environment* **25**, 1219-1232.

Fu, Y., Ballicora, M.A., Leykam, J.F., and Preiss, J. (1998). Mechanism of Reductive Activation of Potato Tuber ADP-glucose Pyrophosphorylase. *J Biol Chem* **273**, 25045-25052.

Gehl, C., Waadt, R., Kudla, J., Mendel, R.-R., and Hänsch, R. (2009). New GATEWAY vectors for High Throughput Analyses of Protein-Protein Interactions by Bimolecular Fluorescence Complementation. *Mol Plant* **2**, 1051-1058.

Geigenberger, P., Kolbe, A., and Tiessen, A. (2005). Redox regulation of carbon storage and partitioning in response to light and sugars. *J Exp Bot* **56**, 1469-1479.

Glaring, M.A., Skryhan, K., Kotting, O., Zeeman, S.C., and Blennow, A. (2012). Comprehensive survey of redox sensitive starch metabolising enzymes in *Arabidopsis thaliana*. *Plant physiology and biochemistry : PPB / Societe francaise de physiologie vegetale* **58**, 89-97.

Grieco, M., Tikkanen, M., Paakkarinen, V., Kangasjarvi, S., and Aro, E.M. (2012). Steady-state phosphorylation of light-harvesting complex II proteins preserves photosystem I under fluctuating white light. *Plant Physiol* **160**, 1896-1910.

Hendriks, J.H.M., Kolbe, A., Gibon, Y., Stitt, M., and Geigenberger, P. (2003). ADP-glucose pyrophosphorylase is activated by posttranslational redox-modification in response to light and to sugars in leaves of *Arabidopsis* and other plant species. *Plant Physiol* **133**, 838-849.

Hertle, A.P., Blunder, T., Wunder, T., Pesaresi, P., Pribil, M., Armbruster, U., and Leister, D. (2013). PGRL1 is the elusive ferredoxin-plastoquinone reductase in photosynthetic cyclic electron flow. *Molecular cell* **49**, 511-523.

Hodges, M., Miginiac-Maslow, M., Decottignies, P., Jacquot, J.-P., Stein, M., Lepiniec, L., Crétin, C., and Gadal, P. (1994). Purification and characterization of pea thioredoxin f expressed in *Escherichia coli*. *Plant Mol Biol* **26**, 225-234.

Holaday, A.S., Martindale, W., Alred, R., Brooks, A.L., and Leegood, R.C. (1992). Changes in Activities of Enzymes of Carbon Metabolism in Leaves during Exposure of Plants to Low Temperature. *Plant Physiol* **98**, 1105-1114.

Holmgren, A. (1985). Thioredoxin. *Annual review of biochemistry* **54**, 237-271.

Jefferson, R.A., Kavanagh, T.A., and Bevan, M.W. (1987). GUS fusions: beta-glucuronidase as a sensitive and versatile gene fusion marker in higher plants. *The EMBO journal* **6**, 3901-3907.

Jelitto, T., Sonnewald, U., Willmitzer, L., Hajirezeai, M., and Stitt, M. (1992). Inorganic pyrophosphate content and metabolites in potato and tobacco plants expressing *E. coli* pyrophosphatase in their cytosol. *Planta* **188**, 238-244.

Kirchsteiger, K., Fernandez, J., Belen Pascual, M., Gonzalez, M., and Javier Cejudo, F. (2012). NADPH Thioredoxin Reductase C Is Localized in Plastids of Photosynthetic and Nonphotosynthetic Tissues and Is Involved in Lateral Root Formation in *Arabidopsis*. *Plant Cell* **24**, 1534-1548.

Kolbe, A., Tiessen, A., Schluemann, H., Paul, M., Ulrich, S., and Geigenberger, P. (2005). Trehalose 6-phosphate regulates starch synthesis via posttranslational redox activation of ADP-glucose pyrophosphorylase. *P Natl Acad Sci USA* **102**, 11118-11123.

Konig, J., Baier, M., Horling, F., Kahmann, U., Harris, G., Schurmann, P., and Dietz, K.J. (2002). The plant-specific function of 2-Cys peroxiredoxin-mediated detoxification of peroxides in the redox-hierarchy of photosynthetic electron flux. *Proc Natl Acad Sci U S A* **99**, 5738-5743.

Koßmann, J., Sonnewald, U., and Willmitzer, L. (1994). Reduction of the chloroplastic fructose-1,6-bisphosphatase in transgenic potato plants impairs photosynthesis and plant growth. *The Plant Journal* **6**, 637-650.

Laemmli, U.K. (1970). Cleavage of Structural Proteins during the Assembly of the Head of Bacteriophage T4. *Nature* **227**, 680-685.

Lee, Y., Kim, S., Lazar, P., Moon, J.C., Hwang, S., Thangapandian, S., Shon, Y., Lee, K.O., Lee, S.Y., and Lee, K.W. (2012). Comparative molecular modeling study of *Arabidopsis* NADPH-dependent thioredoxin reductase and its hybrid protein. *PloS one* **7**, e46279.

Lepisto, A., Pakula, E., Toivola, J., Krieger-Liszakay, A., Vignols, F., and Rintamaki, E. (2013). Deletion of chloroplast NADPH-dependent thioredoxin reductase results in inability to regulate starch synthesis and causes stunted growth under short-day photoperiods. *J Exp Bot* **64**, 3843-3854.

Lepisto, A., Kangasjarvi, S., Luomala, E.-M., Brader, G., Sipari, N., Keranen, M., Keinanen, M., and Rintamaki, E. (2009). Chloroplast NADPH-Thioredoxin Reductase Interacts with Photoperiodic Development in *Arabidopsis*. *Plant Physiol* **149**, 1261-1276.

Lichter, A., and Häberlein, I. (1998). A light-dependent redox signal participates in the regulation of ammonia fixation in chloroplasts of higher plants — ferredoxin: Glutamate synthase is a thioredoxin-dependent enzyme. *J Plant Physiol* **153**, 83-90.

Lintala, M., Schuck, N., Thormahlen, I., Jungfer, A., Weber, K.L., Weber, A.P., Geigenberger, P., Soll, J., Bolter, B., and Mulo, P. (2014). Arabidopsis tic62 trol mutant lacking thylakoid-bound ferredoxin-NADP⁺ oxidoreductase shows distinct metabolic phenotype. *Mol Plant* **7**, 45-57.

Liu, Y.J., Norberg, F.E., Szilagyi, A., De Paepe, R., Akerlund, H.E., and Rasmusson, A.G. (2008). The mitochondrial external NADPH dehydrogenase modulates the leaf NADPH/NADP⁺ ratio in transgenic *Nicotiana sylvestris*. *Plant Cell Physiol* **49**, 251-263.

Livingston, A.K., Cruz, J.A., Kohzuma, K., Dhingra, A., and Kramer, D.M. (2010). An Arabidopsis mutant with high cyclic electron flow around photosystem I (hcef) involving the NADPH dehydrogenase complex. *Plant Cell* **22**, 221-233.

Meyer, Y., Belin, C., Delorme-Hinoux, V., Reichheld, J.-P., and Riondet, C. (2012). Thioredoxin and Glutaredoxin Systems in Plants: Molecular Mechanisms, Crosstalks, and Functional Significance. *Antioxidants & Redox Signaling* **17**, 1124-1160.

Michalska, J., Zauber, H., Buchanan, B.B., Cejudo, F.J., and Geigenberger, P. (2009). NTRC links built-in thioredoxin to light and sucrose in regulating starch synthesis in chloroplasts and amyloplasts. *P Natl Acad Sci USA* **106**, 9908-9913.

Michelet, L., Zaffagnini, M., Morisse, S., Sparla, F., Perez-Perez, M.E., Francia, F., Danon, A., Marchand, C.H., Fermani, S., Trost, P., and Lemaire, S.D. (2013). Redox regulation of the Calvin-Benson cycle: something old, something new. *Front Plant Sci* **4**, 470.

Mikkelsen, R., Mutenda, K.E., Mant, A., Schurmann, P., and Blennow, A. (2005). Alpha-glucan, water dikinase (GWD): a plastidic enzyme with redox-regulated and coordinated catalytic activity and binding affinity. *Proc Natl Acad Sci U S A* **102**, 1785-1790.

Nee, G., Zaffagnini, M., Trost, P., and Issakidis-Bourguet, E. (2009). Redox regulation of chloroplast glucose-6-phosphate dehydrogenase: a new role for f-type thoresoxin. *FEBS Lett* **583**, 2827-2832.

Nikkanen, L., and Rintamäki, E. (2014). Thioredoxin-dependent regulatory networks in chloroplasts under fluctuating light conditions. *Philosophical Transactions of the Royal Society B: Biological Sciences* **369**.

Perez-Ruiz, J.M., Guinea, M., Puerto-Galan, L., and Cejudo, F.J. (2014). NADPH thioredoxin reductase C is involved in redox regulation of the Mg-chelatase I subunit in *Arabidopsis thaliana* chloroplasts. *Mol Plant* **7**, 1252-1255.

Perez-Ruiz, J.M., Gonzalez, M., Spinola, M.C., Sandalio, L.M., and Cejudo, F.J. (2009). The quaternary structure of NADPH thioredoxin reductase C is redox-sensitive. *Mol Plant* **2**, 457-467.

Perez-Ruiz, J.M., Spinola, M.C., Kirchsteiger, K., Moreno, J., Sahrawy, M., and Cejudo, F.J. (2006). Rice NTRC is a high-efficiency redox system for chloroplast protection against oxidative damage. *Plant Cell* **18**, 2356-2368.

Pérez-Ruiz, J.M., and Cejudo, F.J. (2009). A proposed reaction mechanism for rice NADPH thioredoxin reductase C, an enzyme with protein disulfide reductase activity. *FEBS Letters* **583**, 1399-1402.

Pfannschmidt, T., and Liere, K. (2005). Redox regulation and modification of proteins controlling chloroplast gene expression. *Antioxid Redox Signal* **7**, 607-618.

Richter, A.S., Peter, E., Rothbart, M., Schlicke, H., Toivola, J., Rintamaki, E., and Grimm, B. (2013). Posttranslational influence of NADPH-dependent

thioredoxin reductase C on enzymes in tetrapyrrole synthesis. *Plant Physiol* **162**, 63-73.

Sanz-Barrio, R., Corral-Martinez, P., Ancin, M., Segui-Simarro, J.M., and Farran, I. (2013). Overexpression of plastidial thioredoxin f leads to enhanced starch accumulation in tobacco leaves. *Plant Biotechnol J* **11**, 618-627.

Sanz-Barrio, R., Fernandez-San Millan, A., Carballeda, J., Corral-Martinez, P., Segui-Simarro, J.M., and Farran, I. (2012). Chaperone-like properties of tobacco plastid thioredoxins f and m. *J Exp Bot* **63**, 365-379.

Sasaki, Y., Kozaki, A., and Hatano, M. (1997). Link between light and fatty acid synthesis: thioredoxin-linked reductive activation of plastidic acetyl-CoA carboxylase. *Proc Natl Acad Sci U S A* **94**, 11096-11101.

Scheibe, R. (2004). Malate valves to balance cellular energy supply. *Physiol Plant* **120**, 21-26.

Scheibe, R., and Stitt, M. (1988). Comparison of NADP-malate dehydrogenase activation, Q_A reduction and O_2 evolution in spinach leaves. *Plant physiology and biochemistry : PPB / Societe francaise de physiologie vegetale* **26**, 473-481.

Schmitz, J., Heinrichs, L., Scossa, F., Fernie, A.R., Oelze, M.L., Dietz, K.J., Rothbart, M., Grimm, B., Flugge, U.I., and Hausler, R.E. (2014). The essential role of sugar metabolism in the acclimation response of *Arabidopsis thaliana* to high light intensities. *J Exp Bot* **65**, 1619-1636.

Schuermann, P., and Buchanan, B.B. (2008). The ferredoxin/thioredoxin system of oxygenic photosynthesis. *Antioxidants & Redox Signaling* **10**, 1235-1273.

Schwarz, C., Bohne, A.-V., Wang, F., Javier Cejudo, F., and Nickelsen, J. (2012). An intermolecular disulfide-based light switch for chloroplast psbD gene expression in *Chlamydomonas reinhardtii*. *Plant J* **72**, 378-389.

Serrato, A.J., Perez-Ruiz, J.M., Spinola, M.C., and Cejudo, F.J. (2004). A novel NADPH thioredoxin reductase, localized in the chloroplast, which deficiency causes hypersensitivity to abiotic stress in *Arabidopsis thaliana*. *J Biol Chem* **279**, 43821-43827.

Seung, D., Thalmann, M., Sparla, F., Abou Hachem, M., Lee, S.K., Issakidis-Bourguet, E., Svensson, B., Zeeman, S.C., and Santelia, D. (2013). *Arabidopsis thaliana* AMY3 is a unique redox-regulated chloroplastic alpha-amylase. *J Biol Chem* **288**, 33620-33633.

Silver, D.M., Silva, L.P., Issakidis-Bourguet, E., Glaring, M.A., Schriemer, D.C., and Moorhead, G.B. (2013). Insight into the redox regulation of the phosphoglucan phosphatase SEX4 involved in starch degradation. *The FEBS journal* **280**, 538-548.

Stitt, M., Lilley, R.M., Gerhardt, R., and Heldt, H.W. (1989). [32] Metabolite levels in specific cells and subcellular compartments of plant leaves. In *Methods in Enzymology*, B.F. Sidney Fleischer, ed (Academic Press), pp. 518-552.

Suorsa, M., Jarvi, S., Grieco, M., Nurmi, M., Pietrzykowska, M., Rantala, M., Kangasjarvi, S., Paakkarinen, V., Tikkanen, M., Jansson, S., and Aro, E.M. (2012). PROTON GRADIENT REGULATION5 is essential for proper acclimation of *Arabidopsis* photosystem I to naturally and artificially fluctuating light conditions. *Plant Cell* **24**, 2934-2948.

Thormahlen, I., Ruber, J., Von Roepenack-Lahaye, E., Ehrlich, S.M., Massot, V., Hummer, C., Tezycka, J., Issakidis-Bourguet, E., and Geigenberger, P. (2013). Inactivation of thioredoxin f1 leads to decreased light activation of ADP-glucose pyrophosphorylase and altered diurnal starch turnover in leaves of *Arabidopsis* plants. *Plant Cell Environ* **36**, 16-29.

Tikkanen, M., and Aro, E.M. (2014). Integrative regulatory network of plant thylakoid energy transduction. *Trends Plant Sci* **19**, 10-17.

Tikkanen, M., Mekala, N.R., and Aro, E.M. (2014). Photosystem II photoinhibition-repair cycle protects Photosystem I from irreversible damage. *Biochimica et biophysica acta* **1837**, 210-215.

Toivola, J., Nikkanen, L., Dahlstrom, K.M., Salminen, T.A., Lepisto, A., Vignols, F., and Rintamaki, E. (2013). Overexpression of chloroplast NADPH-dependent thioredoxin reductase in *Arabidopsis* enhances leaf growth and elucidates *in vivo* function of reductase and thioredoxin domains. *Frontiers in Plant Science* **4**.

Valerio, C., Costa, A., Marri, L., Issakidis-Bourguet, E., Pupillo, P., Trost, P., and Sparla, F. (2011). Thioredoxin-regulated beta-amylase (BAM1) triggers diurnal starch degradation in guard cells, and in mesophyll cells under osmotic stress. *J Exp Bot* **62**, 545-555.

Wang, P., Liu, J., Liu, B., Feng, D., Da, Q., Wang, P., Shu, S., Su, J., Zhang, Y., Wang, J., and Wang, H.B. (2013). Evidence for a role of chloroplastic m-type thioredoxins in the biogenesis of photosystem II in *Arabidopsis*. *Plant Physiol* **163**, 1710-1728.

Wulff, R.P., Lundqvist, J., Rutsdottir, G., Hansson, A., Stenbaek, A., Elmlund, D., Elmlund, H., Jensen, P.E., and Hansson, M. (2011). The activity of barley NADPH-dependent thioredoxin reductase C is independent of the oligomeric state of the protein: tetrameric structure determined by cryo-electron microscopy. *Biochemistry* **50**, 3713-3723.

Zakharov, A., Giersberg, M., Hosein, F., Melzer, M., Muntz, K., and Saalbach, I. (2004). Seed-specific promoters direct gene expression in non-seed tissue. *J Exp Bot* **55**, 1463-1471.

Zimmermann, G., Kelly, G.J., and Latzko, E. (1976). Efficient purification and molecular properties of spinach chloroplast fructose 1,6-bisphosphatase. *European journal of biochemistry / FEBS* **70**, 361-367.

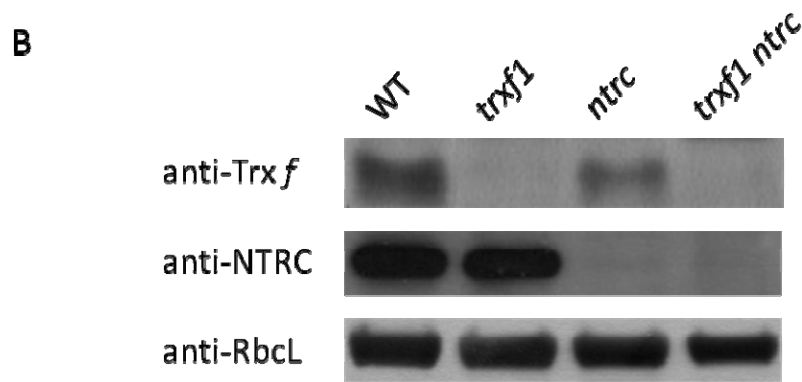
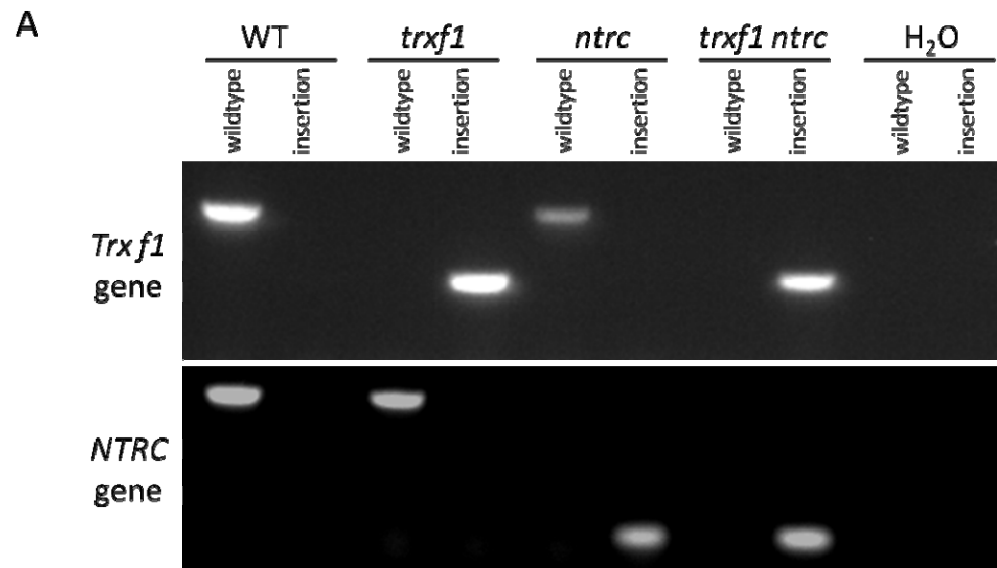


Figure 1: Molecular characterization of *trxf1*, *ntrc* and *trxf1 ntrc* *Arabidopsis* mutants compared to wild-type. **(A)** Genotyping by PCR analysis with different primer combinations (wild-type or insertion) for the identification of T-DNA insertions in *Trx f1* and *NTRC* genes. **(B)** Detection of Trx f and NTRC proteins using Western blot analysis. Representative Western blots are shown of measurements, which were performed in leaves of 5-week old plants grown in an 8h-day with 160 μmol photons $\text{m}^{-2} \text{s}^{-1}$ light regime harvested 4 h into the light period. Rubisco protein level is shown as control.

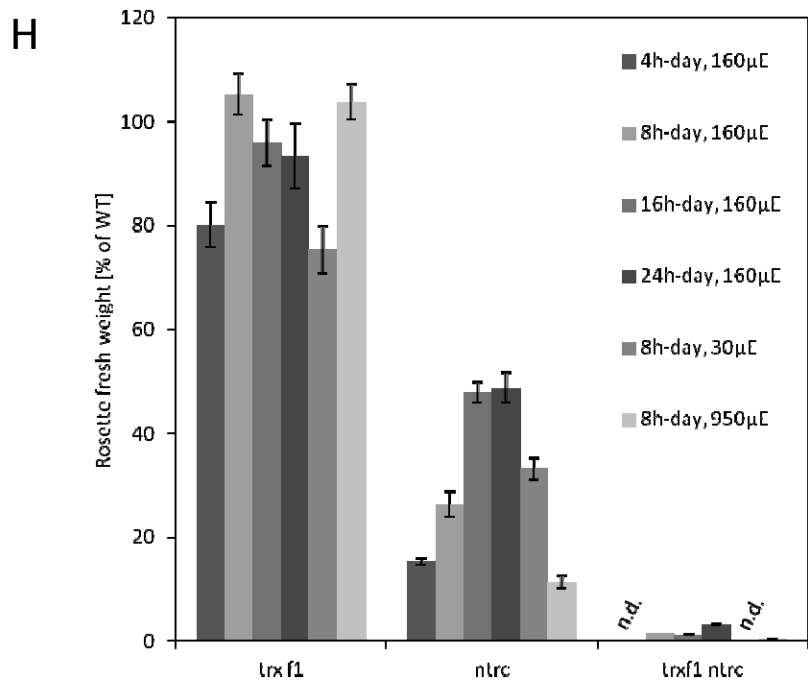
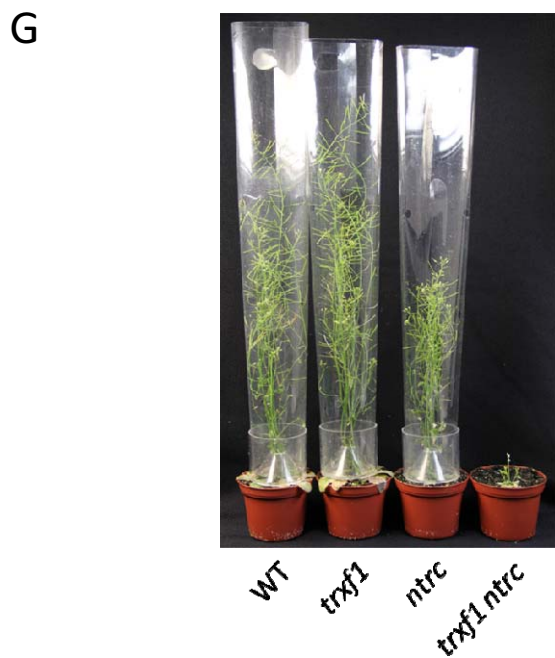
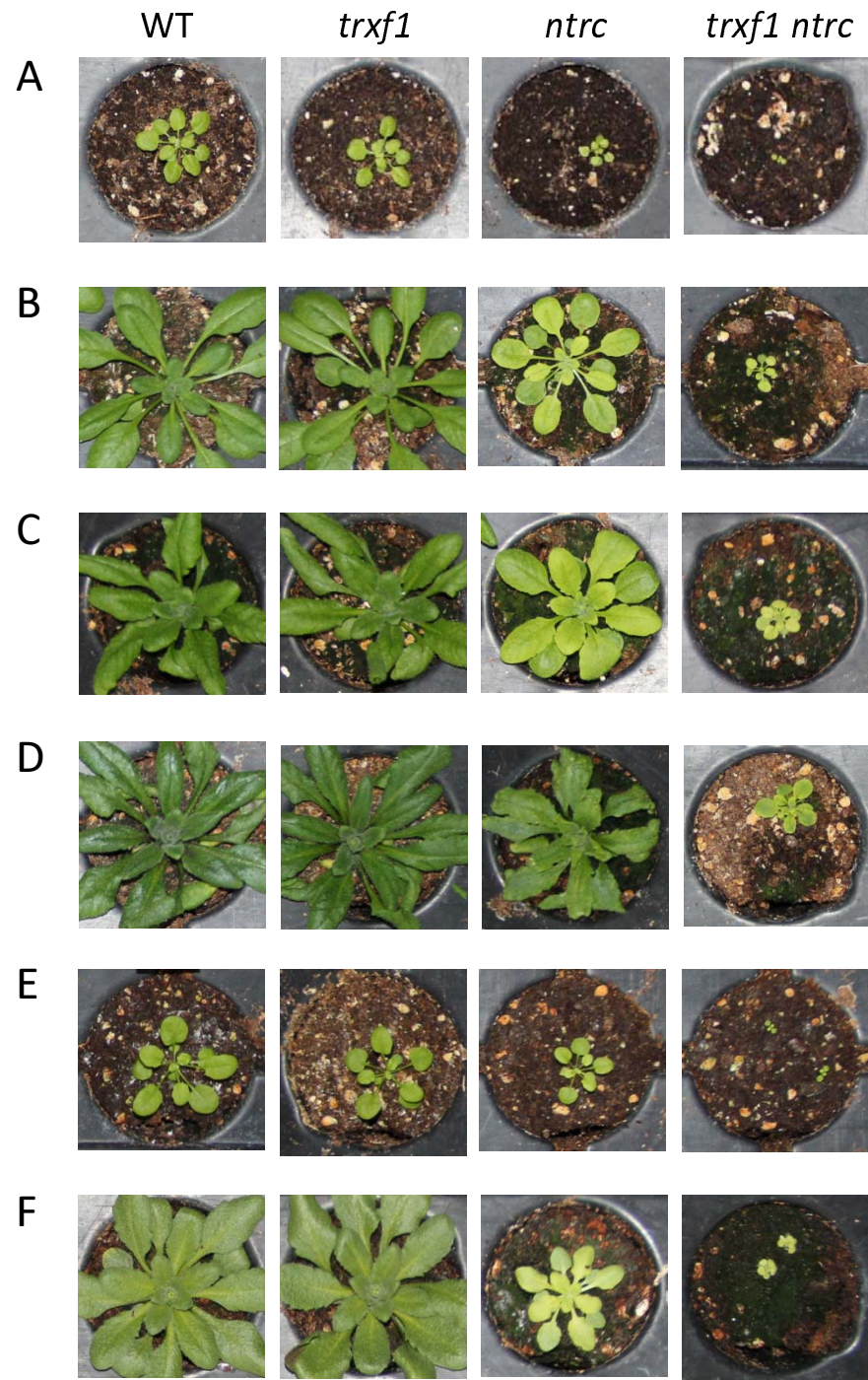


Figure 2: Growth analysis of wild-type, *trxf1*, *ntrc* and *trxf1 ntrc* *Arabidopsis* mutants across different light conditions. **(A), (B), (E) and (F)** correspond to 5 week-old plants, while **(C)** and **(D)** correspond to 4 week-old plants, and **(G)** to 7 week-old plants. In the first week, plants - except **(G)** - were grown in an 8 h-day and 160 μ E regime before they were transferred for additional 3-4 weeks to the conditions indicated below: **(A)** 4 h-day and 160 μ E, **(B)** 8 h-day and 160 μ E, **(C)** 16 h-day and 160 μ E, **(D)** 24 h-day and 160 μ E, **(E)** 8 h-day and 30 μ E, **(F)** 8 h-day and 950 μ E, and **(G)** 16 h-day in greenhouse. In **(H)**, rosette fresh-weights of plants corresponding to the conditions shown in **(A)** to **(F)** are given as percent of wild-type levels in the respective conditions. Results are the mean \pm SE, $n = 30-86$ (wild-type), 15-44 (*trxf1*), 5-44 (*ntrc*) or 70-111 (*trxf1 ntrc*) different plants. All values are significantly different from wild-type according to the student *t*-test ($P < 0.05$), except the *trxf1* mutant in 8 h-, 16 h- and 24 h-day regimes at 160 μ E and in 950 μ E. μ E = μ mol photons $m^{-2} s^{-1}$; n.d. = not detectable (fresh-weight values were below the detection limit)

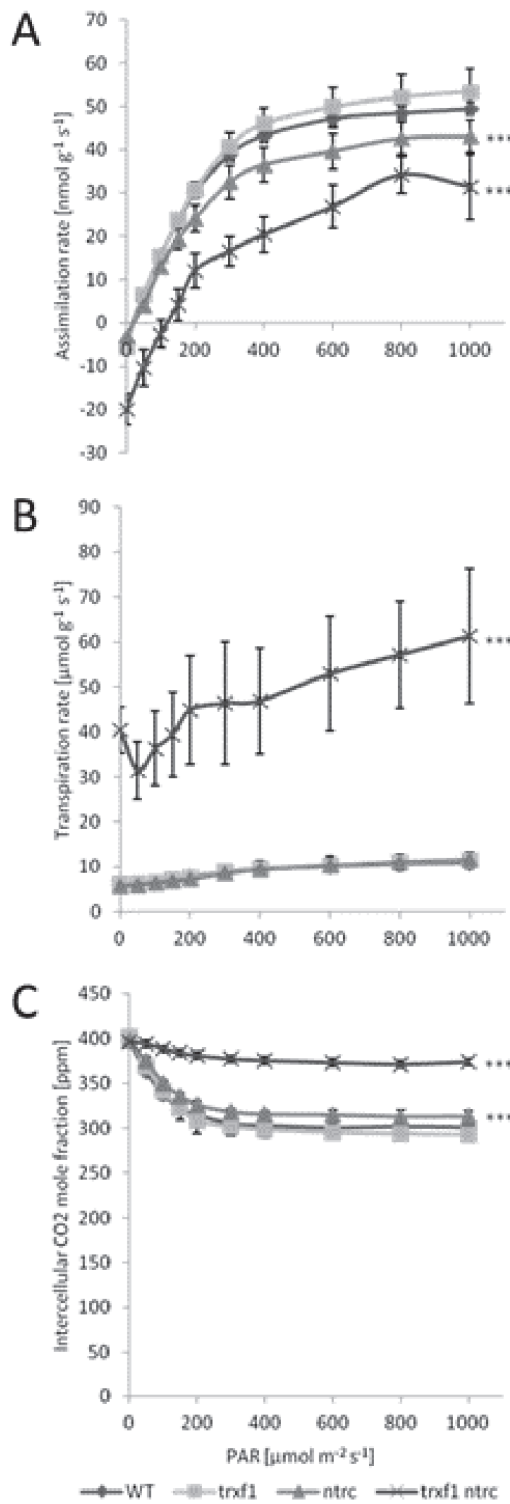


Figure 3: Changes in gas-exchange parameters in leaves of *trx1*, *ntrc* and *trx1 ntrc* Arabidopsis mutants compared to wild-type. **(A)** CO_2 assimilation rate, **(B)** transpiration rate, and **(C)** intercellular CO_2 concentration were measured at different light intensities in leaves from plants growing in an 8 h photoperiod with $160 \mu\text{mol}$ photons $\text{m}^{-2} \text{s}^{-1}$. Results are the mean \pm SE, $n = 10$ (wild-type) or 5 (mutants) different plant replicates. *: $P<0.05$, **: $P<0.01$, ***: $P<0.001$ (according to two-way analysis of variance [Anova]), Tukey test; PAR = photosynthetic active radiation

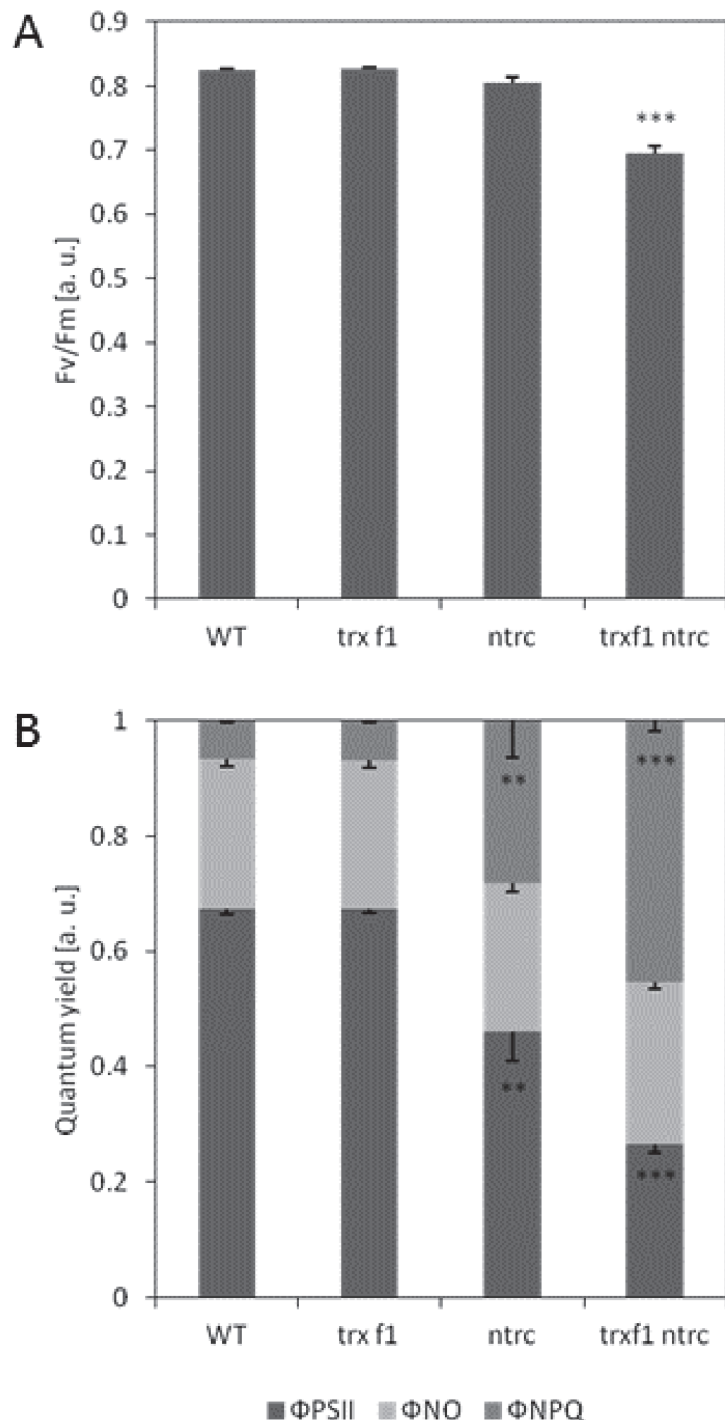


Figure 4: Changes in chlorophyll fluorescence parameters in leaves of *trxf1*, *ntrc* and *trxf1 ntrc* *Arabidopsis* mutants compared to wild-type. Plants growing in an 8 h photoperiod with 160 μmol photons $\text{m}^{-2} \text{s}^{-1}$ were dark adapted for 10 min, before exposure of a far red light saturation pulse (5,000 μmol $\text{m}^{-2} \text{s}^{-1}$ for 0.8 s) to single leaves. Afterwards the maximal chlorophyll a fluorescence was quenched by electron transport with an actinic red light of 166 μmol photons $\text{m}^{-2} \text{s}^{-1}$. Within 10 min the steady state was reached and another saturation pulse was given. In the end, **(A)** the maximal PSII (F_v/F_m), and **(B)** the effective PSII (Φ_{PSII}), the non-regulated energy dissipation (Φ_{NO}) and the regulated energy dissipation (Φ_{NPQ}) quantum yields were calculated. Results are means \pm SE, $n = 11$ different plants.

*: $P < 0.05$, **: $P < 0.01$, ***: $P < 0.001$ (according to student *t*-test);

a. u. = arbitrary unit

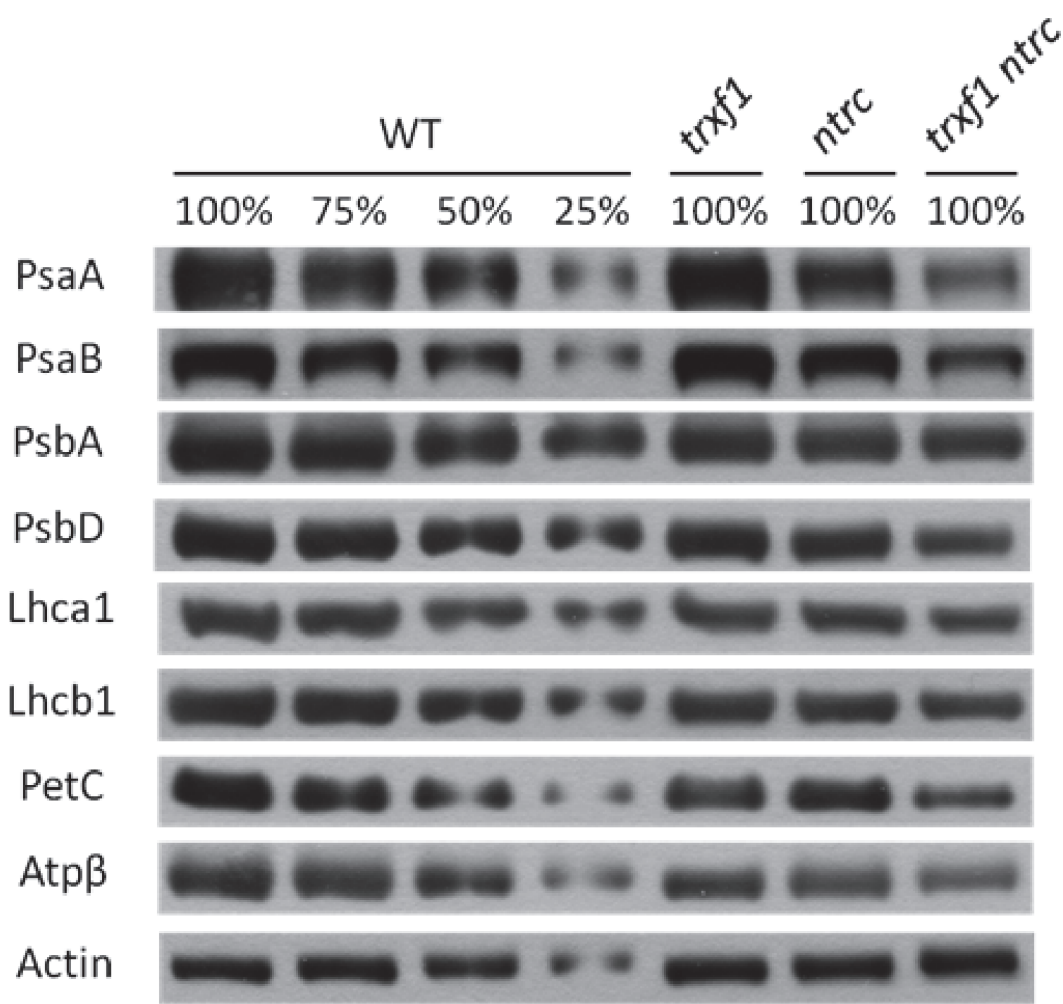


Figure 5: Changes in the levels of proteins involved in photosynthetic electron transport and ATP synthesis in leaves of *trxf1*, *ntrc* and *trxf1 ntrc* *Arabidopsis* mutants compared to wild-type. PsaA, PsaB, PsbA, PsbD, PetC, Lhca1, Lhcb1 and Atp β proteins were detected using specific antibodies. Representative Western blots are shown from 5-week old plants growing in an 8h-day with 160 μ mol photons $m^{-2} s^{-1}$ light regime harvested 4 h into the light period. Actin protein level is shown as control.

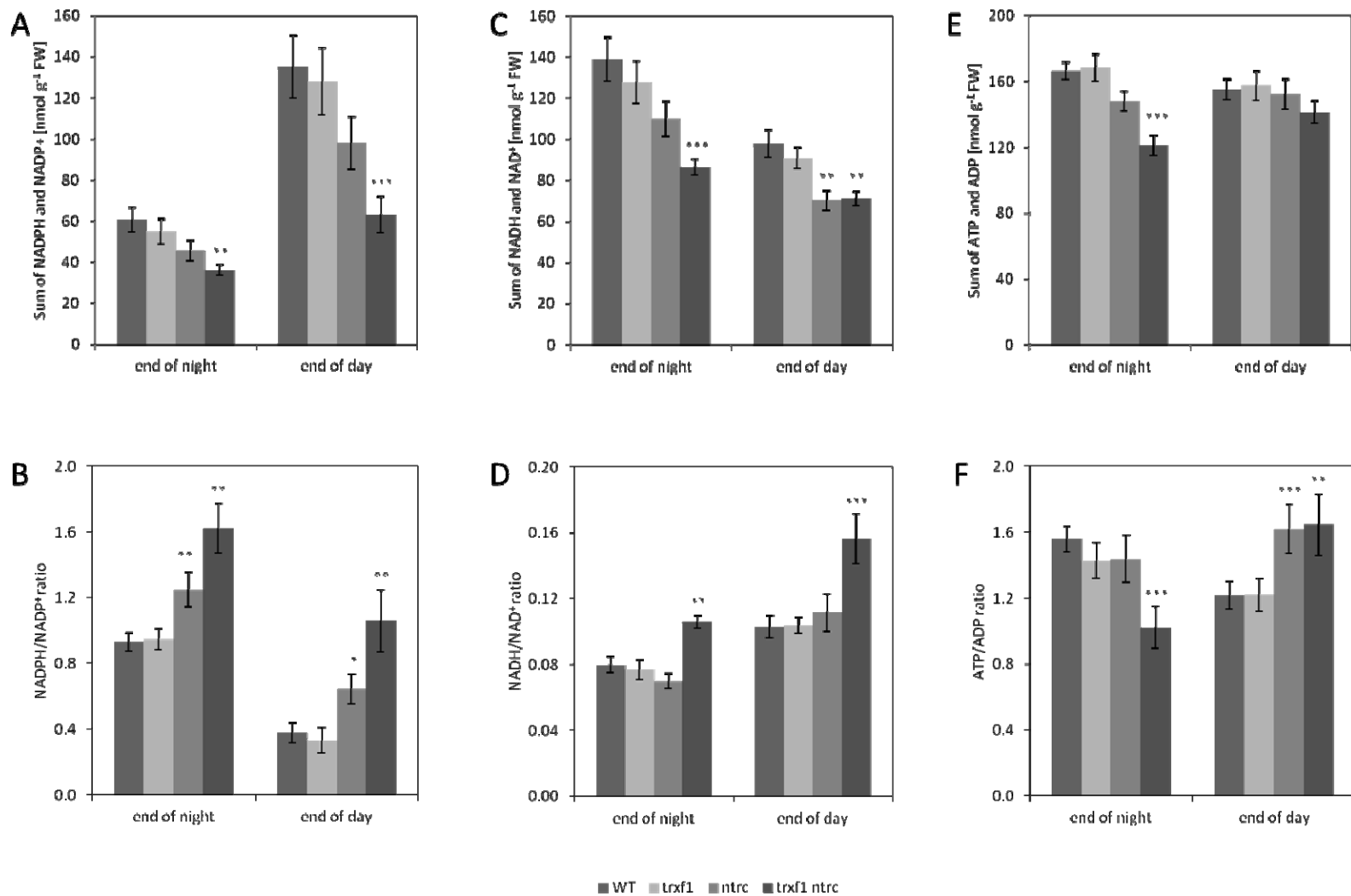


Figure 6: Changes in nucleotide levels in leaves of *trx1*, *ntrc* and *trx1 ntrc* Arabidopsis mutants compared to wild-type. **(A)** Sum of NADPH and NADP, **(B)** NADPH/NADP ratio, **(C)** sum of NADH and NAD, **(D)** NADH/NAD ratio, **(E)** sum of ATP and ADP, and **(F)** ATP/ADP ratio were measured in leaves harvested at the end of day and end of night. Results are means \pm SE, $n = 20-30$ (wild-type) or 10-15 (mutants) different plant replicates. Plants were grown in an 8 h photoperiod with 160 μ mol photons $m^{-2} s^{-1}$. *: $P < 0.05$, **: $P < 0.01$, ***: $P < 0.001$, according to student **(A)** to **(D)** or paired **(E)** to **(F)** *t*-test

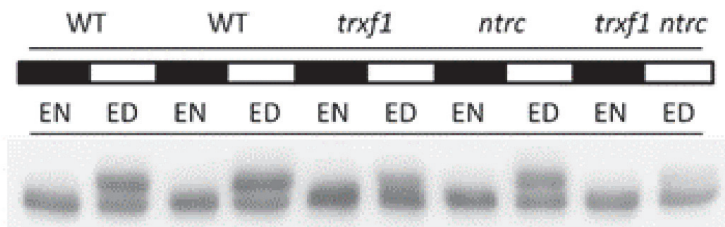
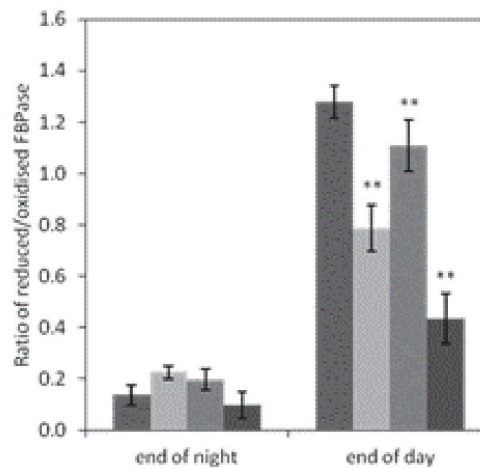
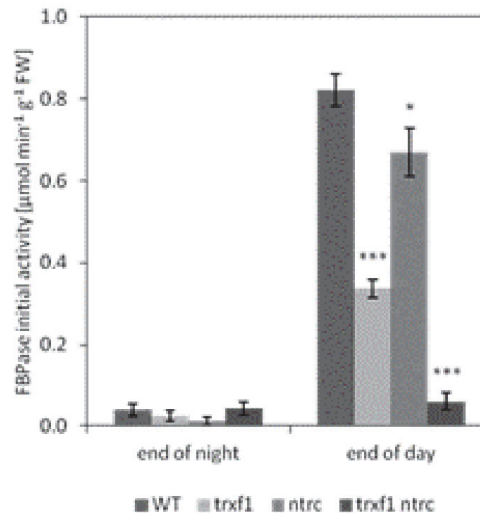
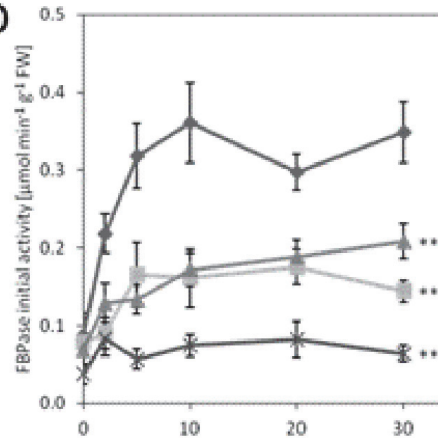
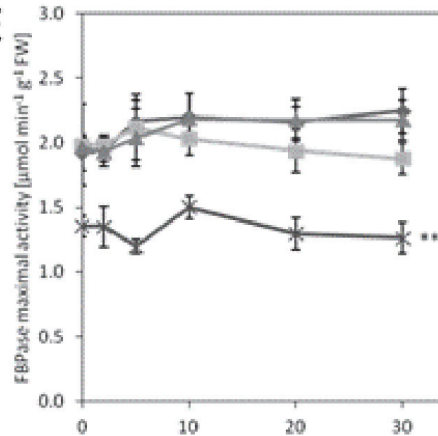
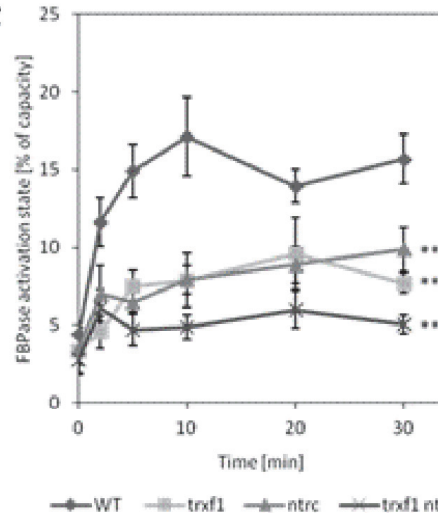
A**B****C****D****E****F**

Figure 7: Light-dependent redox activation of fructose-1,6-bisphosphatase (FBPase) in leaves of *trxf1*, *ntrc* and *trxf1 ntrc* *Arabidopsis* mutants compared to wild-type. **(A)** and **(B)** show the thiol-disulfide reduction state of chloroplast FBPase in leaves harvested at the end of night (EN) and end of day (ED) analyzed by using gel-shift assays: **(A)** Representative gel-shift blot using an antibody specific for chloroplast FBPase, and **(B)** calculated ratio of reduced to oxidized FBPase. **(C)** Corresponding initial enzyme activity of FBPase (assay without DTT) in leaves harvested at the end of night (EN) and end of day (ED). **(D)** to **(F)** Transient light activation of FBPase during a detailed time course. At the end of the night (0 min), plants were illuminated for different time-periods (2, 5, 10, 20 and 30 min) to measure FBPase activity using different assay conditions: **(D)** Initial activity without DTT additions in the assay, **(E)** maximal activity with 10 mM DTT included in the assay, and **(F)** redox-activation state (initial/maximal activity*100). Results are means \pm SE, $n = 8$ (wild-type) or 4 (mutants) different plant replicates **(B)**, $n = 20$ (wild-type) or 10 (mutants) different plant replicates **(C)**, and $n = 8$ (wild-type) or 4 (mutants) different plant replicates **(D)** to **(F)**. All plants were grown in an 8 h photoperiod with 160 μmol photons $\text{m}^{-2} \text{s}^{-1}$. *: $P < 0.05$, **: $P < 0.01$, ***: $P < 0.001$, according to paired t-test **(B)** and **(C)** or two-way analysis of variance [Anova] Tukey test **(D)** to **(F)**

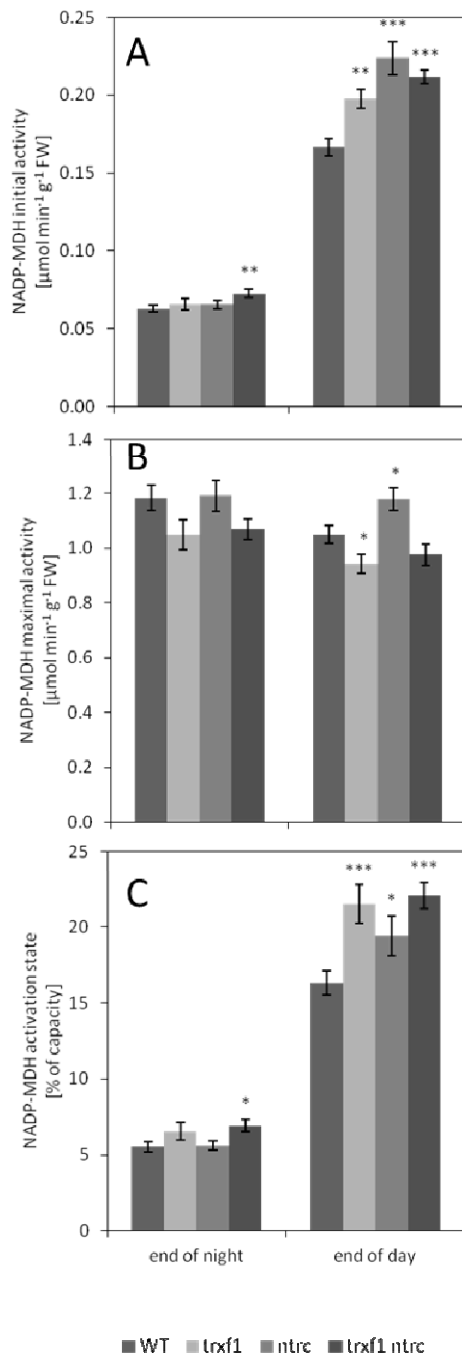


Figure 8: Light-dependent redox activation of NADP-dependent malate dehydrogenase (MDH) in leaves of *trx1*, *ntrc* and *trx1 ntrc* *Arabidopsis* mutants compared to wild-type. **(A)** Initial activity without DTT additions in the assay, **(B)** maximal activity with 10 mM DTT included in the assay, **(C)** redox-activation state (initial/maximal activity*100). Leaves were sampled at the end of night and end of day. Results are means \pm SE, $n=24$ (wild-type) or 12 (mutants) different plant replicates. Plants were grown in an 8 h photoperiod with 160 μmol photons $\text{m}^{-2} \text{s}^{-1}$. *: $P<0.05$, **: $P<0.01$, ***: $P<0.001$ (according to student t-test)

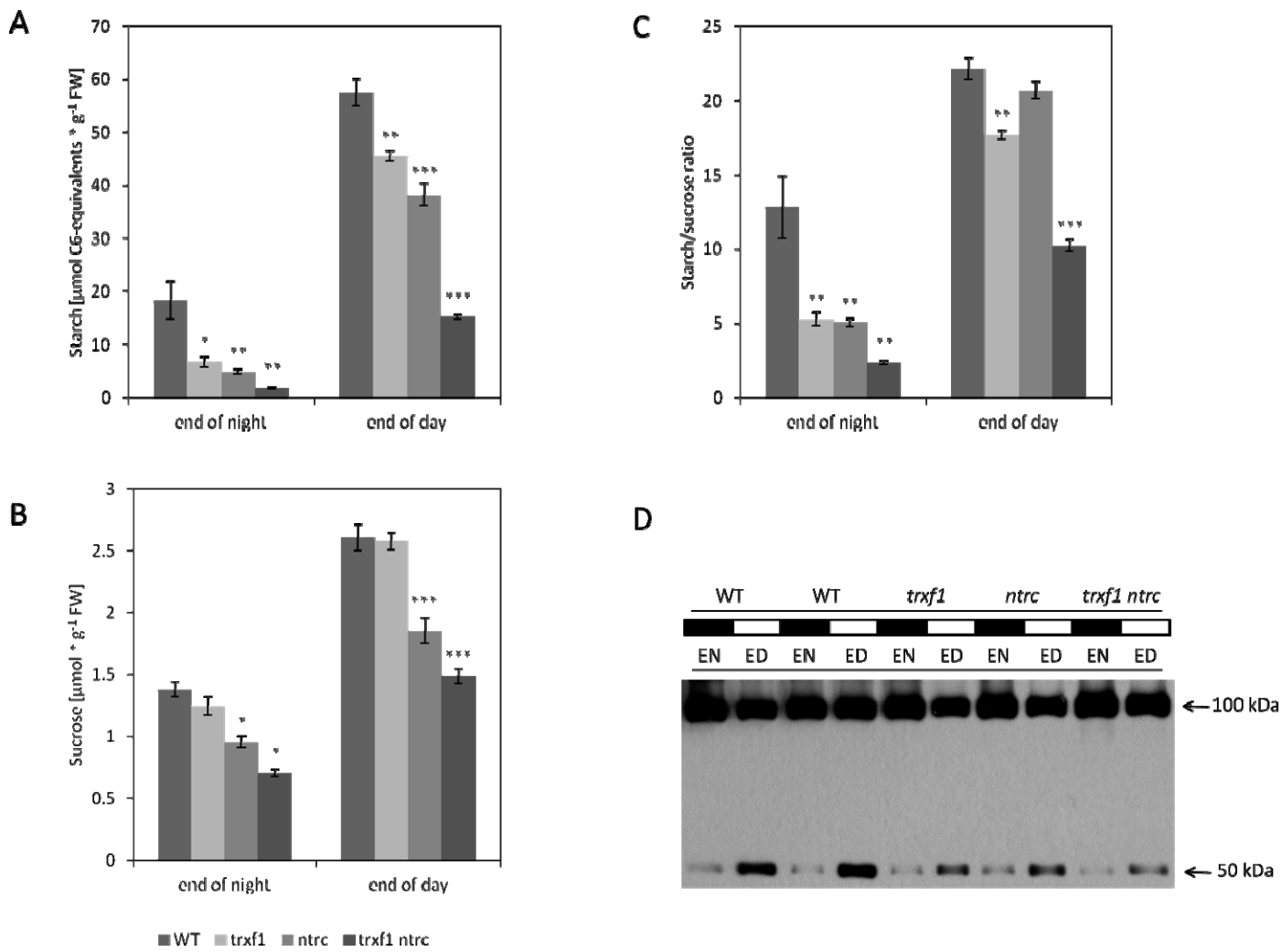


Figure 9: Changes in the accumulation of starch and sucrose and in the thiol-disulfide reduction state of ADP-glucose pyrophosphorylase (AGPase) in leaves of *trxf1*, *ntrc* and *trxf1 ntrc* *Arabidopsis* mutants compared to wild-type. **(A)** Starch level, **(B)** sucrose level, **(C)** starch/sucrose ratio, and **(D)** APS1 monomerisation (representative Western-blot) were measured in leaves sampled at the end of night (EN) and end of day (ED). Results for **(A)** to **(C)** are means \pm SE, $n= 8$ (wild-type) or 4 (mutants) different plant replicates growing in an 8 h photoperiod with 160 μmol photons $\text{m}^{-2} \text{s}^{-1}$. *: $P<0.05$, **: $P<0.01$, ***: $P<0.001$ (according to student *t*-test); APS1 = small subunit of AGPase

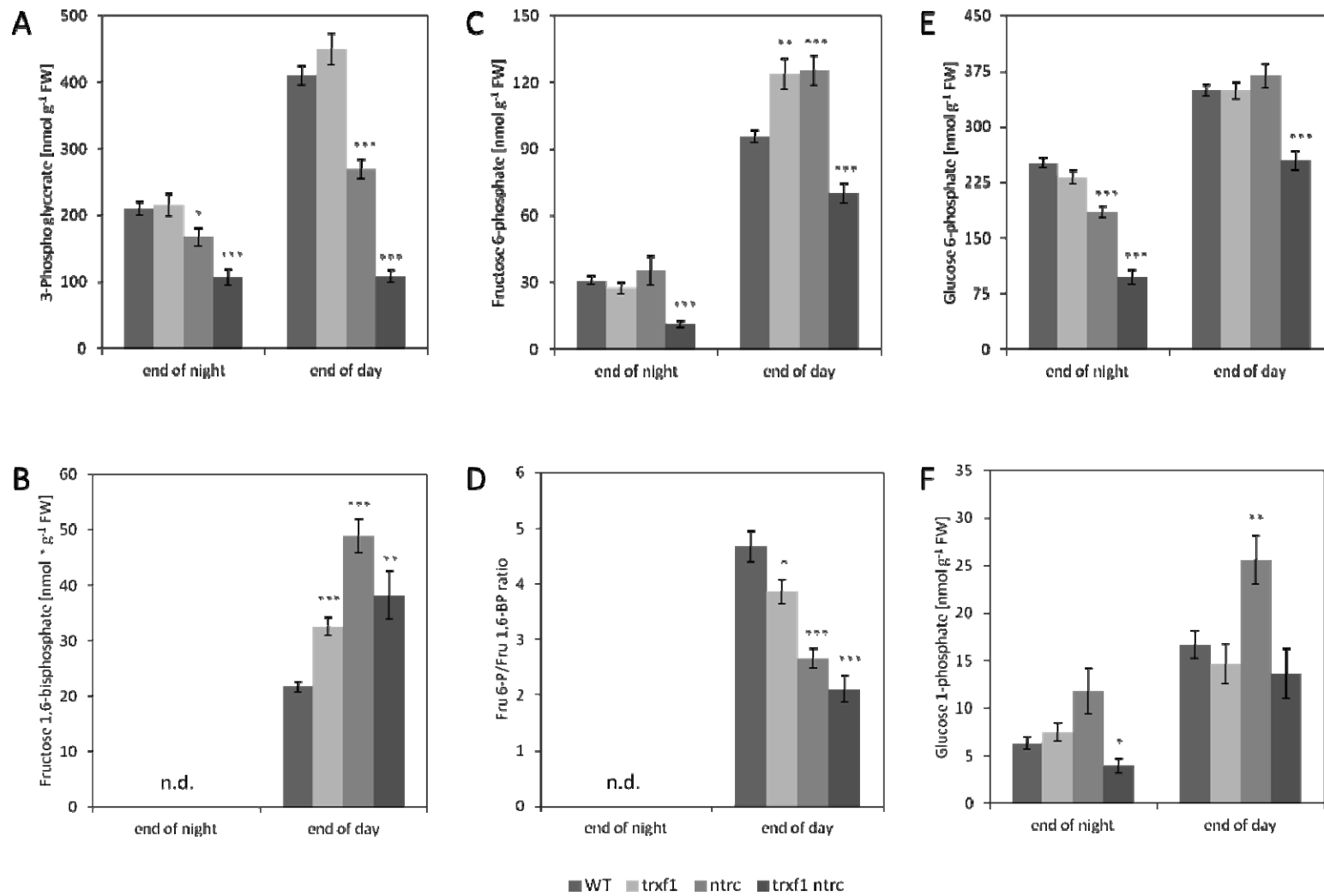
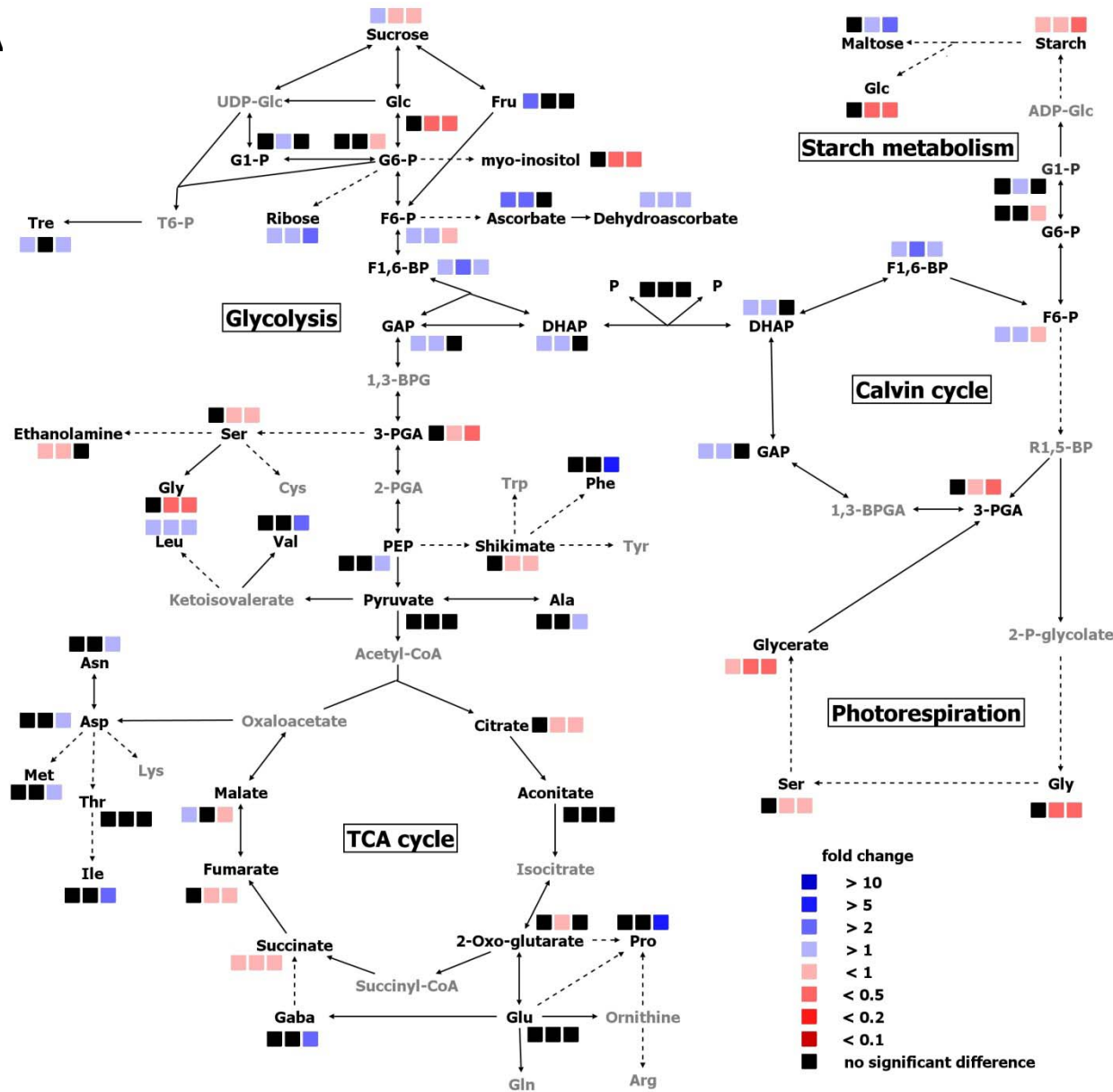


Figure 10: Changes in the in-vivo levels of phosphorylated intermediates in leaves of *trx1*, *ntrc* and *trx1 ntrc* Arabidopsis mutants compared to wild-type. **(A)** 3-phosphoglycerate (3PGA) level, **(B)** fructose-1,6-bisphosphate (FBP) level, **(C)** fructose-6-phosphate (F6P) level, **(D)** F6P/FBP ratio, **(E)** glucose-6-phosphate (G6P) level, and **(F)** glucose-1-phosphate (G1P) level were measured in leaves sampled at the end of the night and end of the day. Results are means \pm SE, $n=30$ (wild-type) or 15 (mutants) different plant replicates growing in an 8 h photoperiod with $160 \mu\text{mol photons m}^{-2} \text{s}^{-1}$. *: $P<0.05$, **: $P<0.01$, ***: $P<0.001$ (according to student *t*-test); n.d. = not detectable (values were below the detection limit)

A



B

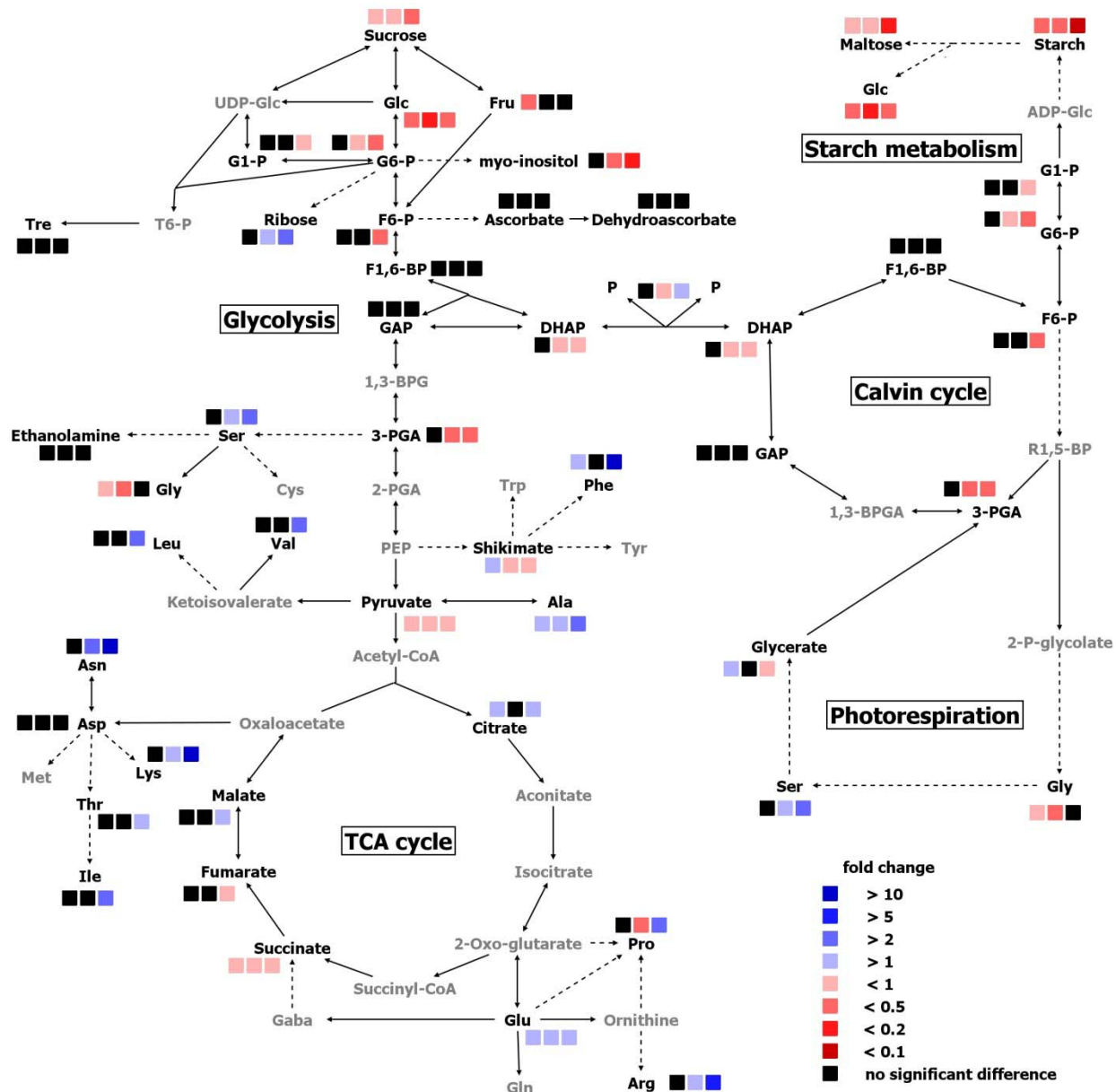
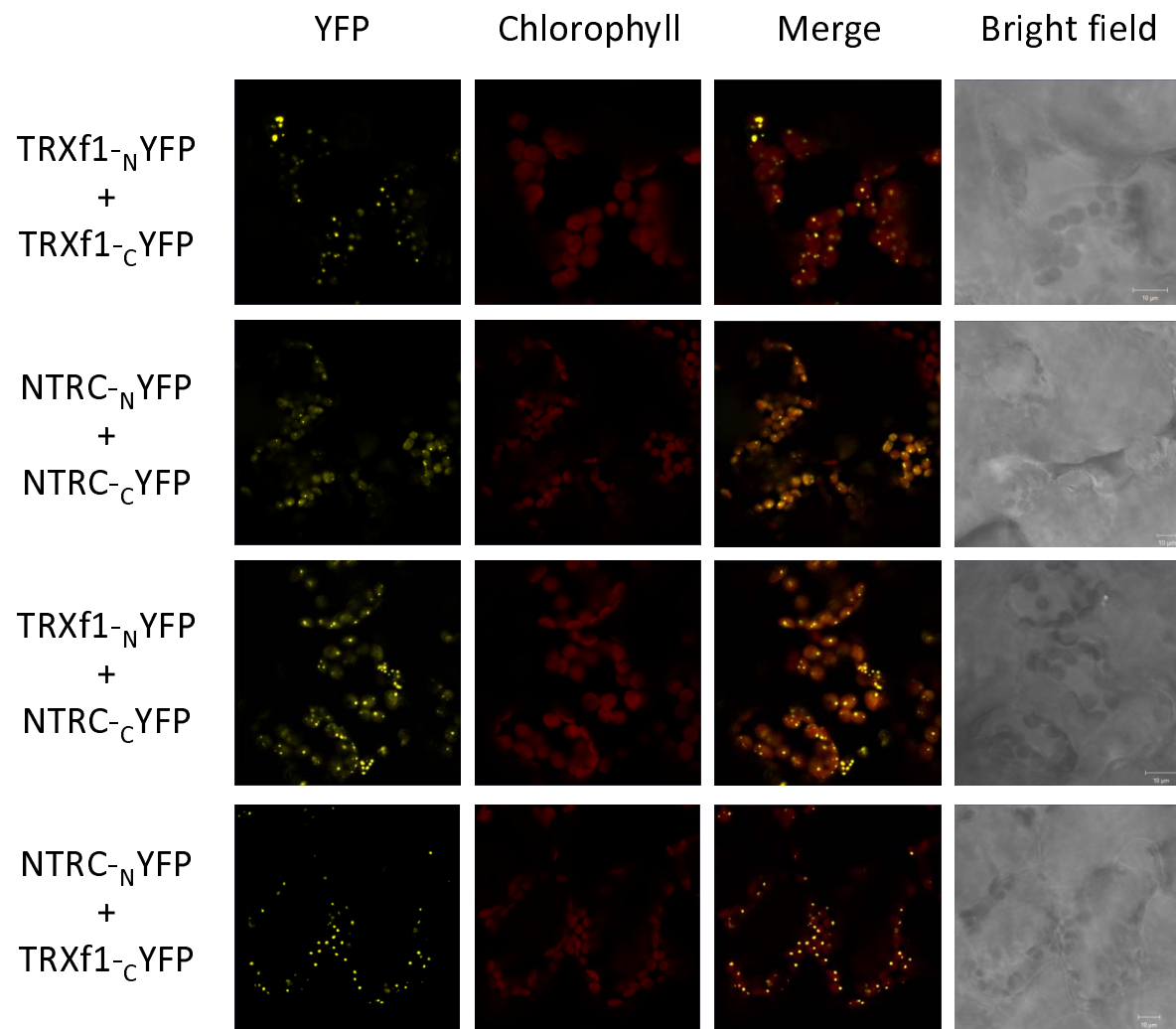


Figure 11: Overview of changes in metabolite profiles from leaves of *trxf1*, *ntrc* and *trxf1 ntrc* Arabidopsis mutants compared to wild-type. Results from leaves sampled at the end of day (**A**) and end of night (**B**) are visualized using Wanted diagrams. Metabolite levels which are significantly different from wild-type according to the student *t*-test ($P<0.05$) are indicated in blue (increase) or red (decrease) color, while black color indicates no significant difference from wild-type. The order of the squares from left to right is *trxf1*, *ntrc* and *trxf1 ntrc* mutants being in first, second and third position, respectively. Data are taken from Supplemental Tables S4 – S7.



continued

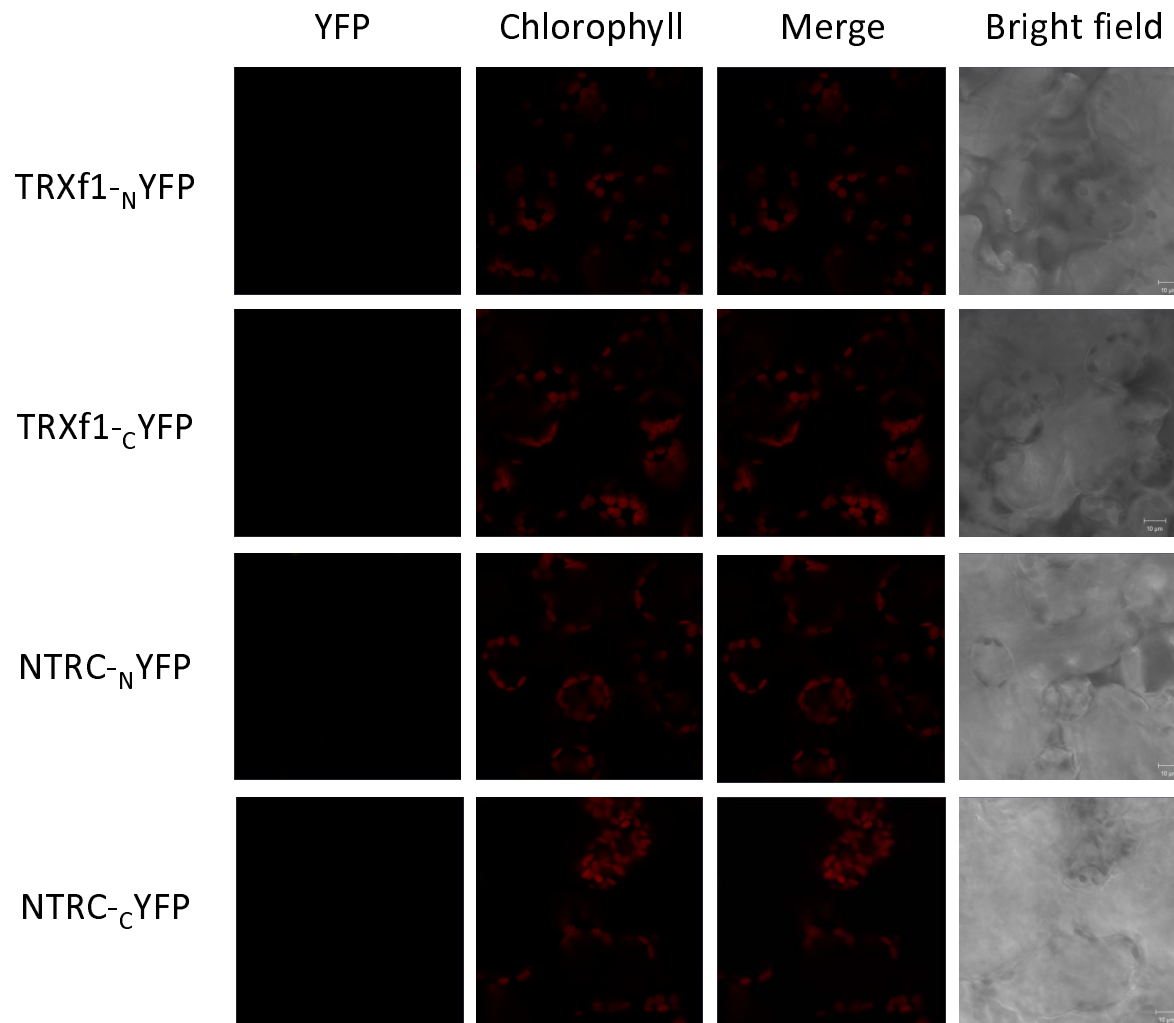
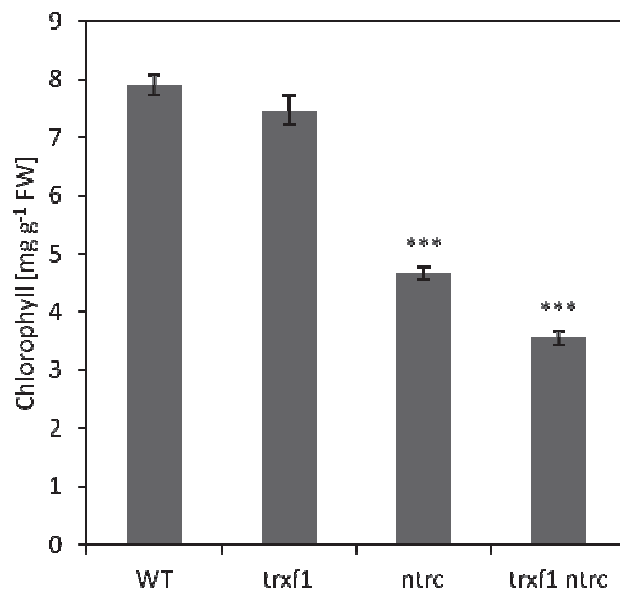
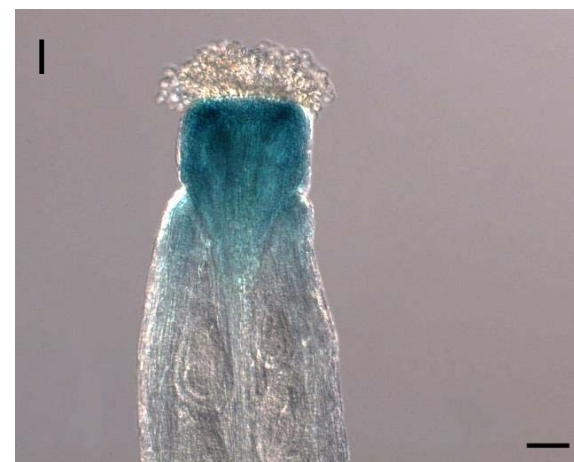
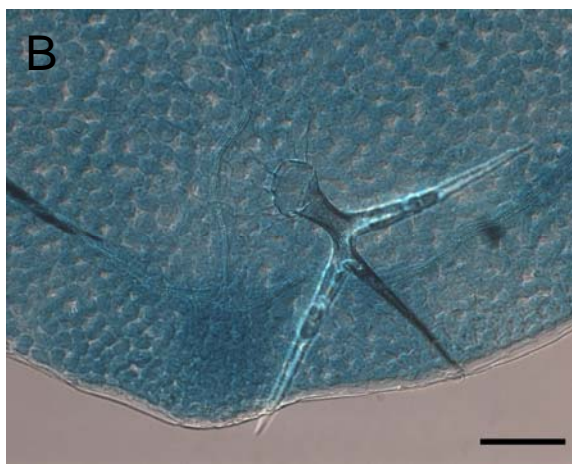
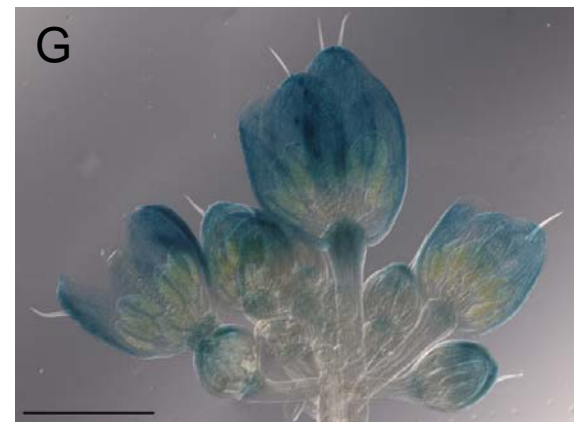


Figure 12: Visualization of protein-protein interactions of NTRC and Trx f1 in *Nicotiana benthamiana* chloroplasts by the BiFC assay. Confocal microscopy picture series present transiently transformed leaf mesophyll cells expressing combinations of the fusion proteins as indicated. Single pictures represent from left to right images of the yellow YFP fluorescence representing the BiFC-signal, the red autofluorescence of chlorophyll, the merge of both fluorescence signals illustrating the overlay of chlorophyll fluorescence and the BiFC-signal, and the bright field channel. No YFP-specific fluorescence signal was detectable in cells expressing fusion proteins separately (negative controls). Pictures were monitored in the channel mode with identical microscope settings. Bars = 10 μ m



Suppl. Figure S1: Changes in chlorophyll content in leaves of *trx1*, *ntrc* and *trx1 ntrc* Arabidopsis mutants compared to wild-type. Results are the mean \pm SE, $n = 24$ (wild-type) or 12 (mutants) different plant replicates growing in an 8 h photoperiod with 160 μmol photons $\text{m}^{-2} \text{s}^{-1}$. *: $P < 0.05$, **: $P < 0.01$, ***: $P < 0.001$ (according to student *t*-test)



Suppl. Figure S2: Histochemical localization of GUS expression in *Arabidopsis* plants transformed with a *Trxf1_{pro}*-GUS reporter gene. GUS staining of 10-day-old seedlings grown in a 16 h photoperiod **(A)** to **(D)**, and of 6-week-old plants having flowered and begun to set seed **(E)** to **(I)**. GUS staining is shown in emerging leaves **(A)** and **(B)**, roots **(C)**, hypocotyl **(D)**, siliques petiol **(E)**, siliques **(F)**, flower **(G)**, sepal **(H)** and stigma **(I)**. No GUS staining was observed in trichomes **(B)**. The following microscopic techniques were used: **(A)**, **(E)** and **(F)** Stereomicroscopy, **(B)**, **(C)**, **(D)**, **(G)**, **(H)** and **(I)** differential interference contrast microscopy, and **(G)** and **(H)** single image merge. Bars = 1000 μ m in **(A)**, **(E)**, **(F)**, **(G)** and **(H)**, and 100 μ m in **(B)**, **(C)**, **(D)** and **(I)**.

Suppl. Table S1:

Statistical analysis for rosette fresh weights of *trxf1*, *ntrc* and *trxf1 ntrc* *Arabidopsis* mutants growing in different light conditions, compared to wild-type. Values are based on the data presented in Figure 2H. Significantly different values from wild-type according to the student t-test ($P<0.05$) are indicated in bold. n.d. = not detectable.

Growth condition	<i>trxf1</i>	<i>ntrc</i>	<i>trxf1 ntrc</i>
4h-day, 160 μ E	0.002	<0.001	n.d.
8h-day, 160 μ E	0.354	<0.001	<0.001
16h-day, 160 μ E	0.484	<0.001	<0.001
24h-day, 160 μ E	0.316	<0.001	<0.001
8h-day, 30 μ E	<0.001	<0.001	n.d.
8h-day, 950 μ E	0.781	<0.001	<0.001

Suppl. Table S2:

Statistical analysis for gas exchange parameters of *trxf1*, *ntrc* and *trxf1 ntrc* Arabidopsis mutants dependent on different light intensities, compared to wild-type. Values are based on the data presented in Figure 3. Significantly different values from wild-type according to the student t-test ($P<0.05$) are indicated in bold. PAR = photosynthetically active radiation.

PAR [$\mu\text{mol m}^{-2} \text{s}^{-1}$]	Assimilation rate			Transpiration rate			Intercellular CO_2 mole fraction		
	<i>trxf1</i>	<i>ntrc</i>	<i>trxf1 ntrc</i>	<i>trxf1</i>	<i>ntrc</i>	<i>trxf1 ntrc</i>	<i>trxf1</i>	<i>ntrc</i>	<i>trxf1 ntrc</i>
0	0.402	0.365	0.011	0.767	0.773	0.002	0.328	0.912	0.693
50	0.958	0.009	0.017	0.789	0.971	0.016	0.446	0.063	<0.001
100	0.863	0.052	0.004	0.864	0.944	0.022	0.682	0.046	<0.001
150	0.762	0.081	0.005	0.882	0.906	0.026	0.996	0.040	<0.001
200	0.797	0.048	0.008	0.851	0.525	0.037	0.670	0.078	<0.001
300	0.576	0.091	<0.001	0.935	0.773	0.052	0.660	0.040	<0.001
400	0.455	0.090	<0.001	0.916	0.909	0.033	0.585	0.047	<0.001
600	0.532	0.058	<0.001	0.852	0.884	0.029	0.404	0.026	<0.001
800	0.529	0.104	0.002	0.794	0.638	0.017	0.208	0.087	<0.001
1000	0.493	0.077	0.071	0.718	0.456	0.028	0.170	0.056	<0.001

Suppl. Table S3:

Statistical analysis for the time course of fructose-1,6-bisphosphatase light activation in leaves of *trxf1*, *ntrc* and *trxf1 ntrc* *Arabidopsis* mutants, compared to wild-type. Values are based on the data presented in Figure 7D-F. Significantly different values from wild-type according to the student t-test ($P<0.05$) are indicated in bold.

Time [min]	Initial activity			Maximal activity			Activation state		
	<i>trxf1</i>	<i>ntrc</i>	<i>trxf1 ntrc</i>	<i>trxf1</i>	<i>ntrc</i>	<i>trxf1 ntrc</i>	<i>trxf1</i>	<i>ntrc</i>	<i>trxf1 ntrc</i>
0	0.802	0.503	0.070	0.837	0.811	0.014	0.521	0.480	0.255
2	0.011	0.044	0.008	0.813	0.939	0.006	0.019	0.097	0.060
5	0.053	0.001	<0.001	0.878	0.642	<0.001	0.023	<0.001	0.002
10	0.039	0.006	0.002	0.589	0.965	0.023	0.051	0.006	<0.001
20	0.010	0.007	<0.001	0.343	0.936	<0.001	0.075	0.010	<0.001
30	<0.001	0.021	<0.001	0.227	0.793	0.002	<0.001	0.026	<0.001

Suppl. Table S4:

Changes in GC-MS based metabolite profiles in leaves of *trxf1*, *ntrc* and *trxf1 ntrc* Arabidopsis mutants compared to wild-type. Leaves were sampled at the end of the day. Results are means \pm SD, $n = 12$. Values which are significantly different from wild type according to the student t-test ($P < 0.05$) are indicated in bold (see also Figure 11A).

Metabolites	WT	<i>trxf1</i>	P-value	<i>ntrc</i>	P-value	<i>trxf1 ntrc</i>	P-value
Sugars							
Fructose	1.00 \pm 0.57	2.03 \pm 0.69	0.001	1.15 \pm 0.37	0.445	0.83 \pm 0.22	0.360
Glucose	1.00 \pm 0.63	1.43 \pm 0.63	0.109	0.39 \pm 0.08	0.006	0.45 \pm 0.24	0.014
Maltose	1.00 \pm 0.26	1.03 \pm 0.20	0.725	1.65 \pm 0.69	0.008	3.13 \pm 1.34	<0.001
Raffinose	1.00 \pm 0.35	1.93 \pm 1.13	0.017	0.25 \pm 0.07	<0.001	0.55 \pm 0.64	0.045
Ribose	1.00 \pm 0.08	1.15 \pm 0.18	0.016	1.55 \pm 0.51	0.003	2.64 \pm 1.14	<0.001
Sucrose	1.00 \pm 0.07	1.11 \pm 0.10	0.004	0.86 \pm 0.14	0.007	0.89 \pm 0.07	0.001
Trehalose	1.00 \pm 0.49	1.38 \pm 0.23	0.028	1.20 \pm 0.44	0.304	1.88 \pm 0.75	0.003
Phosphate ester							
Glycerol-3-phosphate	1.00 \pm 0.27	1.14 \pm 0.17	0.143	1.22 \pm 0.47	0.174	1.85 \pm 1.02	0.016
Phosphoenolpyruvate	1.00 \pm 0.18	1.02 \pm 0.20	0.805	1.35 \pm 0.68	0.112	1.85 \pm 0.53	<0.001
Organic acids							
Aconitate (cis)	1.00 \pm 0.29	0.99 \pm 0.32	0.956	0.84 \pm 0.12	0.086	1.05 \pm 0.36	0.711
Benzoate	1.00 \pm 0.24	1.14 \pm 0.32	0.257	1.33 \pm 0.58	0.096	1.61 \pm 0.29	<0.001
caffeoate (cis)	1.00 \pm 0.10	0.98 \pm 0.10	0.593	1.09 \pm 0.40	0.486	1.33 \pm 0.93	0.247
caffeoate (trans)	1.00 \pm 0.36	1.03 \pm 0.26	0.871	0.92 \pm 0.20	0.594	1.10 \pm 0.26	0.530
3-caffeooyl-quinate (cis)	1.00 \pm 0.10	1.06 \pm 0.16	0.306	0.88 \pm 0.15	0.033	0.91 \pm 0.18	0.138
3-caffeooyl-quinate (trans)	1.00 \pm 0.22	1.23 \pm 0.41	0.112	0.59 \pm 0.12	<0.001	0.74 \pm 0.19	0.005
Citrate	1.00 \pm 0.19	1.09 \pm 0.14	0.202	0.69 \pm 0.24	0.002	0.51 \pm 0.38	0.001

Fumarate	1.00 ± 0.17	1.05 ± 0.10	0.404	0.80 ± 0.19	0.011	0.70 ± 0.22	0.001
Galactonate	1.00 ± 0.12	0.95 ± 0.06	0.268	0.88 ± 0.11	0.015	0.91 ± 0.06	0.029
Glycerate	1.00 ± 0.04	0.61 ± 0.07	<0.001	0.36 ± 0.18	<0.001	0.33 ± 0.44	<0.001
Gulonate	1.00 ± 0.19	1.28 ± 0.19	0.002	1.28 ± 0.38	0.033	1.42 ± 0.36	0.002
Malate	1.00 ± 0.12	1.22 ± 0.19	0.003	1.00 ± 0.24	0.955	0.69 ± 0.28	0.003
Maleate	1.00 ± 0.51	0.85 ± 0.35	0.395	0.94 ± 0.36	0.726	1.51 ± 0.74	0.065
2-methyl-malate	1.00 ± 0.09	0.93 ± 0.17	0.206	0.63 ± 0.18	<0.001	0.61 ± 0.21	<0.001
2-oxo-glutarate	1.00 ± 0.18	0.92 ± 0.21	0.311	0.66 ± 0.12	<0.001	0.83 ± 0.36	0.281
Pyruvate	1.00 ± 0.35	0.79 ± 0.18	0.079	0.85 ± 0.23	0.225	1.02 ± 0.23	0.853
Shikimate	1.00 ± 0.08	1.11 ± 0.23	0.160	0.52 ± 0.12	<0.001	0.51 ± 0.32	<0.001
sinapate (cis)	1.00 ± 0.16	0.95 ± 0.16	0.485	0.97 ± 0.13	0.573	1.07 ± 0.19	0.370
sinapate (trans)	1.00 ± 0.22	0.91 ± 0.17	0.290	1.00 ± 0.22	0.987	1.29 ± 0.40	0.040
Succinate	1.00 ± 0.16	0.80 ± 0.12	0.002	0.57 ± 0.15	<0.001	0.58 ± 0.35	0.002
Threonate	1.00 ± 0.12	0.95 ± 0.18	0.416	0.62 ± 0.05	<0.001	0.64 ± 0.14	<0.001
<u>Amino acids</u>							
Alanine	1.00 ± 0.22	1.12 ± 0.37	0.357	1.07 ± 0.36	0.567	1.36 ± 0.48	0.032
Aspartate	1.00 ± 0.21	1.08 ± 0.33	0.496	1.24 ± 0.62	0.226	1.75 ± 0.60	0.001
Asparagine	1.00 ± 0.23	1.10 ± 0.17	0.368	1.21 ± 0.67	0.359	1.95 ± 0.48	<0.001
Glutamate	1.00 ± 0.27	1.03 ± 0.27	0.797	0.85 ± 0.26	0.179	1.05 ± 0.33	0.676
Glycine	1.00 ± 0.13	1.24 ± 0.38	0.055	0.45 ± 0.17	<0.001	0.43 ± 0.31	<0.001
4-hydroxy-proline (cis)	1.00 ± 0.28	0.77 ± 0.37	0.100	0.38 ± 0.05	0.000	0.85 ± 0.26	0.300
Isoleucine	1.00 ± 0.20	1.16 ± 0.30	0.136	1.48 ± 0.90	0.093	2.30 ± 1.16	0.003
Leucine	1.00 ± 0.172	1.23 ± 0.19	0.007	1.40 ± 0.46	0.018	1.96 ± 1.00	0.007
Methionine	1.00 ± 0.20	1.08 ± 0.31	0.470	1.12 ± 0.25	0.219	1.37 ± 0.44	0.018

Phenylalanine	1.00 ± 0.28	1.21 ± 0.25	0.073	3.16 ± 4.21	0.104	6.74 ± 4.27	0.001
Proline	1.00 ± 0.42	1.58 ± 0.90	0.059	2.30 ± 2.91	0.153	7.16 ± 5.63	0.003
Pyroglutamate	1.00 ± 0.33	1.22 ± 0.20	0.066	1.14 ± 0.38	0.356	1.59 ± 0.51	0.003
Serine	1.00 ± 0.36	0.75 ± 0.32	0.086	0.50 ± 0.19	<0.001	0.57 ± 0.19	0.001
Threonine	1.00 ± 0.21	1.06 ± 0.40	0.672	1.03 ± 0.39	0.845	1.19 ± 0.25	0.059
Valine	1.00 ± 0.15	1.12 ± 0.36	0.313	1.21 ± 0.71	0.339	2.16 ± 1.16	0.005
<u>Sugar alcohols</u>							
Erythritol	1.00 ± 0.14	1.34 ± 0.20	0.003	2.63 ± 2.82	0.072	7.40 ± 3.30	<0.001
Glycerol	1.00 ± 0.14	0.99 ± 0.19	0.918	1.09 ± 0.29	0.328	1.41 ± 0.33	0.001
Mannitol	1.00 ± 0.20	1.04 ± 0.30	0.738	2.91 ± 3.02	0.051	8.07 ± 5.35	0.001
myo-inositol	1.00 ± 0.16	1.19 ± 0.41	0.164	0.44 ± 0.16	<0.001	0.42 ± 0.36	<0.001
Sorbitol	1.00 ± 0.09	0.87 ± 0.11	0.007	1.04 ± 0.15	0.449	1.24 ± 0.34	0.034
<u>Others</u>							
4-amino-butanoate	1.00 ± 0.16	1.67 ± 1.31	0.105	1.17 ± 0.84	0.542	4.92 ± 2.95	0.001
Ascorbate	1.00 ± 0.52	3.40 ± 2.32	0.004	4.22 ± 2.19	<0.001	1.02 ± 0.60	0.947
Dehydroascorbate	1.00 ± 0.20	1.44 ± 0.45	0.011	1.70 ± 0.64	0.003	1.76 ± 0.28	<0.001
Ethanolamine	1.00 ± 0.26	0.59 ± 0.14	<0.001	0.53 ± 0.17	<0.001	1.00 ± 0.13	0.968
Phosphate	1.00 ± 0.13	1.02 ± 0.16	0.793	0.99 ± 0.18	0.847	1.07 ± 0.21	0.337
Putrescine	1.00 ± 0.29	1.06 ± 0.40	0.658	1.28 ± 0.52	0.124	2.02 ± 1.10	0.009
Spermidine	1.00 ± 0.67	1.13 ± 0.56	0.636	0.77 ± 0.47	0.355	0.74 ± 0.35	0.267
Uracil	1.00 ± 0.62	0.92 ± 0.48	0.763	1.24 ± 0.67	0.407	3.42 ± 3.29	0.028

Suppl. Table S5:

Changes in GC-MS based metabolite profiles in leaves of *trxf1*, *ntrc* and *trxf1 ntrc* Arabidopsis mutants compared to wild-type. Leaves were sampled at the end of the night. Results are means \pm SD, $n = 12$. Values which are significantly different from wild type according to the student t-test ($P < 0.05$) are indicated in bold (see also Figure 11B).

Metabolites	WT	<i>trxf1</i>	P-value	<i>ntrc</i>	P-value	<i>trxf1 ntrc</i>	P-value
<u>Sugars</u>							
Arabinose	1.00 \pm 0.09	0.98 \pm 0.08	0.549	0.95 \pm 0.03	0.100	0.70 \pm 0.04	<0.001
Fructose	1.00 \pm 0.34	0.38 \pm 0.04	<0.001	1.14 \pm 0.46	0.397	1.14 \pm 0.68	0.535
Galactose	1.00 \pm 0.33	0.56 \pm 0.15	<0.001	0.31 \pm 0.10	<0.001	0.39 \pm 0.13	<0.001
Glucose	1.00 \pm 0.38	0.35 \pm 0.04	<0.001	0.20 \pm 0.04	<0.001	0.34 \pm 0.12	<0.001
Glucose (beta-1,6-anhydro)	1.00 \pm 0.19	0.83 \pm 0.16	0.025	0.80 \pm 0.16	0.011	1.15 \pm 0.21	0.085
Maltose	1.00 \pm 0.09	0.73 \pm 0.07	<0.001	0.51 \pm 0.04	<0.001	0.19 \pm 0.03	<0.001
Mannose	1.00 \pm 0.32	0.94 \pm 0.19	0.615	0.81 \pm 0.14	0.079	0.99 \pm 0.17	0.905
Psicose	1.00 \pm 0.05	1.09 \pm 0.06	<0.001	0.99 \pm 0.08	0.733	1.02 \pm 0.04	0.230
Ribose	1.00 \pm 0.17	1.04 \pm 0.11	0.464	1.17 \pm 0.11	0.011	2.71 \pm 0.45	<0.001
Sucrose	1.00 \pm 0.03	0.82 \pm 0.09	<0.001	0.53 \pm 0.04	<0.001	0.46 \pm 0.04	<0.001
Trehalose	1.00 \pm 0.28	1.11 \pm 0.19	0.283	0.86 \pm 0.21	0.168	1.08 \pm 0.14	0.386
Xylose	1.00 \pm 0.18	0.88 \pm 0.10	0.055	0.84 \pm 0.11	0.014	1.11 \pm 0.17	0.124
<u>Organic acids</u>							
Citrate	1.00 \pm 0.26	1.53 \pm 0.23	<0.001	0.99 \pm 0.25	0.924	1.23 \pm 0.26	0.036
Fumarate	1.00 \pm 0.20	0.92 \pm 0.11	0.256	0.89 \pm 0.09	0.107	0.59 \pm 0.06	<0.001
Glycerate	1.00 \pm 0.13	1.13 \pm 0.09	0.011	0.90 \pm 0.18	0.120	0.70 \pm 0.09	<0.001
Hexadecanoate	1.00 \pm 0.55	0.58 \pm 0.22	0.026	0.54 \pm 0.17	0.016	0.57 \pm 0.18	0.022

Malate	1.00 ± 0.22	1.06 ± 0.12	0.437	1.12 ± 0.25	0.216	1.54 ± 0.15	<0.001
Maleate	1.00 ± 0.14	1.00 ± 0.16	0.985	1.10 ± 0.20	0.167	1.87 ± 0.22	<0.001
Octadecanoate	1.00 ± 0.62	0.69 ± 0.29	0.134	0.65 ± 0.23	0.088	0.70 ± 0.25	0.134
Pyroglutamate	1.00 ± 0.19	1.05 ± 0.13	0.435	1.66 ± 0.14	<0.001	2.04 ± 0.14	<0.001
Pyruvate	1.00 ± 0.29	0.75 ± 0.18	0.018	0.68 ± 0.18	0.003	0.71 ± 0.19	0.007
Shikimate	1.00 ± 0.07	1.17 ± 0.11	<0.001	0.87 ± 0.09	<0.001	0.69 ± 0.07	<0.001
Sinapate (cis)	1.00 ± 0.11	1.00 ± 0.16	0.991	1.00 ± 0.06	0.993	1.45 ± 0.10	<0.001
Sinapate (trans)	1.00 ± 0.14	1.11 ± 0.09	0.028	1.14 ± 0.11	0.015	1.68 ± 0.14	<0.001
Succinate	1.00 ± 0.14	0.82 ± 0.10	0.002	0.86 ± 0.12	0.018	0.59 ± 0.06	<0.001
Threonate	1.00 ± 0.11	1.24 ± 0.12	<0.001	1.42 ± 0.45	0.009	0.94 ± 0.15	0.310
Amino acids							
Alanine	1.00 ± 0.13	1.25 ± 0.11	<0.001	1.64 ± 0.15	<0.001	3.03 ± 0.19	<0.001
Arginine	1.00 ± 0.25	1.22 ± 0.29	0.057	1.27 ± 0.32	0.031	7.53 ± 3.62	<0.001
Asparagine	1.00 ± 0.43	1.02 ± 0.28	0.881	2.41 ± 1.65	0.014	43.70 ± 9.51	<0.001
Aspartate	1.00 ± 0.48	0.93 ± 0.36	0.686	0.77 ± 0.51	0.272	1.14 ± 0.62	0.543
Glutamate	1.00 ± 0.30	1.40 ± 0.18	<0.001	1.48 ± 0.24	<0.001	1.88 ± 0.12	<0.001
Glycine	1.00 ± 0.43	0.67 ± 0.13	0.027	0.42 ± 0.06	<0.001	0.77 ± 0.26	0.134
Isoleucine	1.00 ± 0.15	1.04 ± 0.29	0.665	1.15 ± 0.30	0.141	3.98 ± 0.54	<0.001
Leucine	1.00 ± 0.16	0.99 ± 0.40	0.952	1.05 ± 0.51	0.731	3.28 ± 0.52	<0.001
Lysine	1.00 ± 0.25	1.14 ± 0.28	0.215	1.52 ± 0.76	0.034	10.21 ± 3.01	<0.001
Phenylalanine	1.00 ± 0.33	1.36 ± 0.37	0.019	0.82 ± 0.22	0.135	10.28 ± 1.84	<0.001
Proline	1.00 ± 0.44	0.80 ± 0.33	0.225	0.49 ± 0.18	0.002	2.36 ± 0.38	<0.001
Serine	1.00 ± 0.27	1.05 ± 0.16	0.547	1.25 ± 0.14	0.010	2.33 ± 0.28	<0.001
Threonine	1.00 ± 0.20	1.07 ± 0.08	0.314	1.13 ± 0.14	0.087	1.99 ± 0.16	<0.001

Valine	1.00 ± 0.19	1.04 ± 0.17	0.578	1.13 ± 0.22	0.124	2.59 ± 0.24	<0.001
<u>Sugar alcohols</u>							
Erythritol	1.00 ± 0.19	1.12 ± 0.07	0.051	1.63 ± 0.23	<0.001	5.96 ± 0.77	<0.001
Glycerol	1.00 ± 0.13	1.12 ± 0.18	0.081	0.99 ± 0.14	0.870	1.33 ± 0.16	<0.001
Inositol (myo)	1.00 ± 0.11	1.00 ± 0.07	0.985	0.47 ± 0.06	<0.001	0.19 ± 0.03	<0.001
Mannitol	1.00 ± 0.64	0.74 ± 0.19	0.200	2.90 ± 0.90	<0.001	18.26 ± 6.04	<0.001
Sorbitol	1.00 ± 0.07	0.90 ± 0.06	0.001	0.96 ± 0.09	0.192	1.37 ± 0.07	<0.001
<u>Others</u>							
Ascorbate	1.00 ± 0.68	0.66 ± 0.25	0.126	0.87 ± 0.81	0.680	1.03 ± 0.32	0.895
Dehydroascorbate	1.00 ± 0.25	0.86 ± 0.11	0.087	0.82 ± 0.23	0.083	1.14 ± 0.29	0.228
Ethanolamine	1.00 ± 0.34	0.85 ± 0.12	0.163	1.02 ± 0.17	0.888	1.34 ± 0.48	0.058
Phosphate	1.00 ± 0.15	1.01 ± 0.14	0.865	0.67 ± 0.14	<0.001	1.88 ± 0.14	<0.001
Putrescine	1.00 ± 0.36	1.06 ± 0.27	0.664	1.36 ± 0.48	0.048	3.65 ± 0.42	<0.001
Spermidine	1.00 ± 0.54	1.34 ± 0.52	0.135	2.62 ± 0.99	<0.001	2.44 ± 1.81	0.021
Uracil	1.00 ± 0.19	0.74 ± 0.18	0.002	0.80 ± 0.16	0.011	4.40 ± 0.56	<0.001

Suppl. Table S6:

Changes in the levels of phosphorylated intermediates and starch in leaves of *trxf1*, *ntrc* and *trxf1 ntrc* *Arabidopsis* mutants compared to wild-type, based on spectrophotometric measurements. Leaves were sampled at the end of the day. Results are normalized to wild-type level and represent means \pm SE, $n = 8-30$ (wild-type) or 4-15 (mutants). Values which are significantly different from wild-type according to the student t-test ($P < 0.05$) are indicated in bold (see also Figure 11A).

Metabolites	WT	<i>trxf1</i>	<i>P</i> -value	<i>ntrc</i>	<i>P</i> -value	<i>trxf1 ntrc</i>	<i>P</i> -value
Dihydroxyacetone phosphate	1.00 \pm 0.03	1.22 \pm 0.06	0.001	1.69 \pm 0.10	<0.001	0.99 \pm 0.14	0.926
Fructose 1,6-bisphosphate	1.00 \pm 0.04	1.50 \pm 0.08	<0.001	2.25 \pm 0.14	<0.001	1.76 \pm 0.20	0.002
Fructose 6-phosphate	1.00 \pm 0.03	1.29 \pm 0.07	0.001	1.31 \pm 0.07	<0.001	0.73 \pm 0.05	<0.001
Glucose 1-phosphate	1.00 \pm 0.09	0.88 \pm 0.12	0.432	1.54 \pm 0.15	0.003	0.82 \pm 0.16	0.282
Glucose 6-phosphate	1.00 \pm 0.02	1.00 \pm 0.03	0.997	1.06 \pm 0.05	0.207	0.73 \pm 0.04	<0.001
Glyceraldehyde 3-phosphate	1.00 \pm 0.04	1.25 \pm 0.09	0.006	1.68 \pm 0.11	<0.001	0.92 \pm 0.09	0.389
3-Phosphoglycerate	1.00 \pm 0.04	1.10 \pm 0.06	0.139	0.66 \pm 0.04	<0.001	0.26 \pm 0.02	<0.001
Starch	1.00 \pm 0.04	0.79 \pm 0.02	0.009	0.66 \pm 0.04	<0.001	0.26 \pm 0.01	<0.001

Suppl. Table S7:

Changes in the levels of phosphorylated intermediates and starch in leaves of *trxf1*, *ntrc* and *trxf1 ntrc* *Arabidopsis* mutants compared to wild-type, based on spectrophotometric measurements. Leaves were sampled at the end of the night. Results are normalized to wild-type level and represent means \pm SE, $n = 8-30$ (wild-type) or 4-15 (mutants). Values which are significantly different from wild-type according to the student t-test ($P < 0.05$) are indicated in bold (see also Figure 11B). n.d. = not detectable.

Metabolites	WT	<i>trxf1</i>	P-value	<i>ntrc</i>	P-value	<i>trxf1 ntrc</i>	P-value
Dihydroxyacetone phosphate	1.00 \pm 0.03	0.96 \pm 0.08	0.608	0.73 \pm 0.03	<0.001	0.65 \pm 0.07	<0.001
Fructose 1,6-bisphosphate	n.d.	n.d.		n.d.		n.d.	
Fructose 6-phosphate	1.00 \pm 0.07	0.88 \pm 0.09	0.322	1.14 \pm 0.21	0.549	0.36 \pm 0.05	<0.001
Glucose 1-phosphate	1.00 \pm 0.11	1.18 \pm 0.16	0.364	1.86 \pm 0.38	0.053	0.62 \pm 0.12	0.042
Glucose 6-phosphate	1.00 \pm 0.03	0.92 \pm 0.04	0.106	0.73 \pm 0.03	<0.001	0.38 \pm 0.04	<0.001
Glyceraldehyde 3-phosphate	n.d.	n.d.		n.d.		n.d.	
3-Phosphoglycerate	1.00 \pm 0.05	1.03 \pm 0.08	0.771	0.80 \pm 0.07	0.026	0.51 \pm 0.06	<0.001
Starch	1.00 \pm 0.20	0.36 \pm 0.05	0.014	0.26 \pm 0.02	0.007	0.09 \pm 0.01	0.002

RESULTS

Chapter 3 – Disruption of both chloroplastic and cytosolic FBPases genes results in dwarf phenotype and important starch and metabolite changes in *Arabidopsis thaliana*

José A. Rojas-González, Mauricio Soto-Súarez, Ángel García-Díaz, María C. Romero-Puertas, Luisa M. Sandalio, Ángel Mérida, Ina Thormählen, Peter Geigenberger, Antonio J. Serrato, Mariam Sahrawy (2014) Disruption of both chloroplastic and cytosolic FBPases genes results in dwarf phenotype and important starch and metabolite changes in *Arabidopsis thaliana*. *Manuscript submitted, first revision (revision–major) (J Exp Bot).*

1 **Disruption of both chloroplastic and cytosolic FBPases genes results in dwarf**
2 **phenotype and important starch and metabolite changes in *Arabidopsis***
3 ***thaliana***

4

5 José A. Rojas-González¹, Mauricio Soto-Suárez^{1*}, Ángel García-Díaz^{1**}, María C.
6 Romero-Puertas¹, Luisa M. Sandalio¹, Ángel Mérida², Ina Thormählen³, Peter
7 Geigenberger³, Antonio J. Serrato¹ and Mariam Sahrawy^{1§}

8

9

10 ¹Departamento de Bioquímica, Biología Molecular y Celular de Plantas. Estación
11 Experimental del Zaidín. Consejo Superior de Investigaciones Científicas.
12 C/Profesor Albareda 1, 18008, Granada, Spain.

13 ²Instituto de Bioquímica Vegetal y Fotosíntesis. CSIC-US. Avda Américo
14 Vespucio, 49. 41092-Sevilla, Spain.

15 ³Ludwig Maximilians University of Munich. Biology Department I, Plant
16 Metabolism, Grosshaderner Str. 2-4, 82152 Planegg, Germany.

17 joseantonio.rojas@eez.csic.es; mauricio.soto@cragenomica.es;
18 AGarciaDiaz@mednet.ucla.edu; maria.romero@eez.csic.es;
19 luisamaria.sandalio@eez.csic.es; angel@ibvf.csic.es; thormaehlen@biologie.uni-
20 muenchen.de; geigenberger@biologie.uni-muenchen.de; aserrato@eez.csic.es;
21 sahrawy@eez.csic.es

22

23

24 [§]Author for correspondence: Mariam Sahrawy, Department of Plant Biochemistry
25 and Molecular and Cell Biology, EEZ-CSIC, Profesor Albareda 1, 18008
26 Granada, Spain.

27 E-mail: mariam.sahrawy@eez.csic.es.

28 Tel.: +34 958 181600, Fax +34 958 129600

29

30 Running title: Plant FBPases control sugar synthesis and growth

1 Date of submission: 27 Octobre 2014
2 Number of Tables: 2
3 Number of Figures: 11
4 Total word count: 9448
5 Supplementary data: 2 Figures, 4 tables

6

7 **Footnotes:**

8 This work has been funded by research project BIO2009-07297 from the Spanish
9 Ministry of Science and Innovation and the European Fund for Regional
10 Development and project BIO2012-33292 from the Spanish Ministry of Economy
11 and Competitiveness, project P07-CVI-2795 and BIO 154 from the Andalucian
12 Regional Government, Spain. Mauricio Soto-Suárez has been supported by a
13 postdoctoral contract from the Andalucian Regional Government and the CSIC.
14 José A. Rojas González has been supported by a contract from the Andalucian
15 Regional Government. Peter Geigenberger gratefully acknowledges support from
16 the Deutsche Forschungsgemeinschaft.

17

18 *Present address: Centre for Research in Agricultural Genomics CSIC-IRTA-UAB-UB,
19 Parc de Recerca UAB, Edifici CRAG, Campus UAB, Bellaterra (Cerdanyola del Vallès),
20 08193, Barcelona, Spain.

21 ** Present address: Department of Medicine (Division of Hematology-Oncology), David
22 Geffen School of Medicine, University of California Los Angeles (UCLA); Los Angeles,
23 CA, USA.

24

25 Key words: fructose-1,6-bisphosphatase, chloroplastic, cytosolic, knockout mutants,
26 sucrose, starch, metabolites

27

28

29

30

31

32

1 **Abstract**

2 In this study we provide evidence for the role of FBPases in plant development
3 and carbohydrate synthesis and distribution by analyzing two *Arabidopsis*
4 (*Arabidopsis thaliana*) T-DNA knockout mutant lines, *cyfbp* and *cfbp1*, and one
5 double mutant *cyfbp cfbp1* which affect each FBPase isoform, cytosolic and
6 chloroplastic, respectively. cyFBP is involved in sucrose synthesis, whilst cFBP1
7 is key enzyme in Calvin cycle. In addition to the smaller rosette size and lower
8 photosynthesis rate the lack of cFBP1 in the mutants *cfbp1* and *cyfbp cfbp1* leads
9 to a lower content in soluble sugars, less starch accumulation and a greater
10 superoxide dismutase (SOD) activity. The mutants also had some developmental
11 alterations, including stomata opening defects and higher root vascular layers.
12 Complementation also confirmed that the mutant phenotypes were caused by
13 disruption of the cFBP1 gene. Plants without the cyFBP, *cyfbp* mutant showed
14 higher starch content in the chloroplasts, but this did not greatly affect the
15 phenotype. Notably, the sucrose content in *cyfbp* was close to that found in the
16 wild-type. The *cyfbp cfbp1* double mutant displayed features of both parental lines
17 but had the *cfbp1* phenotype. All the mutants accumulated F1,6BP and triose-
18 phosphates during light period. These results prove that while the lack of cFBP1
19 induces important changes in a wide range of metabolites such as amino acids,
20 sugars, and organic acids, the lack of cyFBP activity in *Arabidopsis* essentially
21 provokes a carbon metabolism imbalance which does not compromise the
22 viability of the double mutant *cyfbp cfbp1*.

23

24

25

26

27

28

29

30

31

32

33

34

1 **Introduction**

2 Sucrose and starch are the major end products in higher plants, and their functions
3 are essential for plant development (Geigenberger, 2011a). The rate of net CO₂
4 fixation determines the rate of starch and sucrose synthesis. The photosynthetic
5 carbon reduction cycle (the Calvin-Benson cycle) is responsible for the formation
6 of these carbohydrates after the fixation and reduction of the atmospheric CO₂, the
7 first important intermediate metabolites being the triose-phosphates (TPs). By
8 condensation TPs form fructose-1,6-bisphosphate (F1,6BP) which are used to
9 synthesize starch in the chloroplast, and sucrose in the cytosol. Fructose-1,6-
10 bisphosphatase (FBPase) catalyze the breakdown of F1,6BP to fructose-6-
11 phosphate (F6P) and Pi (Zimmermann *et al.*, 1976). Three FBPases have so far
12 been described in the plant cell, the cytosolic enzyme (cyFBP) which is involved
13 in sucrose synthesis and gluconeogenesis (Cséke and Buchanan, 1986), and two
14 other chloroplastidial isoforms (cFBP1 and cFBP2) (Serrato *et al.*, 2009b; Serrato
15 *et al.*, 2009a). The chloroplastic FBPase (cFBP1; EC 3.1.3.11) is a key enzyme of
16 the Calvin-Benson pathway and is involved in the regeneration of the ribulose-
17 1,5-bisphosphate and the starch synthesis pathway.
18 cyFBP and cFBP1 display a similar tertiary structure with the exception of an
19 extra sequence of 20-30 amino acids in the regulatory domain of the cFBP1
20 (called “loop 170”), which holds three cysteines, two of these can form disulphide
21 bonds that can be reduced by plastidial thioredoxins *f* (TRX *f*) during light
22 activation (Chiadmi *et al.*, 1999). The novel isoform cFBP2 lacks the loop 170 in
23 its sequence, it is not redox regulated by TRX *f* and the affinity for substrate FBP
24 is 6.6-fold lower than that of cFBP1 (Serrato *et al.*, 2009b; Serrato *et al.*, 2009a).
25 The cytosolic isoform activity is inhibited by an excess of substrate and shows
26 allosteric inhibition by adenosine monophosphate (AMP) and fructose-2,6-
27 bisphosphate (F2,6BP). cyFBP and sucrose phosphate synthase (SPS) are
28 considered major sites for controlling sucrose synthesis (MacRae and Lunn,
29 2006). Additionally, pyrophosphate: fructose-6-phosphate 1-phosphotransferase
30 (PFP), which catalyzes the reversible interconversion of F6P and F1,6BP is also
31 considered as an important regulatory point of primary carbon metabolism toward
32 glycolysis or gluconeogenesis in the cytosol (Nielsen and Stitt, 2001).

33 Considerable effort has been made to investigate which steps control the
34 biosynthesis and distribution of carbohydrates in plant cells. By using various

1 transgenic approaches in different plant species, the roles of chloroplast and
2 cytosolic FBPases have been analysed in this context (Koßman *et al.*, 1994;
3 Sahrawy *et al.*, 2004). These results depended on the genetically manipulated
4 plant species, the level of repression or overexpression of the gene selected
5 (chloroplastic and cytosolic FBPase) (Sharkey *et al.*, 1992; Strand *et al.*, 2000;
6 Zrenner *et al.*, 1996) and the tissue (leaf) or organ analyzed (fruit or tuber)
7 (Obiadalla-Ali *et al.*, 2004). Most of the data reported on photosynthesis rate,
8 starch and sucrose content and general phenotypes. Nevertheless, these studies
9 have not led to clear and consistent results on the specific role of FBPases. In
10 general, the use of these transgenic strategies has given rise to some confusion on
11 the function of FBPases in sucrose and starch levels in plants and its turnover, and
12 the results to date remain imprecise making it impossible to draw unambiguous
13 conclusions.

14 To shed light on this confusing information we have performed for the first
15 time a comprehensive analysis of *Arabidopsis* cyFBP and cFBP1 loss-of-function
16 mutants, as well as the corresponding double mutant. The main objective was to
17 determine the extent of contribution of each FBPase to photosynthesis, plant
18 development, reactive oxygen metabolism, carbon partitioning and metabolic
19 profiles in leaves over a day/night period. We provide physiological, biochemical,
20 and metabolic evidence that cFBP1 activity is critical for normal plant
21 development and important for wide metabolic processes, whilst cyFBP appears
22 to affect essentially starch levels.

23

24 **Materials and Methods**

25

26 *Plant material and growth conditions*

27 *Arabidopsis thaliana* wild-type (ecotype Columbia; wt) and mutant plants, *cyfbp*,
28 line SALK_064456 (At1G43670) corresponding to the mutant line *fins1* (Cho and
29 Yoo, 2011), and *cfbp1*, line GK-472G06-019879 (At3g54050) (Serrato *et al.*,
30 2009a), were grown in soil during 20 days in culture chambers under long-day
31 conditions (16 h light/8 h darkness) at 22°C during the light and 20°C during
32 darkness. The light intensity was set at 120 $\mu\text{mol m}^{-2} \text{ s}^{-1}$. The double mutant,
33 stated *cyfbp cfbp1*, was obtained by manual crossing of single mutant *cyfbp* and
34 *cfbp1*. The oligonucleotides used for the genotyping (Table S1) and the

1 homozygous selection was: CYFBP F and R for *cyfbp*, CFBP1 F and R for *cfbp1*,
2 in conjunction with the oligonucleotides (LBSALK and GABI) hybridizing with
3 the T-DNA sequence. Five plants were harvested at intervals of 5 days for 30
4 days, then the leaves per rosette were counted, and the fresh weight per plant and
5 area were measured. For root length measurements seedlings were grown in
6 vertical plates. *Arabidopsis cfbp1* and *cyfbp* mutants were complemented with
7 pGWB4-derived constructions expressing the GFP-translationally fused proteins
8 cFBP1:GFP and cyFBP:GFP under the control of 1 kb of their respective
9 promoters (Figure S1A).

10

11 *Gas exchange measurements and PSII photochemical efficiency*

12 Photosynthetic gas exchange was measured using a portable infrared gas analyzer
13 LI-6400 (LI-COR Biosciences, Inc., Lincoln, NE, USA), which allows
14 environmental conditions inside the chamber to be precisely controlled. The CO₂-
15 assimilation rate was determined in the upper leaf of the wild-type and mutant
16 plants grown for three weeks by changing light intensities (light curve), with the
17 range from 0 to 2000 μmol quanta $\text{m}^{-2} \text{s}^{-1}$. To measure the CO₂ response (CO₂
18 curve), the CO₂ concentration was changed with the range: 400 to 50 and 50 to
19 1500 $\mu\text{mol/mol}$ and the irradiance was set at 1000 μmol quanta $\text{m}^{-2} \text{s}^{-1}$. The
20 photosynthetic parameters were calculated by using LI-6400 6.1 software.
21 Photosyn Assistant, software developed by Dundee Scientific (Parsons and
22 Ogston, 1999) was used to estimate the following parameters, dark respiration
23 (R_d), light compensation point (Γ), and the maximum photosynthesis rate (A_{max}),
24 from the A to light (A/Q) as well as the maximum rate of Rubisco carboxylation
25 (V_{cmax}), maximum rate of electron transport (ETRs) (J_{max}), and triose-P use
26 (TPU) from A to intercellular CO₂ concentration (A/C_i) curves, to help in the
27 comparison between the mutants.

28 Parameters of chlorophyll fluorescence emission were measured at 22°C with the
29 chlorophyll fluorometer PAM 2000 (Walz, Effeltrich, Germany). The maximum
30 quantum yield of PSII (F_v/F_m) was calculated from the parameters using the
31 following equation: F_v/F_m=(F_m-F_o)/F_m, where F_o is the initial minimal
32 fluorescence emitted from leaves dark-adapted for 15 min and F_m the maximal
33 fluorescence elicited by saturating actinic light.

34

1 *Determination of photosynthetic pigments*

2 After pigment extraction in 80% acetone, the content of chlorophyll *a* (chl*a*) and *b*
3 (chl*b*), and carotenoids was spectrophotometrically quantified according to the
4 method of Lichtenthaler and Wellburn (1983).

5

6 *Stomata characterization*

7 The shape and number of the stomata and epidermal cells were observed and
8 measured from a similar leaf used for gas exchange determinations. Digital
9 photographs of a 427-fold magnification were taken using a scanning electron
10 microscope of variable pressure [VPSEM] Zeiss (LEO 1430VP) from six different
11 fields per leaf of adaxial and abaxial epidermis of 3 individual genotype. Adobe
12 Photoshop software was used for cell numbers counting and stomata density
13 quantification.

14

15 *Oxidative metabolism assays*

16 H₂O₂ concentration in leaf extracts was measured by spectrofluorimetry using
17 homovalinic acid (Ex= 325 and Em= 425 nm) and horseradish peroxide as
18 described elsewhere (Pazmiño *et al.*, 2011). The content of carbonyl groups was
19 measured by derivatization with 2,4-dinitrophenylhydrazine, according to
20 Romero-Puertas *et al* (2002). Glycolate oxidase (GOX; EC 1.1.3.1) activity was
21 assayed spectrophotometrically according with Kerr and Groves (1975). Activity
22 of catalase (CAT; EC 1.11.1.6) was determined as described by Aebi (1984).
23 Superoxide dismutase (SOD) isoenzymes were individualized by native-PAGE on
24 10% acrylamide gels and were localized by a photochemical method (Beauchamp
25 and Fridovich, 1971). Lipid peroxidation was determined by the thiobarbituric
26 acid-reacting substances method (Buege and Aust, 1972).

27

28 *Determination of sugars*

29 Carbohydrates were extracted from frozen 20-day-old *Arabidopsis* leaf rosettes
30 with 80% ethanol (v/v) at 80°C, followed by further washing with 50% ethanol at
31 80°C (Stitt *et al.*, 1978). After centrifugation, sucrose, glucose, and fructose were
32 measured enzymatically in the extraction solution by determining the reduction of
33 NADP at 340 nm according to (Sekin, 1978). Starch was extracted with 50 mM
34 Hepes pH 7.6, 1% Triton X-100 buffer, and filtered through two layers of

1 Miracloth (Millipore, MA, USA) and centrifuged. The pellet was resuspended in
2 Percoll 90% (v/v), centrifuged and then the pellet was resuspended in ethanol and
3 measured as glucose from the extract, following incubation with α -amylase and
4 amyloglucosidase.

5

6 *RT-PCR analysis*

7 Total RNA was extracted and RT-PCR was carried out as described by Barajas-
8 López et al.(2007). Primers used are listed in Table S1.

9

10 *Light and electron microscopy*

11 After sample processing (as described in(de Dios Barajas-Lopez *et al.*, 2007)),
12 semi-thin sections (1mm) of *Arabidopsis* leaves and roots were stained with
13 toluidine blue for structure visualization in an OLYMPUS BX51 light microscope
14 and ultra-thin sections (70 to 90 nm) were examined by transmission electron
15 microscopy (TEM) of high resolution [HRTEM] LIBRA 120-EDX-Carl Zeiss
16 SMT.

17

18 *Protein Extraction, Western Blotting and FBPase and PFP enzymatic activities*

19 Protein concentration of extracts was determined with the Bradford assay (1976).
20 Western-blotting and FBPase assays were performed according to Serrato *et al.*
21 (2009a). The modified method of Kombrink (1984) was used to measure PFP
22 activity.

23

24 *Measurement of hexose-phosphates, triose-phosphates and 3-PGA*

25 Leaf samples of wild-type *Arabidopsis* and mutants (6 biological replicates) were
26 snap-frozen in liquid nitrogen, ground to a fine powder using a liquid nitrogen-
27 cooled Mixer Mill MM200 (Retsch, <http://www.retsch.com>), and extracted to
28 measure hexose-phosphates (Glc6-P, Fru6-P, Glc1-P, Fru1,6-BP), triose-
29 phosphates (GAP, DHAP), and 3-PGA using enzymatic assays coupled to
30 NAD(P)H-fluorescence analysis, as previously described in Thormählen *et al.*
31 (2013).

32

33

34

1 *GC-MS analysis of polar primary compounds*
2 50 mg of leaf samples prepared as above was extracted and the relative metabolite
3 contents were determined by GC-MS, as previously described in Thormahlen *et*
4 *al.* (2013). For the visualization and analysis of networks with related
5 experimental data Wanted version 2.1.0 (IPK Gatersleben, Germany) was applied
6 as a tool.

7

8 **Results**

9

10 *T-DNA insertions knock out the expression of both FBPase isoforms*

11 The T-DNA insertions are located in intron 11 and exon 1 (positions +1111 and
12 +111 with respect to the start codon) for *cyfbp* and *cfbp1*, respectively (Fig. 1A).
13 In figure 1B it can be observed no *cyFBP* expression in the *cyfbp* mutant,
14 corroborating previous results by Cho and Yoo (2011), and only a very faint
15 *cFBP1* signal in *cfbp1*. Interestingly, *cyFBP* transcript and protein increased in
16 *cfbp1* whereas the amount of *cFBP1* mRNA augmented in the *cyfbp* mutant
17 rosette (Fig. 1B-C). We generated the double mutant *cyfbp cfbp1* by crossing the
18 respective single knockout mutants. In each case, we confirmed the complete loss
19 of the respective proteins (Fig. 1C) by western-blot analysis using specific
20 antibodies (Serrato *et al.*, 2009a). The negligible *in vitro* FBPase activity in the
21 double mutant validated our FBPase assay conditions, corroborating that the 80%
22 of FBPase activity measured in *cyfbp* and the 40% of FBPase activity obtained in
23 *cfbp1* were due to the cFBP1 and cyFBP activities, respectively (Fig. 1D). No
24 compensation by PFP activity (using specific assay conditions in the sense of the
25 F1,6BP hydrolysis) was observed in any FBPase mutant, being similar in *cyfbp*
26 and wt and surprisingly lower when cFBP1 was lacking (Figure S1C).

27

28 *Changes in the phenotypes of cyfbp, cfbp1 and cyfbp cfbp1 mutants*

29 The appearance of the *cyfbp* is slightly lesser than in the wild-type plants (Fig.
30 2A) and no major difference is observed for this mutant. However, the absence of
31 cFBP1 has a dramatic effect on plant development (Livingston *et al.*, 2010) and
32 the rosettes of both *cfbp1* and double mutant resulted in less leaves, smaller size
33 and lower growth rates than in the wild-type (Fig. 2A-B). Fresh weight and leaf
34 area decreased by 7-fold and 5-fold, in *cfbp1* and *cyfbp cfbp1* mutants respectively

1 when compared with the wild-type (Fig. 2B). Nevertheless, seed viability and
2 germination were normal for all the mutants (Fig. 2C). Root growth analysis
3 showed that *cfbp1* and *cyfbp cfbp1* roots were ~50% shorter and the root-growth
4 speed was 2-fold slower than wild-type and *cyfbp* roots (Fig. 2D).

5 SEM analysis of stomata morphology of the abaxial side of *Arabidopsis* leaves
6 showed a higher stomatal closure in *cfbp1* and double mutants in relation to the
7 full open stomata of wild-type plants under environmental conditions. As shown
8 in Figure 3 B, C, and D and Table S2, the stomatal density (SD) on the adaxial
9 side of the *cyfbp*, *cfbp1* and *cyfbp cfbp1* mutants proved to be 41%, 23%, and 29%
10 lower, respectively, than found on the adaxial surface of the wild-type leaves.
11 However, the same mutants had 46%, 62% and twice as many stomata/mm² on
12 the abaxial side than in wild-type, respectively. Related to leaf size, the stomatal
13 index (SI) values of the rosette *cyfbp*, *cfbp1*, and *cyfbp cfbp1* mutant leaves were
14 lower, respectively, than those of wild-type (Table S2).

15

16 *Cell structure alterations of cyfbp, cfbp1 and cyfbp cfbp1 mutants*

17 The structure of non-flowering rosette leaf and root cross-sections analyzed by
18 light microscopy showed different cell types in leaves, epidermis, mesophyll
19 (palisade and spongy), xylem, phloem, and stomata (Fig. 4 A-C). Cell structure of
20 *cyfbp* mutant is similar to that of the control plant, but chloroplasts contained
21 more starch granule when examined in a magnification micrograph (Fig. 4 G-I).
22 The *cfbp1* mutant had a higher surface of intercellular spaces, and few
23 chloroplasts with less starch granule (only one in some cases) (Fig. 4 I). Some of
24 the chloroplasts displayed a centrifugal position only on the far side of the light
25 source (Fig. 4 C). *cyfbp cfbp1* showed similar cell structure as its *cfbp1* parental
26 (data not shown).

27 The *cfbp1* mutation resulted in a greater number of cell layers in the root vascular
28 cylinder, and there were twice as many vascular tissue cells in the layer, in
29 comparison with the wild-type root (Fig. 4 D and F). However, no disorganization
30 was detected and the shape and size of cells were normal. The root structure of the
31 *cyfbp* mutant showed slightly higher number of the cells of the vascular cylinder
32 than in control (Fig. 4 D and E).

33 The observations with a transmission electron microscope showed disturbances in
34 the cell structure of the *cfbp1* and double mutant, characterized by a diminished

1 number of thylakoids and grana lamellae but without disrupting the chloroplast
2 ultrastructure (Fig. 5). A higher number of plastoglobuli were detected in *cfbp1*
3 and *cyfbp cfbp1* chloroplast than in wild-type (Fig. 5C-D). A lower starch content
4 was observed in *cfbp1* and double mutant than in *cyfbp* and wild-type (Fig. 5A-B).

5

6 *Pigment content decreases drastically in cfbp1 and cyfbp cfbp1*

7 The chlorophyll *a* (Chla) and *b* (Chlb), and carotenoid content were considerably
8 reduced (~40-50%) in the *cfbp1* and *cyfbp cfbp1* mutants in relation to that found
9 in the wild-type, whilst the *cyfbp* mutant displayed values similar to those of the
10 wild-type (Fig. 6).

11

12 *Effect of FBPases removal on CO₂ assimilation and PSII photochemical efficiency*

13 With an open gas-exchange system, CO₂ assimilation rates (A) were determined
14 on attached leaves of plants grown under 120 $\mu\text{mol m}^{-2} \text{s}^{-1}$ and ambient CO₂. The
15 light-response curves (A/Q) at ambient CO₂ are shown in Figure 7A. Under these
16 conditions, the photosynthesis rate of the wild-type had a maximum of 13.5 μmol
17 $\text{m}^{-2} \text{s}^{-1}$ at 2000 $\mu\text{mol m}^{-2} \text{s}^{-1}$. At light intensities <250 $\mu\text{mol m}^{-2} \text{s}^{-1}$, the *cyfbp*
18 mutant assimilation rate was similar to wild-type plants, while at higher intensities
19 the assimilation rate was a ~33% lower. At light intensities between 100 and 500
20 $\mu\text{mol m}^{-2} \text{s}^{-1}$ (standard growth conditions), the A of the *cfbp1* and *cyfbp cfbp1*
21 mutants showed superimposed curves with values nearby 1, indicating an
22 impaired CO₂ assimilation capacity and a poor photosynthesis/respiration ratio. At
23 higher intensities, both *cfbp1*-containing mutants presented lower CO₂ fixation
24 (~6-fold) than did the wild-type, reaching a maximum of 3.4 $\mu\text{mol m}^{-2} \text{s}^{-1}$ (Fig.
25 7A). Transpiration (E) and stomatal conductance (gs) values were higher at lower
26 irradiance in *cfbp1* and *cyfbp cfbp1* leaves in relation to wild-type plants (Fig.
27 7B-C). However, when light intensity was increasing, E and gs converged to
28 reach wild-type and *cyfbp* mutant values at 2000 $\mu\text{mol m}^{-2} \text{s}^{-1}$ (Fig. 7B-C).

29 The response of net photosynthesis to increasing internal leaf CO₂ concentration
30 (Ci) at 1000 $\mu\text{mol m}^{-2} \text{s}^{-1}$ (A/Ci curve) exhibited a similar behaviour (Fig. 7D).
31 The photosynthesis rate of wild-type plants increased to a maximum of 16.2 at
32 1300 ppm of CO₂. At the same concentration of CO₂, the *cyfbp* mutant decreased
33 by 25%, whereas, *cfbp1* and *cyfbp cfbp1* *Arabidopsis* plants lowered their
34 photosynthetic rate 2-fold. This suggests that cFBP1 deficiency rather than cyFBP

1 exerts a stronger effect on CO₂ fixation. Transpiration values of *cfbp1* mutant
2 were higher than the other mutant lines and control plants at all CO₂
3 concentrations assayed (Fig. 7E). Curiously, transpiration and conductance in
4 *cyfbp cfbp1* mutant (Fig. 7 E-F) displayed high values at lower CO₂
5 concentrations but declined slowly at higher concentrations, reaching levels
6 similar to those of the wild-type plants. No significant differences were detected
7 for the E and gs of the wild-type and *cyfbp* mutant in relation to the intercellular
8 CO₂ concentration.

9 We used the Photosynthesis Assistant program, version 1.1.2 , which is based on
10 the von Caemmerer and Farquhar equations (Caemmerer and Farquhar, 1981)
11 (Table 1) to help in the interpretation, comparison and modeling of photosynthesis
12 of plants grown under different environmental conditions. Based on A/Q curves,
13 we found that respiration rates (Rd) increased by 1.6- and 1.3-fold in *cfbp1* and
14 double mutant, respectively, in relation to wild-type plants but the differences did
15 not significantly differ (Table 1). The light compensation point exhibited higher
16 values in *cfbp1* and double mutant, but only *cfbp1* data significantly differed.
17 Amax of *cfbp1* and *cyfbp cfbp1* proved 2 and 3 times lower, respectively, than that
18 of the wild-type and *cyfbp*, as indicated in the A/Q curves (Fig. 7).

19 The response of net CO₂ uptake to increasing intercellular CO₂ (Ci), the A/Ci
20 curve, showed clear differences between *cfbp1* and double mutant in relation to
21 wild-type plants. A lack of plastidial FBPase and of both FBPases caused the
22 plants to decrease 37 and 34% in *Vcmax*, 42 and 40% in *Jmax*, and 25 and 25% in
23 TPU, respectively, suggesting the damaged of the CO₂ assimilation process (Table
24 2). By contrast, the values of both *Jmax* and *Vcmax* of plants lacking only cyFBP
25 were similar to control values.

26 The chlorophyll fluorescence analysis of PSII (Fv/Fm) showed a significant
27 decrease of the photochemical performance for the *cfbp1* and *cyfbp cfbp1* mutants
28 (Table 1), indicating a lower quantum efficiency of linear electron transport
29 through PSII in these two mutants, in agreement with the above *Jmax* data.

30

31

32

33

34

1 *Oxidative metabolism in the mutants*
2 FBPases removal affects reactive oxygen metabolism in *Arabidopsis* mutants, and
3 resulted in an increase of H₂O₂ accumulation by 42%, 60%, and 51%, in *cyfbp*,
4 *cfbp1* and double mutants, respectively (Fig. 8A), and of the content of carbonyl
5 group by 4-, 9- and 2-fold in the *cyfbp*, *cfbp1* and *cyfbp cfbp1*, respectively (Fig.
6 8B). However, lipid peroxidation did not change significantly in any of the
7 mutants in relation to wild-type (Fig. 8C). In order to establish possible sources of
8 H₂O₂ two enzymes were studied, the GOX, an enzyme from the photorespiratory
9 pathway in peroxisomes and the SOD, which removes O₂[−] and at the same time
10 produces H₂O₂. GOX activity increased in the three mutants, *cfbp1* being the
11 highest (1.3-fold; Fig. 8D). SOD isoforms activity showed a low increase of
12 FeSOD, and MnSOD in *cyfbp* and a strong induction of the CuZnSOD in *cfbp1*
13 and *cyfbp cfbp1* (Fig. 8E). The expression analysis revealed a significant induction
14 of the plastid isoform CuZnSOD2 and of FeSOD3 in all mutants, the highest
15 changes being in the *cfbp1* lines (Fig. 8F). The CAT, involved in the
16 detoxification of H₂O₂, showed a significant increase in all the lines mainly in
17 *cfbp1* (1.5-fold) and double mutant (1.8-fold; Fig. 8G). However, the rise of CAT
18 was insufficient to avoid protein oxidative damages (Fig. 8B). No differences in
19 the non-enzymatic antioxidants ascorbate and dehydroascorbate were found,
20 although the ratio ASC/DHA increased in the *cfbp1* and double mutant and
21 decreased in the *cyfbp* (Table S3 and S4).

22
23 *Day/night cycle of carbohydrate accumulation in cyfbp, cfbp1, and cyfbp cfbp1*
24 The level of soluble sugars, such as glucose, fructose, and sucrose in wild-type
25 and mutants plants were analyzed every 4 h over a 24-h period (Fig. 9). Glucose
26 accumulated during the central light period in all the lines and declined as
27 darkness approached, but the concentrations were slightly lower than the wild-
28 type line (Fig. 9A). Compared to wild-type plants, all FBPase mutants showed a
29 4-h delayed glucose-accumulation peak at 8 h and a dramatic drop 4 h before the
30 end of the day (the wild-type displaying a constant and negative slope from points
31 4-h to 16-h). *cyfbp* showed fructose amounts similar to those of the wild-type,
32 excepting the points corresponding to wild-type peak-like shape at 4 h and 20 h
33 (Fig. 9B), whilst this amount decreased drastically in the *cfbp1* background. The
34 wild-type and *cyfbp* plants accumulated fructose at the beginning of the light

1 period, this diminishing after 8 h of illumination while *cfbp1* fructose
2 concentration was almost constant over the photoperiod (around 0.2 µg/mg.FW).
3 Fructose level in the *cyfbp cfbp1* leaves fell sharply (fructose depletion) at 16 h,
4 followed by a sharp rise during the period coinciding with the starch degradation.
5 In FBPase mutant lines, the inflection point in sucrose accumulation occurs at 8 h
6 of the light period (occurring a slightly before in wild-type), reaching maximum
7 accumulations during the first half of the night period, and decreasing rapidly at
8 the end of this period, with a similar profile in all plant lines (Fig. 9C). *cfbp1* had
9 a lesser sucrose content over the photoperiod, and although *cyfbp cfbp1* showed
10 similar profile to *cfbp1* at the beginning of the light period, there was a gradual
11 recovery ending with an accumulation peak close to that of wild-type sucrose
12 concentration at night (20 h).

13 It was noteworthy that after 8 h illumination, *cyfbp* mutant plants displayed a
14 starch content that was approximately 4-fold higher than in the wild-type (Fig.
15 9D). On the contrary, the starch content was ~3-fold lower in *cfbp1* in relation to
16 that found in control plants. The amount of starch detected for the double mutant
17 plants was double than that of the *cfbp1* content, but lower than in the wild-type
18 and *cyfbp*, revealing that the low quantity of starch accumulated is not exclusively
19 due to a limitation in the carbon fixation capacity of *cfbp1*. Staining with Lugol
20 solution plantlets confirmed the higher starch accumulation in *cyfbp* mutant (Fig.
21 9E). The foliar sucrose/starch ratio, an indicator of photo-assimilate allocation
22 (Table 2), was positive toward the starch content (<1) for the *cyfbp* line
23 throughout the photoperiod, indicating an increased starch content in the
24 chloroplasts when cyFBP is lacking. Conversely, this ratio was balanced towards
25 the sucrose synthesis in *cfbp1* (>1) whilst in *cyfbp cfbp1* the ratios were lower and
26 even <1.

27

28 *Effect of the loss of cyFBP, cFBP1 and of both FBPases on leaf metabolite levels*
29 Tables S3 and S4 show the changes in leaf metabolite levels at the end of the
30 night and after 8 h of illumination (middle of the day). The lack of cyFBP activity
31 induced a slight decrease in sugars during the night period, with the exception of
32 maltose and trehalose, whilst most sugars increased in the light period, the rise in
33 isomaltose content being statistically significant. The *cfbp1* and *cyfbp cfbp1*
34 mutant plants in the light and at the end of the night showed between 50 and 90%

1 decreases in relation to the wild-type in the levels of most of the sugars analyzed,
2 such as sucrose, glucose, fructose, isomaltose, trehalose, suggesting a strong
3 impairment of the Calvin-Benson cycle.

4 As expected, during the day the lack of cytosolic or chloropastic FBPases led to
5 an accumulation of fructose-1,6-bisphosphate (F1,6BP) content, which was
6 around 4-, 17- and 60-fold higher in *cfbp1*, *cyfbp*, and *cyfbp cfbp1*, respectively
7 (Fig. 11). An important increase of TPs (dihydroxyacetone phosphate-DHAP and
8 glyceraldehyde 3-phosphate-GAP) was observed, mainly in the double mutant,
9 and of the 3-phosphoglycerate (3-PGA), the first carbon assimilates synthesized
10 after CO₂ fixation and reduction (Table S4). At the end of the night, the hexose-P
11 and DHAP pools declined sharply in all the mutants. During the light period, the
12 level of 3-PGA increased in all mutants, principally in the *cyfbp* mutant, and a
13 marked decrease resulted in the *cfbp1* and *cyfbp cfbp1* in the night (Table S3).

14 Interestingly, the lack of cFBP1 led to marked changes in the levels of organic
15 acids. As revealed by Table S3 and S4, organic acid level decreased after 8 h light
16 and more intensely at night period, especially in the *cfbp1* and *cyfbp cfbp1*
17 mutants. It is worth mentioning the low content detected of glycerate, malate,
18 fumarate, gluconate, succinate, and threonate found in the metabolite group,
19 indicating possible effects on the TCA cycle in the mitochondria. During
20 illumination, the *cyfbp* mutant displayed an increase in the gluconate and gulonate
21 content.

22 Lack of cFBP1 also led to changes in the levels of amino acids. Threonine
23 increased by 16- and 8-fold in the night and 9- and 5-fold at midday in the *cfbp1*
24 and *cyfbp cfbp1* lines, respectively, compared to the wild-type leaf. After 8 h of
25 light, *cfbp1* registered an increase in glycine and proline. Meanwhile, the amounts
26 of serine and leucine in *cfbp1* and double mutant plants reached half the values
27 found in the wild-type. The changes in the levels of glycine, serine and glycerate
28 suggest that photorespiration is strongly affected. In contrast, only the aspartate
29 increased (3-fold) in the night in the *cyfbp* line.

30 During the light period, the group of sugar alcohols metabolites increased in the
31 *cyfbp* line and generally decreased in *cfbp1* and *cyfbp cfbp1* (Table S4). However,
32 the erythritol, glycerol, myo-inositol, and maltitol contents were significantly
33 different in the *cfbp1* and double mutant lines. The higher content of the ascorbate
34 by 3- and 5-fold in *cfbp1* and *cyfbp cfbp1* mutant lines respectively is interesting

1 when compared to wild-type in the night. The *cyfbp* mutant also displayed an
2 increase in dehydroascorbate, a product of the ascorbic acid pathway. This
3 suggests changes in the redox status and the possible activation of detoxifying
4 mechanism.

5 The Wanted diagrams provide an overview map of the clear metabolic changes in
6 *cyfbp*, *cfbp1*, and *cyfbp cfbp1* at the end of the night (Fig. 10 A) and during the
7 light period (Fig. 10B). These diagrams reveal that the lack of different FBPase
8 isoforms disturbs various central metabolic processes, affecting the plant
9 physiology and the development as shown above.

10

11 **Discussion**

12 The existence of different FBPases in plants makes it difficult to predict the
13 precise role or the specific metabolic contribution of each of the isoforms. In
14 previous studies using the antisense strategy in *A. thaliana* and other plant species
15 (potato, tomato or rice); several authors have reported that FBPases play an
16 important role during the regulation of primary photosynthetic metabolism and
17 carbohydrate synthesis in plants (Koßman *et al.*, 1994; Lee *et al.*, 2008;
18 Obiadalla-Ali *et al.*, 2004). However, most of the results were dissimilar and
19 confusing, possibly due to specific plant metabolic adaptations in response to
20 particular life cycles or environmental conditions.

21 The aim of this work is to understand the interrelation between the two main
22 gluconeogenic pathways and the overall contribution of the FBPase isoforms
23 cyFBP and cFBP1 through the study of three *Arabidopsis* mutants: *cyfbp*
24 (affecting sucrose synthesis), *cfbp1* (affecting Calvin cycle/starch synthesis) and
25 *cyfbp cfbp1*. Whilst Cho and Yo (2011) reported the role of *fins1* (*cyfbp*) in
26 fructose signalling, in this study we have carried out a comprehensive
27 physiological and metabolic characterization of this mutant under normal growth
28 conditions, together with *cfbp1* mutant analysis and the line obtained by
29 combining both FBPase mutations. The null *cyfbp* mutant showed a normal
30 phenotype whilst plant growth was only slightly affected, indicating that, in
31 *Arabidopsis*, sucrose synthesis could be possible with hexoses or hexose-Ps
32 exported from the chloroplasts (Fettke *et al.*, 2011), probably due to an enhanced
33 starch turnover. Several results obtained with this mutant support this hypothesis:
34 there is (i) no compensation of FBPase activity by the cytosolic PFP (Figure S1C),

1 (ii) a starch over-accumulation (Fig. 9D and E) and a higher content of starch
2 degradation products (Table S3 and S4), and (iii) an up-regulated expression of
3 the maltose transporter (MEX1), the plastidic glucose translocator (pGlcT) and
4 the glucose 6-phosphate/phosphate translocator 1 (GPT1) and 2 (GPT2) (Figure
5 S2A) (Cho *et al.*, 2011). In a similar way, the lack of the TP translocator in the
6 Arabidopsis *tpt-2* mutant (blocking TP export into cytosol) induces a higher starch
7 accumulation compared with wild-type plants, but maintaining a similar sucrose
8 content. Interestingly, despite showing a non-altered sucrose level, cyFBP is
9 down-regulated in *tpt-2* (Figure S2B) (Cho *et al.*, 2011). All these results suggest
10 that *A. thaliana* could circumvent the cytosolic gluconeogenic pathway by
11 accumulating and mobilizing more starch to export hexose/hexose-phosphates
12 from the chloroplast to the cytosol with only a little loss in the photosynthetic
13 efficiency. On the contrary to cyFBP, the absence of cFBP1 leads to a dramatic
14 phenotype suggesting the impairment of many physiological processes, mainly
15 photosynthesis and CO₂ fixation, as we have evidenced in this work; being cyFBP
16 up-regulation not enough to compensate the cFBP1 loss (Fig. 1B and C). Our
17 original hypothesis presumed that an additive/synergic negative effect of the two
18 mutations over cell gluconeogenesis could have led to a lethal condition.
19 However, to our surprise, *cyfbp cfbp1* is viable, displaying a *cfbp1* phenotype
20 (Figure 2). Expression experiments only revealed a slight higher transcript
21 accumulation of the plastidial isoform *cFBP2* in *cyfbp cfbp1* (Figure S1B).
22 However, observing the negligible FBPase activity observed in this mutant, the
23 contribution of cFBP2 and PFP seems to be very limited (Figure S1C). Moreover,
24 the lack of *cFBP2* induction in *cfbp1* makes uncertain to substitute cFBP1
25 function in the chloroplast (Figure S1B).

26 The chlorotic aspect of *cfbp1* and *cyfbp cfbp1* leaves reflects that the mutation
27 directly determine the photosynthetic potential and primary production in these
28 mutants. Therefore, the chlorophyll fluorescence results indicating that the lack of
29 *cFBP1* affected the PSII and the photosynthetic electron transport rates are in line
30 with a previous work in which the authors describe an Arabidopsis mutant with a
31 loss-of-function allelic variant of *cFBP1* (*hfc1*, from *high fluorescence*
32 *chlorophyll 1*), which constitutively induces the cyclic electron flow (CEFI) to
33 balance the chloroplast energy budget (Livingston *et al.*, 2010). The decline of
34 PSII efficiency and the rate of photosynthetic electron transport (Jmax, based on

1 NADPH requirement) for *cfbp1* and *cyfbp cfbp1*, indicates that CO₂ assimilation
2 was limited as well by the rate of electron transport and RuBP regeneration.
3 Furthermore, chloroplastic FBPase activity removal led to a decrease in Vcmax
4 and TPU, and consequently, as the metabolite analysis corroborated, an increasing
5 accumulation of TP in all mutant lines (specially in *cfbp1* and *cyfbp cfbp1*). It
6 seems that the drastic changes in the organic acids malate, fumarate and succinate,
7 could lead to the stomata failure of the *cfbp1* mutant epidermis at midday (Fig. 3),
8 resulting in a limited CO₂ gas exchange (Araujo *et al.*, 2011; Driscoll *et al.*, 2006;
9 Zheng *et al.*, 2013). No relevant difference in the photosynthesis rate was detected
10 in the case of the *cyfbp* line. After gathering all this information, we could
11 conclude that cFBP1 is a real “photosynthesis-limiting” enzyme.

12 Surprisingly, it was observed a greater number of cell layers in the root
13 vascular cylinder of *cfbp1* root tissues in comparison with the wild-type,
14 suggesting that root ontogenetic factors are involved in order to counteract the
15 metabolism imbalance, highlighting the coordination existing between green and
16 non-green organs. It would be interesting to know what the physiological
17 significance of this root re-modelling is and the nature of the factors implicated in
18 (i.e. hormones and/or transcription factors).

19 Besides, photosynthetic light reactions providing NADPH and ATP necessary
20 for CO₂ fixation and carbohydrate synthesis inevitably go along with the
21 production of harmful reactive oxygen species (ROS) (Mittler, 2002), whilst
22 photorespiration is required to remove 2-phosphoglycolate produced by the
23 oxygenase reaction of Rubisco (Bauwe *et al.*, 2010). Thus, alterations observed in
24 PSII of *cfbp1* and *cyfbp cfbp1* mutants could led to a likely increase in O₂⁻
25 production and the induction of GOX causing an accumulation of H₂O₂ in
26 peroxisomes of all mutant lines. This situation was confirmed by the strong
27 induction of CuZnSOD and FeSOD3 (Fig. 8E and F) (Kliebenstein *et al.*, 1998).
28 Despite the induction of CAT (Fig. 8G), there is an important oxidative protein
29 damage in all mutants. In addition, lack of both FBPases, mainly cFBP1, provokes
30 changes in the reactive oxygen metabolism and triggers an adjustment of the ratio
31 ASC/DHA as a detoxifying mechanism. Low sugar level can result in the
32 enhancement of ROS responses. However the complexity of sugar signalling and
33 sugar-modulated gene expression could place soluble carbohydrates in a pivotal
34 role in the pro-oxidant and antioxidant balance (Couee *et al.*, 2006).

1 The comprehensive GC-TOF MS and fluorescence spectroscopy metabolite
2 analysis provided an overview of visible metabolic alteration in the FBPase
3 mutants, especially significant in *cfbp1* and *cyfbp cfbp1*, underlying the dramatic
4 change in their phenotypes. The inactivation of cyFBP leads to an overall
5 accumulation of F1,6BP, hexose-P, and thus of TP during the light period
6 resulting in the rise in the starch level. However, sub-cellular metabolite analysis
7 will be required to confirm this interpretation (Geigenberger *et al.*, 2011b). Most
8 of the sugar amounts rose, mainly maltose and isomaltose, the main products of
9 starch mobilization in the chloroplast, whilst sucrose level was similar to that of
10 wild-type. In this way, Cho and co-workers (2011) also showed that *Arabidopsis*
11 plants defective in the maltose transporter (MEX1) and the plastidic glucose
12 translocator (pGlcT) resulted in severely reduced photosynthetic activities,
13 decrease of sucrose content and starch turnover and growth retardation. A
14 remarkable increase in trehalose content was detected in the *cyfbp* mutants. In
15 fact, some authors have proposed that trehalose-6-phosphate (Tre6P), the
16 intermediate of trehalose synthesis, is a component in a signalling pathway that
17 mediates the regulation of the accumulation and/or turnover of transitory starch in
18 *Arabidopsis* leaves, potentially linking the management of these reserves to the
19 availability and demand for sucrose (Martins *et al.*, 2013). Also, the positive
20 effects of trehalose include a decrease of photo-oxidative damage, as a potential
21 protective element (Bae *et al.*, 2005). Reflecting the *cyfbp* phenotype, no effect
22 was detected in the amino-acid biosynthesis or other metabolic pathways when
23 *cyFBP* was lacking.

24 On the contrary, the inactivation of the *cFBP1* had a profound effect on
25 photosynthetic carbon metabolism and photorespiration, leading in general to
26 alterations in the redox-status as revealed by changes in ascorbate levels. Besides,
27 it also affected other pathways in the plants, such as amino acids and organic acid
28 metabolism in mitochondria. As expected, the lack of *cFBP1* in the light led to an
29 accumulation of F1,6BP, TPs, and 3PGA, and to a decline in the levels of hexose-
30 P and many sugars, including sucrose, glucose, fructose, and trehalose (signalling)
31 and maltose (starch degradation) leading to a small rosette size. On the other
32 hand, amino-acid synthesis was also affected, serine content diminished in the
33 *cfbp1* and the double mutant, whilst the glycine level rose in *cfbp1* during the light
34 period. Both amino acids are involved in photorespiratory and non-

1 photorespiratory pathways, and the opposite changes in serine and glycine content
2 indicate that, during photorespiration, glycine decarboxylase activity is altered.
3 Timm and colleagues suggest that serine, possibly together with glycine acts as a
4 metabolic signal for the transcriptional regulation of photorespiration, particularly
5 in the glycine-to-serine interconversion reactions (Timm *et al.*, 2013). Moreover,
6 during an imbalance between sucrose/starch synthesis and the production of
7 phosphorylated intermediates in the Calvin-Benson cycle, the photorespiration
8 might provide the cell with an alternative pathway for the synthesis of sink
9 products, such as glycine and serine (Harley and Sharkey, 1991). The rise in the
10 levels of aspartate, proline, and threonine, seems to indicate that carbon starvation
11 may have led to degradation of proteins instead of starch for plants needs.

12 In addition, the inactivation of chloroplast FBPase in *cfbp1* and *cyfbp cfbp1*
13 led to a fall in the levels of several organic acids involved in the tricarboxylic acid
14 cycle (TCA) in mitochondria, which could be a secondary consequence of the
15 decrease in carbon fixation. Among them, L-tryptophan, L-phenylalanine, L-
16 tyrosine and shikimate, a precursor in aromatic amino acid biosynthesis. These
17 aromatic amino acids (AAAs) can be precursors of numerous natural products in
18 plants, such as pigments, alkaloids, hormones, and cell wall components.

19 Finally, an even sharper increase in the F1,6BP and TPs accumulation is
20 observed in *cyfbp cfbp1* as a consequence of both cFBP1 and cyFBP inactivation
21 and thus a decline of sucrose content. Despite displaying a similar *cfbp1*
22 phenotype and metabolite profile, it is interesting to observe some *cyfbp*
23 behaviours such as the changes in starch level, suggesting a combined inheritance
24 in this mutant and raising the interesting question of how can these plants increase
25 the starch content in the absence of cFBP1. Moreover, the survival of the double
26 mutant lacking enzymes that regulate essential metabolic steps is remarkable. The
27 slightly higher *cFBP2* gene expression in *cyfbp cfbp1* mutant might suggest a
28 possible compensation of the depleted carbohydrate metabolism. Thus, the
29 redundant function of the plastidial FBPases could not be considered.

30 To sum up, taken together our results of the analysis of individual and double
31 knockout cFBP1 and cyFBP mutants lead us to suggest that both FBPases play
32 important roles in sucrose and starch synthesis and contribute significantly to
33 regulate carbohydrate turnover in plants. In addition, the lack of cFBP1 induces
34 cell structural deficiencies, and reduced plant growth. The cFBP2 isoform could

1 not substitute the function of the other two isoforms. In addition, our study has
2 uncovered a relationship between sugar turnover, biomass, protein content and
3 other important metabolic pathways, the most important being photorespiration,
4 amino-acid synthesis and the TCA cycle.

5

6

7 **Supplementary data**

8 Supplementary data can be found at *JXB* online.

9

10 **Supplementary Figure S1.** A, Phenotype reversion in *cyfbp* and *cfbp1* mutants
11 complemented with translationally GFP-fused FBPases (under the control of a 1-
12 kb promoter region) cloned into pGWB4 vector. B, cFBP2 gene expression using
13 semiquantitative RT-PCR in rosette leaves of 20-day-old *Arabidopsis* plants. C,
14 PFP enzymatic activity.

15

16 **Supplementary Figure S2.** A, maltose transporter (MEX1), plastidic glucose
17 translocator (pGlcT) and glucose 6-phosphate/phosphate translocator 1 (GPT1)
18 and 2 (GPT2) gene expression using semiquantitative RT-PCR in rosette leaves of
19 20-day-old *Arabidopsis* plants. B-C, Western-blot analysis using anti-cyFBP y
20 anti-cFBP1 antibody.

21

22 **Supplementary Table S1.** Gene-specific oligonucleotides used for semi-
23 quantitative PCR.

24

25 **Supplementary Table S2.** Stomatal density and stomatal index in epidermis of
26 leaves of the wild-type (WT) and *cyfbp*, *cfbp1*, and *cyfbp cfbp1* mutants at the
27 adaxial and abaxial surfaces.

28

29 **Supplementary Tables S3 and S4.** Changes in *Arabidopsis* leaf metabolite levels
30 at the end of the night (**S3**) and after 8 h illumination (**S4**) in *cyfbp*, *cfbp1* and
31 *cyfbp cfbp1* knockout lines relative to the wild type. Metabolite profiling was
32 made using GC-TOF-MS analysis and fluorescence spectroscopy. Results are
33 means \pm SD ($n = 6$). Values that are significantly different from the wild type
34 according to Student's *t*-test are indicated in bold (P value < 0.05).

1 **Acknowledgments**

2 The authors thank Maria Trinidad Moreno for her technical support, and English
3 translators for helpful editorial feedback on the manuscript. The microscopy
4 assays and observations were carried out at the Scientific Instrumentation Centre
5 of the University of Granada (Spain).

6

References

Aebi H. 1984. Catalase in vitro. *Methods Enzymol* **105**, 121-126.

Araujo WL, Nunes-Nesi A, Osorio S, Usadel B, Fuentes D, Nagy R, Balbo I, Lehmann M, Studart-Witkowski C, Tohge T, Martinoia E, Jordana X, Damatta FM, Fernie AR. 2011. Antisense inhibition of the iron-sulphur subunit of succinate dehydrogenase enhances photosynthesis and growth in tomato via an organic acid-mediated effect on stomatal aperture. *Plant Cell* **23**, 600-627.

Bae H, Herman E, Sicher R. 2005. Exogenous trehalose promotes non-structural carbohydrate accumulation and induces chemical detoxification and stress response proteins. *Plant Science* **168**, 8.

Bauwe H, Hagemann M, Fernie AR. 2010. Photorespiration: players, partners and origin. *Trends Plant Sci* **15**, 330-336.

Beauchamp C, Fridovich I. 1971. Superoxide dismutase: improved assays and an assay applicable to acrylamide gels. *Analytical Biochemistry* **44**, 276-287.

Bradford MM. 1976. A rapid and sensitive method for the quantitation of microgram quantities of protein utilizing the principle of protein-dye binding. *Anal Biochem* **72**, 248-254.

Buege J, Aust S. 1972. Microsomal lipid peroxidation. *Methods in Enzymology* **52**, 302-310.

Caemmerer Sv, Farquhar G. 1981. Some relationships between the biochemistry of photosynthesis and the gas exchange of leaves. *Planta* **153**, 376-387.

Couee I, Sulmon C, Gouesbet G, El Amrani A. 2006. Involvement of soluble sugars in reactive oxygen species balance and responses to oxidative stress in plants. *J Exp Bot* **57**, 449-459.

Cséke C, Buchanan B. 1986. Regulation of the formation and utilization of photosynthate in leaves. *Biochimica et Biophysica Acta* **853**, 43-63.

Chiadmi M, Navaza A, Miginiac-Maslow M, Jacquot JP, Cherfils J. 1999. Redox signalling in the chloroplast: structure of oxidized pea fructose-1,6-bisphosphate phosphatase. *EMBO J* **18**, 6809-6815.

Cho MH, Lim H, Shin DH, Jeon JS, Bhoo SH, Park YI, Hahn TR. 2011. Role of the plastidic glucose translocator in the export of starch degradation products from the chloroplasts in *Arabidopsis thaliana*. *New Phytol* **190**, 101-112.

Cho YH, Yoo SD. 2011. Signaling role of fructose mediated by FINS1/FBP in *Arabidopsis thaliana*. *PLoS Genet* **7**, e1001263.

de Dios Barajas-Lopez J, Serrato AJ, Olmedilla A, Chueca A, Sahrawy M. 2007. Localization in roots and flowers of pea chloroplastic thioredoxin f and thioredoxin m proteins reveals new roles in nonphotosynthetic organs. *Plant Physiol* **145**, 946-960.

Driscoll SP, Prins A, Olmos E, Kunert KJ, Foyer CH. 2006. Specification of adaxial and abaxial stomata, epidermal structure and photosynthesis to CO₂ enrichment in maize leaves. *J Exp Bot* **57**, 381-390.

Fettke J, Malinova I, Albrecht T, Hejazi M, Steup M. 2011. Glucose-1-phosphate transport into protoplasts and chloroplasts from leaves of *Arabidopsis*. *Plant Physiol* **155**, 1723-1734.

Geigenberger P. 2011a. Regulation of starch biosynthesis in response to a fluctuating environment. *Plant Physiology* **155**, 1566-1577.

Geigenberger P, Tiessen A, Meurer J. 2011b. Use of non-aqueous fractionation and metabolomics to study chloroplast function in *Arabidopsis*. *Methods Mol Biol* **775**, 135-160.

Harley P, Sharkey T. 1991. An improved model of C3 photosynthesis at high CO₂:reversed O₂ sensitivity explained by lack of glycerate reentry into the chloroplast. *Photosynthesis Research* **27**, 169-178.

Kerr MW, Groves D. 1975. Purification and properties of glycolate oxidase from *Pisum sativum* leaves. *Phytochemistry* **14**, 359-362.

Kliebenstein DJ, Monde RA, Last RL. 1998. Superoxide dismutase in *Arabidopsis*: an eclectic enzyme family with disparate regulation and protein localization. *Plant Physiol* **118**, 637-650.

Kombrink E, Kruger NJ, Beevers H. 1984. Kinetic properties of pyrophosphate:fructose-6-phosphate phosphotransferase from germinating castor bean endosperm. *Plant Physiol* **74**, 395-401.

Koßman J, Sonnewald U, L.Willmitzer. 1994. Reduction of the chloroplastic fructose-1,6-bisphosphatase in transgenic potato plants impairs photosynthesis and plant growth. *The Plant Journal* **6**, 637-650.

Lee SK, Jeon JS, Bornke F, Voll L, Cho JI, Goh CH, Jeong SW, Park YI, Kim SJ, Choi SB, Miyao A, Hirochika H, An G, Cho MH, Bhoo SH, Sonnewald U, Hahn TR. 2008. Loss of cytosolic fructose-1,6-bisphosphatase limits photosynthetic sucrose synthesis and causes severe growth retardations in rice (*Oryza sativa*). *Plant Cell Environ* **31**, 1851-1863.

Lichtenthaler H, Wellburn A. 1983. Determinations of total carotenoids and chlorophylls a and b of leaf extracts in different solvents. *Biochemical Society Transactions* **11**, 591-592.

Livingston AK, Cruz JA, Kohzuma K, Dhingra A, Kramer DM. 2010. An Arabidopsis mutant with high cyclic electron flow around photosystem I (hcef) involving the NADPH dehydrogenase complex. *Plant Cell* **22**, 221-233.

MacRae EA, Lunn JE. 2006. Control of sucrose biosynthesis. In *WC Plaxton, MT Mcmanus, eds, Advances in Plant Research: Control of Primary Metabolism in Plants Vol. 22*, Blackwell, Oxford, pp 234-257.

Martins MC, Hejazi M, Fettke J, Steup M, Feil R, Krause U, Arrivault S, Vosloh D, Figueroa CM, Ivakov A, Yadav UP, Piques M, Metzner D, Stitt M, Lunn JE. 2013. Feedback inhibition of starch degradation in Arabidopsis leaves mediated by trehalose 6-phosphate. *Plant Physiology* **163**, 1142-1163.

Mittler R. 2002. Oxidative stress, antioxidants and stress tolerance. *Trends Plant Sci* **7**, 405-410.

Nielsen TH, Stitt M. 2001. Tobacco transformants with strongly decreased expression of pyrophosphate:fructose-6-phosphate expression in the base of their young growing leaves contain much higher levels of fructose-2,6-bisphosphate but no major changes in fluxes. *Planta* **214**, 106-116.

Obiadalla-Ali H, Fernie AR, Lytovchenko A, Kossmann J, Lloyd JR. 2004. Inhibition of chloroplastic fructose 1,6-bisphosphatase in tomato fruits leads to decreased fruit size, but only small changes in carbohydrate metabolism. *Planta* **219**, 533-540.

Parsons R, Ogston S. 1999. Photosyn Assistant Ver. 1.1.2. Dundee. Scientific, Dundee.

Pazmiño DM, Rodriguez-Serrano M, Romero-Puertas MC, Archilla-Ruiz A, Del Rio LA, Sandalio LM. 2011. Differential response of young and adult leaves to herbicide 2,4-dichlorophenoxyacetic acid in pea plants: role of reactive oxygen species. *Plant Cell Environ* **34**, 1874-1889.

Romero-Puertas M, Palma J, Gómez M, Río Ld, Sandalio L. 2002. Cadmium causes the oxidative modification of proteins in pea plants. *Plant, Cell and Environment* **25**, 677-686.

Sahrawy M, Avila C, Chueca A, Canovas FM, Lopez-Gorge J. 2004. Increased sucrose level and altered nitrogen metabolism in *Arabidopsis thaliana* transgenic plants expressing antisense chloroplastic fructose-1,6-bisphosphatase. *J Exp Bot* **55**, 2495-2503.

Sekin S. 1978. Enzymatic determination of glucose, fructose and sucrose in tobacco. *Tobacco Science* **23**, 75-77.

Serrato AJ, de Dios Barajas-Lopez J, Chueca A, Sahrawy M. 2009b. Changing sugar partitioning in FBPase-manipulated plants. *J Exp Bot* **60**, 2923-2931.

Serrato AJ, Yubero-Serrano EM, Sandalio LM, Munoz-Blanco J, Chueca A, Caballero JL, Sahrawy M. 2009a. cpFBPaseII, a novel redox-independent chloroplastic isoform of fructose-1,6-bisphosphatase. *Plant Cell Environ* **32**, 811-827.

Sharkey T, Sutch L, Vanderveer P, Micallef B. 1992. Carbon partitioning in a *Flaveria linearis* mutant with reduced cytosolic fructose bisphosphatase. *Plant Physiology* **100**, 210-215.

Stitt M, Bulpin PV, ap Rees T. 1978. Pathway of starch breakdown in photosynthetic tissues of *Pisum sativum*. *Biochim Biophys Acta* **544**, 200-214.

Strand A, Zrenner R, Trevanion S, Stitt M, Gustafsson P, Gardestrom P.
2000. Decreased expression of two key enzymes in the sucrose biosynthesis pathway, cytosolic fructose-1,6-bisphosphatase and sucrose phosphate synthase, has remarkably different consequences for photosynthetic carbon metabolism in transgenic *Arabidopsis thaliana*. *Plant J* **23**, 759-770.

Thormählen I, Ruber J, von Roepenack-Lahaye E, Ehrlich SM, Massot V, Hummer C, Tezycka J, Issakidis-Bourguet E, Geigenberger P. 2013.
Inactivation of thioredoxin f1 leads to decreased light activation of ADP-glucose pyrophosphorylase and altered diurnal starch turnover in leaves of *Arabidopsis* plants. *Plant Cell Environ* **36**, 16-29.

Timm S, Florian A, Wittmiss M, Jahnke K, Hagemann M, Fernie AR, Bauwe H. 2013. Serine acts as a metabolic signal for the transcriptional control of photorespiration-related genes in *Arabidopsis*. *Plant Physiol* **162**, 379-389.

Zheng Y, Xu M, Hou R, Shen R, Qiu S, Ouyang Z. 2013. Effects of experimental warming on stomatal traits in leaves of maize (*Zea mays L.*). *Ecol Evol* **3**, 3095-3111.

Zimmermann G, Kelly GJ, Latzko E. 1976. Efficient purification and molecular properties of spinach chloroplast fructose 1,6-bisphosphatase. *European Journal of Biochemistry* **70**, 361-367.

Zrenner R, Krause KP, Apel P, Sonnewald U. 1996. Reduction of the cytosolic fructose-1,6-bisphosphatase in transgenic potato plants limits photosynthetic sucrose biosynthesis with no impact on plant growth and tuber yield. *Plant J* **9**, 671-681.

Table 1. Photosynthetic parameters of WT, *cyfbp*, *cfbp1* and *cyfbp cfbp1* mutant plants. Values were obtained from the A/Q and A/Ci curves using the Photosyn Assistant software as described in Materials and Methods.

	Amax	Γ	Rd	Vcmax	Jmax	TPU	Fv/Fm
wt	9.5 ± 0.5	14.6±1.5	-1.1 ±0.3	30.6 ±4.9	154±33	11.1±1.4	0.83±0.01
<i>cyfbp</i>	9.3 ± 0.5	16.7±5.4	-1.25 ±0.0	31.1 ±4.2	143 ±25	10.1±1.4	0.83±0.01*
<i>cfbp1</i>	4.2±0.4**	67.3±23*	-1.81 ±0.7	19.4±2.1*	88 ±12*	8.4 ±1.2*	0.77±0.01***
<i>cyfbp cfbp1</i>	3.2±0.7 **	50.4±31	-1.41 ±0.5	20.1±4.0	92±23*	8.4±1.2*	0.77±0.03***

Values are the mean ± standard error of five to ten independent determinations. Fv/Fm was determined in 10 leaves from different plants. Values are mean ± SD. Asterisks indicate that mean values are significantly different between wild-type and FBPase mutant plants (*, P<0.05; **, P<0.01; ***, P<0.001).

Table 2. Sucrose/starch ratio in leaves of Arabidopsis wild-type, *cyfbp*, *cfbp1*, and *cyfbp cfbp1* mutants.

Hours	wt	<i>cyfbp</i>	<i>cfbp1</i>	<i>cyfbp cfbp1</i>
0	0.87	0.66	5.15	1.91
4	1.11	0.48	3.18	1.05
8	1.39	0.29	1.89	0.20
12	0.72	0.67	2.85	1.14
16	1.02	0.73	1.42	0.96
20	1.16	0.91	3.00	3.02

Figure legends

Figure 1

Analysis of mutant lines. (A) Genomic structure of *cyFBP* and *cFBP1*. Exons and introns are indicated as thick and thin black bars, respectively. Insertion sites of T-DNA in mutant lines *cyfbp* and *cfbp1* at intron 11 and exon 1, respectively, are indicated by triangles. (B) Expression profile of each FBPase using specific oligonucleotides in the *cyfbp* and *cfabp1* mutants and wildtype, 18s was used as housekeeping gene. (C) Western blot analysis of crude leaf extracts of *cyfbp*, *cfabp1*, *cyfbp cfbp1* mutants and wild-type. Proteins (25 µg) were separated by SDS-PAGE electrophoresis, transferred to nitrocellulose filters and immunolabeled with rabbit antiserum raised against Ab cyFBPase and Ab cFBPase1 proteins (see Material and methods). Bands are approximately 40 kDa, and RbcLS was used as loading control. (D) FBPase activity was determined in wt and mutants extract plants.

Figure 2

Growth of *cyfbp*, *cfabp1*, *cyfbp cfbp1* mutants and the wild-type plants. Seeds of mutant and wild-type plants were sown in soil and cultured in a growth cabinet under 16-h light/8-h dark. Pictures were taken 21 days after sowing. A: *cyfbp*, *cfabp1*, *cyfbp cfbp1* mutants and WT. B: leaf number per rosette; fresh weight (FW) in mg per plant and leaf area in cm² of mutants and wild-type during the experimental time course plotted against the number of days after germination of seeds. C: rate of seed germination. D: root growth rate in the first 24 h after germination.

Figure 3

Scanning electron micrographs illustrating morphological differences and stomata of “adaxial” leaves surfaces from *Arabidopsis* wild-type (wt) (A), *cyfbp* (B), *cfabp1* (C) and *cyfbp cfbp1* (D) mutants. Scale Bars: 10µm.

Figure 4

Light microscopy images of mesophyll cells and roots from the wild type, *cyfbp*, *cfabp1*, and *cyfbp cfbp1* mutants of *Arabidopsis* plants grown for 21 days under a 16 h light/ 8 h dark regime. Semi-thin cross-section of leaves and roots from the wild type (A, E, and

H), *cyfbp* mutant (B, F and I), *cfbp1* mutant (C, G, and J), and *cyfbp cfbp1* (D) were stained with toluidine blue (which stains proteins). Scale bars: 100 μ m.

Figure 5

Transmission electron microscopy analysis of leaf sections from WT (A), *cyfbp1* (B), *cfbp1* (C), and *cyfbp cfbp1* (D) plants. Leaves plants were collected at 4 h in a 16 h light/8 h dark photoperiod, fixed, embedded and sectioned as described in the Materials and Methods. Symbols: G, grana; S, starch; V, vacuole and P, plastoglobule. Chl: chloroplast, CW: cell wall, M: mitochondrion.

Figure 6

Pigment content in chlorophyll a and b and carotenoids in wild-type and *cyfbp*, *cfbp1* and *cyfbp cfbp1* plants. Values are means +/- SE of measurements on at least 5-7 leaves of three different plants. Error bars show the standard error of the squared mean. Significant differences between means within a time point are indicated with * (P<0.05-*), P<0.01--**, P<0.001--***).

Figure 7

Photosynthetic capacity of wild type and *cyfbp*, *cfbp1*, and *cyfbp cfbp1* mutants. Plants were grown in a controlled growth cabinet under 100 μ mol $m^{-2} s^{-1}$ light regimes for 20 days. Photosynthetic carbon fixation rates were determined in the newest fully expanded leaf, as a function of increasing irradiance (A) at saturating CO_2 (400 μ mol mol^{-1} ; A/Q response curve) and a function of increasing CO_2 concentration (D) at saturating-light levels (1000 μ mol $m^{-2} s^{-1}$; A/Ci response curve). Transpiration (E) and stomatal conductance (gs) were determined in the same leaves (B, E and C, F). Values represent the mean of 8 plants \pm SE.

Figure 8

Reactive oxygen metabolism in *Arabidopsis* WT and *cyfbp*, *cfbp1* and *cyfbp cfbp1* mutants. (A) Determination of H_2O_2 by fluorometry. (B) Protein oxidation measured as carbonyl group content. (C) Lipid peroxidation measured as malondyaldehyde (MDA) content. (D) Glycolate oxidase (GOX) activity. (E) Relative intensity of Mn-SOD, Fe-SOD and CuZn-SOD activities quantified by the Bio-Rad software Quantity one. (F) Analysis of mRNA SODs expression by qRT-PCR. (G) Catalase (CAT) activity. Each

bar represents mean \pm SE of three independent experiments. Differences between mutant plants and WT were significant at P<0.05 (*), P<0.01 (**) and P<0.001 (***). (R.I., relative intensity).

Figure 9

Changes in the intracellular content of glucose (A), fructose (B), sucrose (C) and starch (D) in wild-type (wt), *cyfbp*, *cfbp1*, and *cyfbp cfbp1* mutant plants. The rosette leaves were collected at 0, 4, 8, 12, 16, and 20 h (4 h dark) of the photoperiod. The results are the mean \pm SE from three individual *Arabidopsis* rosettes of three different experiments. (E) Plantlets of wild-type and mutants plants were harvested after 8 h illumination and at the end of the night and stained in Lugol solution.

Figure 10

Summary of metabolite profiling of leaves at the end of the night (A) and after 8 h of light (B) as analyzed by gas chromatography coupled with mass spectroscopy (GC-MS) and enzymatic assays coupled to fluorescence spectroscopy. Ratios are given between *cyfbp*, *cfbp1*, *cyfbp cfbp1* and wildtype in colour coding: red, significantly lower than the wild-type; blue, significantly higher than the wild type (Student's t-test, P<0.05, n=6). Data set of metabolite profiling see Supplementary Table S3 and S4.

Figure 11

Simplified scheme of the major changes (in metabolism, photosynthesis, and gene regulation) occurring in FBPase mutants and their impact on end-products accumulation (sucrose and starch). TP, trioses phosphate; F1,6BP, fructose-1,6-phosphate; F6P, fructose-6-phosphate.

Figure 1

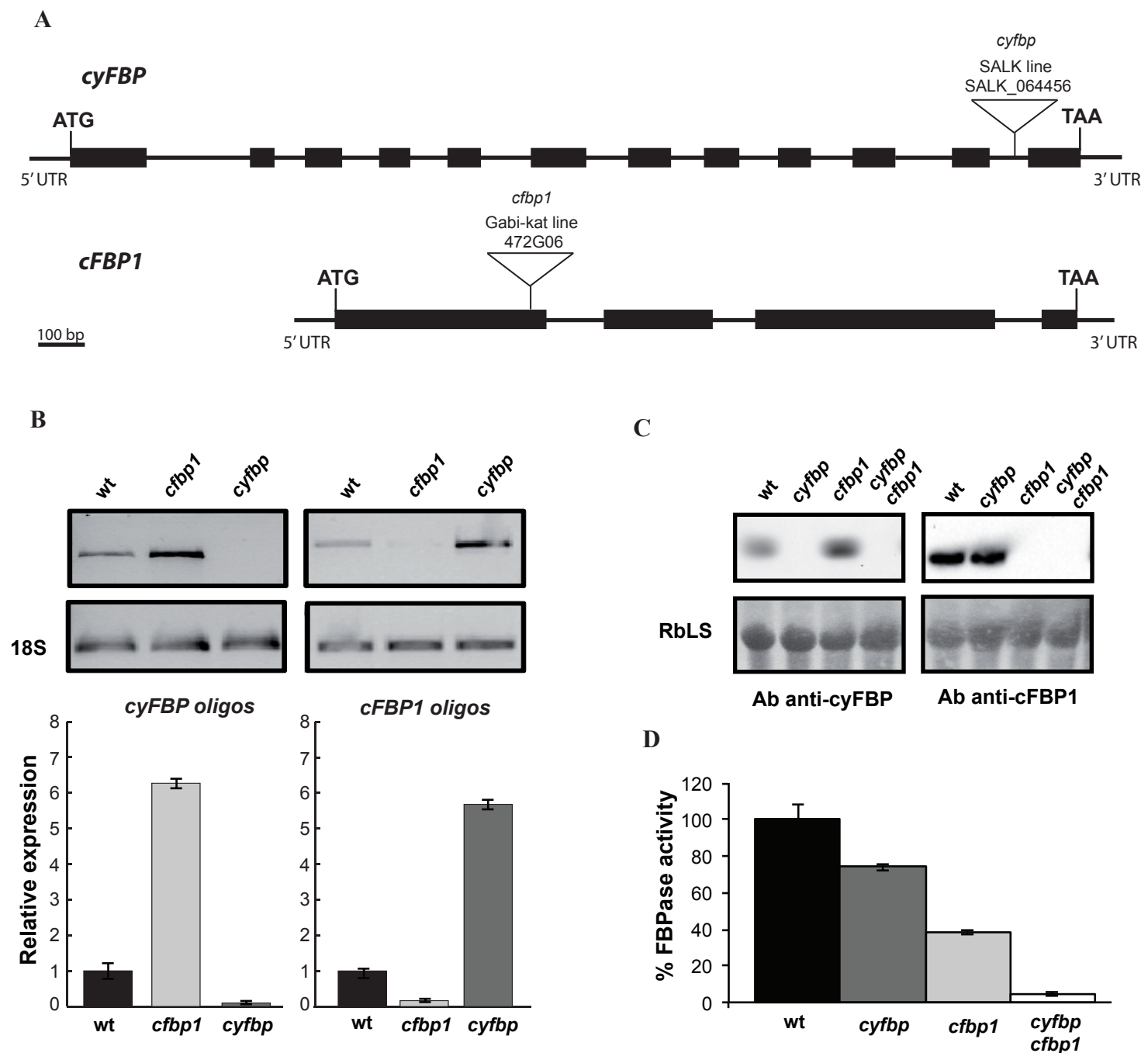
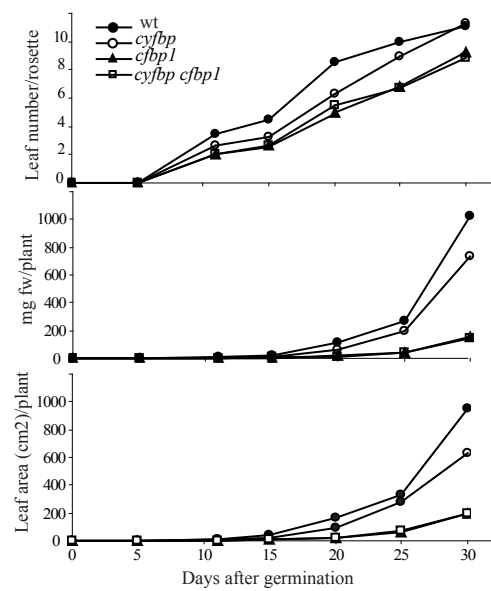


Figure 2

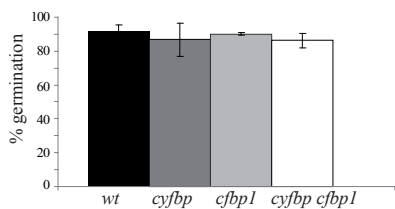
A



B



C



D

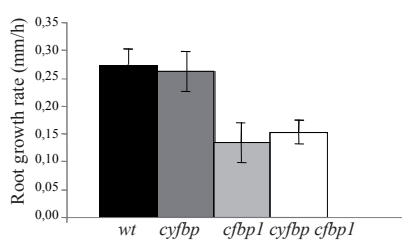


Figure 3

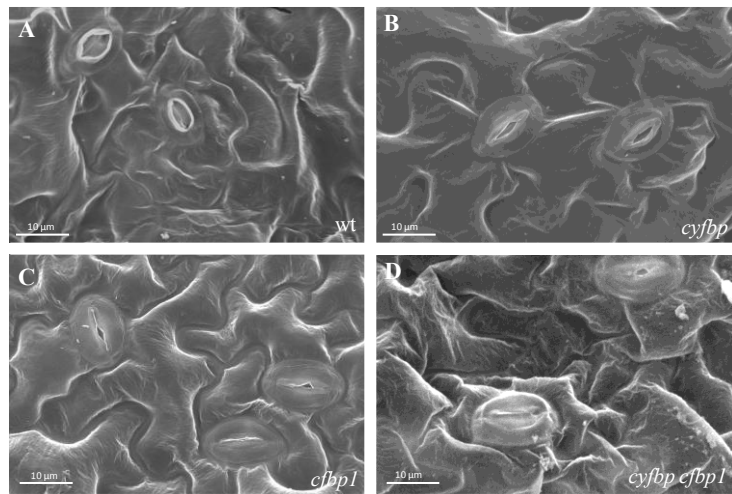


Figure 4

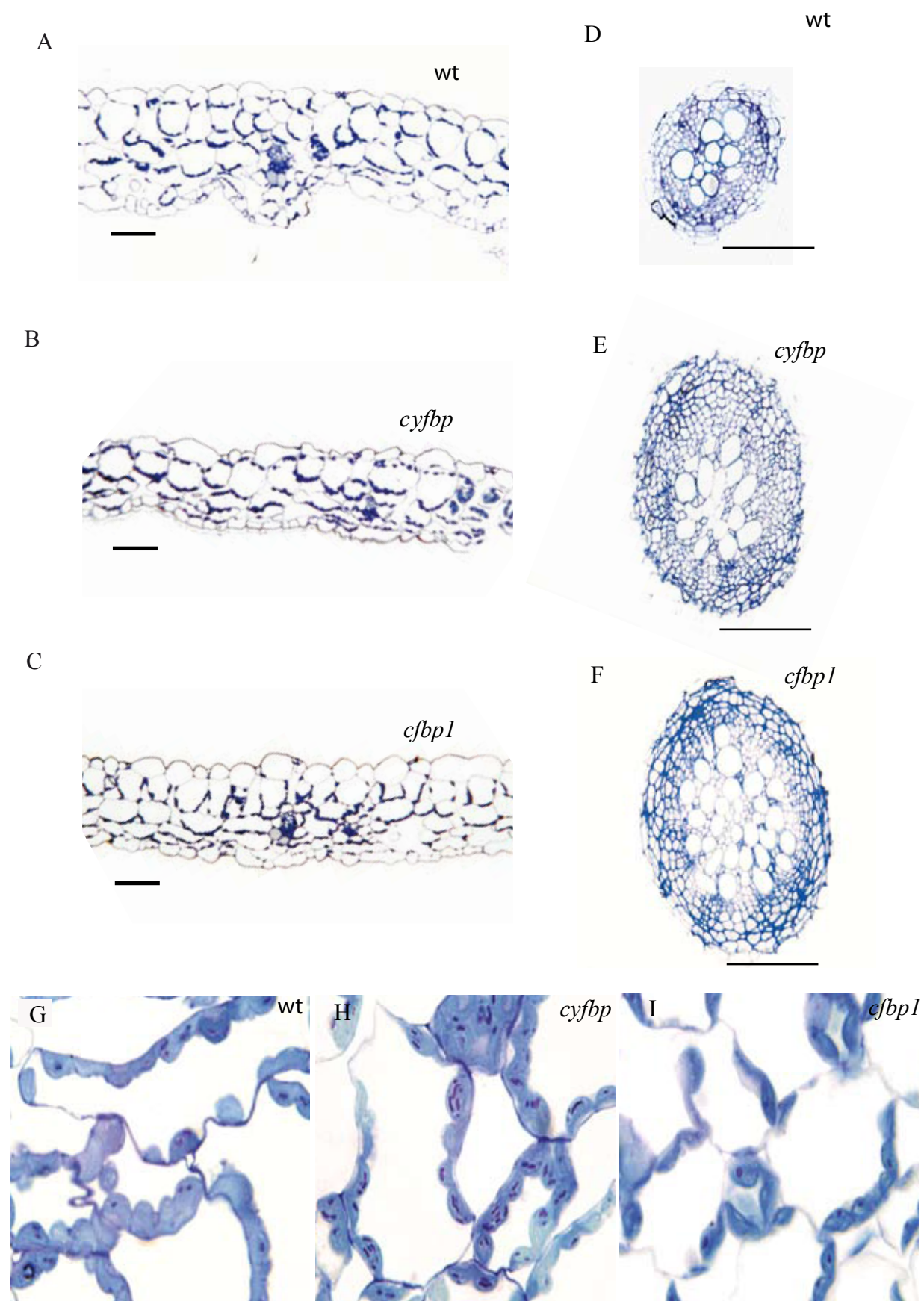


Figure 5

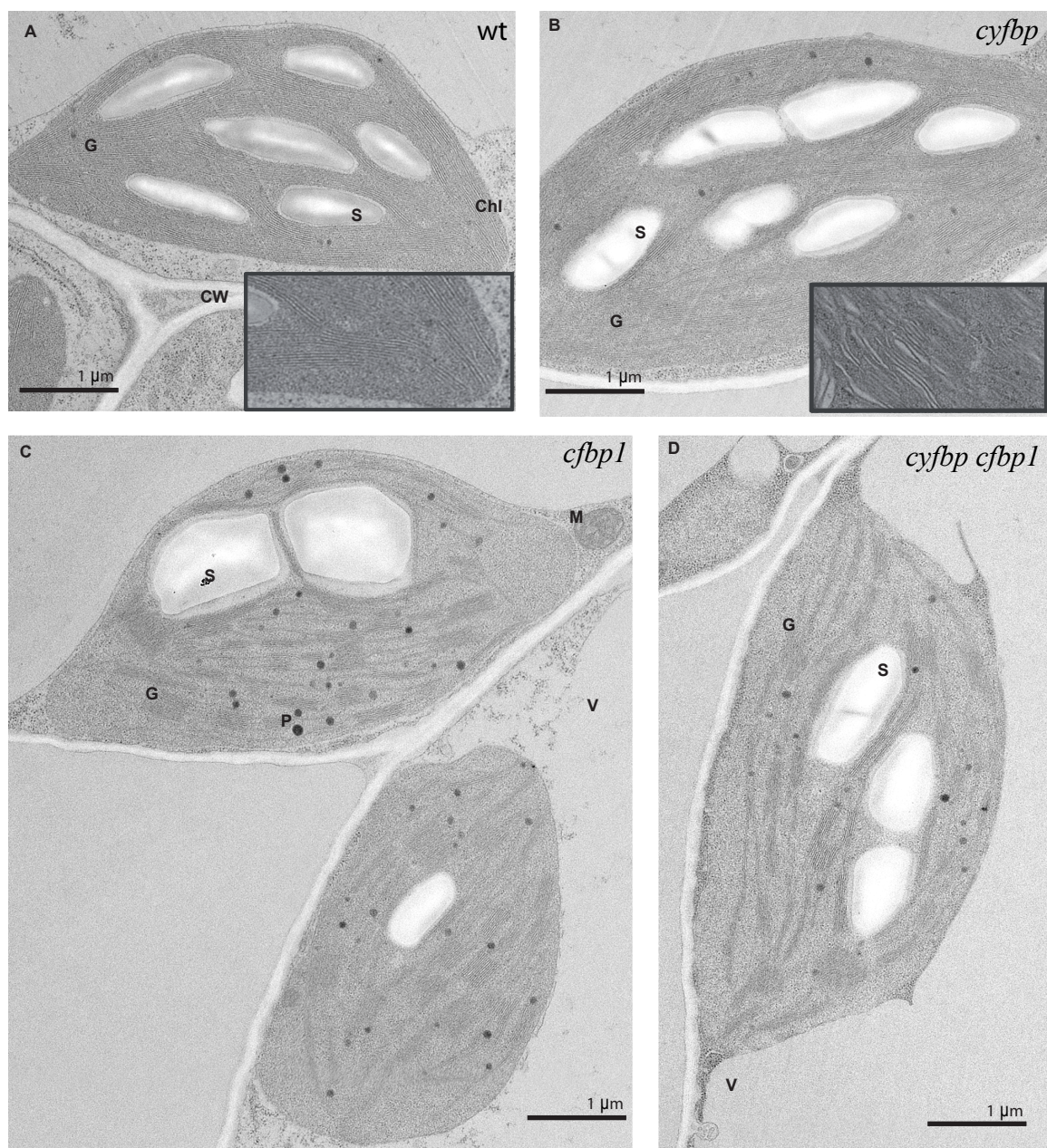


Figure 6

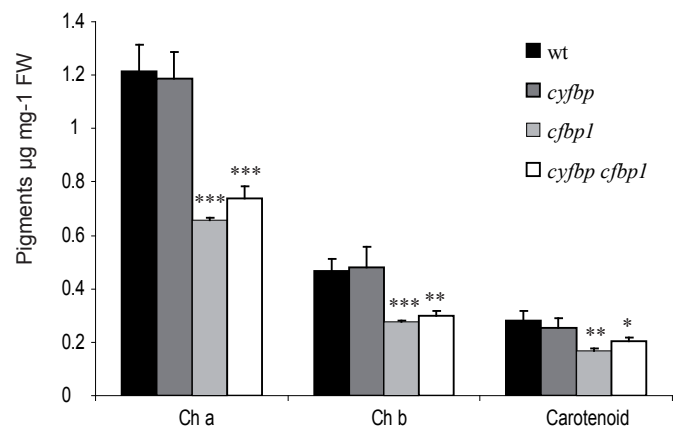


Figure 7

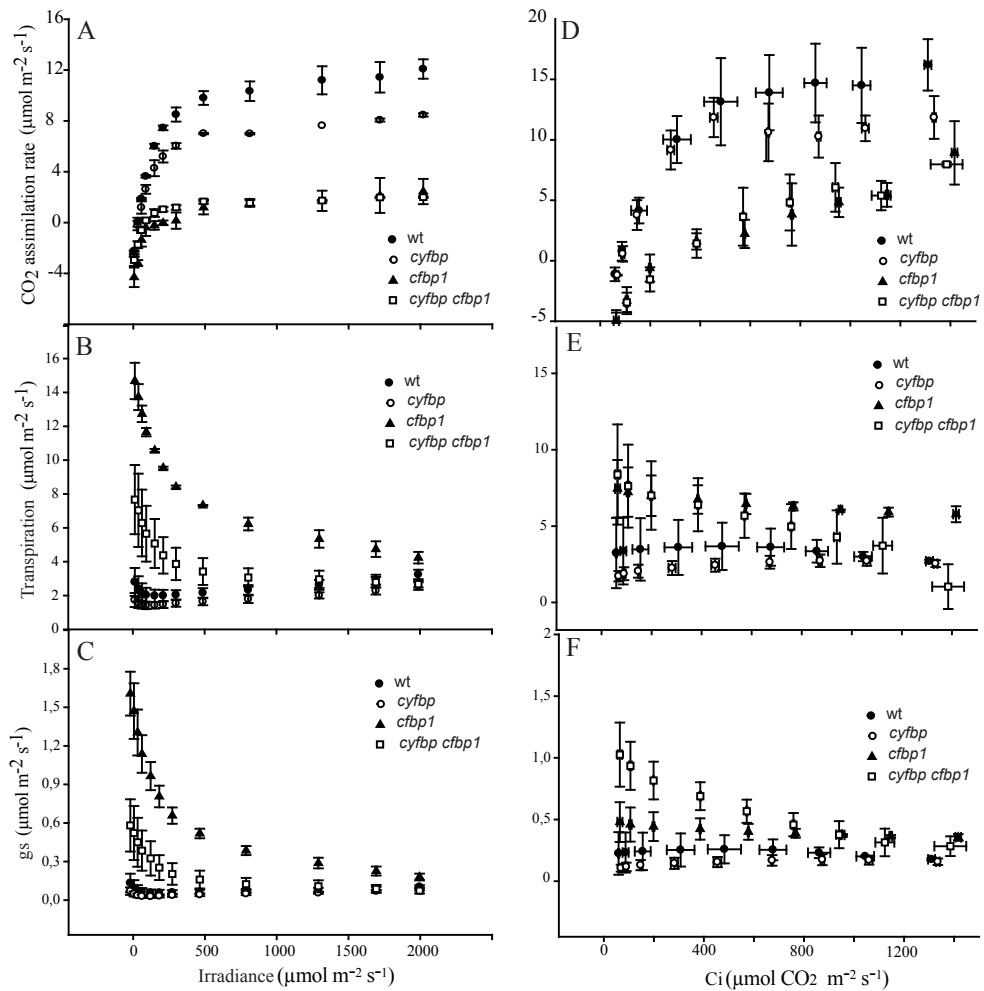


Figure 8

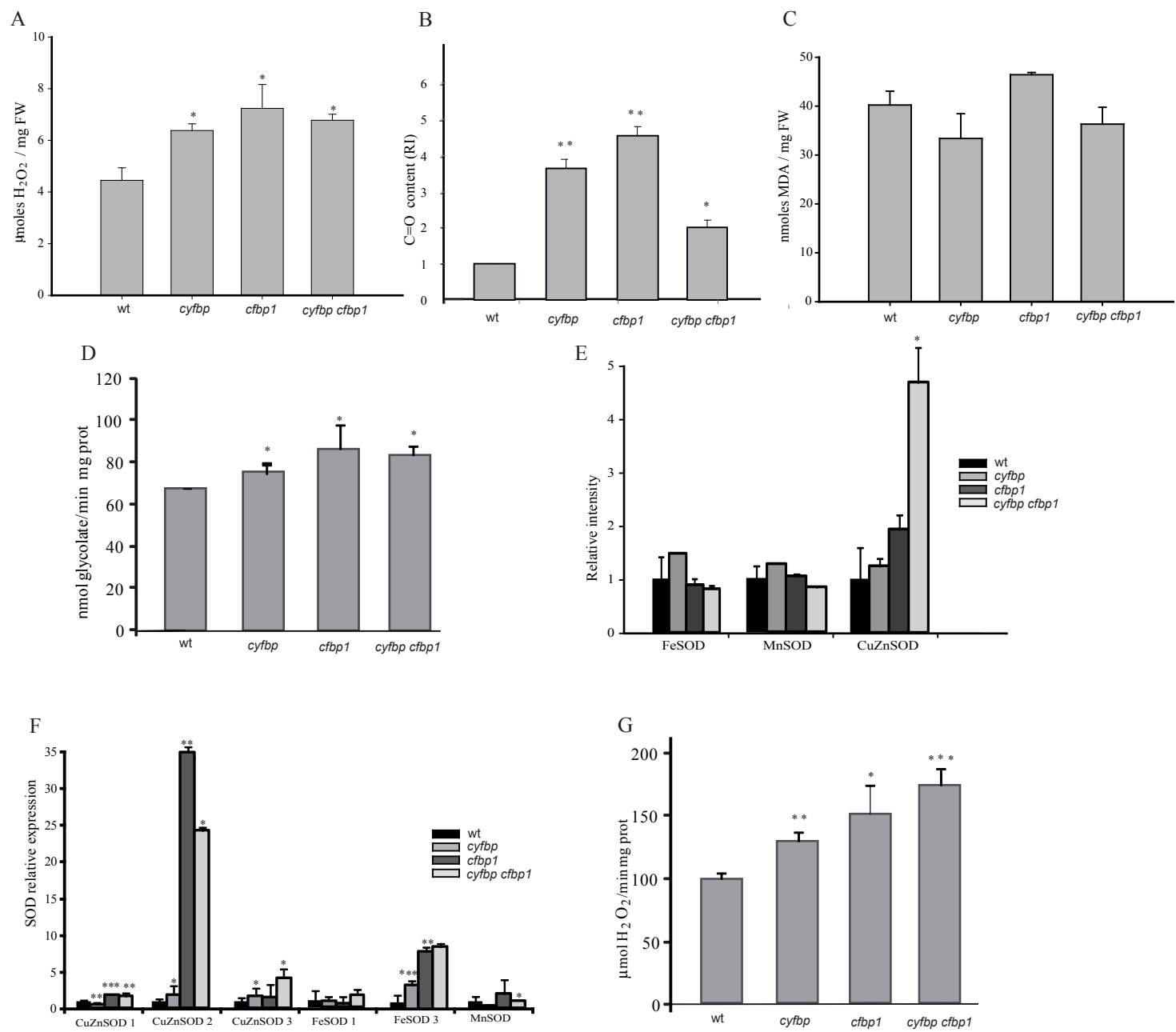


Figure 9

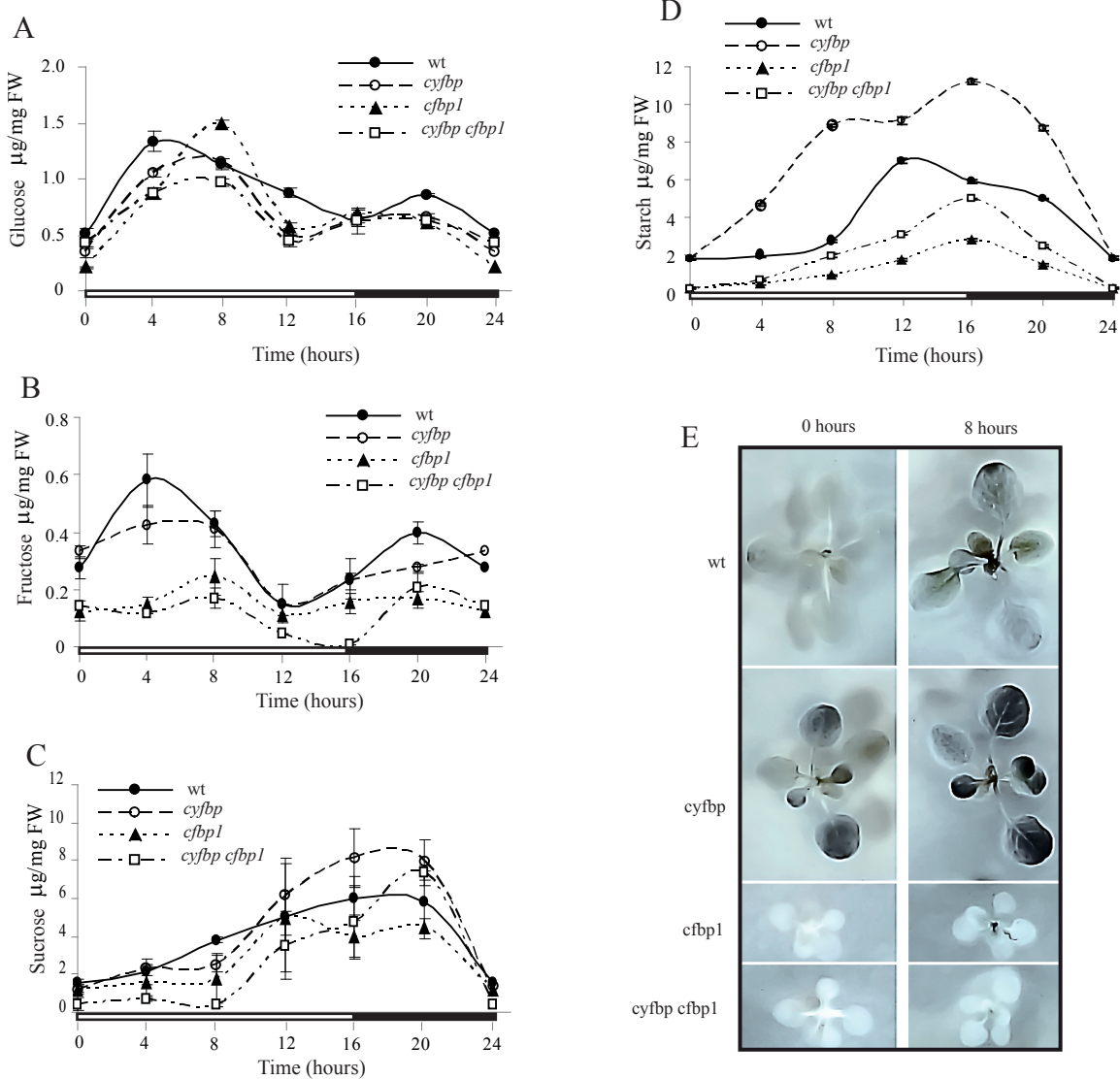


Figure 10

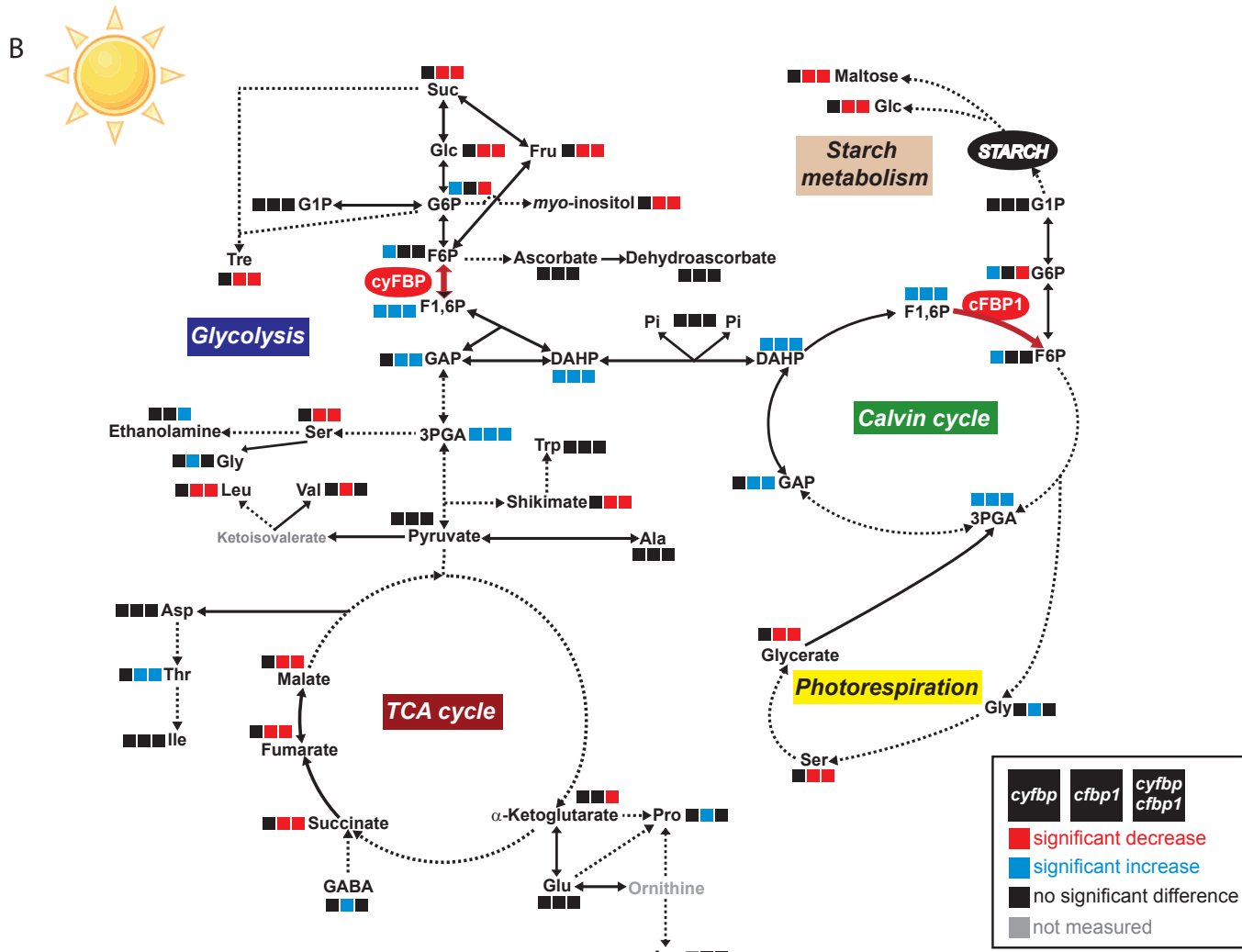
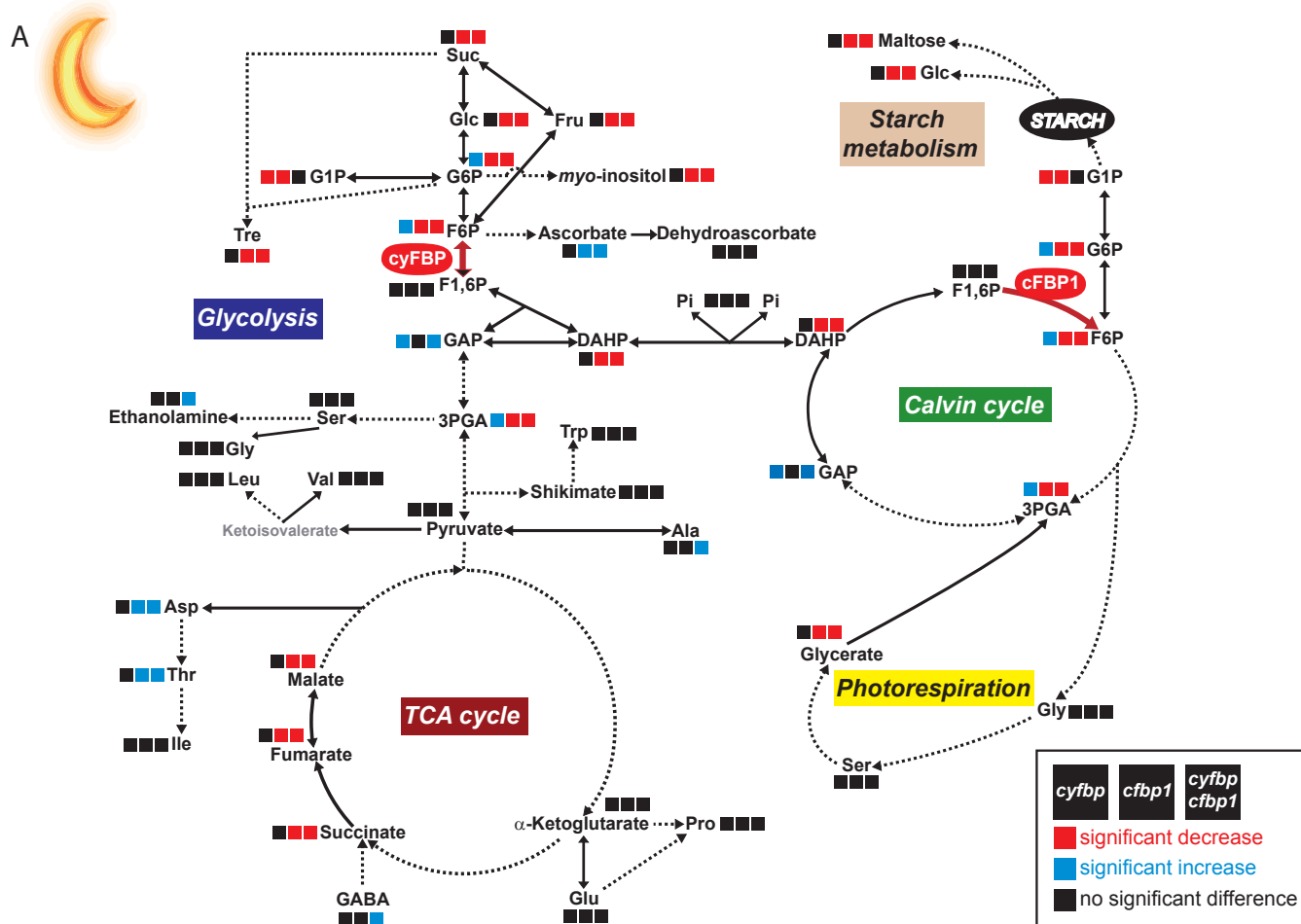
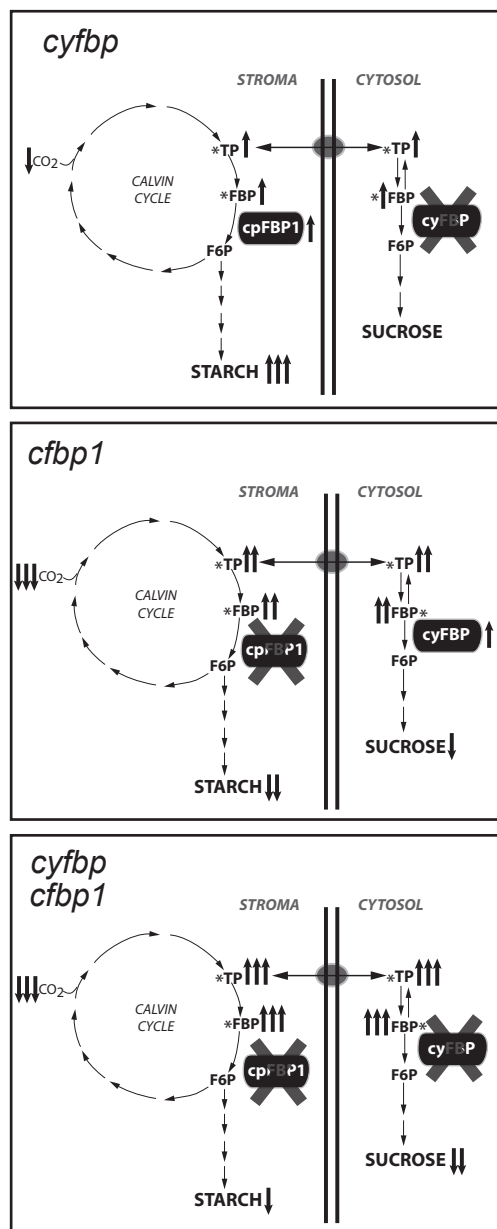


Figure 11



Supplementary Table S1 Gene-specific oligonucleotides used for semi-quantitative PCR

Oligos	Gene Analyzed	Primer sequence
CYFBP F	AT1G43670	GAGAGACAGAGACAGTAAG
CYFBP R		ACCCGGCTGACAAGAAAAGCCCCAA
LBSALK		TGGTTCACGTAGTGGGCCATCG
CFBP F	AT3G54050	GATATCTCAGCTCTGGGTC
CFBP1 R		GATGTATCTCAGTCGGTTGG
GABI		CCCATTGGACGTGAATGTAGACAC
AtCII5	AT5G64380	TTGTCTCGAACGATATCGTC
AtCII3		GATTGTCCCCGAGTTGGG
18s RNA F	Arabidopsis	AATATACGCTATTGGAGCTGG
18s RNA R		ATGGCTCATTAAATCAGTTAT
FeSOD1 F	AT4G25100	TGCTCTTCTGAGTGTGTGCG
FeSOD1 R		TGAATAATGGGCCATGCCAAC
FeSOD3 F	AT5G23310	CATCAGTGAGCCCTGTATGGTAC
FeSOD3 R		ATACTCTCAGTCACGTGCGGGTC
MnSOD1 F	AT3G10920	GAGATGAACCAGTTCCAGCTCAG
MnSOD1 R		CAACGTACCACACAGCTGAGTTG
CuZnSOD1 F	AT1G08830	AACTCAGCCTGGCTACTGGAAAC
CuZnSOD1 R		CACACAACTACCAAACCCAGGTC
CuZnSOD2 F	AT2G28190	GAACAATGGTGAAGGCTGTG
CuZnSOD2 R		GTGACCACCTTCCCAAGAT
CuZnSOD3 F	AT5G18100	AGTATTCCATACTCGGGAGGGCG
CuZnSOD3 R		GCATCCGCAGATGATTGAAGTCC
GPT1 5	AT4G24620	AAGTTCTGCCCTGCAAAAGC
GPT1 3		CGTACAGGTCACTCACATTGC
GPT2 5	AT1G61800	AGTGGCACAAAGTGTGTTTACC
GPT2 3		TCCTCACTGCTTCGCCTGTGAGT
pGlcT 5	AT5G16450	TTTCTCTGGCATGCACTGG
pGlcT 3		CTATTCCCTCCAGTGATCGACC
MEX1 5	AT5G1752	TTGATGTGGCTCACTGGTTCG
MEX1 3		GTTGTGACCATAAGCCACTGC

Supplementary Table S2. Stomatal density and stomatal index in epidermis of leaves of the wild-type and *cyfbp*, *cfbp1*, and *cyfbp cfbp1* mutants at the adaxial and abaxial surfaces.

	Stomatal density		Stomatal index (%)	
	Adaxial	Abaxial	Adaxial	Abaxial
Wild-type	384±26	215±13	23±2	12±1
<i>cyfbp</i>	228±20 *	315±36 *	15±1 *	16±3
<i>cfbp1</i>	296±30 *	349±67 *	10±1 *	18±2 *
<i>cyfbp cfbp1</i>	274±44 *	442±41 *	11±1 *	14±3

Stomatal density, number stomata/mm²; ± S.D. (n=8)

Stomatal index, SI = number of stomata/(number of epidermal cells + number of stomata) × 100

Data represents average ±SD for three different leaves per experiment. Asterisks (*) indicate a significant differences between means (Student's t-test, P <0.005).

(SD density of stomata=number of stomata per mm²) and stomata index determination (SI= number of stomata/ (number of epidermal cells + number of stomata) × 100)

Supplementary Table S3. Changes in *Arabidopsis* leaf metabolite levels at the end of the night in *cyfbp*, *cfbp1* and *cyfbp cfbp1* knockout lines relative to the wild type. Metabolite profiling was performed using GC-TOF-MS analysis and fluorescence spectroscopy. Results are means \pm SD ($n = 6$). Values that are significantly different from the wild type according to Student's *t*-test are indicated in bold (*P* value < 0.05).

Metabolites	WT	cyfbp	p-value	Dark		cyfbp x cfbp1	p-value
				cfbp1	p-value		
Sugars							
Arabinose	1,00 \pm 0,20	0,89 \pm 0,50	0,623	0,56 \pm 0,19	0,003	0,76 \pm 0,20	0,066
Fructose	1,00 \pm 0,80	0,65 \pm 0,78	0,460	0,12 \pm 0,04	0,023	0,15 \pm 0,05	0,026
Fucose	1,00 \pm 0,28	0,90 \pm 0,50	0,690	0,47 \pm 0,16	0,002	0,53 \pm 0,12	0,007
Galactose	1,00 \pm 0,60	0,83 \pm 0,63	0,638	0,52 \pm 0,15	0,088	0,61 \pm 0,18	0,157
Glucose	1,00 \pm 0,71	0,67 \pm 0,57	0,391	0,11 \pm 0,07	0,013	0,07 \pm 0,02	0,010
Isomaltose	1,00 \pm 0,07	0,67 \pm 0,72	0,477	n.d.		n.d.	
Maltose	1,00 \pm 0,27	1,42 \pm 0,83	0,271	0,20 \pm 0,07	<0,001	0,35 \pm 0,09	<0,001
Mannose	1,00 \pm 0,58	0,80 \pm 0,58	0,559	0,27 \pm 0,08	0,012	0,33 \pm 0,10	0,019
Psicose	1,00 \pm 0,35	1,10 \pm 0,67	0,744	0,40 \pm 0,13	0,006	0,53 \pm 0,16	0,013
Rhamnose	1,00 \pm 0,26	0,95 \pm 0,63	0,865	0,85 \pm 0,26	0,347	0,86 \pm 0,19	0,316
Ribose	1,00 \pm 0,40	0,79 \pm 0,49	0,429	1,08 \pm 0,46	0,766	1,11 \pm 0,30	0,583
Sedoheptulose (beta-2,7-anhydro-)	1,00 \pm 0,39	0,84 \pm 0,53	0,556	0,61 \pm 0,23	0,063	0,64 \pm 0,17	0,065
Sucrose	1,00 \pm 0,23	1,00 \pm 0,63	0,997	0,17 \pm 0,05	0,000	0,25 \pm 0,07	<0,001
Trehalose	1,00 \pm 0,39	1,37 \pm 1,21	0,489	0,36 \pm 0,15	0,004	0,40 \pm 0,13	0,005
Xylose	1,00 \pm 0,22	0,75 \pm 0,44	0,243	0,34 \pm 0,12	0,000	0,34 \pm 0,10	<0,001
Phosphate esters							
Dihydroxyacetone phosphate	1,00 \pm 0,10	0,98 \pm 0,12	0,782	0,42 \pm 0,05	<0,001	0,42 \pm 0,08	<0,001
Fructose 6-phosphate	1,00 \pm 0,11	1,22 \pm 0,08	0,003	0,79 \pm 0,15	0,017	0,74 \pm 0,14	0,005
Fructose 1,6-bisphosphate				n.d.			
Glucose 1-phosphate	1,00 \pm 0,24	0,68 \pm 0,22	0,041	0,69 \pm 0,10	0,016	0,80 \pm 0,04	0,079
Glucose 6-phosphate	1,00 \pm 0,09	1,13 \pm 0,04	0,007	0,64 \pm 0,06	<0,001	0,65 \pm 0,07	<0,001
Glyceraldehyde 3-phosphate	1,00 \pm 0,20	1,30 \pm 0,20	0,034	0,89 \pm 0,37	0,548	2,76 \pm 1,09	0,004
Glycerol 3-phosphate	1,00 \pm 0,28	0,60 \pm 0,29	0,035	0,85 \pm 0,31	0,407	0,66 \pm 0,23	0,046
3-Phosphoglycerate	1,00 \pm 0,16	1,27 \pm 0,21	0,031	0,51 \pm 0,07	<0,001	0,62 \pm 0,07	<0,001
Organic acids							
Benzoate	1,00 \pm 0,29	0,98 \pm 0,58	0,955	0,93 \pm 0,19	0,640	0,84 \pm 0,24	0,334
Butanoate (4-amino-)	1,00 \pm 0,65	0,67 \pm 0,64	0,394	1,34 \pm 0,74	0,418	2,01 \pm 0,48	0,012
Fumarate	1,00 \pm 0,26	0,77 \pm 0,44	0,303	0,28 \pm 0,12	<0,001	0,13 \pm 0,04	<0,001
Galactonate	1,00 \pm 0,22	0,88 \pm 0,50	0,616	0,86 \pm 0,36	0,427	0,70 \pm 0,20	0,034
Gluconate	1,00 \pm 1,41	0,07 \pm 0,04	0,137	0,10 \pm 0,02	0,191	0,06 \pm 0,01	0,306

Glutarate (2-oxo-)	1,00 ± 0,32	1,16 ± 0,68	0,609	0,96 ± 0,21	0,817	0,94 ± 0,23	0,732
Glycerate	1,00 ± 0,30	0,82 ± 0,46	0,447	0,50 ± 0,10	0,003	0,37 ± 0,11	<0,001
Gulonate	1,00 ± 0,92	0,91 ± 1,03	0,881	0,12 ± 0,02	0,042	0,09 ± 0,03	0,037
Hexadecanoate	1,00 ± 0,40	1,31 ± 1,17	0,548	1,07 ± 0,45	0,797	0,90 ± 0,25	0,631
Malate	1,00 ± 0,32	0,87 ± 0,55	0,640	0,25 ± 0,12	<0,001	0,15 ± 0,04	<0,001
Maleate	1,00 ± 0,37	0,95 ± 0,55	0,853	0,83 ± 0,39	0,465	0,54 ± 0,21	0,025
Nicotinate	1,00 ± 0,31	0,87 ± 0,48	0,586	0,76 ± 0,23	0,150	0,94 ± 0,27	0,726
Octadecanoate	1,00 ± 0,45	1,14 ± 1,09	0,773	1,05 ± 0,46	0,856	0,86 ± 0,25	0,522
Pyruvate	1,00 ± 0,35	1,04 ± 0,69	0,910	1,08 ± 0,29	0,658	0,84 ± 0,24	0,376
Quinate	1,00 ± 0,35	0,88 ± 0,55	0,750	1,18 ± 0,36	0,505	1,26 ± 0,37	0,350
Shikimate	1,00 ± 0,27	1,02 ± 0,55	0,942	0,77 ± 0,25	0,155	0,84 ± 0,21	0,266
Sinapate (cis-)	1,00 ± 0,40	0,78 ± 0,43	0,374	0,83 ± 0,34	0,449	0,71 ± 0,27	0,161
Sinapate (trans-)	1,00 ± 0,40	0,73 ± 0,38	0,256	0,86 ± 0,33	0,528	0,69 ± 0,27	0,157
Succinate	1,00 ± 0,36	1,39 ± 0,93	0,361	0,35 ± 0,13	0,002	0,30 ± 0,07	<0,001
Threonate	1,00 ± 0,20	0,77 ± 0,42	0,264	0,51 ± 0,18	0,001	0,35 ± 0,11	<0,001

Amino acids

Alanine	1,00 ± 0,38	0,78 ± 0,50	0,409	1,09 ± 0,40	0,703	2,01 ± 0,35	<0,001
Arginine				n.d.			
Aspartate	1,00 ± 0,50	0,92 ± 0,60	0,803	3,61 ± 2,30	0,022	3,64 ± 0,99	<0,001
Glutamate	1,00 ± 0,96	0,77 ± 0,67	0,647	2,92 ± 2,03	0,063	2,03 ± 0,76	0,066
Glycine	1,00 ± 1,22	0,46 ± 0,37	0,320	0,56 ± 0,22	0,404	0,70 ± 0,23	0,564
Isoleucine	1,00 ± 1,17	0,54 ± 0,43	0,391	1,20 ± 0,37	0,692	0,83 ± 0,09	0,726
Leucine	1,00 ± 1,08	0,60 ± 0,49	0,433	0,65 ± 0,26	0,464	0,70 ± 0,10	0,509
Proline	1,00 ± 1,86	0,26 ± 0,32	0,356	0,28 ± 0,07	0,367	0,30 ± 0,05	0,379
Pyroglutamate	1,00 ± 0,21	0,88 ± 0,40	0,538	1,05 ± 0,44	0,803	1,27 ± 0,30	0,093
Serine	1,00 ± 0,46	1,01 ± 0,82	0,986	0,55 ± 0,18	0,050	1,16 ± 0,33	0,500
Threonine	1,00 ± 0,41	0,78 ± 0,44	0,396	16,00 ± 6,45	<0,001	8,56 ± 1,51	<0,001
Tryptophan	1,00 ± 0,21	0,88 ± 0,64	0,763	0,91 ± 0,25	0,622	1,04 ± 0,23	0,840
Valine	1,00 ± 0,61	0,90 ± 0,53	0,768	0,93 ± 0,24	0,802	1,14 ± 0,25	0,604

Sugar alcohols

Erythritol	1,00 ± 0,39	0,97 ± 0,54	0,922	0,88 ± 0,19	0,504	0,82 ± 0,24	0,355
Glycerol	1,00 ± 0,26	0,88 ± 0,50	0,603	0,65 ± 0,17	0,021	0,65 ± 0,16	0,018
Inositol (myo-)	1,00 ± 0,34	1,09 ± 0,62	0,772	0,20 ± 0,05	<0,001	0,20 ± 0,05	<0,001
Maltitol	1,00 ± 0,87	0,85 ± 0,73	0,757	0,08 ± 0,03	0,027	0,06 ± 0,03	0,040
Mannitol	1,00 ± 0,73	0,67 ± 0,36	0,346	0,77 ± 0,44	0,524	1,21 ± 0,39	0,669

Others

Ascorbate	1,00 ± 0,89	1,76 ± 1,12	0,220	3,14 ± 1,60	0,017	5,48 ± 1,66	<0,001
Dehydroascorbate dimer	1,00 ± 0,58	1,28 ± 0,72	0,475	0,80 ± 0,25	0,451	0,89 ± 0,32	0,698
Ethanolamine	1,00 ± 0,68	0,96 ± 1,13	0,941	1,11 ± 0,63	0,774	2,99 ± 1,54	0,016
Phosphate	1,00 ± 0,21	0,75 ± 0,40	0,198	0,90 ± 0,32	0,524	1,14 ± 0,29	0,349
Spermidine	1,00 ± 0,36	0,74 ± 0,44	0,317	0,86 ± 0,30	0,496	0,69 ± 0,31	0,174
Uracil	1,00 ± 0,32	1,12 ± 0,84	0,745	1,16 ± 0,32	0,410	0,93 ± 0,25	0,681

n.d.: not detectable

Supplementary Table S4. Changes in Arabidopsis leaf metabolite levels after 8 h illumination (16 h light/8 h dark) in *cyfbp*, *cfbp1*, and *cyfbp cfbp1* knockout lines compared relative to the wild type. Metabolite profiling was performed using GC-TOF-MS analysis and fluorescence spectroscopy. Results are means \pm SD ($n = 6$). Values that are significantly different from the wild type according to Student's *t*-test are indicated in bold (P value < 0.05).

Metabolites	WT	cyfbp	p-value	Light		cyfbp x cfbp1	p-value
				cfbp1	p-value		
Sugars							
Arabinose	1,00 \pm 0,43	1,48 \pm 1,17	0,369	0,58 \pm 0,10	0,042	0,56 \pm 0,20	0,047
Fructose	1,00 \pm 0,83	1,54 \pm 1,50	0,458	0,13 \pm 0,03	0,028	0,10 \pm 0,06	0,024
Fucose	1,00 \pm 0,40	1,45 \pm 1,15	0,381	0,50 \pm 0,11	0,015	0,40 \pm 0,15	0,006
Galactose	1,00 \pm 0,57	2,71 \pm 2,15	0,090	0,48 \pm 0,19	0,059	0,52 \pm 0,21	0,080
Glucose	1,00 \pm 0,68	1,74 \pm 1,72	0,348	0,11 \pm 0,04	0,010	0,07 \pm 0,04	0,008
Isomaltose	1,00 \pm 0,53	4,51 \pm 3,54	0,037	0,47 \pm 0,10	0,090	0,29 \pm 0,09	0,033
Maltose	1,00 \pm 0,42	3,93 \pm 4,27	0,126	0,22 \pm 0,08	0,018	0,21 \pm 0,07	0,001
Mannose	1,00 \pm 0,59	1,63 \pm 1,30	0,307	0,27 \pm 0,08	0,013	0,25 \pm 0,10	0,011
Psicose	1,00 \pm 0,36	2,33 \pm 1,82	0,110	0,28 \pm 0,10	<0,001	0,34 \pm 0,11	0,002
Rhamnose	1,00 \pm 0,43	1,66 \pm 1,35	0,277	0,79 \pm 0,16	0,277	0,67 \pm 0,21	0,118
Ribose	1,00 \pm 0,36	1,77 \pm 1,51	0,256	1,18 \pm 0,34	0,390	1,22 \pm 0,44	0,370
Sedoheptulose (beta-2,7-anhydro-)	1,00 \pm 0,43	1,31 \pm 1,04	0,512	0,47 \pm 0,10	0,014	0,36 \pm 0,13	0,005
Sucrose	1,00 \pm 0,43	2,21 \pm 2,01	0,179	0,55 \pm 0,13	0,034	0,27 \pm 0,07	0,002
Trehalose	1,00 \pm 0,44	2,37 \pm 2,31	0,182	0,31 \pm 0,11	0,004	0,31 \pm 0,17	0,005
Xylose	1,00 \pm 0,48	1,40 \pm 1,05	0,421	0,35 \pm 0,08	0,009	0,30 \pm 0,10	0,006
Phosphate ester							
Dihydroxyacetone phosphate	1,00 \pm 0,05	1,26 \pm 0,14	0,002	1,65 \pm 0,55	0,017	3,08 \pm 0,29	<0,001
Fructose 6-phosphate	1,00 \pm 0,08	1,23 \pm 0,13	0,004	0,97 \pm 0,11	0,631	0,99 \pm 0,10	0,887
Fructose 1,6-bisphosphate	1,00 \pm 0,38	4,61 \pm 2,00	0,002	16,54 \pm 11,60	0,009	59,76 \pm 7,22	<0,001
Glucose 1-phosphate	1,00 \pm 0,27	1,06 \pm 0,43	0,776	1,05 \pm 0,21	0,741	0,74 \pm 0,16	0,065
Glucose 6-phosphate	1,00 \pm 0,06	1,25 \pm 0,06	<0,001	0,95 \pm 0,05	0,108	0,91 \pm 0,06	0,033
Glyceraldehyde 3-phosphate	1,00 \pm 0,33	4,83 \pm 1,13	<0,001	12,54 \pm 5,20	<0,001	29,77 \pm 3,92	<0,001
Glycerol 3-phosphate	1,00 \pm 0,42	0,74 \pm 0,50	0,359	0,63 \pm 0,30	0,111	0,45 \pm 0,20	0,017
3-Phosphoglycerate	1,00 \pm 0,09	2,88 \pm 0,24	<0,001	1,85 \pm 0,54	0,004	2,27 \pm 0,15	<0,001
Organic acids							
Benzoate	1,00 \pm 0,37	1,47 \pm 1,26	0,399	0,60 \pm 0,18	0,039	0,57 \pm 0,22	0,036
Butanoate (4-amino-)	1,00 \pm 0,57	1,17 \pm 1,20	0,760	2,86 \pm 1,65	0,026	2,27 \pm 1,63	0,102
Fumarate	1,00 \pm 0,40	1,18 \pm 0,95	0,678	0,29 \pm 0,09	0,002	0,14 \pm 0,05	<0,001
Galactonate	1,00 \pm 0,44	1,23 \pm 0,91	0,599	0,49 \pm 0,18	0,026	0,37 \pm 0,12	0,007
Gluconate	1,00 \pm 0,29	2,01 \pm 1,04	0,044	0,29 \pm 0,10	0,002	0,28 \pm 0,14	<0,001

Glutarate (2-oxo-)	1,00 ± 0,48	1,71 ± 1,64	0,334	0,65 ± 0,31	0,158	0,51 ± 0,24	0,049
Glycerate	1,00 ± 0,40	1,80 ± 1,17	0,146	0,24 ± 0,04	<0,001	0,26 ± 0,10	0,001
Gulonate	1,00 ± 0,37	2,87 ± 1,17	0,004	0,06 ± 0,02	<0,001	0,04 ± 0,02	<0,001
Hexadecanoate	1,00 ± 0,46	3,24 ± 4,00	0,204	0,76 ± 0,42	0,361	0,58 ± 0,39	0,117
Malate	1,00 ± 0,47	0,71 ± 0,46	0,302	0,29 ± 0,15	0,005	0,14 ± 0,10	0,001
Maleate	1,00 ± 0,31	0,91 ± 0,53	0,729	0,49 ± 0,25	0,010	0,29 ± 0,11	<0,001
Nicotinate	1,00 ± 0,34	1,04 ± 0,68	0,906	0,49 ± 0,15	0,007	0,58 ± 0,20	0,026
Octadecanoate	1,00 ± 0,48	3,24 ± 4,19	0,222	0,80 ± 0,50	0,487	0,56 ± 0,39	0,111
Pyruvate	1,00 ± 0,37	1,36 ± 1,06	0,453	0,69 ± 0,26	0,124	0,60 ± 0,27	0,061
Quinate	1,00 ± 0,59	1,47 ± 1,25	0,421	0,91 ± 0,44	0,759	1,08 ± 1,10	0,884
Shikimate	1,00 ± 0,39	1,40 ± 1,00	0,378	0,62 ± 0,12	0,044	0,49 ± 0,16	0,014
Sinapate (cis-)	1,00 ± 0,31	1,09 ± 0,65	0,760	0,52 ± 0,10	0,005	0,37 ± 0,13	<0,001
Sinapate (trans-)	1,00 ± 0,40	1,02 ± 0,74	0,953	0,53 ± 0,20	0,028	0,39 ± 0,13	0,006
Succinate	1,00 ± 0,35	1,56 ± 0,75	0,127	0,18 ± 0,05	<0,001	0,11 ± 0,04	<0,001
Threonate	1,00 ± 0,44	1,11 ± 0,80	0,776	0,30 ± 0,09	0,003	0,22 ± 0,08	0,002

Amino acids

Alanine	1,00 ± 0,43	1,43 ± 1,27	0,453	1,16 ± 0,43	0,525	1,22 ± 0,53	0,445
Arginine	1,00 ± 0,48	n.d.		0,76 ± 0,08	0,243	0,83 ± 0,59	0,651
Aspartate	1,00 ± 1,10	0,61 ± 0,58	0,466	0,78 ± 0,35	0,645	0,63 ± 0,41	0,462
Glutamate	1,00 ± 0,84	4,16 ± 4,49	0,122	2,38 ± 2,55	0,236	1,20 ± 0,94	0,699
Glycine	1,00 ± 0,23	1,10 ± 0,97	0,829	3,25 ± 2,01	0,036	1,81 ± 1,23	0,184
Isoleucine	1,00 ± 0,26	1,67 ± 1,67	0,357	1,21 ± 0,14	0,110	1,03 ± 0,29	0,874
Leucine	1,00 ± 0,31	1,80 ± 1,75	0,295	0,59 ± 0,12	0,012	0,57 ± 0,22	0,019
Proline	1,00 ± 0,36	2,27 ± 3,03	0,332	1,50 ± 0,29	0,026	1,79 ± 1,17	0,148
Pyroglutamate	1,00 ± 0,37	1,00 ± 0,64	0,993	0,81 ± 0,28	0,332	0,61 ± 0,22	0,052
Serine	1,00 ± 0,43	0,88 ± 0,37	0,631	0,50 ± 0,18	0,024	0,40 ± 0,09	0,008
Threonine	1,00 ± 0,42	0,75 ± 0,34	0,271	8,50 ± 2,06	<0,001	4,74 ± 1,43	<0,001
Tryptophan	1,00 ± 0,55	1,98 ± 1,86	0,247	0,72 ± 0,28	0,292	0,57 ± 0,36	0,166
Valine	1,00 ± 0,38	1,59 ± 1,48	0,363	0,50 ± 0,12	0,012	0,68 ± 0,20	0,104

Sugar alcohols

Erythritol	1,00 ± 0,42	1,16 ± 0,97	0,713	0,54 ± 0,21	0,037	0,49 ± 0,24	0,041
Glycerol	1,00 ± 0,39	1,72 ± 1,41	0,256	0,48 ± 0,11	0,010	0,50 ± 0,25	0,022
Inositol (myo-)	1,00 ± 0,47	1,57 ± 1,34	0,348	0,13 ± 0,05	0,001	0,14 ± 0,05	0,001
Maltitol	1,00 ± 0,47	5,00 ± 4,43	0,052	0,06 ± 0,03	<0,001	0,03 ± 0,02	<0,001
Mannitol	1,00 ± 0,92	1,19 ± 1,12	0,772	0,64 ± 0,28	0,423	0,51 ± 0,25	0,281

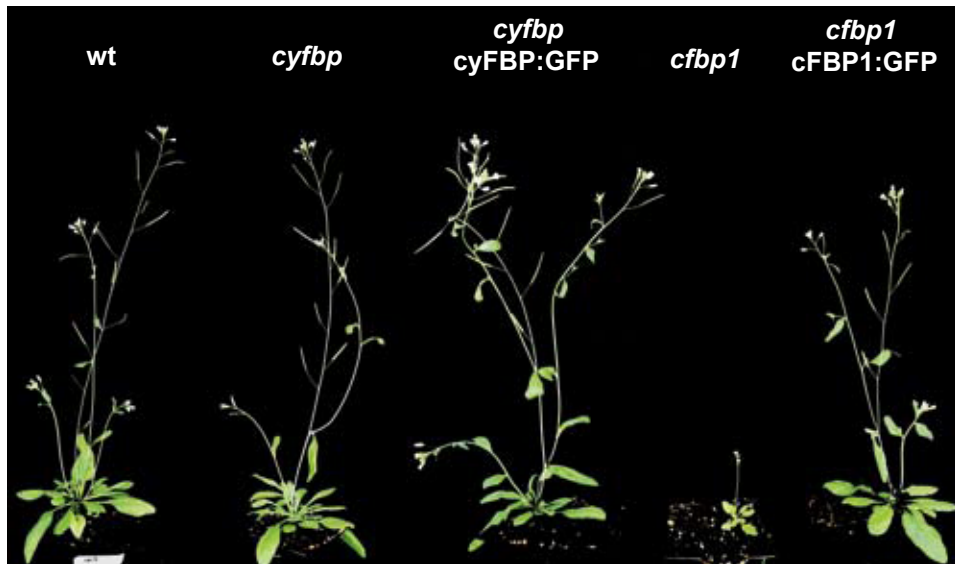
Others

Ascorbate	1,00 ± 0,70	0,70 ± 0,52	0,422	1,15 ± 0,60	0,693	1,29 ± 0,80	0,525
Dehydroascorbate dimer	1,00 ± 0,56	3,71 ± 3,43	0,086	0,60 ± 0,24	0,136	0,48 ± 0,18	0,054
Ethanolamine	1,00 ± 0,68	0,96 ± 1,19	0,950	1,90 ± 1,47	0,205	4,38 ± 2,63	0,012
Phosphate	1,00 ± 0,45	1,41 ± 1,12	0,424	0,67 ± 0,29	0,162	0,61 ± 0,35	0,125
Spermidine	1,00 ± 0,42	1,10 ± 0,80	0,784	0,55 ± 0,22	0,044	0,42 ± 0,19	0,012
Uracil	1,00 ± 0,46	1,16 ± 0,85	0,702	0,66 ± 0,26	0,150	0,64 ± 0,31	0,139

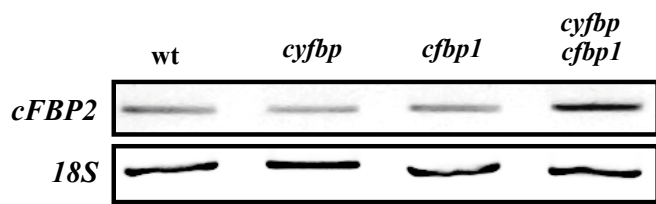
n.d.: not detectable

Supplementary Figure S1

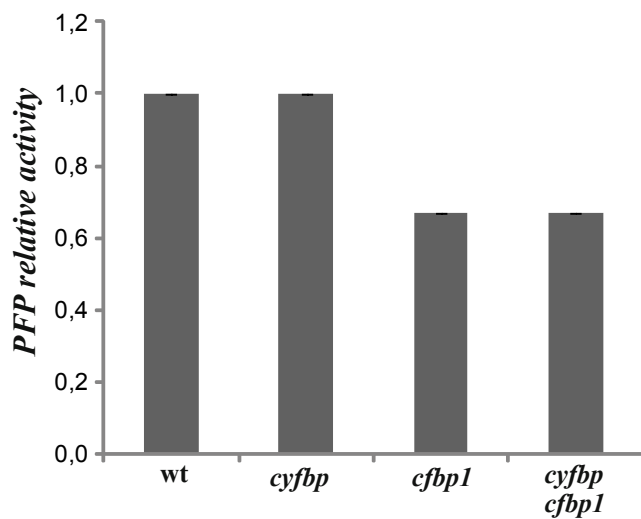
A



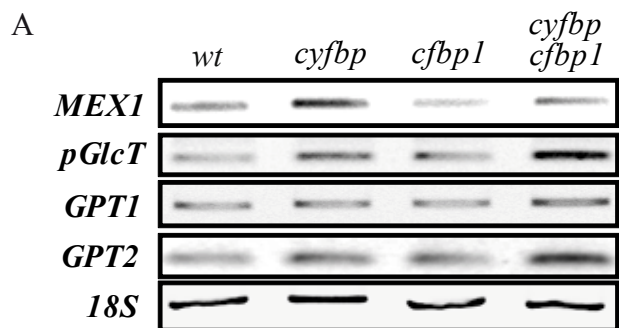
B



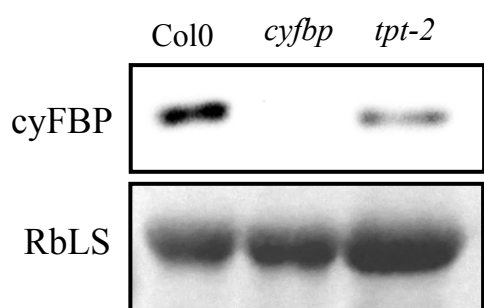
C



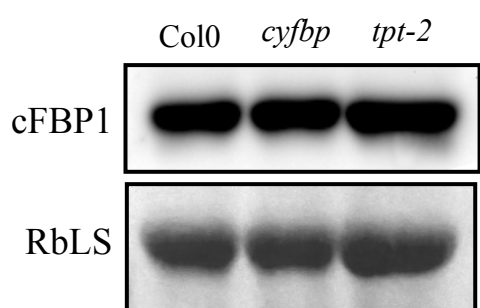
Supplementary Figure S2



B



C



RESULTS

Chapter 4 - *Arabidopsis tic62 trol* mutant lacking thylakoid-bound ferredoxin-NADP⁺ oxidoreductase shows distinct metabolic phenotype

Minna Lintala, Natalie Schuck, Ina Thormählen, Andreas Jungfer, Katrin L. Weber, Andreas P.M. Weber, Peter Geigenberger, Jürgen Soll, Bettina Böltner, Paula Mulo (2014) *Arabidopsis tic62 trol* mutant lacking thylakoid-bound ferredoxin-NADP⁺ oxidoreductase shows distinct metabolic phenotype. *Mol Plant.* 7(1):45-57.

Arabidopsis *tic62 trol* Mutant Lacking Thylakoid-Bound Ferredoxin–NADP⁺ Oxidoreductase Shows Distinct Metabolic Phenotype

Minna Lintala^{a,2}, Natalie Schuck^{b,c,2}, Ina Thormählen^d, Andreas Jungfer^{b,c}, Katrin L. Weber^e, Andreas P.M. Weber^e, Peter Geigenberger^d, Jürgen Soll^{b,c}, Bettina Böltner^{b,c,1}, and Paula Mulo^{a,1}

a Molecular Plant Biology, Department of Biochemistry, University of Turku, FI-20014 Turku, Finland

b Munich Center for Integrated Protein Science CiPSM, Ludwig-Maximilians-Universität München, Feodor-Lynen-Strasse 25, D-81377 Munich, Germany

c Department of Biology I, Botany, Ludwig-Maximilians-Universität München, Großhaderner Strasse 2–4, D-82152 Planegg-Martinsried, Germany

d Department of Biology I, Plant Metabolism Group, Ludwig-Maximilians-Universität München, Großhaderner Strasse 2–4, D-82152 Planegg-Martinsried, Germany

e Institute for Plant Biochemistry, Cluster of Excellence on Plant Sciences (CEPLAS), Universitätsstrasse 1, D-40225 Düsseldorf, Germany

ABSTRACT Ferredoxin–NADP⁺ oxidoreductase (FNR), functioning in the last step of the photosynthetic electron transfer chain, exists both as a soluble protein in the chloroplast stroma and tightly attached to chloroplast membranes. Surface plasmon resonance assays showed that the two FNR isoforms, LFNR1 and LFNR2, are bound to the thylakoid membrane via the C-terminal domains of Tic62 and TROL proteins in a pH-dependent manner. The *tic62 trol* double mutants contained a reduced level of FNR, exclusively found in the soluble stroma. Although the mutant plants showed no visual phenotype or defects in the function of photosystems under any conditions studied, a low ratio of NADPH/NADP⁺ was detected. Since the CO₂ fixation capacity did not differ between the *tic62 trol* plants and wild-type, it seems that the plants are able to funnel reducing power to most crucial reactions to ensure survival and fitness of the plants. However, the activity of malate dehydrogenase was down-regulated in the mutant plants. Apparently, the plastid metabolism is able to cope with substantial changes in directing the electrons from the light reactions to stromal metabolism and thus only few differences are visible in steady-state metabolite pool sizes of the *tic62 trol* plants.

Key words: carbon assimilation; ferredoxin–NADP⁺ oxidoreductase; photosynthesis; chloroplast; stromal metabolism; Tic62; TROL

INTRODUCTION

The light reactions of photosynthesis are linked to carbon metabolism via the ferredoxin–NADP⁺ oxidoreductase (FNR) enzyme, a 35-kDa flavoprotein found in chloroplasts as well as in non-photosynthetic plastids (Morigasaki et al., 1993). In *Arabidopsis thaliana*, the leaf-type chloroplast-targeted FNR isoforms LFNR1 and LFNR2 are encoded by two distinct nuclear genes, At5g66190 and At1g20020, respectively, which share 82% identity on amino acid level (Hanke et al., 2005; Lintala et al., 2007). In chloroplasts, both isoforms are evenly distributed between the thylakoid membranes and soluble stroma (Hanke et al., 2005), and a small quantity is additionally found attached to the inner chloroplast envelope membrane via the Tic62 protein (62-kDa subunit of translocon of inner chloroplast membrane) (Kuchler et al., 2002).

As FNR is involved in producing reducing equivalents for stromal primary metabolism, it may have a regulatory impact on distribution of electrons to various targets. In addition to

FNR, electrons are distributed directly from ferredoxin (Fd) to various reactions, such as nitrogen and sulphur metabolism, biosynthesis of chlorophyll, phytochrome and fatty acids, as well as regulation and maintenance of stromal redox balance (Hanke and Mulo, 2013). Members of the thioredoxin (Trx) protein family also accept electrons from Fd via Fd-Trx reductase (FTR), and are required for activation of numerous chloroplast enzymes, including fructose-1,6-bisphosphate phosphatase, sedoheptulose-1,7-bisphosphate phosphatase,

¹ To whom correspondence should be addressed. P.M. E-mail pmulo@utu.fi, tel. +358-2-3337915, fax +358-2-3338075. B.B. E-mail boeltner@bio.lmu.de, tel. +49-89-218074759, fax +49-89-218074752.

² These authors contributed equally to this work.

© The Author 2013. Published by the Molecular Plant Shanghai Editorial Office in association with Oxford University Press on behalf of CSPB and IPPE, SIBS, CAS.

doi:10.1093/mp/sst129, Advance Access publication 16 September 2013

Received 19 June 2013; accepted 28 August 2013

ribulose-5-phosphate kinase, NADP-glyceraldehyde-3-phosphate dehydrogenase, and rubisco activase involved in the Calvin–Benson cycle, as well as ADP-glucose pyrophosphorylase (AGPase) involved in starch synthesis, ATP synthase involved in ATP production and NADP-malate dehydrogenase (NADP-MDH) involved in export of redox-equivalents from the chloroplast to the cytosol (Schürmann and Buchanan, 2008; Thormählen et al., 2013). In addition to this, chloroplasts contain an NADPH-Trx reductase C (NTRC) combining both NTR and Trx activities on a single polypeptide to efficiently regulate chloroplast target enzymes such as 2-Cys peroxiredoxins (Pérez-Ruiz et al., 2006) or AGPase (Michalska et al., 2009) using NADPH as reducing power. Obviously, the fraction of electrons fed to these pathways must be balanced with the rates of enzyme activity to avoid over-reduction of the stromal acceptors, which might lead to formation of potentially damaging reactive oxygen species (ROS).

As the membrane binding and attachment site may affect the enzyme activity and ultimately determine which metabolic pathways are supplied with electrons, a number of studies have attempted to localize FNR at the thylakoid membranes over the past 30 years. A number of loci have been suggested: specific FNR-binding proteins (Vallejos et al., 1984; Shin et al., 1985; Chan et al., 1987; Soncini and Vallejos, 1989; Shin et al., 1990), PSI (Andersen et al., 1992), the NDH-complex (Guedeney et al., 1996; Quiles and Cuello, 1998), and the Cyt b₆f complex (Clark et al., 1984; Zhang et al., 2001). Previously, two novel FNR-binding proteins, Tic62 (Benz et al., 2009) and TROL (thylakoid rhodanese-like protein; Juric et al., 2009), have been characterized. Indeed, these proteins share an FNR-binding domain, which is characteristic only for the Tic62 and TROL proteins of vascular plants indicating a young evolutionary origin (Balsera et al., 2007).

Tic62 is encoded by a single nuclear gene (At3g18890). It is composed of two distinct structural domains: the N-terminal NADP(H)-binding module and the C-terminal domain containing conserved polyproline type II (PPII) helices capable of binding FNR (Kuchler et al., 2002; Juric et al., 2009; Alte et al., 2010). In the C-terminus of *Arabidopsis* Tic62, four FNR-binding domains have been identified, although this number varies in other plants (Balsera et al., 2007). Tic62 is a functional NADPH-dependent dehydrogenase shuttling between the chloroplast membranes and soluble stroma in a redox-dependent way: a low plastidial NADPH/NADP⁺ ratio leads to strong attachment of Tic62 to the membrane, while, under reducing conditions, Tic62 is localized predominantly in the stroma (Stengel et al., 2008). Tic62 builds large (>250-kDa) protein complexes together with FNR at the thylakoid membranes (Benz et al., 2009). The association between FNR and Tic62 is increased under acidic conditions and in darkness (Benz et al., 2009; Alte et al., 2010). These complexes are not directly involved in photosynthesis, but rather the recruitment of FNR by Tic62 to the thylakoid membranes appears to protect FNR from inactivation during the non-photosynthetic periods of the night (Benz et al., 2009, 2010).

The TROL protein, in turn, is an intrinsic thylakoid protein of 66 kDa encoded by a single nuclear gene in *Arabidopsis* (At4g01050; Juric et al., 2009). A small amount of the unprocessed form of the protein is also found in association with the inner envelope membrane. TROL contains a single serine/proline rich FNR-binding region at its C-terminus, similar to that of Tic62, and indeed the TROL–FNR protein complexes at the thylakoid membranes are smaller (190 kDa) than those composed of Tic62 and FNR (Benz et al., 2009; Juric et al., 2009). In contrast to *tic62* mutant plants, *trol* mutants possessed slightly retarded development and thicker leaves than the wild-type (WT). Notably, although no differences in linear electron transfer between *trol* mutants and WT plants could be detected upon lower light intensities, photosystem (PS)II-driven electron transfer (ETR) and non-photochemical quenching (NPQ) in *trol* mutants were affected upon increasing illumination, indicating the impact of the TROL protein in photosynthetic reactions (Juric et al., 2009).

Because membrane recruitment of FNR may be an important mechanism to control the activity of the enzyme and distribution of the electrons to stromal reactions, we have analyzed the *tic62 trol* double mutant plants, which do not possess any FNR at the thylakoid membranes, neither in protein complexes nor as free membrane-associated proteins. Here, we show that, despite the low NADPH/NADP⁺ ratio detected in the *tic62 trol* mutants, the visual phenotype and the function of photosystems in the mutants did not differ from those of the WT. This implies that the soluble pool of FNR is sufficient to support autotrophic growth of the plants, and that the plants are able to funnel NADPH to the most crucial reactions (i.e. carbon assimilation) to ensure survival and proper fitness of the plants. The *tic62 trol* double mutant revealed distinct differences in metabolic parameters relative to WT, such as changes in the activities of enzymes that are involved in NADPH metabolism (NADP-MDH) or starch biosynthesis (AGPase), and specific alterations in metabolite levels.

RESULTS

Affinity of LFNR1 and LFNR2 to the FNR-Binding Domains in Tic62 and TROL

We have shown previously that the affinity of PsFNR to one repetitive motif from Tic62 (MRM; FNR-Membrane-Recruiting-Motif; Alte et al., 2010) is pH-dependent. To determine the relative affinity of different leaf FNR (LFNR) isoforms to the three repetitive motifs in pea Tic62 and TROL proteins (Figure 1A), interaction between synthetic peptides and the heterologously expressed LFNR isoforms was analyzed using surface plasmon resonance (Biacore T200). We applied binding buffers with different pH values, similar to the experiments described in Benz et al. (2009), but, in contrast to the former approach, the different LFNR isoforms were coupled to a CM5 chip and the relative binding of the respective peptides was analyzed (Figure 1B). PsFNR showed distinct interactions with the different peptides in a concentration-dependent manner:

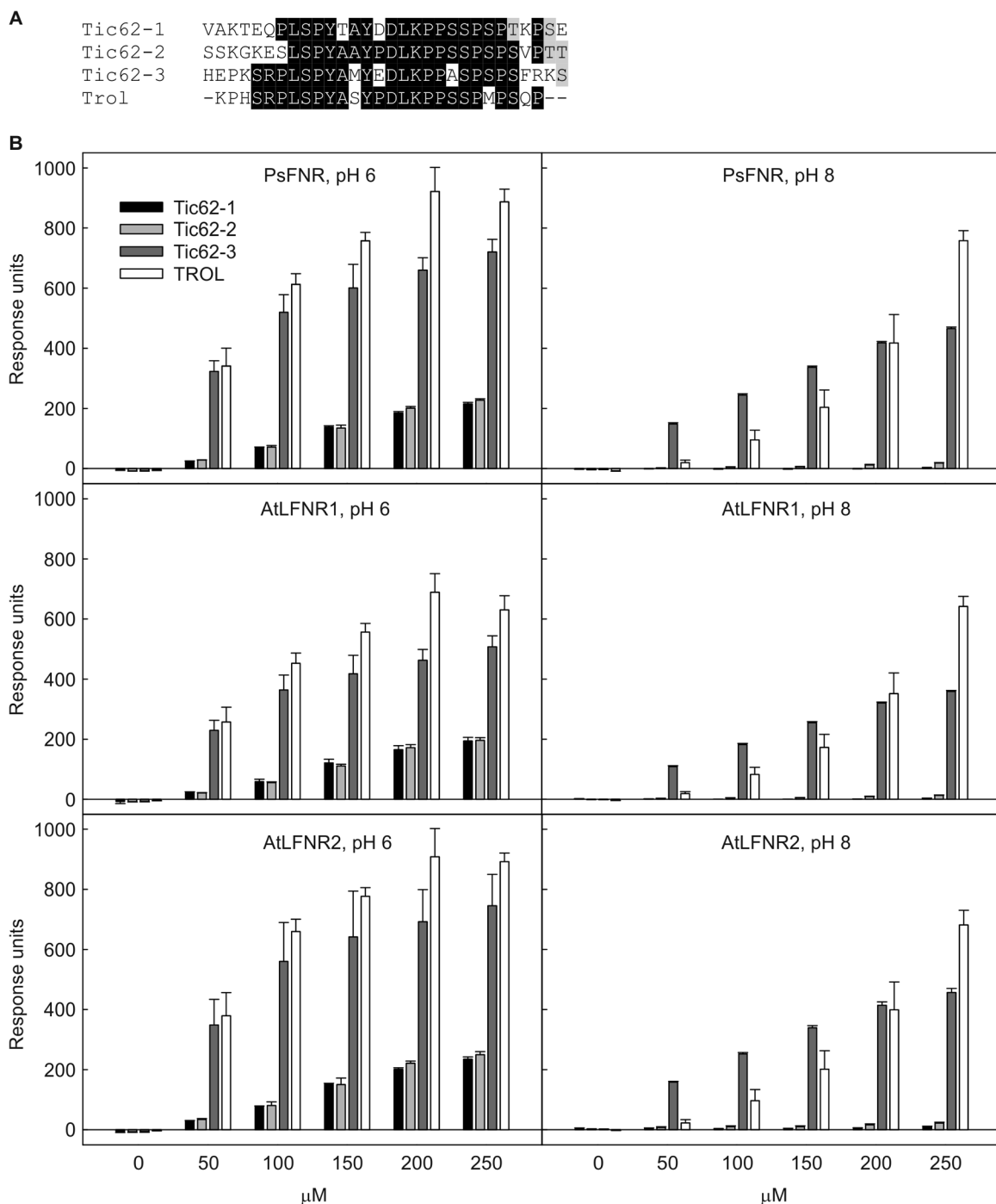


Figure 1. Interaction of FNR with Tic62 and TROL Peptides.

(A) Sequence comparison of the synthetic Tic62 and TROL peptides used for surface plasmon resonance analysis. Black boxes indicate identical, gray boxes similar amino acids.

(B) Surface plasmon resonance analyses of binding affinities of PsFNR, AtLFNR1, and AtLFNR2 (analytes) with synthetic peptides of Tic62 and TROL as ligands. Analyses were performed at two different pH values (6 and 8) with different molarities of analytes. Results are presented as mean \pm SD, $n = 3$.

with Tic62-3 as well as TROL, it interacted about three times stronger calculated by the value of obtained response units than with Tic62-1 and Tic62-2, respectively. This holds true for both pH 6 and pH 8, though the lower pH in general leads to stronger interactions. Interestingly, at pH 8, the Tic62-3

peptide showed the strongest binding to FNR (except for 200 and 250- μ M concentration), whereas, at pH 6, the TROL peptide was bound more strongly (Figure 1B). This appears to contradict the results published by Juric et al. (2009), who reported TROL having a higher affinity for FNR than Tic62 as

judged by a yeast two-hybrid assay. AtLFNR1 and AtLFNR2 basically exhibited the same interaction behavior as the pea isoform, with the LFNR1 having slightly lower affinity compared to pea and *Arabidopsis* LFNR2.

Visual and Molecular Phenotype of *tic62 trol* Mutant Plants

To study the effect of a complete loss of MRMs at the thylakoids, the *tic62* (SAIL_124_G04; Benz et al., 2009) and *trol* (SAIL_27_B04; Juric et al., 2009) mutant plants were crossed. Two homozygote lines (*tic62 trol* 2–6–8 and *tic62 trol* 2–1–18) devoid of Tic62 and TROL proteins were identified and further characterized. Results are shown from the line 2–1–18.

The *tic62 trol* double mutant plants showed no visual phenotype under any of the studied conditions (short day (SD) 8 h/16 h light/dark; long day 16 h/8 h light/dark; SD at 10°C; SD under constantly changing 5 min 50 μ mol photons $m^{-2} s^{-1}$, 1 min 500 μ mol photons $m^{-2} s^{-1}$; SD under 500 μ mol photons $m^{-2} s^{-1}$), and the double mutant plants proved to be as healthy and vigorous as the WT (Supplemental Figure 1). It is worth mentioning that, in contrast to the earlier report showing decreased rosette size of the *trol* plants (Juric et al., 2009), no such changes in the visual phenotype of *trol* plants could be detected under any of our growth conditions (Supplemental Figure 1). In line with the earlier study (Benz et al., 2009), the phenotype of *tic62* plants did not differ from WT plants (Supplemental Figure 1). Accordingly, no marked differences could be detected in the pigment (chlorophyll *a* and *b*, neoxanthin, lutein, β -carotene), pheophytin, and α -tocopherol content between WT and mutant plants (Table 1).

The quantities of the Tic62 and TROL proteins in the mutant plants were verified by Western blotting using an antibody raised against the FNR-bindings motif of pea Tic62, which recognized both Tic62 and TROL proteins (Figure 2A). Despite the predicted molecular weight of 62 kDa, Tic62 co-migrated with the 116-kDa marker, while TROL migrated with the 66-kDa marker. The *tic62* mutant plants lacked the Tic62 protein, but no clearup- or down-regulation of TROL protein could be observed. Equally, *trol* mutant plants lacked the TROL protein without changes in the content of the Tic62 protein. As expected, the double mutant plants showed complete loss of both Tic62 and TROL protein (Figure 2A). The total amount of FNR protein in the *trol* plants did not show marked difference compared to WT, whereas the total FNR content in the *tic62* and *tic62 trol* mutant was lower than in the WT. Nevertheless, the soluble pool of FNR protein was increased especially in *tic62* and *tic62 trol* mutant plants, while the thylakoid pool of FNR was clearly smaller in *tic62* mutant plants and completely missing from the *tic62 trol* mutant plant thylakoids (Figure 2B). Thylakoids were isolated under very mild conditions with no detergent present; thus, it is highly unlikely that the FNR was lost during the isolation procedure, but rather was not attached to the thylakoid membrane due to the lack of its binding partners Tic62 and TROL. Moreover, in line with the previous studies (Benz et al., 2009; Juric et al., 2009), the

analysis of thylakoid protein complexes by blue native (BN) PAGE showed that several large protein complexes composed of FNR together with Tic62 were missing from *tic62* plants, while TROL and FNR were found together only in one protein complex of around 140 kDa (Figure 2B). Additionally, the TROL protein was present independently of FNR in at least one small complex. In *trol* plants, the TROL-containing complexes were not detected. The thylakoid membranes of *tic62 trol* double mutant plants did not respond to Tic62 or FNR antibodies when separated by BN gel, indicating that FNR is attached to thylakoid membrane protein complexes which are stable under BN-PAGE conditions only via Tic62 and TROL. Intriguingly, the monomeric FNR protein detected at the thylakoid membranes of *tic62* and *trol* plants was also completely missing from the thylakoids of the *tic62 trol* plants (Figure 2B), indicating that 'free' FNR is detached from complexes during sample preparation or gel electrophoresis and no FNR is bound to thylakoid membranes independently of Tic62 or TROL.

As the simultaneous depletion of Tic62 and TROL completely hindered FNR complex formation at the thylakoid membrane (Figure 2B), we wanted to test whether *psae*, *ndho*, or *pgr5* mutant plants show a similar kind of defect in FNR complex formation as *tic62*, *trol*, and *tic62 trol*. These mutants lack the complexes/subunits previously suggested to be involved in the membrane binding of FNR (Andersen et al., 1992; Guedeney et al., 1996; Quiles and Cuello, 1998; DalCorso et al., 2008). To this end, mutant thylakoids were subjected to BN-PAGE and the gels were immunoblotted with FNR antibody. Figure 3 clearly shows that all FNR-containing complexes were present at the thylakoid membranes of WT, *ndho*, *psae*, and *pgr5*. In line with our previous results, the loss of LFNR1 resulted in complete loss of FNR from the thylakoid membranes, whereas, in the *fnr2* mutant plants, FNR was present as a free protein and in small amounts in complex with TROL (Figure 3; Lintala et al., 2007, 2009).

Photosynthetic Properties of the *tic62 trol* Plants

To study the effect of complete loss of FNR from the thylakoid membranes on the photosynthetic performance of photosystem II (PSII), chlorophyll fluorescence measurements were performed. In our hands, neither ETR nor NPQ differed between the WT and the *tic62*, *trol*, or *tic62 trol* mutant plants under different actinic light intensities (Figure 4A and 4B). Deeper insight into the ability of plants to induce NPQ was gained by analyzing the de-epoxidation state of the xanthophyll cycle pigments. In accordance with the fluorescence measurements, no drastic differences could be detected in the accumulation of violaxanthin, antheraxanthin, and zeaxanthin between the WT and the *tic62 trol* plants under standard growth conditions or after 1 h of high light illumination (500 μ mol photons $m^{-2} s^{-1}$) (Table 1). Also, the photosynthetic protein complexes showed similar composition and quantity in all plant lines (WT, *tic62*, *trol*, and *tic62 trol*) when studied either by BN-PAGE (Figure 2B) or SDS-PAGE (Figure 4C).

Table 1. Pigment, Pheophytin, and α -Tocopherol Composition of WT and *tic62 trol* Leaves.

	WT	<i>tic62 trol</i>
Chl <i>a</i>	15 815 \pm 1925	13 886 \pm 1442
Chl <i>b</i>	5057 \pm 502	4481 \pm 476**
Chl <i>a/b</i>	3.13 \pm 0.22	3.10 \pm 0.10
Pheophytin	141 \pm 22	121 \pm 19
Lutein	1621 \pm 215	1421 \pm 147
β -carotene	958 \pm 137	850 \pm 66
Neoxanthin	293 \pm 29	260 \pm 26
Antheraxanthin	35 \pm 7	37 \pm 5
Violaxanthin	341 \pm 52	308 \pm 42
α -tocopherol	111 \pm 23	91 \pm 11
Zeaxanthin (HL)	6.5 \pm 1.0	5.6 \pm 0.9

Pigments were measured from leaf discs punched from plants grown under standard short-day conditions, except zeaxanthin after 1 h high light treatment (HL, 500 μ mol photons m^{-2} s $^{-1}$).

Pigments are expressed in ng cm^{-2} . Data are presented as mean \pm SD, $n = 11$ –12. ** statistically significant difference from WT ($P < 0.01$).

Moreover, no differences in the capacity of PSII could be detected between the *tic62 trol* plants and WT when challenged by intense illumination (1000 μ mol photons m^{-2} s $^{-1}$; Figure 4D), indicating that the mutant plants were as tolerant against photoinhibition as WT.

Consistently with the fluorescence measurements, no changes in the apparent rate of CO_2 assimilation could be detected when the *tic62 trol* plants were grown under standard conditions. Furthermore, the light and CO_2 responses of photosynthetic CO_2 assimilation (Figure 4E and 4F) were similar in WT and mutant plants. Also, the content of Calvin–Benson cycle peptides RbcS and RbcL did not differ between the *tic62 trol* mutant and WT (Figure 4E).

Analysis of the NADPH/NADP $^{+}$ Redox State in the *tic62 trol* Plants

As FNR is catalyzing the conversion of NADP $^{+}$ to NADPH, we next aimed to analyze the steady-state NADPH and NADP $^{+}$ pool sizes as well as the NADPH/NADP $^{+}$ redox state in the *tic62 trol* plants. The NADPH and NADP $^{+}$ contents were measured at the end of the dark period, in the middle of the light period, and at the end of the light period. Interestingly, the quantity of NADP(H) was much lower in the plants harvested at the end of the dark period than those harvested during illumination, but these diurnal alterations were not significantly different between the *tic62 trol* plants and WT (Figure 5A). The changes in the total amount of NADP(H) upon day/night alterations were found to be much stronger than previously appreciated. However, a smaller pool size of NADP(H) in the dark versus light has already been reported in previous studies, such as for spinach leaves (Heineke et al., 1991). Intriguingly, a significant decrease in the NADPH/

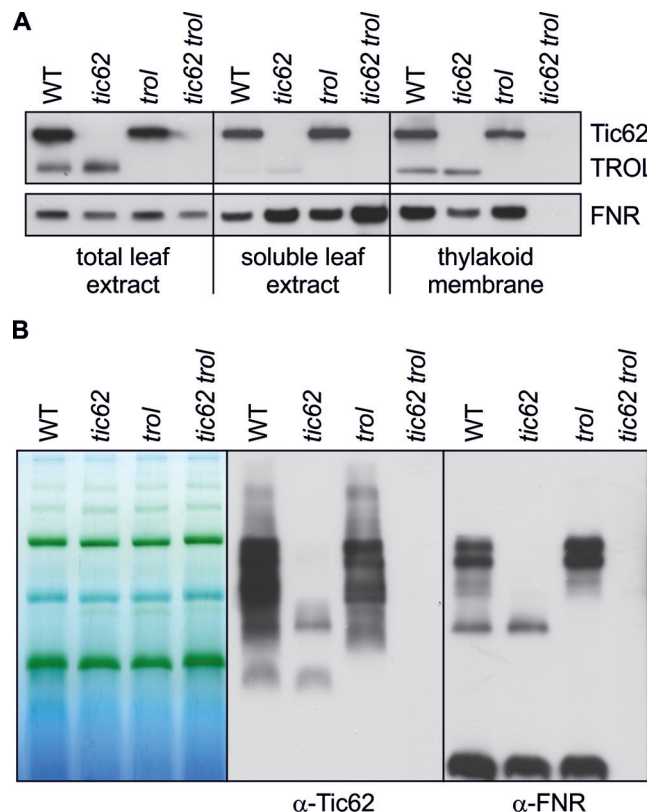


Figure 2. Tic62, TROL, and FNR Protein Content in the WT, *tic62*, *trol*, and *tic62 trol* Plants.

(A) SDS-PAGE of the WT, *tic62*, *trol*, and *tic62 trol* plant total leaf extract, soluble leaf extract, and thylakoid membranes. 10 μ g of protein was loaded on gel and proteins were immunodetected with Tic62 and FNR antibodies.

(B) BN-PAGE of the WT, *tic62*, *trol*, and *tic62 trol* plants. The first panel shows the thylakoid protein complexes, and the second and third panels show the respective Western blots labeled with Tic62 or FNR antibody, respectively. 5 μ g of chlorophyll was loaded on the gel.

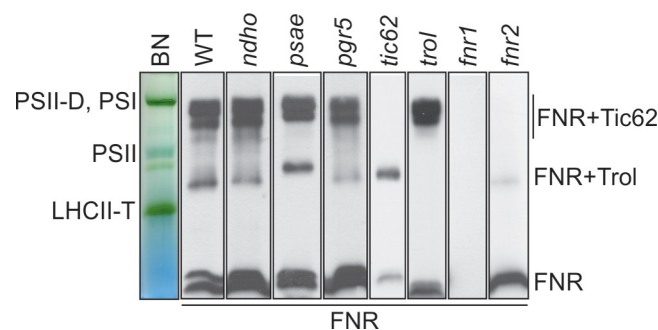


Figure 3. Interaction of FNR with Various Thylakoid Membrane Protein Complexes.

Molecular analysis of FNR-containing thylakoid protein complexes in WT, *ndho*, *psae*, *pgr5*, *tic62*, *trol*, *fnr1*, and *fnr2* plants. Protein complexes were separated using BN-PAGE, the gel was Western blotted, and proteins were detected with FNR-specific antibody. 5 μ g of chlorophyll was loaded on the gel.

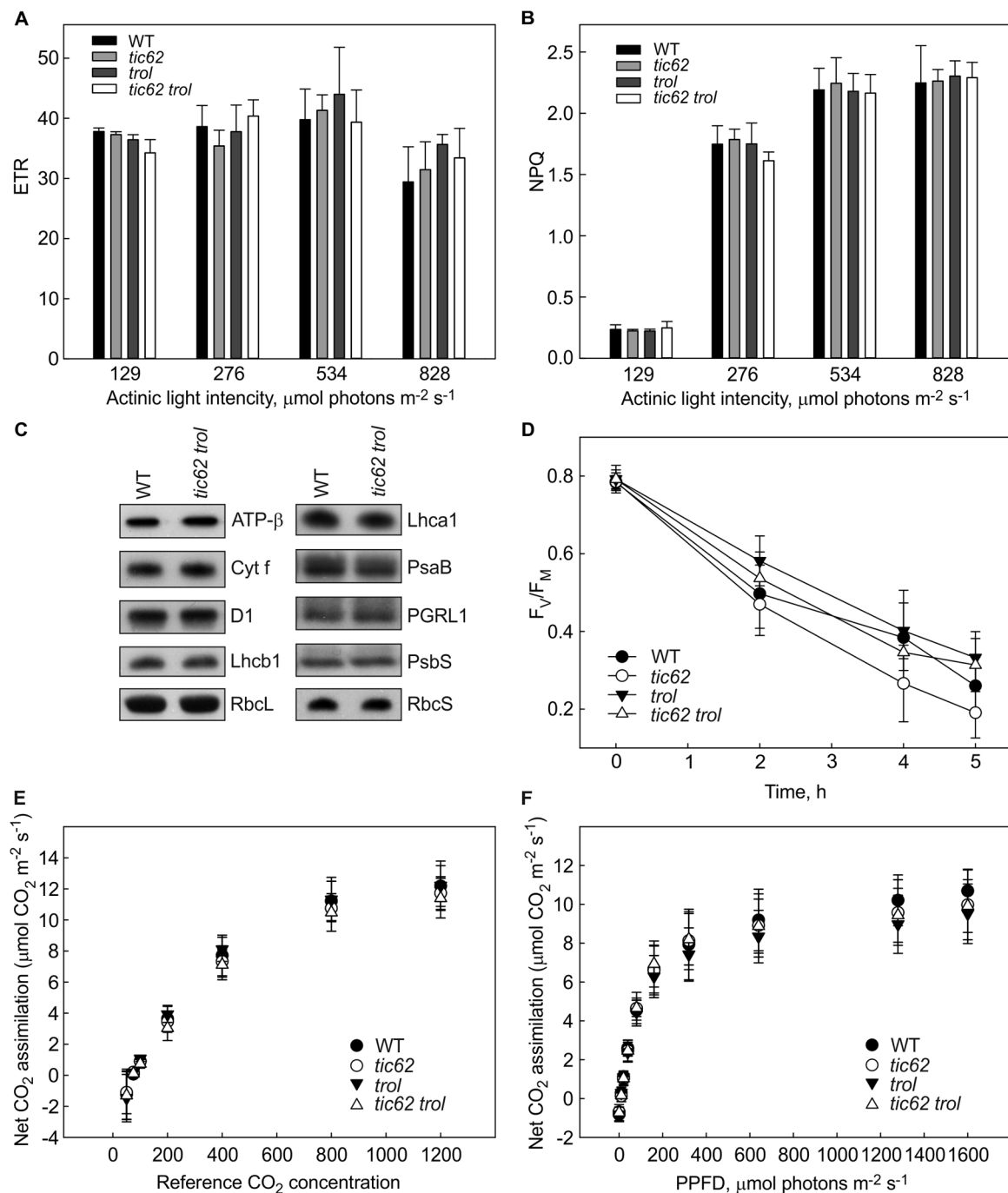


Figure 4. Photosynthetic Electron Transfer Properties of the WT, *tic62*, *trol*, and *tic62 trol* Plants.

(A) Electron transfer of PSII (ETR) and (B) NPQ capacity of the WT, *tic62*, *trol*, and *tic62 trol* plants.

(C) The content of photosynthetic proteins in the WT and *tic62 trol* plants. The gels were loaded according to linear range of the antibody and the membranes were immunolabeled with antibodies against ATP- β , Cyt f, D1, Lhcb1, Lhca1, PsaB, PGRL1, PsbS, RbcL, and RbcS.

(D) Photoinhibition of the WT, *tic62*, *trol*, and *tic62 trol* plants. The leaves were illuminated under 1000 $\mu\text{mol photons m}^{-2} \text{s}^{-1}$ (+10°C) for the indicated time and the PSII efficiency recorded as F_v/F_m .

(E) CO_2 assimilation efficiency of the WT, *tic62*, *trol*, and *tic62 trol* plants under various reference CO_2 concentrations.

(F) CO_2 assimilation efficiency of the WT, *tic62*, *trol*, and *tic62 trol* plants under various light intensities.

NADP $^+$ ratio was detected in the *tic62 trol* plants when plants were analyzed during the light period (Figure 5B). In contrast to the large decrease in NADPH/NADP $^+$ redox state,

the NADH/NAD $^+$ redox status was not substantially affected, indicating that the *tic62 trol* mutation affected specifically the NADP system (Figure 5C). The decrease in the NADPH/

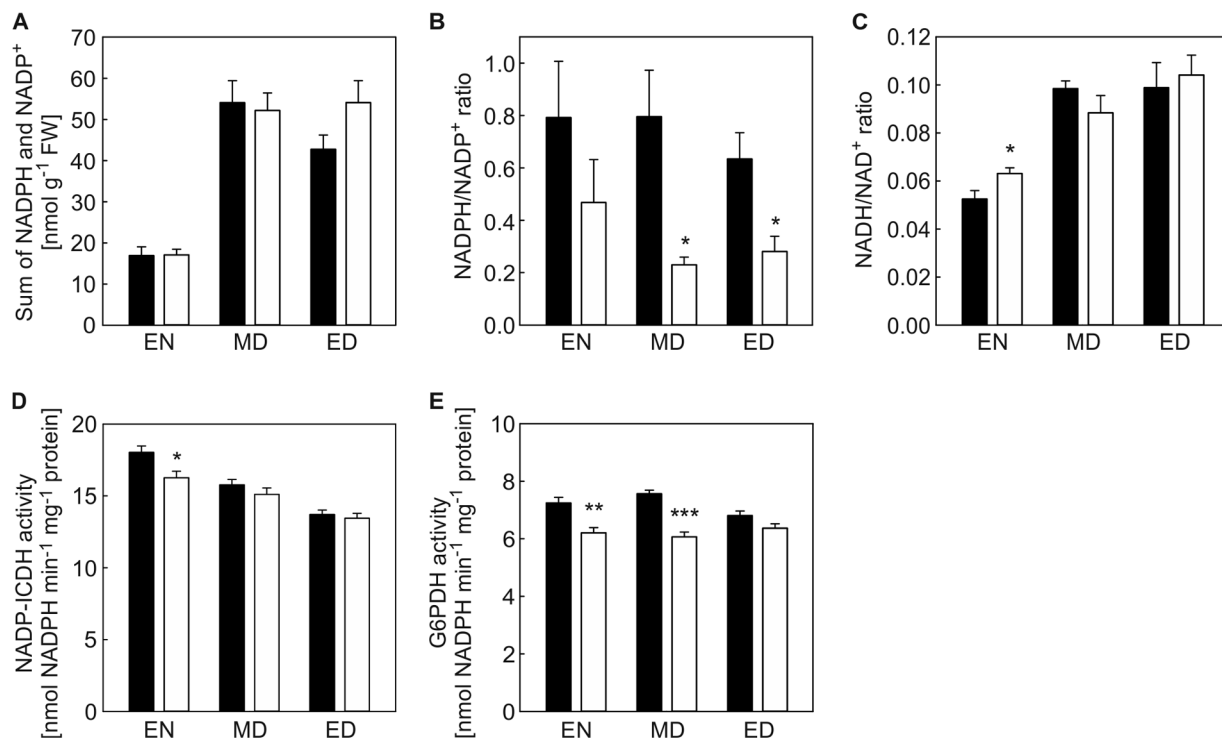


Figure 5. NADP(H) Metabolism in the WT (Black Bars) and *tic62 trol* Plants (White Bars).

(A) The total content of NADPH and NADP⁺ of the WT and *tic62 trol* plants.

(B) NADPH/NADP⁺ ratio of the WT and *tic62 trol* plants.

(C) NADH/NAD⁺ ratio of the WT and *tic62 trol* plants.

(D) Spectrophotometric determination of the activity of NADP-ICDH.

(E) Spectrophotometric determination of the activity of G6PDH. All measurements were performed in the end of the night/dark period (EN), in the middle of the day/light period (MD), and in the end of the day/light period (ED). Results are presented as mean \pm SE, $n = 4$. Statistically significant difference from WT (* $P < 0.05$; ** $P < 0.01$; *** $P < 0.005$).

NADP⁺ ratio could be due to an inhibition of FNR activity that may be attributable to the overall decrease in FNR protein level (see above) or the loss of FNR membrane association. Alternatively, metabolic reactions using or generating NADPH could have been activated or inhibited in response to altered FNR membrane binding. We therefore measured the activity of selected enzymes involved in NADPH metabolism, such as isocitrate dehydrogenase (NADP-ICDH) and glucose-6 phosphate dehydrogenase (G6PDH), which are proposed to be involved in generation of NADPH in the cytosol and in the plastid. Our results show that the *tic62 trol* mutation led to a significant decrease in NADP-ICDH and G6PDH activities (Figure 5D and 5E), which could partly be responsible for the decrease in the NADPH/NADP⁺ ratios (Figure 5B).

Analysis of Stromal Metabolism in the *tic62 trol* Plants

The AGPase enzyme catalyzes the first committed step in starch biosynthesis by generating ADP-glucose from glucose-1-phosphate and ATP in the chloroplast stroma, simultaneously liberating inorganic pyrophosphate (PPi) (reviewed in Stitt and Zeeman, 2012). AGPase is subject to posttranslational redox-regulation by reversible disulfide-bond

formation between the two small subunits (APS1) of the heterotetrameric enzyme (Geigenberger, 2011). To investigate the AGPase redox-activation state in the *tic62 trol* mutant, leaf samples were taken at the end of the dark period, in the middle of the light period, and at the end of the light period to analyze the monomer/dimer ratio of the APS1 subunits. Results show that, at the end of the dark period, AGPase redox activation was significantly higher in the leaves of the *tic62 trol* plants than those of WT, whereas, in the subsequent light period, this effect disappeared or was slightly reverted (Figure 6A). When starch levels were analyzed, no statistically significant difference could be detected in the accumulation of starch between the *tic62 trol* mutant plants and the WT, except a slight increase in the starch content in the *tic62 trol* plants at the end of the dark period that corresponds to the redox activation of AGPase under these conditions (Figure 6A and 6B). This difference was emphasized when the plants were challenged by dim light (50 μ mol photons $m^{-2} s^{-1}$), leading to a significant increase in starch content in the *tic62 trol* mutant relative to WT (Figure 6C). We also measured the redox-activation state of stromal NADP-MDH, which is involved in the export of excess NADPH from the stroma to the cytosol via the malate valve (Scheibe et al., 1990). Results show that, in

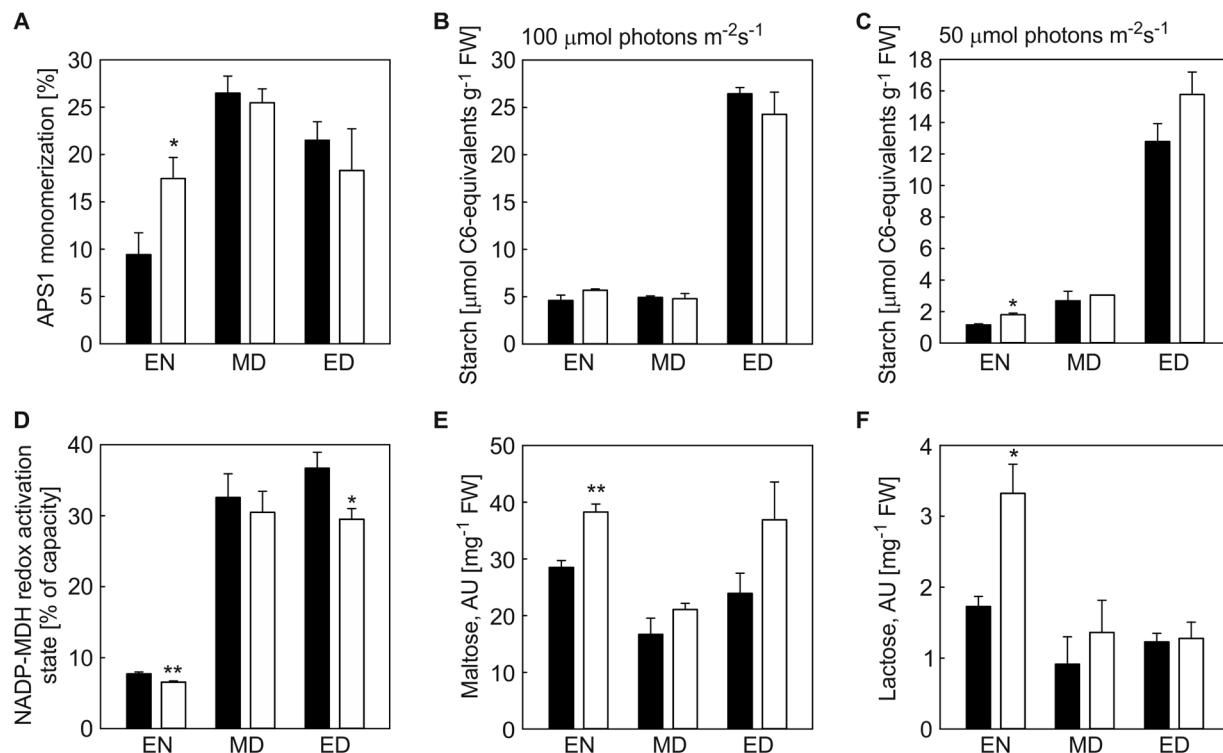


Figure 6. Starch Accumulation and Stromal Metabolism in the WT (Black Bars) and *tic62 trol* Plants (White Bars).

(A) Redox-activation state of AGPase measured as monomer/dimer ratio of the two APS1 small subunits.
 (B) Starch content in the WT and *tic62 trol* plants grown under 100 $\mu\text{mol photons m}^{-2} \text{s}^{-1}$ or (C) grown under 50 $\mu\text{mol photons m}^{-2} \text{s}^{-1}$.
 (D) Redox activation of NADP-MDH, measured as the ratio of apparent/maximal enzyme activity, in the WT and *tic62 trol* plants.
 (E) Content of maltose and (F) lactose in the WT and *tic62 trol* plants. Concentrations of maltose and lactose are given in arbitrary units (AU) mg^{-1} fresh weight. All measurements were performed in the end of the night/dark period (EN), in the middle of the day/light period (MD), and in the end of the day/light period (ED). Results are presented as mean \pm SE, $n = 4$. Statistically significant difference from WT (* $P < 0.05$; ** $P < 0.01$).

the *tic62 trol* mutant, redox activation of NADP-MDH was significantly decreased relative to the WT (Figure 6D).

To further analyze effects on metabolite levels, a metabolic fingerprint of the *tic62 trol* plants was obtained (Supplemental Figure 2). Most amino acids were found at a similar level in the *tic62 trol* and WT plants, but the content of β -alanine, aspartic acid, and proline was slightly increased in the *tic62 trol* plants as compared to WT, although the difference could only be detected at the end of the light period. The content of asparagine, in contrast, was higher in the WT plants than in *tic62 trol*, but only in the middle of the light period. The levels of malonic acid and succinic acid were increased in the double mutant at the end of the light period and the end of the dark period, respectively, whereas the content of maleic acid was decreased. No apparent changes could be detected in the accumulation of any other organic acid, not even malate. The sugar content (fructose, glucose, mannose, sucrose, xylose) of the *tic62 trol* plants tended to be higher as compared to WT (Supplemental Figure 2). However, significant differences were only observed for maltose and lactose after the dark period (Figure 6E and 6D, and Supplemental Figure 2). Overall, the steady-state metabolite levels in the mutant lines were very close to those observed in WT.

DISCUSSION

LFNR1 and LFNR2 Interact with Tic62 and TROL

The detailed analysis of affinity properties of the different FNR isoforms from *Arabidopsis* and pea to distinct repetitive motifs of Tic62 and TROL revealed that the pH-dependent binding behavior is consistent among all FNRs—acidic pH leads to more pronounced binding of all FNRs to all peptides (Figure 1). This is perfectly in line with our previously published observations (Benz et al., 2009). Thus, we can extend the model from pea FNR and a single Tic62 repeat to AtLFNR1 and AtLFNR2 as well as the other two repetitive motifs in Tic62 and the single one in TROL. Under conditions when FNR is needed for electron transfer from Fd to NADP⁺ in the stroma, namely in the light during active photosynthesis, the pH at the thylakoids is more alkaline due to protons being pumped into the thylakoid lumen, which leads to detachment of FNR from Tic62 and TROL. When photosynthetic activity decreases and finally completely ceases in the night, the stroma is acidified. This, in turn, increases the affinity of FNR to its binding partners at the membrane, where it is then stored overnight until needed again at dawn (Benz et al., 2010).

The third repeat of Tic62 and the MRM in TROL has generally a higher affinity to all FNR isoforms than Tic62-1 and Tic62-2 MRMs under all conditions tested. A marked difference between the otherwise very similar MRMs from Tic62 and TROL (Figure 1B) is the pI of the peptides: 62-1 = 4.78; 62-2 = 8.11; 62-3 = 9.4; TROL = 9.53. Thus, both Tic62-3 and TROL MRMs have a basic pI above 9 and are positively charged under the two different pH conditions applied in our experiments. Since the MRMs form PPII helices, which interact with FNR via van der Waals interactions as well as via salt bridges, the different charge might influence the binding capacity. It is tempting to speculate that the third, most exposed repeat is responsible for 'catching' FNR molecules and only if all terminal motifs are loaded with FNR will it start binding to the second and first MRM. It might also be the case, as deduced from our analytical ultracentrifugation analysis (Benz et al., 2009), that, for sterical reasons, not all repeats bind two FNR molecules, as theoretically possible, but that the terminal repeat is predominantly responsible for FNR binding. This would be in line with the data reported by Juric et al. (2009) showing that TROL has in general a higher binding affinity. The single repeat at the C-terminus of TROL binds equally or even more strongly to FNR as the third Tic62 repeat. Since TROL is an integral membrane protein and cannot relocate depending on the stromal redox state as Tic62 does, attachment of FNR to either Tic62 or TROL might influence the flexibility of the system.

NADPH Is Funneled towards Carbon Assimilation in the *tic62 trol* Plants

Our results show that the *tic62 trol* double mutant plants are completely lacking FNR from the thylakoid membranes (Figure 2). Interestingly, this led to changes in plastid metabolism rather than in photosynthetic carbon assimilation. Although the exclusively soluble pool of FNR is sufficient to support expeditious function of photosystems followed by efficient carbon assimilation (Figure 4), the ratio of NADPH/NADP⁺ was found to be compromised in the *tic62 trol* plants (Figure 5). It should be noted that, in addition to relocation of FNR, the total content of chloroplast FNR was markedly decreased in the *tic62 trol* plants (Benz et al., 2009; Juric et al., 2009; Figure 2). This leads us to two possible interpretations: (1) the decreased amount of total FNR may result in lower production of NADPH or (2) the soluble form of FNR is less efficient in the reduction of NADP⁺ to NADPH than the membrane-bound FNR.

Intriguingly, the *tic62 trol* plants were tolerant against both long- and short-term high light illumination. The capacity of PSII in the high-light-treated *tic62 trol* plants, measured as F_v/F_m , did not differ from that of WT and the ETR and NPQ capacities of the *tic62 trol* plants were similar to WT under all studied actinic light intensities (Figure 4). Additionally, no significant changes in the function of the xanthophyll cycle and accumulation of antioxidative compounds (i.e. α -tocopherol and zeaxanthin) could be detected (Table 1). The identical

ETR and NPQ capacity between the WT and *tic62 trol* plants are in contrast to the previous study reporting changes in the photosynthetic performance of the *trol* mutant, especially under high light intensities (Juric et al., 2009). This discrepancy may result from differences in growth conditions of the plants and/or experimental set-up, though we cannot completely exclude the possibility of adaptive processes in the *trol* background which could have led to masking of the previously observed phenotype. As the *tic62 trol* plants show no symptoms of oxidative stress under any conditions studied, it is conceivable that the electrons originating from the light reactions are funneled towards other reactions acting as safety valves in the chloroplasts. Previous studies describing *Arabidopsis* mutants with considerable changes in the chloroplast redox metabolism, such as *tapx sapx* (Kangasjärvi et al., 2008) and *NADP-mdh* (Hebbelmann et al., 2012) suggest extensive metabolic adaptation, which enables maintenance of a chloroplast redox homeostasis resulting in WT appearance of the mutant plants. This remarkable resilience is also reflected in the metabolic fingerprints obtained from the *tic62 trol* plants, which indicated a very similar metabolite state as observed in WT.

Indeed, the posttranslational redox activation of AGPase was up-regulated in the *tic62 trol* plants (Figure 6). More starch accumulated in the low-light-grown *tic62 trol* plants during the dark period, whereas no significant differences in the starch content could be detected between the *tic62 trol* mutant and WT in the light (Figure 6). The slightly higher maltose level detected in *tic62 trol* (Figure 6) is in line with the altered starch metabolism, since starch may be degraded in the light, the resulting sugars undergoing oxidation in the cytoplasm. AGPase has been found to be rapidly activated by reduction of an intermolecular disulfide bond between the Cys residues joining the two small APS1 subunits of this heterotetrameric enzyme (Geigenberger et al., 2011). While light activation of AGPase involves the Fd/Trx f system (Hendriks et al., 2003; Kolbe et al., 2005; Thormählen et al., 2013), the NADPH/NTRC system can also activate AGPase in the dark in response to sugars (Tiessen et al., 2002; Michalska et al., 2009). Thus, it is possible that the higher AGPase activity detected in the *tic62 trol* plants after the dark period results from the activating effect of increased sugar content.

It is remarkable that, even if the ratio of NADPH/NADP⁺ is decreased in the *tic62 trol* mutants, the plants are able to secure the function of most crucial pathways, namely carbon assimilation (Figure 4). It can be speculated that the soluble FNR is in close physical proximity to the Calvin cycle enzymes to ensure electron flow to carbon assimilation. Indeed, FNR has been shown to be co-localized in the stroma of pea chloroplasts with glyceraldehyde-3-phosphate dehydrogenase (Negi et al., 2008), which, in turn, is co-localized with phosphoglycerate kinase (Anderson et al., 2003), triose phosphate isomerase, aldolase (Anderson et al., 2005), and transketolase (Anderson et al., 2006). If the decreased NADPH amount was threatening to the plants, we would expect alternative

pathways of generating NADPH to be up-regulated. Therefore, we checked the activation status of the G6PDH, which is the key enzyme of the oxidative pentose phosphate cycle in the cytosol and plastids (Kruger and von Schaewen, 2003) and that of NADP-ICDH, which produces NADPH in the plastids, cytosol, mitochondria, and peroxisomes (Hodges et al., 2003). Under normal conditions, plastidial G6PDH is activated by oxidation in the dark to ensure production of NADPH when photosynthetic activity ceases and no Trx is reduced, whereas several Calvin cycle enzymes are activated upon reduction in the light (Schürmann and Buchanan, 2008; Née et al., 2009). In contrast to our expectations, the activities of both G6PDH and NADP-ICDH were lower in the *tic62 trol* plants than in WT (Figure 5). This indicates that the oxidative pentose phosphate pathway as well as NADP-ICDH is not activated to compensate for the shortage of NADPH. Rather, it seems that the lower activity of G6PDH in the mutants results from the expeditious flow of electrons from Fd to Trx, which agrees with the increased activation state of AGPase (Figure 6). Moreover, as the plants direct NADPH towards carbon fixation, the allocation of reducing power in the form of malate (Scheibe et al., 1990) is likely to be decreased in the *tic62 trol* plants (Figure 6). Malate is also needed as a counter-ion for the chloroplast import of 2-oxoglutarate (Weber and Flügge, 2002), produced by cytosolic NADP-ICDH, and thus it is tempting to speculate that the activities of NADP-MDH and NADP-ICDH may be co-regulated. Additionally, the decreased NADPH/NADP⁺ ratio might have led to the decreased NADP-MDH activation state, as it is known that decreased NADPH/NADP⁺ level inhibits the ability of Trxs to redox activate the enzyme (Scheibe and Jacquot, 1983).

METHODS

Plant Material and Growth Conditions

Arabidopsis thaliana (L.) ecotype Columbia (Col-0) T-DNA insertion mutant lines (Alonso et al., 2003) *tic62* (SAIL_124G04; Benz et al., 2009) and *trol* (SAIL_27_B04; Juric et al., 2009) were cross-fertilized and the homozygote double mutants were identified from F2 generation by PCR and confirmed by immunoblotting. Insertion mutant information was obtained from the SIGnAL website at <http://signal.salk.edu>. The plants were grown under 100 μmol photons $\text{m}^{-2} \text{s}^{-1}$ in light/dark cycle of 8/16 h or 16/8 h at 23°C on soil:vermiculite mixture. Plants for metabolite analysis were grown on 1/2 MS plates without sugar under 100 μmol photons $\text{m}^{-2} \text{s}^{-1}$ (16/8 h). After 12 d, the seedlings were snap frozen in liquid nitrogen after 16 h light, 8 h dark, and 8 h light (noon), respectively. This was performed with four replicas per plant line and time point.

SDS-PAGE, BN-PAGE, and Western Blotting

Thylakoid membranes and crude soluble protein extract were isolated as described (Rintamäki et al., 1996; Lintala et al., 2007). Protein content was determined using Bio-Rad

protein Assay kit (www.bio-rad.com/) and chlorophyll content as described (Porra et al., 1989). Proteins were separated using SDS-PAGE (14% acrylamide and 6 M urea), or non-urea Next gels (Amresco-inc., www.amresco-inc.com/). Gels were blotted on PVDF membrane, blocked with 5% milk, and proteins immunodetected using standard detection systems. For separation of thylakoid protein complexes, BN-PAGE was performed as in Sirpiö et al. (2007). BN gels were further electro-blotted. Gels were loaded according to protein or chlorophyll concentration, as indicated, within a linear immuno response with respective antibody. Equal loading of the gels was verified with the staining of the membranes by Coomassie Brilliant Blue. Antibodies were purchased from Agrisera (ATP-β, Lhcb1, Lhca1, PsaB, PGRL1, PsbS, RbcL, and RbcS; www.agrisera.com) or were kind gifts from H.V. Scheller (FNR; Cyt f). The immunodetection of the small subunits of AGPase (APS1) monomerization was performed as described in Thormählen et al. (2013).

Enzyme Activity Measurements

NADP-MDH activities were determined according to Scheibe and Stitt (1988). Briefly, 20 mg frozen tissue were re-suspended in 100 μl extraction buffer. The rate of NADPH decrease was measured at 340 nm in an Anthos reader HT-3 (Anthos Mikrosysteme GmbH, www.anthos.de/). Enzyme activities of G6PDH and NADP-ICDH were measured as described in Leterrier et al. (2012). 20 mg frozen tissue was re-suspended in 100 μl extraction buffer. NADPH was monitored at 340 nm in an Anthos reader HT-3.

Pigment Analysis

Pigments (Chl *a* and *b*, neoxanthin, violaxanthin, antheraxanthin, zeaxanthin, lutein, and β-carotene) and α-tocopherol were extracted and analyzed as described in Lehtimäki et al. (2011).

Photosynthetic Parameters

Minimal fluorescence (F_0) was measured under a measuring beam after 20 min dark adaptation and maximal fluorescence (F_M) by applying 0.7 s saturating flash by using Dual-PAM-100 (Walz, www.walz.com/). Leaves were illuminated for 20 min by distinct actinic light intensities (129, 276, 534, and 828 μmol photons $\text{m}^{-2} \text{s}^{-1}$) and steady-state fluorescence (F_s) was recorded. Thereafter, maximal fluorescence of light adapted leaves (F_M') was measured after applying a second saturating flash. NPQ and ETR were recorded and calculated by the Dual-PAM-100 software.

For photoinhibition experiments, detached leaves were floated overnight on water in the dark for 16 h, and then illuminated with 1000 μmol photons $\text{m}^{-2} \text{s}^{-1}$ for indicated time at +10°C. PSII efficiency as variable to maximal fluorescence (F_v/F_M , where $F_v = F_M - F_0$) was recorded using the Plant Efficiency Analyzer (Hansatech Instruments, www.hansatech-instruments.com) after 30-min dark adaptation.

Metabolite Analysis

For determination of NAD(P) (H) contents, extraction of material was performed as described in [Hajirezaei et al. \(2002\)](#). 25 mg frozen tissue were re-suspended in 250 μ l 0.1 M HClO_4 (NAD $^+$ and NADP $^+$) or 250 μ l 0.1 M KOH (for NADH and NADPH, respectively) and incubated for 10 min on ice. Samples were centrifuged at 20 000 g for 10 min at 4°C and the supernatant was heated to 95°C for 2 min. The pH was adjusted to 8.0–8.5 by addition of an equal volume 0.2 M Tris (pH 8.4), 0.1 M KOH or 0.2 M Tris (pH 8.4), 0.1 M HClO_4 , respectively. The photometric measurement was performed according to [Gibon et al. \(2004\)](#). The detection mix for NAD(H) contained 0.3 M Tricine/KOH (pH 9), 12 mM EDTA, 1.5 M EtOH, 0.3 mM phenazine ethosulfate (PES), 1.8 mM methylthiazolylidiphenyl-tetrazolium bromide (MTT), 18 U ml $^{-1}$ alcohol dehydrogenase (ADH). For NADP(H), the mix consisted of 0.3 M Tricine/KOH (pH 9), 12 mM EDTA, 9 mM glucose 6-phosphate, 0.3 mM PES, 1.8 mM MTT, 18 U ml $^{-1}$ G6PDH. Absorption was monitored at 570 nm at 30°C in an Anthos reader HT-3 (Anthos Mikrosysteme GmbH, [www.anthos.de/](#)). Starch contents were determined as in [Thormählen et al. \(2013\)](#).

Preparation of samples for metabolic analysis was performed as described in [Fiehn \(2007\)](#). Samples were harvested by shock freezing the plate in liquid nitrogen. Leaves were then ground in liquid nitrogen and 50 mg of leaf powder was used for extraction with 1.5 ml of a pre-chilled (-20°C) mixture of $\text{H}_2\text{O}/\text{methanol}/\text{chloroform}$ (1:2.5:1). 50 μM ribitol was added as an internal standard. Following incubation under gentle agitation for 6 min at 4°C on a rotating device, samples were centrifuged for 2 min at 20 000 g at RT. 25–50 μl of the supernatant were dried and used for further analysis by gas chromatography/electron-impact time-of-flight mass spectrometry, as previously described ([Lee and Fiehn, 2008](#)). Metabolite content is expressed relative to the internal standard ribitol. All samples were analyzed with three independent biological replicates.

Surface Plasmon Resonance

Peptides for Tic62 and TROL were synthesized at Panatecs ([www.panatecs.com](#)) at 99% purity and dissolved in the appropriate buffer. PsFNR, AtLFNR1, and AtLFNR2 in pET21d (resulting in a C-terminal hexa-histidine tag) were transformed into BL21 (DE3) cells. Inoculated cultures were incubated under continuous shaking at 37°C until they reached an OD of 0.4, when they were transferred to 12°C. At an OD of \sim 0.6, expression was induced by adding 0.2 mM IPTG and cells were grown overnight. The cells were harvested by centrifugation and the pellet re-suspended in 50 mM Tris, 150 mM NaCl, 1 mM phenylmethylsulfonyl fluoride, pH 8. Rupture was achieved by two passages through a tissue lyser (Microfluidics; [www.microfluidicscorp.com](#)) and soluble proteins were obtained by centrifugation at 20 000 g for 30 min. The cell lysate was brought to 1 mM imidazole and incubated with equilibrated Ni-sepharose for 2 h at 4°C. The column was washed with 35

column volumes of binding buffer containing 1 mM imidazole and eluted with 3 column volumes of buffer with 150 mM imidazole. Buffer exchange to 10 mM HEPES pH 8 was achieved by passage over a PD10 column (GE Healthcare; [http://gelifesciences.com/](#)) and this was then subjected to anion exchange chromatography. Relevant peak fractions were pooled and the buffer exchanged to 10 mM HEPES, 150 mM NaCl, pH 7, for the final binding studies. Buffer exchange to pH 6 was performed by dialysis over night at 4°C.

Surface plasmon resonance analyses were performed on a Biacore T200 (GE Healthcare; [www.gelifesciences.com/](#)) on a CM5 chip at 25°C. The ligands were coupled from a solution of 1 mg ml $^{-1}$ in 10 mM acetate buffer pH 4.5 (Tic62) or pH 5 (TROL), respectively. The chip was activated by 1-ethyl-3-(3-dimethylaminopropyl)carbodiimide/N-hydroxysuccinimide, blocked with ethanolamine and coupled with the respective peptides. The flow rate was 10 $\mu\text{l min}^{-1}$ and contact time 160 s. Dissociation was allowed for 300 s and the chip was regenerated in 10 mM NaOH for 10 s after each step. LFNR1 and LFNR2 were applied at 0, 0.25, 0.5, 0.75, 1, 2, 3, 4, and 5 μM concentration. Data were evaluated with a program, T100 Evaluation Software, provided by GE Healthcare.

SUPPLEMENTARY DATA

Supplementary Data are available at *Molecular Plant Online*.

FUNDING

This work was supported by the Academy of Finland (grant numbers 263667, 118637, 256784 to M.L. and P.M.); the Deutsche Forschungsgemeinschaft (grant numbers Ge 878/5-1 to P.G. and Ge 878/8-1 to P.G. and I.T.; SFB 594 to J.S., B.B., and N.S.) and the Munich Center for Integrated Protein Science CiPSM (to J.S. and A.J.). Funding for the SIGnAL indexed insertion mutant collection was provided by the National Science Foundation. APMW appreciates support from the Deutsche Forschungsgemeinschaft, grants IRTG 1525-1 and EXC 1028.

ACKNOWLEDGMENTS

Dr. Peter Gollan is thanked for revising the language, and Ilaf Bilal and Juuso Hakala for excellent technical assistance. We thank the Salk Institute Genomic Analysis Laboratory for providing the sequence-indexed *Arabidopsis* T-DNA insertion mutants. No conflict of interest declared.

REFERENCES

Alonso, J.M., Stepanova, A.N., Leisse, T.J., Kim, C.J., Chen, H.M., Shinn, P., Stevenson, D.K., Zimmerman, J., Barajas, P., Cheuk, R., et al. (2003). Genome-wide insertional mutagenesis of *Arabidopsis thaliana*. *Science*. **301**, 653–657.

Alte, F., Stengel, A., Benz, J.P., Petersen, E., Soll, J., Groll, M., and Bolter, B. (2010). Ferredoxin:NADPH oxidoreductase is recruited to thylakoids by binding to a polyproline type II helix in a pH-dependent manner. *Proc. Natl Acad. Sci. U.S.A.* **107**, 19260–19265.

Andersen, B., Scheller, H.V., and Moller, B.L. (1992). The PSI-E subunit of photosystem I binds ferredoxin:NADP⁺ oxidoreductase. *FEBS Lett.* **311**, 169–173.

Anderson, J.B., Carol, A.A., Brown, V.K., and Anderson, L.E. (2003). A quantitative method for assessing co-localization in immunolabeled thin section electron micrographs. *J. Struct. Biol.* **143**, 95–106.

Anderson, L.E., Chrostowski, J., and Carol, A.A. (2006). Enzyme co-localization with transketolase, xylulose-5-P-epimerase and phosphoribosomerase in pea leaf chloroplasts. *Plant Sci.* **171**, 686–698.

Anderson, L.E., Gatla, N., and Carol, A.A. (2005). Enzyme co-localization in pea leaf chloroplasts: Glyceraldehyde-3-P dehydrogenase, triose-P isomerase, aldolase and sedoheptulose bisphosphatase. *Photosynth Res.* **83**, 317–328.

Balsera, M., Stengel, A., Soll, J., and Bolter, B. (2007). Tic62: a protein family from metabolism to protein translocation. *BMC Evol. Biol.* **7**, 43.

Benz, J.P., Lintala, M., Soll, J., Mulo, P., and Bolter, B. (2010). A new concept for ferredoxin–NADP(H) oxidoreductase binding to plant thylakoids. *Trends Plant Sci.* **15**, 608–613.

Benz, J.P., Stengel, A., Lintala, M., Lee, Y.H., Weber, A., Philipp, K., Gugel, I.L., Kaieda, S., Ikegami, T., Mulo, P., et al. (2009). *Arabidopsis* Tic62 and ferredoxin–NADP(H) oxidoreductase form light-regulated complexes that are integrated into the chloroplast redox poise. *Plant Cell.* **21**, 3965–3983.

Chan, R.L., Ceccarelli, E.A., and Vallejos, R.H. (1987). Immunological studies of the binding protein for chloroplast ferredoxin–NADP⁺ reductase. *Arch. Biochem. Biophys.* **253**, 56–61.

Clark, R.D., Hawkesford, M.J., Coughlan, S.J., Bennett, J., and Hind, G. (1984). Association of ferredoxin–NADP⁺ oxidoreductase with the chloroplast cytochrome *b-f* complex. *FEBS Lett.* **174**, 137–142.

DalCorso, G., Pesaresi, P., Masiero, S., Aseeva, E., Schunemann, D., Finazzi, G., Joliot, P., Barbato, R., and Leister, D. (2008). A complex containing PGRL1 and PGR5 is involved in the switch between linear and cyclic electron flow in *Arabidopsis*. *Cell.* **132**, 273–285.

Fiehn, O. (2007). Validated high quality automated metabolome analysis of *Arabidopsis thaliana* leaf disks: quality control charts and standard operating procedures. In *Concepts in Plant Metabolomics*, Nikolau, B.J., and Wurtele, E.S., eds (Dordrecht, The Netherlands: Springer), pp. 1–18.

Geigenberger, P. (2011). Regulation of starch biosynthesis in response to a fluctuating environment. *Plant Physiol.* **155**, 1566–1577.

Geigenberger, P., Tiessen, A., and Meurer, J. (2011). Use of non-aqueous fractionation and metabolomics to study chloroplast function in *Arabidopsis*. *Methods Mol. Biol.* **775**, 135–160.

Gibon, Y., Blaesing, O.E., Hannemann, J., Carillo, P., Hohne, M., Hendriks, J.H., Palacios, N., Cross, J., Selbig, J., and Stitt, M. (2004). A robot-based platform to measure multiple enzyme activities in *Arabidopsis* using a set of cycling assays: comparison of changes of enzyme activities and transcript levels during diurnal cycles and in prolonged darkness. *Plant Cell.* **16**, 3304–3325.

Guedeney, G., Corneille, S., Cuine, S., and Peltier, G. (1996). Evidence for an association of *ndh* B, *ndh* J gene products and ferredoxin-NADP-reductase as components of a chloroplastic NAD(P)H dehydrogenase complex. *FEBS Lett.* **378**, 277–280.

Hajirezaei, M.R., Peisker, M., Tschiersch, H., Palatnik, J.F., Valle, E.M., Carrillo, N., and Sonnewald, U. (2002). Small changes in the activity of chloroplastic NADP(+)–dependent ferredoxin oxidoreductase lead to impaired plant growth and restrict photosynthetic activity of transgenic tobacco plants. *Plant J.* **29**, 281–293.

Hanke, G., and Mulo, P. (2013). Plant type ferredoxins and ferredoxin-dependent metabolism. *Plant Cell Environ.* **36**, 1071–1084.

Hanke, G.T., Okutani, S., Satomi, Y., Takao, T., Suzuki, A., and Hase, T. (2005). Multiple iso-proteins of FNR in *Arabidopsis*: evidence for different contributions to chloroplast function and nitrogen assimilation. *Plant Cell and Environ.* **28**, 1146–1157.

Hebbelmann, I., Selinski, J., Wehmeyer, C., Goss, T., Voss, I., Mulo, P., Kangasjärvi, S., Aro, E.M., Oelze, M.L., Dietz, K.J., et al. (2012). Multiple strategies to prevent oxidative stress in *Arabidopsis* plants lacking the malate valve enzyme NADP–malate dehydrogenase. *J. Exp. Bot.* **63**, 1445–1459.

Heineke, D., Riens, B., Grosse, H., Hoferichter, P., Peter, U., Flugge, U.I., and Heldt, H.W. (1991). Redox transfer across the inner chloroplast envelope membrane. *Plant Physiol.* **95**, 1131–1137.

Hendriks, J.H., Kolbe, A., Gibon, Y., Stitt, M., and Geigenberger, P. (2003). ADP-glucose pyrophosphorylase is activated by post-translational redox-modification in response to light and to sugars in leaves of *Arabidopsis* and other plant species. *Plant Physiol.* **133**, 838–849.

Hodges, M., Flesch, V., Galvez, S., and Bismuth, E. (2003). Higher plant NADP⁺-dependent isocitrate dehydrogenases, ammonium assimilation and NADPH production. *Plant Physiol. Biochem.* **41**, 577–585.

Juric, S., Hazler-Pilepic, K., Tomasic, A., Lepedus, H., Jelicic, B., Puthiyaveetil, S., Bionda, T., Vojta, L., Allen, J.F., Schleiff, E., et al. (2009). Tethering of ferredoxin:NADP⁺ oxidoreductase to thylakoid membranes is mediated by novel chloroplast protein TROL. *Plant J.* **60**, 783–794.

Kangasjärvi, S., Lepistö, A., Hannikainen, K., Piippo, M., Luomala, E.M., Aro, E.M., and Rintamäki, E. (2008). Diverse roles for chloroplast stromal and thylakoid-bound ascorbate peroxidases in plant stress responses. *Biochem. J.* **412**, 275–285.

Kolbe, A., Tiessen, A., Schluepmann, H., Paul, M., Ulrich, S., and Geigenberger, P. (2005). Trehalose 6-phosphate regulates starch synthesis via posttranslational redox activation of ADP-glucose pyrophosphorylase. *Proc. Natl Acad. Sci. U.S.A.* **102**, 11118–11123.

Kruger, N.J., and von Schaewen, A. (2003). The oxidative pentose phosphate pathway: structure and organisation. *Curr. Opin. Plant Biol.* **6**, 236–246.

Kuchler, M., Decker, S., Hormann, F., Soll, J., and Heins, L. (2002). Protein import into chloroplasts involves redox-regulated proteins. *EMBO J.* **21**, 6136–6145.

Lee, D., and Fiehn, O. (2008). High quality metabolomic data for *Chlamydomonas reinhardtii*. *Plant Methods*. **4**, 7.

Lehtimäki, N., Shunmugam, S., Jokela, J., Wahlsten, M., Carmel, D., Keränen, M., Sivonen, K., Aro, E.M., Allahverdiyeva, Y., and Mulo, P. (2011). Nodularin uptake and induction of oxidative stress in spinach (*Spinacia oleracea*). *J. Plant Physiol.* **168**, 594–600.

Leterrier, M., Barroso, J.B., Valderrama, R., Palma, J.M., and Corpas, F.J. (2012). NADP-dependent isocitrate dehydrogenase from *Arabidopsis* roots contributes in the mechanism of defence against the nitro-oxidative stress induced by salinity. *Sci. World J.* Article ID 694740, 10.1100/2012/694740.

Lintala, M., Allahverdiyeva, Y., Kangasjärvi, S., Lehtimäki, N., Keränen, M., Rintamäki, E., Aro, E.M., and Mulo, P. (2009). Comparative analysis of leaf-type ferredoxin–NADP⁺ oxidoreductase isoforms in *Arabidopsis thaliana*. *Plant J.* **57**, 1103–1115.

Lintala, M., Allahverdiyeva, Y., Kidron, H., Piippo, M., Battchikova, N., Suorsa, M., Rintamäki, E., Salminen, T.A., Aro, E.M., and Mulo, P. (2007). Structural and functional characterization of ferredoxin–NADP⁺-oxidoreductase using knock-out mutants of *Arabidopsis*. *Plant J.* **49**, 1041–1052.

Michalska, J., Zauber, H., Buchanan, B.B., Cejudo, F.J., and Geigenberger, P. (2009). NTRC links built-in thioredoxin to light and sucrose in regulating starch synthesis in chloroplasts and amyloplasts. *Proc. Natl Acad. Sci. U S A.* **106**, 9908–9913.

Morigasaki, S., Jin, T., and Wada, K. (1993). Comparative studies on ferredoxin–NADP⁺ oxidoreductase isoenzymes derived from different organs by antibodies specific for the radish root-enzyme and leaf-enzyme. *Plant Physiol.* **103**, 435–440.

Née, G., Zaffagnini, M., Trost, P., and Issakidis-Bourguet, E. (2009). Redox regulation of chloroplastic glucose-6-phosphate dehydrogenase: a new role for f-type thioredoxin. *FEBS Lett.* **583**, 2827–2893.

Negi, S.S., Carol, A.A., Pandya, S., Braun, W., and Anderson, L.E. (2008). Co-localization of glyceraldehyde-3-phosphate dehydrogenase with ferredoxin–NADP reductase in pea leaf chloroplasts. *J. Struct. Biol.* **161**, 18–30.

Pérez-Ruiz, J.M., Spinola, M.C., Kirchsteiger, K., Moreno, J., Sahrawy, M., and Cejudo, F.J. (2006). Rice NTRC is a high-efficiency redox system for chloroplast protection against oxidative damage. *Plant Cell*. **18**, 2356–2368.

Porra, R.J., Thompson, W.A., and Kriedemann, P.E. (1989). Determination of accurate extinction coefficients and simultaneous-equations for assaying chlorophyll-A and chlorophyll-B extracted with 4 different solvents: verification of the concentration of chlorophyll standards by atomic-absorption spectroscopy. *Biochim. Biophys. Acta*. **975**, 384–394.

Quiles, M.J., and Cuello, J. (1998). Association of ferredoxin–NADP oxidoreductase with the chloroplastic pyridine nucleotide dehydrogenase complex in barley leaves. *Plant Physiol.* **117**, 235–244.

Rintamäki, E., Kettunen, R., and Aro, E.M. (1996). Differential D1 dephosphorylation in functional and photodamaged photosystem II centers: dephosphorylation is a prerequisite for degradation of damaged D1. *J. Biol. Chem.* **271**, 14870–14875.

Scheibe, R., and Jacquot, J.P. (1983). NADP regulates the light activation of NADP-dependent malate-dehydrogenase. *Planta*. **157**, 548–553.

Scheibe, R., and Stitt, M. (1988). Comparison of NADP-malate dehydrogenase activation, Q_A reduction and O₂ evolution in spinach leaves. *Plant Physiol. Biochem.* **26**, 473–481.

Scheibe, R., Rudolph, R., Reng, W., and Jaenicke, R. (1990). Structural and catalytic properties of oxidized and reduced chloroplast NADP-malate dehydrogenase upon denaturation and renaturation. *Eur. J. Biochem.* **189**, 581–587.

Schürmann, P., and Buchanan, B.B. (2008). The ferredoxin/thioredoxin system of oxygenic photosynthesis. *Antioxid. Redox Sign.* **10**, 1235–1274.

Shin, M., Ishida, H., and Nozaki, Y. (1985). A new protein factor, connectein, as a constituent of the large form of ferredoxin–NADP reductase. *Plant Cell Physiol.* **26**, 559–563.

Shin, M., Tsujita, M., Tomizawa, H., Sakihama, N., Kamei, K., and Oshino, R. (1990). Proteolytic degradation of ferredoxin–NADP reductase during purification from spinach. *Arch. Biochem. Biophys.* **279**, 97–103.

Sirpiö, S., Allahverdiyeva, Y., Suorsa, M., Paakkarinen, V., Vainonen, J., Battchikova, N., and Aro, E.M. (2007). TLP18.3, a novel thylakoid lumen protein regulating photosystem II repair cycle. *Biochem. J.* **406**, 415–425.

Soncini, F.C., and Vallejos, R.H. (1989). The chloroplast reductase-binding protein is identical to the 16.5-kDa polypeptide described as a component of the oxygen-evolving complex. *J. Biol. Chem.* **264**, 21112–21115.

Stengel, A., Benz, P., Balsara, M., Soll, J., and Böltner, B. (2008). TIC62 redox-regulated translocon composition and dynamics. *J. Biol. Chem.* **283**, 6656–6667.

Stitt, M., and Zeeman, S.C. (2012). Starch turnover: pathways, regulation and role in growth. *Curr. Opin. Plant Biol.* **15**, 282–292.

Thormählen, I., Ruber, J., von Roepenack-Lahaye, E., Ehrlich, S.M., Massot, V., Hummer, C., Tezycka, J., Issakidis-Bourguet, E., and Geigenberger, P. (2013). Inactivation of thioredoxin f1 leads to decreased light activation of ADP-glucose pyrophosphorylase and altered diurnal starch turnover in leaves of *Arabidopsis* plants. *Plant. Cell Environ.* **36**, 16–29.

Tiessen, A., Hendriks, J.H., Stitt, M., Branscheid, A., Gibon, Y., Farre, E.M., and Geigenberger, P. (2002). Starch synthesis in potato tubers is regulated by post-translational redox modification of ADP-glucose pyrophosphorylase: a novel regulatory mechanism linking starch synthesis to the sucrose supply. *Plant Cell*. **14**, 2191–2213.

Vallejos, R.H., Ceccarelli, E., and Chan, R. (1984). Evidence for the existence of a thylakoid intrinsic protein that binds ferredoxin–NADP⁺ oxidoreductase. *J. Biol. Chem.* **259**, 8048–8051.

Weber, A., and Flügge, U. (2002). Interaction of cytosolic and plastidic nitrogen metabolism in plants. *J. Exp. Bot.* **53**, 865–874.

Zhang, H., Whitelegge, J.P., and Cramer, W.A. (2001). Ferredoxin:NADP⁺ oxidoreductase is a subunit of the chloroplast cytochrome b6f complex. *J. Biol. Chem.* **276**, 38159–38165.

Supplementary information

Supplementary figures

Figure S1. The phenotype of *Arabidopsis* WT, *tic62*, *trol* and *tic62 trol* plants. The plants were grown for five weeks under standard short day conditions ($100 \mu\text{mol photons m}^{-2} \text{ s}^{-1}$).

Figure S2. Metabolic analyses of the *tic62 trol* and WT plants. The plants were grown under $100 \mu\text{mol photons m}^{-2} \text{ s}^{-1}$ (16/8h) on MS plates without sugar. After 12 days the seedlings were snap frozen in liquid nitrogen after 16 h light, 8 h dark and 8 h light (noon), respectively. Blue bars denote for WT and red bars for *tic62 trol*. Concentrations of metabolites are given in arbitrary units mg^{-1} fresh weight. Values are presented as mean \pm SE, n=4. Statistically significant difference from WT (*P < 0.05; **P < 0.01).

Supplementary methods

For amino acid analysis, approximately 100 mg of frozen tissue were ground in liquid nitrogen with a mortar and pestle. The fine powder was transferred to a microtube, weighed, and mixed with 1.2 ml of 50 % ethanol. After heating at 70°C for 5 min, the extract was cooled and clarified by centrifugation at 18 800 g for 5 min at 4°C. The supernatant was dried under vacuum and re-dissolved in water. Then, the suspension was reacted with AccQFluor reagent (Waters, <http://www.waters.com/>). The derivatives were separated using an AccQTag amino acid analysis column (Waters) on a Waters HPLC system. (Kinoshita et al., 2011).

For monitoring nitrate, rosette leaves were ground in 0.1 % (W/V) SDS, and the resultant extracts were centrifuged at 18 800 g for 20 min at 4°C. After repeating the centrifugation step, the supernatants were subjected to nitrate determination using a flow injection analyzer (NOX-1000W; Tokyo Chemical Industry, <http://www.tciamerica.com/>). Ammonium and glyoxylate were quantified spectrophotometrically as described previously (Bräutigam et al., 2007).

For organic acid analysis, soluble metabolite fractions were extracted with methanol (Sato et al., 2004). The samples were ultrafiltered through a 10 kDa cut-off filter (Ultrafree-MC; Millipore, <http://www.millipore.com/>), and the filtrate was analyzed by CE/MS (G1310A/G1600A/G6130A; Agilent Technologies, <http://www.agilent.com/>) using with a FunCap-CE/Type S capillary (GL Sciences, <http://www.glsciences.com/>).

Supplementary references

Bräutigam, A., Gagneul, D. and Weber, A. P. M. (2007). High-throughput colorimetric method for the parallel assay of glyoxylic acid and ammonium in a single extract. *Anal. Biochem.* **362**, 151-153.

Kinoshita, H., Nagasaki, J., Yoshikawa, N., Yamamoto, A., Takito, S., Kawasaki, M., Sugiyama, T., Miyake, H., Weber, A. P. M. and Taniguchi, M. (2011). The chloroplastic 2-oxoglutarate/malate transporter has dual function as the malate valve and in carbon/nitrogen metabolism. *Plant J.* **65**, 15-26.

Sato, S., Soga, T., Nishioka, T. and Tomita, M. (2004). Simultaneous determination of the main metabolites in rice leaves using capillary electrophoresis mass spectrometry and capillary electrophoresis diode array detection. *Plant J.* **40**, 151-163.

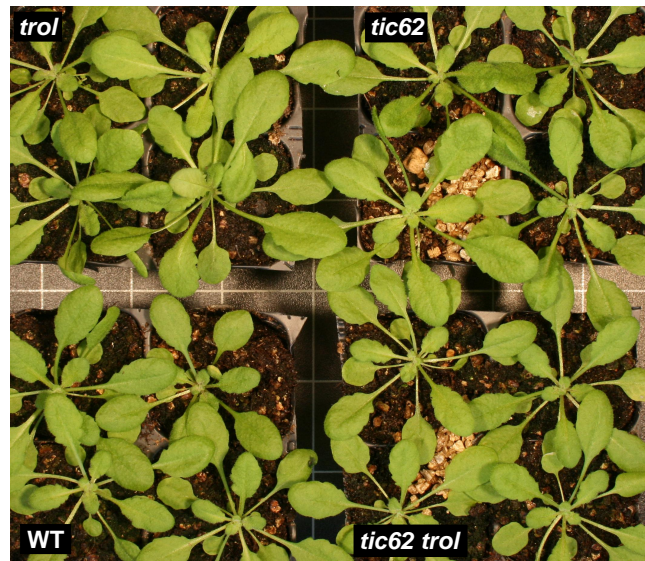
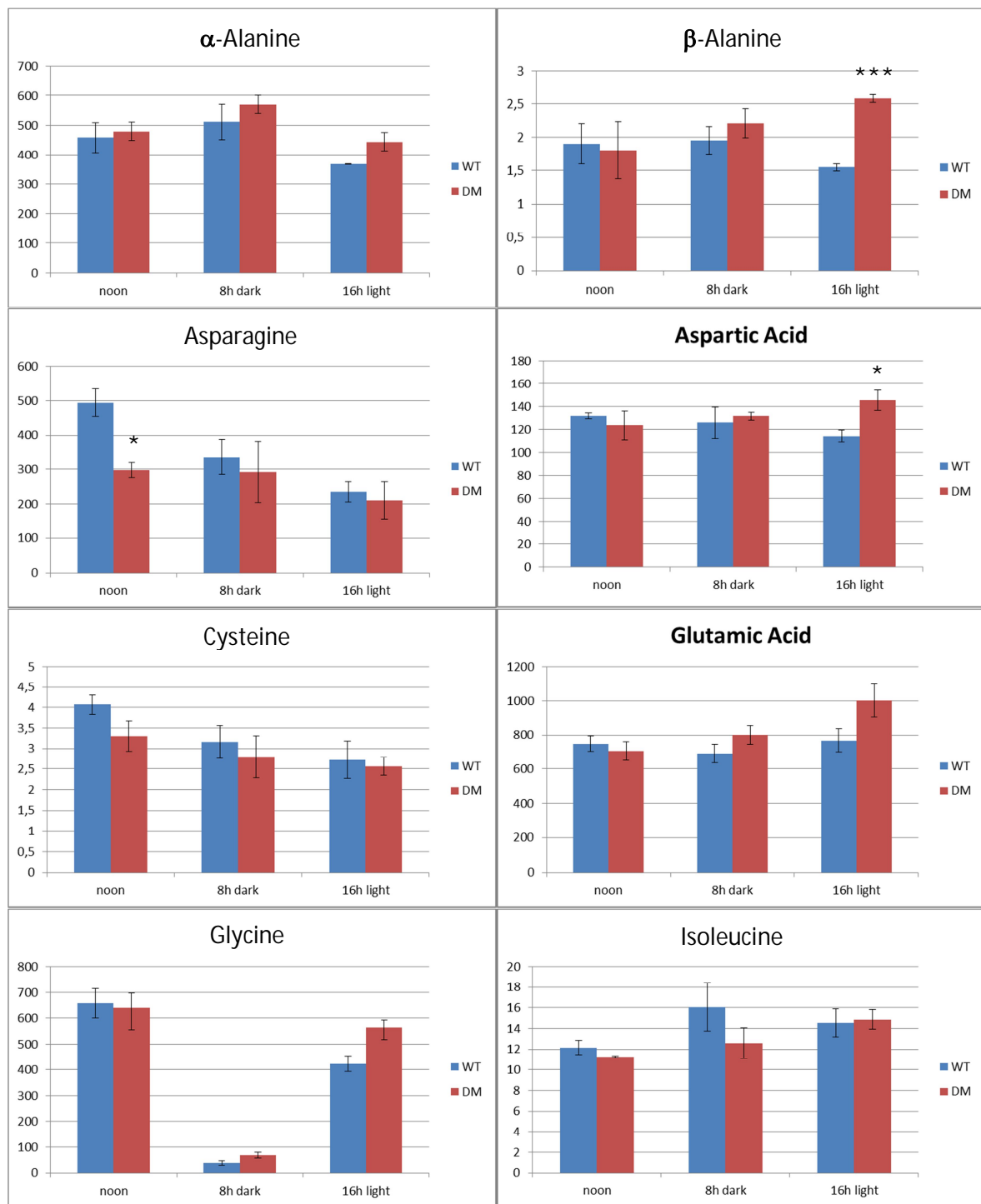
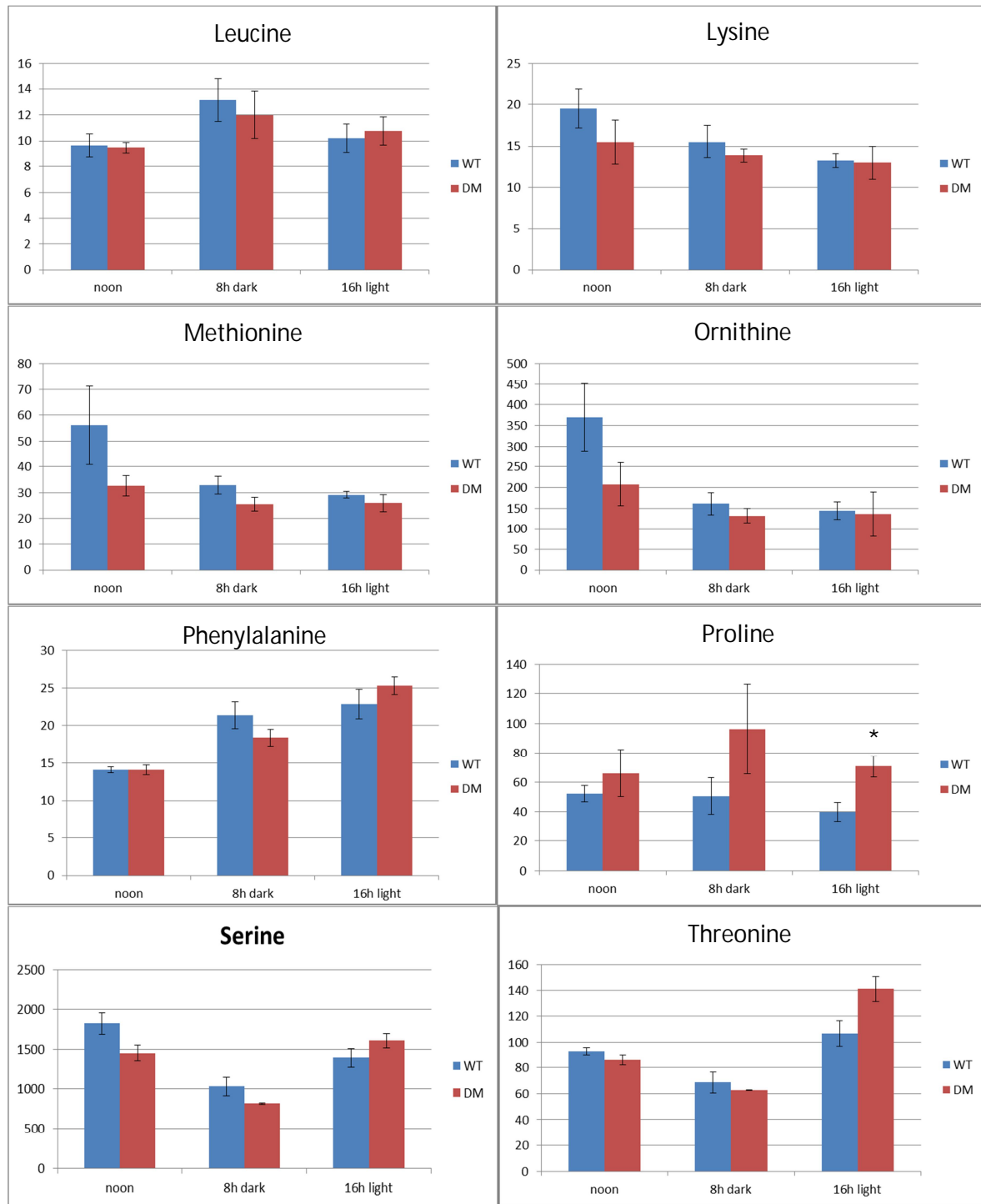


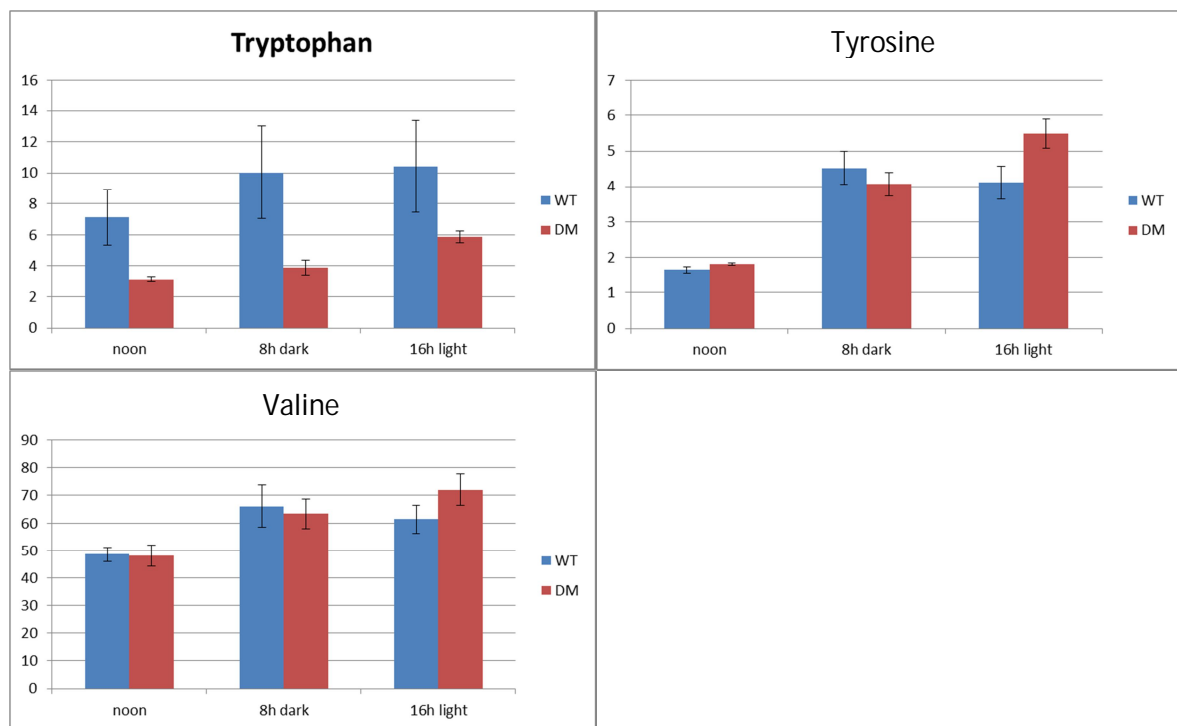
Figure S1. The phenotype of *Arabidopsis* WT, *tic62*, *trol* and *tic62 trol* plants. The plants were grown for five weeks under standard short day conditions ($100 \mu\text{mol photons m}^{-2} \text{ s}^{-1}$).

Figure S2

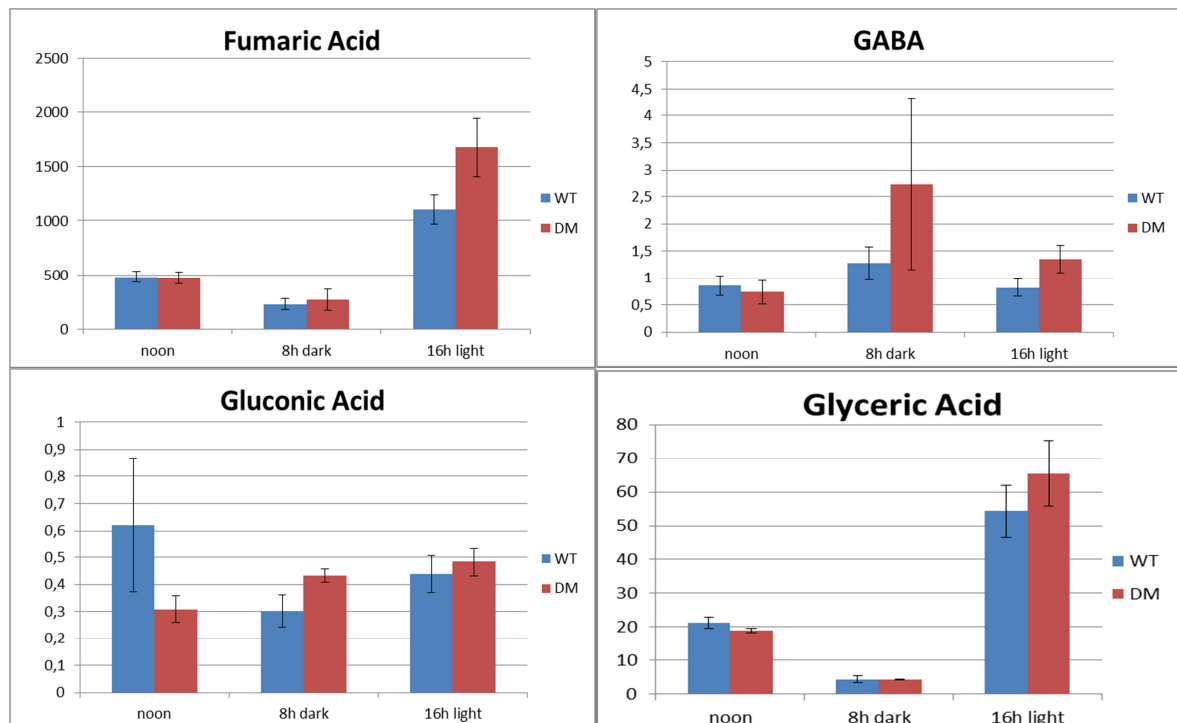
Amino acids

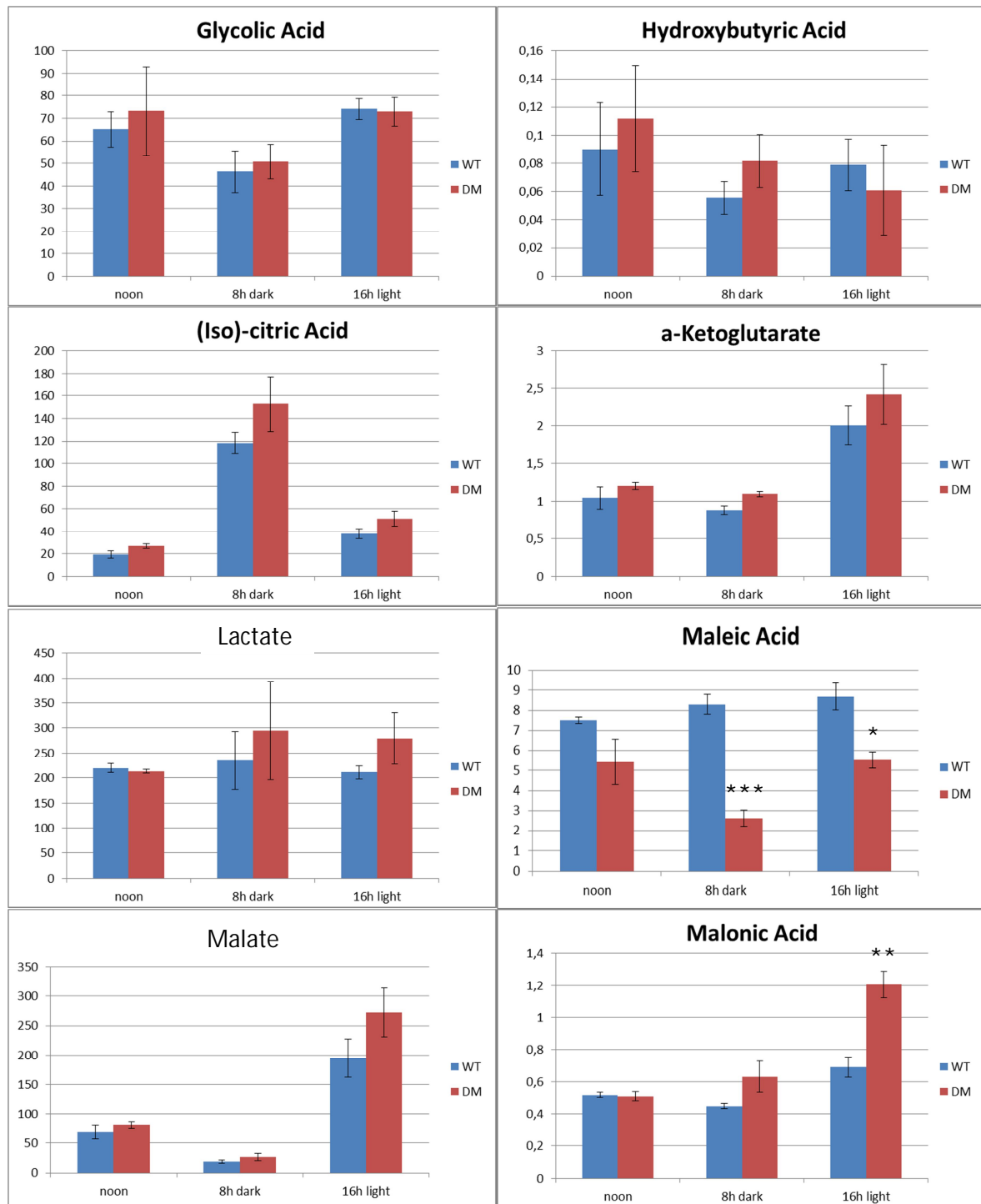


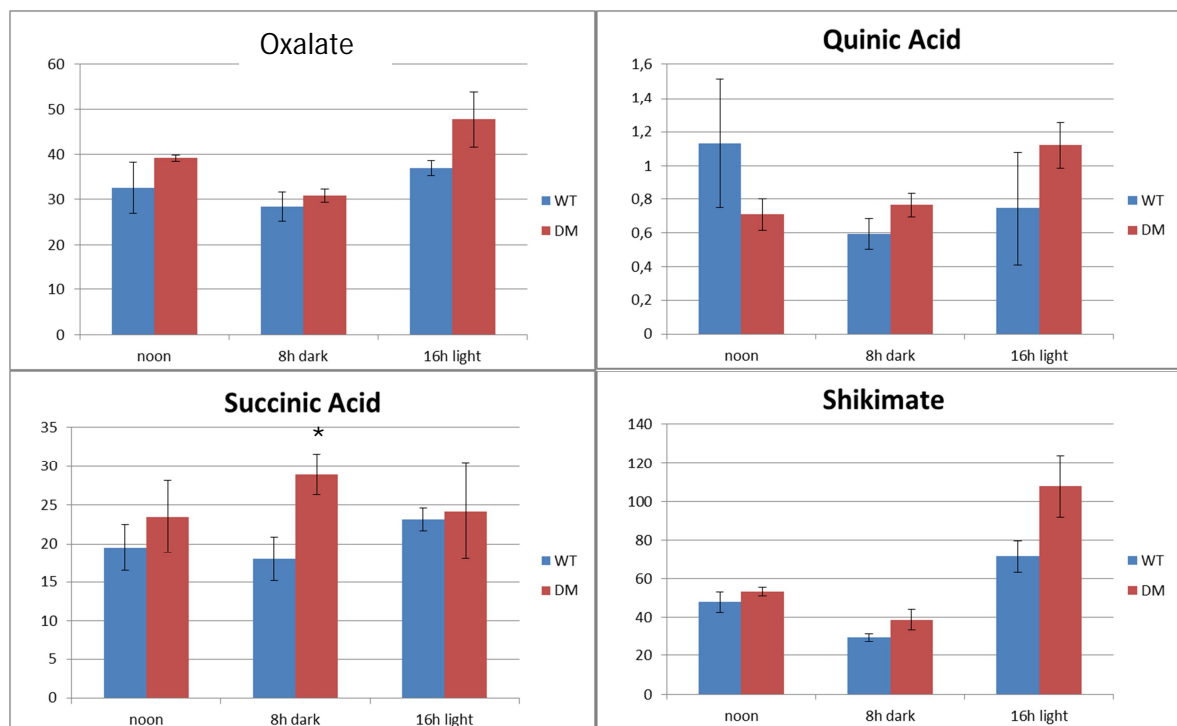




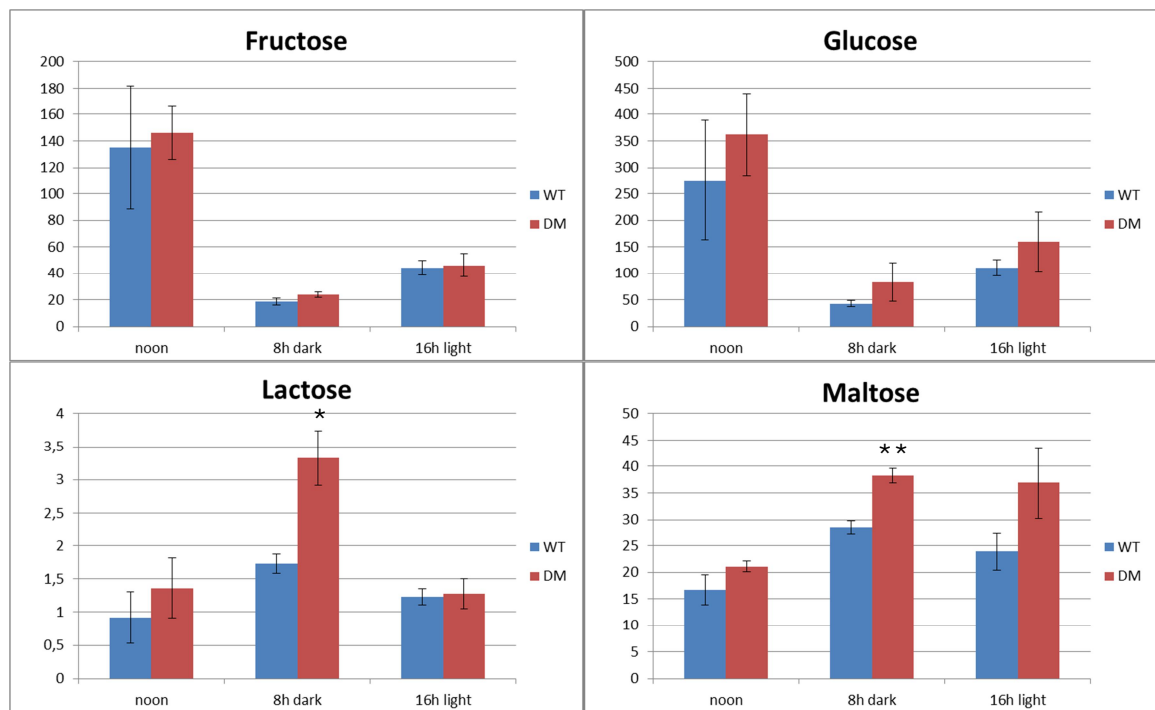
Organic acids

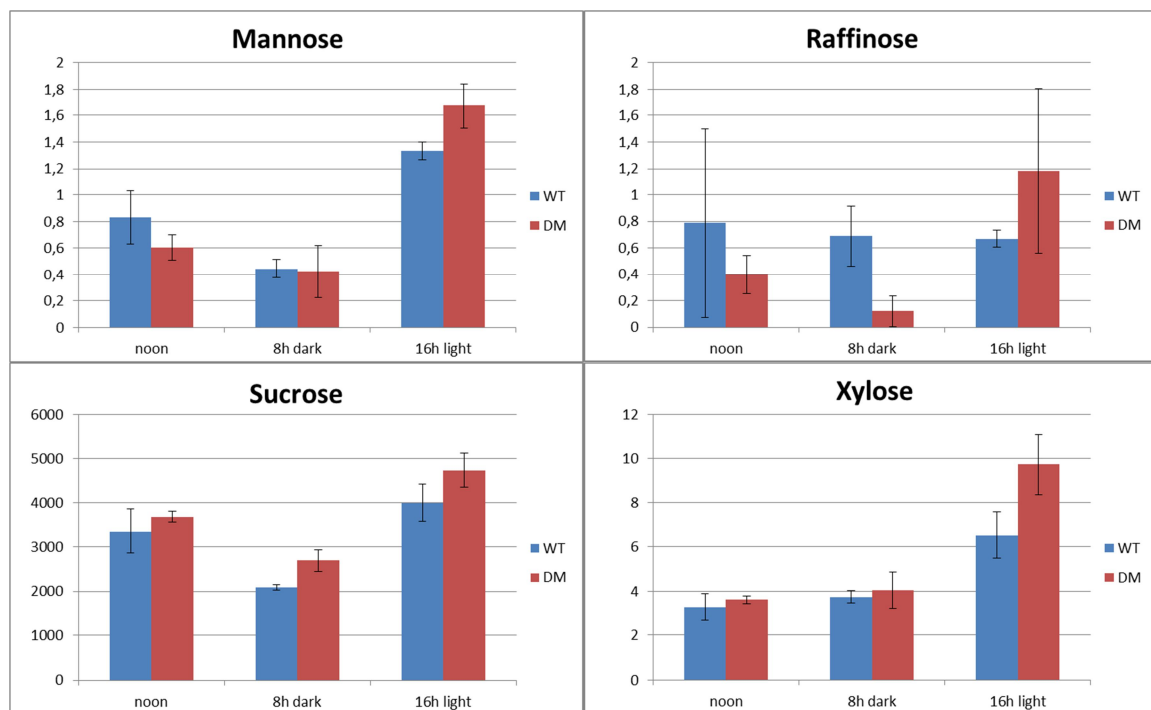




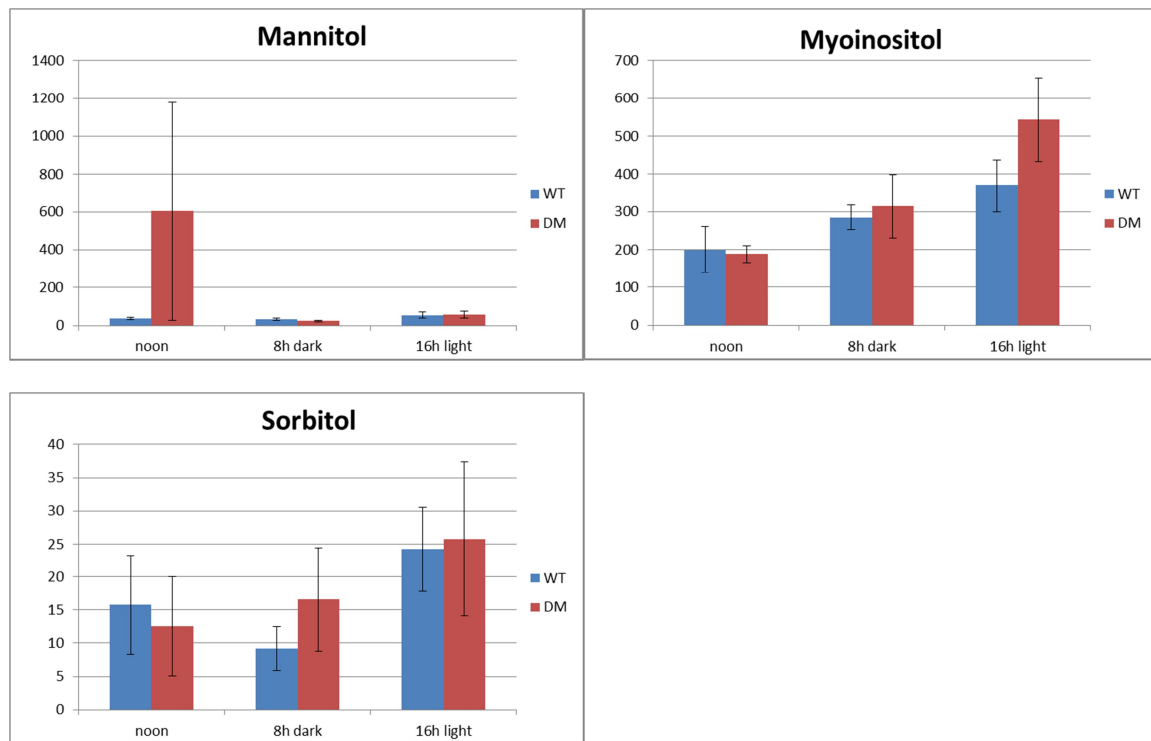


Sugars





Sugar alcohols



Misc.

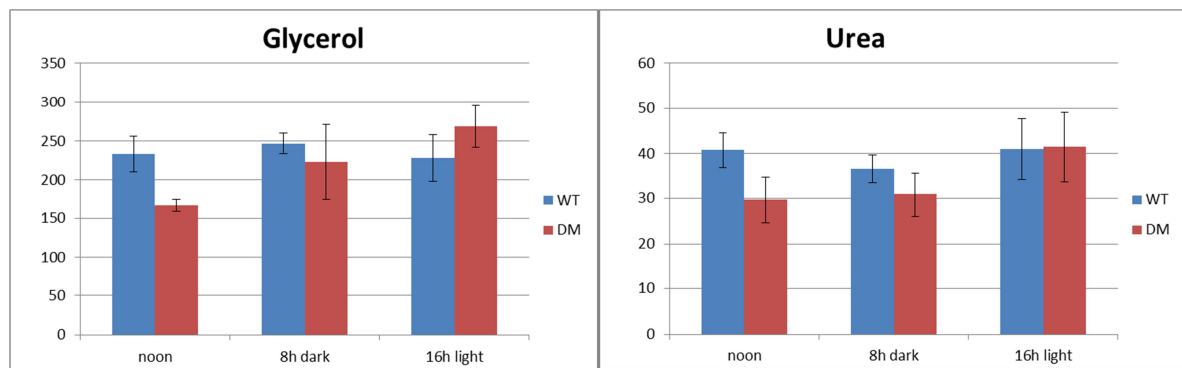


Figure S2. Metabolic analyses of the *tic62 trol* and WT plants. The plants were grown under 100 μmol photons $\text{m}^{-2} \text{s}^{-1}$ (16/8h) on MS plates without sugar. After 12 days the seedlings were snap frozen in liquid nitrogen after 16 h light, 8 h dark and 8 h light (noon), respectively. Blue bars denote for WT and red bars for *tic62 trol*. Concentrations of metabolites are given in arbitrary units mg^{-1} fresh weight. Values are presented as mean \pm SE, n=4. Statistically significant difference from WT (*P < 0.05; **P < 0.01).

Discussion

Trx *f1* and NTRC participate cooperatively in regulating carbon assimilation

The present study revealed a disturbed electron flux of the photosynthetic light reaction due to the lack of the redox regulatory components Trx *f1* and NTRC in *Arabidopsis* leaves, whereas the changes were even absent or only slightly in the single knockout plants *trx f1* or *ntrc*, respectively (Chapter 1, Chapter 2). This is in line with a previous study concerning NTRC-deficient plants (Lepistö et al. 2009). A direct disturbance on the functionality of the PSs due to disturbed redox processes could have led to the less efficient electron transport. More reasonable is a secondary effect by the elevated NADPH/NADP⁺ and ATP/ADP ratios observed in the *ntrc* and even stronger in the *trxf1 ntrc* mutants (Chapter 2), since the photosynthetic light reaction needs sufficient acceptors for its optimal performance (Baker 2008, Foyer et al. 2012). No shortage in levels of the primary light reaction products NADPH and ATP provides reducing power and energy to the plant, and suggests a restriction of downstream processes in the photosynthetic electron flux. The CBC is a significant anabolic process, consuming the major part of photosynthetically produced NADPH and ATP for carbon fixation (Scheibe and Dietz 2011). Indeed, gas exchange measurements revealed an inhibited CO₂ assimilation rate, more severe in leaves, lacking both redox regulators Trx *f1* and NTRC, while intercellular CO₂ concentrations and transpiration rates were increased (Chapter 2). These facts suggest a disturbed CO₂ fixation activity by the CBC without limitations in carbon availability.

A similar pattern of decreased CO₂ assimilation and increased transpiration rates dependent on different light intensities was observed in plants with a deficiency of the redox-sensitive plastidial FBPase isoform cFPB1 (Chapter 3). Interestingly, the growth phenotypes occur very similar as well, showing pale green leaves and a strongly retarded growth, while the plants were still viable and produced seeds. The strong growth impairment of the *cfpb1* mutants leads to the suggestion that cFPB1 is the predominant FBPase isoform in chloroplasts of *Arabidopsis*, and the second isoform cFPB2 plays a minor role (Serrato et al. 2009). The FBPase is part of the regeneration phase in the CBC and known as exclusively redox-activated by Trx *f* (Michelet et al. 2013). Despite the latter fact, the single knockout plants of Trx *f1* show no retardation in growth under normal conditions and no change in photosynthetic electron transfer or carbon assimilation rates (Chapter 1, Chapter 2). Alternative metabolic processes in the plant could

DISCUSSION

have been able to cope the loss of *Trx f* in redox-activating CBC enzymes, but this is in contradiction to the strongly impaired growth phenotype of *cfbp1* mutants, revealing the importance of the plastidial FBPase activity (Chapter 3). More reasonable would be a redundant function of *Trx f1*. Western blot analyses confirmed that the second isoform *Trx f2* represents only about 3 % of the overall *Trx f* content in leaves of *Arabidopsis* (Chapter 1), which might not be sufficient to replace *Trx f1*, since the FBPase activity was 40-50% decreased in the single mutant *trx f1* (Chapter 2).

Intriguingly, the direct measurement of plastidial FBPase revealed decreased activities and redox activation states not only in leaves of the *trx f1* mutant, but also in the *ntrc* single mutant (Chapter 2). An almost completely abolished activation was observed in the combined knockout plants of *Trx f1* and NTRC, so that NTRC might have compensated the loss of *Trx f1* in the single mutant by the activation of the FBPase. In confirmation with the decreased FBPase activities during the day, elevated levels of F1,6BP as substrate of the FBPase and decreased ratios of F6P/F1,6BP in leaves of the single and double mutants of the two redox regulatory components were detected (Chapter 2). Strongly elevated F1,6BP leaf levels, as well as the impairments in photosynthetic activity and retardations in growth were revealed in plants with deficiencies in plastidial FBPase by several studies (Chapter 3, Koßmann et al. 1994, Livingston et al. 2010). These facts provide strong evidences that *Trx f* is not the exclusive redox regulator of FBPase, and leads to the suggestion that NTRC has unexpected functions in regulating photosynthetic carbon assimilation in cooperation with *Trx f1* in *Arabidopsis* leaves.

Trx f1 and NTRC participate cooperatively in regulating starch metabolism

Previous studies with *Arabidopsis* plants deficient in NTRC protein revealed negative effects on the transient starch accumulation, accompanied by a decreased thiol-based activation of AGPase as key enzyme of starch synthesis (Michalska et al. 2009, Lepistö et al. 2013). Additionally, it was shown that recombinant proteins of *Trx f* and *m* were able to redox-activate the AGPase *in vitro* (Ballicora et al. 2000, Geigenberger et al. 2005), however, the knowledge about the *in vivo* relevance of Trxs in regulating starch synthesis was still lacking. In this study the biochemical property of *Trx f1* as most efficient redox activator for AGPase compared to other Trxs was confirmed, and showed similar efficiencies compared to NTRC (Chapter 1). While NTRC influences the AGPase activation during the day, but also in darkness with elevated sugar levels (Chapter 2, Michalska et al. 2009), the redox activation by *Trx f1* is strictly

DISCUSSION

light-dependent (Chapter 1). A decreased reduction of the redox-sensitive and catalytic AGPase subunit APS1 was observed in leaves and illuminated chloroplasts of the *trx f1* single mutant, whereas sugar-infiltrated leaves did not change the redox state of AGPase (Chapter 1, Chapter 2). In leaves with a deficiency in both Trx *f1* and NTRC the starch content and AGPase redox activation decreased even stronger, in the end of the day with similar levels as in wild-type leaves in the end of the night (Chapter 2). This suggests an additive effect on starch synthesis by Trx *f1* and NTRC, being most probably the main redox regulators for this pathway.

The strong growth retardation of plants lacking Trx *f1* and NTRC might be a consequence of both an affected starch metabolism and a less efficient CO₂ fixation during the day (see discussion above), since the double knockout mutants only partly recovered their growth phenotype under constant light conditions (Chapter 2). Plants growing with constant light are independent of a functional starch synthesis, because the essential carbon availability in form of soluble sugars provided by photosynthesis is not interrupted through the night (Caspar et al. 1985, Gibon *et al.* 2004, Geigenberger 2011). The affected starch synthesis and carbon fixation in the *trxf1 ntrc* mutants during the day was accompanied by a strong sugar starvation, especially in the end of the night (Chapter 2). In contrast to this, several levels of amino acids were strongly increased, which was similarly observed in a previous study about the *ntrc* single mutant (Lepistö *et al.* 2009). The elevated amino acids are most likely due to a facilitated protein degradation as a strategy of the plant to provide alternative carbon sources (Osuna *et al.* 2007, Usadel *et al.* 2008), or to an adaptive response for equilibrating the osmotic situation in the tissue, since the soluble sugars decreased (Fernie *et al.* 2002, Faix *et al.* 2012). Interestingly, an increase of remobilization products of starch, such as maltose, was measured during the day, which was more pronounced in the double mutant *trxf1 ntrc* (Chapter 2). This indicates a possible involvement of the redox regulatory proteins Trx *f1* and NTRC in the degradation of starch and supports previous *in vitro* studies, revealing a thiol-based regulation of starch degrading enzymes (Valerio *et al.* 2011, Glaring *et al.* 2012). The *in vivo* relevance of the redox regulatory influence on starch degradation processes has to be solved in future.

Surprisingly, *Arabidopsis* leaves lacking the primary anchor proteins of the FNR protein, named Tic62 and TROL, showed an increased redox activation of the AGPase exclusively in the end of the night, accompanied by partly significant elevated starch levels (Chapter 4). During the darkness elevated sugar levels are able to induce the APS1 monomerisation through the NTRC system (Michalska *et al.* 2009), but not through the transfer of electrons by Trx *f* (Chapter 1). The sugars in the *tic62 trol* mutant tended to be higher (Chapter 4), so that the NTRC could

DISCUSSION

have redox-activated the AGPase during the night. Another possible explanation suggests a redirection of electrons from NADPH to the FNR for the reduction of Fdx (Vojta et al. 2012), which then provides the redox power to the *Trx f* system, and subsequently redox-activates the AGPase. This could also explain the lower G6PDH activity (Chapter 4), since the main plastidial isoform is known to be redox-deactivated through *Trx f*-dependent reduction of disulfides (Wakao and Benning 2005, Nee et al. 2009), and the increased starch degradation products (see discussion above). Under acidic conditions, which are indicated during the night in the chloroplast stroma, the FNR increases its interaction with Tic62 and TROL in wild-type leaves (Chapter 4, Benz et al. 2009, Alte et al. 2010). Possibly, the completely soluble FNR in the *tic62 trol* mutant leaves during the night changes its activity to the direction of NADP⁺ production, attributable to the lack of electron pressure from light-reduced Fdx, and causes an unusual reduction of Trxs during the night. In plastids of the root system the reverse way of FNR activity is known for a NADPH-dependent reduction of Trxs (Meyer et al. 2012), so that in chloroplast the reversibility of FNR activity might be possible dependent on the binding to TIC62 and TROL.

Trx f1 and NTRC are critical for the NADP redox poise in *Arabidopsis* leaves

Similar results of previous studies confirm observations of the present study on diurnal NADP metabolism in wild-type leaves (Chapter 2, Chapter 4, Liu et al. 2008, Beeler et al. 2014). During the day an increased pool of NADPH and NADP⁺ was accompanied by a decrease in the NADPH/NADP⁺ ratio compared to the night. This is most likely attributable to a daytime provision of sufficient electron acceptors for the FNR system to maintain photosynthetic electron flux, and to the active CBC as the main NADPH consumer during the day, respectively (Baker 2008, Scheibe and Dietz 2011). In the end of the day and night elevated ratios of NADPH/NADP⁺ ratios were observed in *Arabidopsis* leaves lacking NTRC (Chapter 2). NADPH is the reducing equivalent for the conversion of NTRC disulfides to dithiols as the prerequisite for the oxidoreductase activity, and it is assumed that NTRC is able to operate also in the night (Perez-Ruiz et al. 2006, Michalska et al. 2009, Cejudo et al. 2012). Possibly, a deficiency of NTRC protein resulted in an increased ratio of NADPH/NADP⁺ due to the diminished utilization of its substrate. Additionally, NADPH is used by several anabolic processes, especially the CBC, but also e.g. the lipid and protein synthesis (Scheibe and Dietz 2011). A decreased redox activation of these processes attributable to the lack of NTRC might

DISCUSSION

have led to the increased NADPH/NADP⁺ ratios (see discussion above). The *trx f1* single mutant showed no alterations in the NADPH/NADP⁺ ratio. This is surprising, since the double knockout *trxf1 ntrc* revealed even stronger effects than the *ntrc* single mutant, and the chloroplastic NADP-MDH activation state was increased in all mutants. The NADP-MDH is able to balance the NADP homeostasis by channelling excess NADPH to the cytosol via the malate valve, and thereby recycling sufficient NADP⁺ to keep the photosynthetic electron transport running (Scheibe et al. 2005). The strictly light-dependent activation of the NADP-MDH by Trxs is inhibited at low NADPH/NADP⁺ ratios and *vice versa*. The lack of Trx *f1* alone might have increased the NADPH/NADP⁺ ratio in the chloroplast, which was not detectable in whole leaf extracts, but induced a stronger NADP-MDH activity to keep the plastidial redox homeostasis (Chapter 2). Since Trx *f* and *m* are known to regulate the NADP-MDH *in vitro* (Collin et al. 2003), the redox activation was still possible in plants lacking Trx *f1*. This is in confirmation with observations on transgenic tobacco plants separately overexpressing Trx *f* and *m*, which show decreased NADP-MDH activation states (Rey et al. 2013). The photosynthetic electron transport was not affected in the *trx f1* single mutant (Chapter 1, Chapter 2), possibly attributable to an efficient NADP redox poise by the higher NADP-MDH activity.

The increase of NADPH/NADP⁺ reached its highest value in plants with a combined deficiency of Trx *f1* and NTRC (Chapter 2). This was accompanied by a strong decrease of PSI core protein abundance. Due to a limited electron transfer on the acceptor side of PSI by the elevated NADPH/NADP⁺ ratios, the PSI complex is threatened to cope with a high electron pressure delivered by the electron transport chain. PSI reacts very sensitive to excess electrons, since its repair capacity is limited, while PSII exhibits a dynamic regulation of protein turnover (Suorsa et al. 2012, Tikkanen et al. 2014). It is worth to mention that also the NADH/NAD⁺ ratio rose significantly in the *trxf1 ntrc* mutant leaves (Chapter 2), most likely due to the strongly reducing conditions in the chloroplasts, which subsequently led to an overall imbalance in redox homeostasis reflected by the reduction states of the pyridine nucleotide pool. The malate valve indirectly transports NADPH outside of the chloroplast by the formation of malate or subsequent NADH in the cytosol (Scheibe et al. 2005). Additionally, the mitochondrial electron transport chain provides the possibility to oxidize excess reducing equivalents by the involvement of alternative plant-specific enzymes, such as external NAD(P)H dehydrogenases and alternative oxidases, which uncouple the electron transfer from the ATP synthesis (Rasmusson and Walls 2010, Geigenberger and Fernie 2014). The decreased ATP/ADP ratios

DISCUSSION

during the night, elevated CO₂ release in darkened leaves and diminished levels of TCA cycle intermediates suggest an affected mitochondrial respiration in the *trxf1 ntrc* mutants, possibly due to the elevated NAD(P)H/NAD(P)⁺ ratios (Chapter 2). Finally, these results provide strong evidence for important roles of the combined action by the two redox regulatory components Trx f1 and NTRC in balancing the redox homeostasis of *Arabidopsis* leaves.

Contrarily, plants lacking the FNR anchor proteins Tic62 and TROL revealed a strong decrease in the diurnal NADPH/NADP⁺ ratios without affecting growth or photosynthesis (Chapter 4). The NADP-MDH activation state was decreased during day and night, most likely to avoid additional regeneration of NADP⁺ (see discussion above). Previous studies reported of several potential adaptation processes in plants with disturbed redox metabolism in chloroplasts, which includes e.g. the malate valve, feedback-regulation of the photosynthetic light reaction, the antioxidant system, alternative respiratory mechanisms or the photorespiratory metabolism (Scheibe et al. 2005, Hald et al. 2008, Kangasjärvi et al. 2008, Liu et al. 2008, Hebbelmann et al. 2012). This suggests, a high flexibility to maintain the redox homeostasis for an efficient photosynthetic electron flow and plastidial metabolism, and could explain the ability of the *tic62 trol* mutant to cope the strongly altered NADP metabolism without affecting growth. An overall decrease in FNR content was detected in whole leaf extracts and in isolated thylakoid membranes, lacking both TIC 62 and TROL or only TIC62, while the *trol* single mutant was not affected (Chapter 4). This is in confirmation with previous studies (Benz et al. 2009, Juric et al. 2009). Intriguingly, the soluble pool of FNR in the stroma was strongly increased in the *tic62 trol* mutants compared to the wild-type (Chapter 4). A decrease of overall FNR content or activity below about 80% of wild-type level would induce a decrease of photosynthetic electron flow (Scheibe and Dietz 2011), which was not the case in the *tic62 trol* mutants (Chapter 4). Possibly, the loss of FNR-membrane association and the increased soluble FNR content changed the activity to the direction of NADPH oxidation (see discussion above), or metabolic processes consuming NADPH as reducing power were induced. The measurement of G6PDH and Isocitrate dehydrogenase as known NADPH-producing enzymes revealed diminished activities (Chapter 4), indicating one possible explanation. Finally, the underlying mechanisms, which have led to the strongly altered NADPH/NADP⁺ ratio in the *tic62 trol* mutant leaves, are not yet fully understood.

Trx f1 and NTRC are involved in the plant growth acclimation to varying light conditions

The lack of a visible growth phenotype for *Arabidopsis* plants defective in Trxs f1, suggested a high redundancy of the different Trx isoforms under normal growth conditions (Laugier et al. 2013), despite the unique property of Trx f1 as most efficient redox regulator for the photosynthesis-related carbon metabolism in chloroplasts (Meyer et al. 2012, Michelet et al. 2013). Interestingly, the mutant plant lacking Trx f1 demonstrated no alterations in growth compared to the wild-type when grown under an 8h or even longer light period, but low light conditions as well as very short light periods decreased the rosette fresh weight (Chapter 1, Chapter 2). The disability to acclimate to the reduced light energy was most likely due to its important role in redox-activating CBC and starch synthesis enzymes (see discussion above). Under normal light conditions a sugar and starch limitation was observed in the end of the night (Chapter 1, Chapter 2), which might have been increased under very short day or low light conditions, consequently leading to a growth limitation.

The *ntrc* single mutant was subjected to even stronger growth limitations, and not able to recover wild-type rosette fresh weights in any light condition (Chapter 2). The strongest growth impairment was observed in plants treated with high light. The disturbed NADP redox homeostasis might have increased the electron pressure to the PSs (see discussion above), especially under high light conditions, which could have led to the induction of an elevated ROS production as harmful consequence for plant growth (Noctor et al. 2014). NTRC is involved in the redox activation of 2-Cys peroxiredoxins as H₂O₂-scavenging enzymes (Perez-Ruiz et al. 2006, Kirchsteiger et al. 2009, Pulido et al. 2010), but the reports about H₂O₂ levels in *ntrc* leaves are inconsistent. One study revealed increased H₂O₂ levels exclusively after re-illumination of 3-days-darkened plants (Perez-Ruiz et al. 2006), while another study showed already increased levels under a normal light/dark cycle of 16h/8h (Pulido et al. 2010). Lepistö et al. (2013) tested the evolution of different ROS in *Arabidopsis* leaves under short as well as long day conditions, and observed exclusively an elevated formation of the hydroxyl radical in 16h-day grown *ntrc* plants compared to wild-type. But still, increased ROS production could be an explanation for the strongest growth impairment under high light in plants lacking NTRC. Alternatively, the *ntrc* mutant was subjected to sugar depletion (Chapter 2), and it was reported that the high light acclimation is dependent on sufficiently available soluble sugars (Schmitz et al. 2014). In contrast to the *trx f1* mutant, in plants lacking the NTRC protein the acclimation to low light conditions was improved by developing rosette fresh weights similar to normal growth conditions, while a growth inhibition was also detectable under very short days (Chapter

DISCUSSION

2). With increasing light periods the growth acclimation was more successful, which is in line with a previous report (Lepistö et al. 2009), indicating that long day conditions increases the rosette fresh weight compared to short days in the *ntrc* mutant plants. However, long day conditions and continuous light only partly recovered the growth impairment compared to the wild-type, suggesting additional disturbances beside the affected starch synthesis due to the lack of NTRC in *Arabidopsis* plants (see discussion above).

Intriguingly, studies with transgenic lines overexpressing *Trx f1* (Sanz Barrio et al. 2013) or NTRC (Toivola et al. 2013), observed elevated leaf dry weights and carbon resources as starch and soluble sugars in tobacco or an increased rosette biomass in *Arabidopsis*, respectively. This is in confirmation with the results of the present study, which show that the single mutants *trx f1* and *ntrc* are subjected to growth retardations under specific conditions (Chapter 2). A transgenic approach with a combined overexpression of both redox components could be interesting for industrial applications, expecting higher biomass yields and carbon resources than already observed, since the growth of the *trxf1 ntrc* mutants was even stronger affected compared to the single mutants (Chapter 2). The rosette fresh weights were drastically reduced and the acclimation to different light conditions was almost abolished in plants lacking both *Trx f1* and NTRC. Compared to normal growth conditions with 160 µE and an 8h- or 16h-day regime, the relative rosette fresh weights were even more decreased in plants, growing under a 4h-day, low or high light. Only with constant light the plants developed an increased relative rosette biomass compared to the normal light conditions, most likely due to the independency of impaired starch metabolism (see discussion above). Overall, the combined lack of *Trx f1* and NTRC in *Arabidopsis* revealed an additively affected growth acclimation to varying light conditions, which provides further evidence for cooperative redox regulatory functions in the photosynthetic-related carbon metabolism.

Physical interaction of *Trx f1* and NTRC *in vivo* underpin their cooperative regulation of photosynthetic carbon metabolism

The combined deficiency of *Trx f1* and NTRC in *Arabidopsis* plants demonstrate a cooperative role of both redox regulators, since the effects on carbon assimilation, photosynthetic end product synthesis, NAD(P) metabolism and growth were additively increased compared to the single mutants (see discussion above). *In vivo* experiments, using the bimolecular fluorescence complementation method, revealed a direct interaction of *Trx f1* and NTRC (Chapter 2), so that

DISCUSSION

a redundant function might not be the only explanation for the synergistic effects. This confirms recent observations on transgenic *Arabidopsis* plants, expressing a full-length NTRC protein with either a defective NTR or Trx domain in the background of the *ntrc* knockout (Toivola et al. 2013). Especially, the complemented *ntrc* plants, expressing an inactive Trx domain in the NTRC protein, were able to recover almost completely the phenotypic behaviour of wild-type plants, which suggests an involvement of other electron-transferring proteins such as Trxs in the functionality of NTRC domains.

In the same study computational three-dimension modelling revealed Trx *f* as most potential interaction partner for NTRC attributable to the similarities to the electrostatic surface properties of the Trx domain (Toivola et al. 2013). The proposed prerequisite for the disulfide reductase activity of NTRC is the formation of homo-dimers to enable electron transfer between the NTR domain of one subunit to the Trx domain of the second subunit (Perez-Ruiz and Cejudo 2009, Lee et al. 2012). The thiol-disulfide exchange between the NTR and the Trx domain includes the possibility of a conformational change, which exposes the catalytic site of the NTR domain, and might facilitate an interaction with free Trxs (Bernal-Bayard 2012, Toivola et al. 2013). An earlier study suggested that Trxs and NTRC act independently due to their low efficiency to distribute electrons to each other *in vitro* (Bohrer et al. 2012). However, the described assay conditions might have decreased an electron transfer to or from free Trxs due to a possible formation of oligomeric structures or caused by the relative protein concentrations, which were not presenting the *in vivo* situation (Toivola et al. 2013). The direct interaction of Trx *f1* and NTRC could explain their synergistic functions in photosynthetic carbon metabolism and redox homeostasis as revealed in this study (Chapter 2, see discussion above). New questions arise addressed to the mechanisms behind the interaction, and to the specificity and flexibility of this cooperative system to control plants redox regulatory network in chloroplasts, especially in reaction to fluctuating light conditions.

References

Alte F, Stengel A, Benz JP, Petersen E, Soll J, Groll M, Böltner B (2010) Ferredoxin:NADPH oxidoreductase is recruited to thylakoids by binding to a polyproline type II helix in a pH-dependent manner. *Proc Natl Acad Sci USA*. 107(45):19260-5.

Arsova B, Hoja U, Wimmelbacher M, Greiner E, Üstün S, Melzer M, Petersen K, Lein W, Börnke F (2010) Plastidial thioredoxin z interacts with two fructokinase-like proteins in a thiol-dependent manner: evidence for an essential role in chloroplast development in *Arabidopsis* and *Nicotiana benthamiana*. *Plant Cell*. 22(5):1498-515.

Baker NR (2008) Chlorophyll fluorescence: a probe of photosynthesis in vivo. *Annu Rev Plant Biol*. 59:89-113.

Ballicora MA, Frueauf JB, Fu Y, Schürmann P, Preiss J (2000) Activation of the potato tuber ADP-glucose pyrophosphorylase by thioredoxin. *J Biol Chem*. 275(2):1315-20.

Beeler S, Liu HC, Stadler M, Schreier T, Eicke S, Lue WL, Truernit E, Zeeman SC, Chen J, Kötting O (2014) Plastidial NAD-dependent malate dehydrogenase is critical for embryo development and heterotrophic metabolism in *Arabidopsis*. *Plant Physiol*. 164(3):1175-90.

Belin C, Bashandy T, Cela J, Delorme-Hinoux V, Riondet C, Reichheld JP (2014) A comprehensive study of thiol reduction gene expression under stress conditions in *Arabidopsis thaliana*. *Plant Cell Environ*. doi: 10.1111/pce.12276. [Epub ahead of print]

Benitez-Alfonso Y, Cilia M, San Roman A, Thomas C, Maule A, Hearn S, Jackson D (2009) Control of *Arabidopsis* meristem development by thioredoxin-dependent regulation of intercellular transport. *Proc Natl Acad Sci USA*. 106(9):3615-20.

Benz JP, Lintala M, Soll J, Mulo P, Böltner B (2010) A new concept for ferredoxin-NADP(H) oxidoreductase binding to plant thylakoids. *Trends Plant Sci*. 15(11):1360-85.

Benz JP, Stengel A, Lintala M, Lee YH, Weber A, Phillippar K, Gügel IL, Kaieda S, Ikegami T, Mulo P, Soll J, Böltner B (2009) *Arabidopsis* Tic62 and ferredoxin-NADP(H) oxidoreductase form light-regulated complexes that are integrated into the chloroplast redox poise. *Plant Cell*. 21(12):3965-83.

REFERENCES

Bernal-Bayard P, Hervás M, Cejudo FJ, Navarro JA (2012) Electron transfer pathways and dynamics of chloroplast NADPH-dependent thioredoxin reductase c (NTRC). *J Biol Chem.* 287(40):33865-72.

Bohrer AS, Massot V, Innocenti G, Reichheld JP, Issakidis-Bourguet E, Vanacker H (2012) New insights into the reduction systems of plastidial thioredoxins point out the unique properties of thioredoxin z from *Arabidopsis*. *J Exp Bot.* 63(18):6315-23.

Buchanan BB, Holmgren A, Jaquot JP, Scheibe R (2012) Fifty years in the thioredoxin field and a bountiful harvest. *Biochim Biophys Acta.* 1820(11):1822-9.

Caspar T, Huber SC, Somerville C (1985) Alterations in growth, photosynthesis, and respiration in a starchless mutant of *Arabidopsis thaliana* (L.) deficient in chloroplast phosphoglucomutase activity. *Plant Physiol.* 79(1):11-7.

Cejudo FJ, Ferrández J, Cano B, Puerto-Galán L, Guinea M (2012) The function of the NADPH thioredoxin reductase C-2-Cys peroxiredoxin system in plastid redox regulation and signalling. *FEBS Lett.* 586(18):2974-80.

Chibani K, Tarrago L, Schürmann P, Jacquot JP, Rouhier N (2011) Biochemical properties of poplar thioredoxin z. *FEBS Lett.* 585(7):1077-81.

Choi YA, Kim SG, Kwon YM (1999) The plastidic glutamine synthetase activity is directly modulated by means of redox change at two unique cysteine residues. *Plant Sci.* 149(2):175-182.

Collin V, Issakidis-Bourguet E, Marchand C, Hirasawa M, Lancelin JM, Knaff DB, Miginiac-Maslow M (2003) The *Arabidopsis* plastidial thioredoxins: new functions and new insights into specificity. *J Biol Chem.* 278(26):23747-52.

Collin V, Lamkemeyer P, Miginiac-Maslow M, Hirasawa M, Knaff DB, Dietz KJ, Issakidis-Bourguet E (2004) Characterization of plastidial thioredoxins from *Arabidopsis* belonging to the new y-type. *Plant Physiol.* 136(4):4088-95.

Courteille A, Vesa S, Sanz-Barrio R, Cazalé AC, Becuwe-Linka N, Farran I, Havaux M, Rey P, Rumeau D (2013) Thioredoxin m4 controls photosynthetic alternative electron pathways in *Arabidopsis*. *Plant Physiol.* 161(1):508-20.

REFERENCES

Crevillén P, Ventriglia T, Pinto F, Orea A, Mérida A, Romero JM (2005) Differential pattern of expression and sugar regulation of *Arabidopsis thaliana* ADP-glucose pyrophosphorylase-encoding genes. *J Biol Chem.* 280(9):8143-9.

Cross JM, Clancy M, Shaw JR, Greene TW, Schmidt RR, Okita TW, Hannah LC (2004) Both subunits of ADP-glucose pyrophosphorylase are regulatory. *Plant Physiol.* 135(1): 137-144.

Faix B, Radchuk V, Nerlich A, Hümmer C, Radchuk R, Emery R J N, Keller H, Götz KP, Weschke W, Geigenberger P, Weber H (2012) Barley grains, deficient in cytosolic small subunit of ADP-glucose pyrophosphorylase, reveal coordinate adjustment of C:N metabolism mediated by an overlapping metabolic-hormonal control. *Plant J.* 69(6):1077-93.

Fernie AR, Tiessen A, Stitt M, Willmitzer L, Geigenberger P (2002) Altered metabolic fluxes result from shifts in metabolite levels in sucrose phosphorylase-expressing potato tubers. *Plant Cell Environ.* 25(10):1219-32.

Foyer CH, Neukermans J, Queval G, Noctor G, Harbinson J (2012) Photosynthetic control of electron transport and the regulation of gene expression. *J Exp Bot.* 63(4):1637-1661.

Fu Y, Ballicora MA, Preiss J (1998) Mutagenesis of the glucose-1-phosphate-binding site of potato tuber ADP-glucose pyrophosphorylase. *Plant Physiol.* 117(3):989-96.

Geigenberger P (2011) Regulation of starch biosynthesis in response to a fluctuating environment. *Plant Physiol.* 155(4):1566-77.

Geigenberger P and Fernie AR (2014) Metabolic control of redox and redox control of metabolism in plants. *Antioxid Redox Signal.* 21(9):1389-421.

Geigenberger P, Kolbe A, Tiessen A (2005) Redox regulation of carbon storage and partitioning in response to light and sugars. *J Exp Bot.* 56(416):1469-79.

Ghosh HP and Preiss J (1966) Adenosine diphosphate glucose pyrophosphorylase. A regulatory enzyme in the biosynthesis of starch in spinach leaf chloroplasts. *J Biol Chem.* 241(19):4491-504.

Gibon Y, Bläsing OE, Palacios-Rojas N, Pankovic D, Hendriks JHM, Fisahn J, Höhne M, Günther M, Stitt M (2004) Adjustment of diurnal starch turnover to short days: depletion of sugar during the night leads to a temporary inhibition of carbohydrate utilization, accumulation

REFERENCES

of sugars and post-translational activation of ADP-glucose pyrophosphorylase in the following light period. *Plant J.* 39(6):847-62.

Glaring MA, Skryhan K, Kötting O, Zeeman SC, Blennow A (2012) Comprehensive survey of redox sensitive starch metabolising enzymes in *Arabidopsis thaliana*. *Plant Physiol Biochem.* 58:89-97.

Hädrich N, Hendriks JHM, Kötting O, Arrivault S, Feil R, Zeeman SC, Gibon Y, Schulze WX, Stitt M, Lunn JE (2012) Mutagenesis of cystein 81 prevents dimerization of the APS1 subunit of ADP-glucose pyrophosphorylase and alters diurnal starch turnover in *Arabidopsis thaliana* leaves. *Plant J.* 70(2):231-42.

Hald S, Nandha B, Gallois P, Johnson GN (2008) Feedback regulation of photosynthetic electron transport by NADP(H) redox poise. *Biochim Biophys Acta.* 1777(5):433-40.

Hanke G and Mulo P (2013) Plant type ferredoxins and ferredoxin-dependent metabolism. *Plant Cell Environ.* 36(6):1071-84.

Hanke GT, Okutani S, Satomi Y, Takao T, Suzuki A, Hase T (2005) Multiple iso-proteins of FNR in *Arabidopsis*: evidence for different contributions to chloroplast function and nitrogen assimilation. *Plant Cell Environ.* 28(9):1146-57.

Hebbelmann I, Selinski J, Wehmeyer C, Goss T, Voss I, Mulo P, Kangasjärvi S, Aro EM, Oelze ML, Dietz KJ, Nunes-Nesi A, Do PT, Fernie AR, Talla SK, Raghavendra AS, Linke V, Scheibe R (2012) Multiple strategies to prevent oxidative stress in *Arabidopsis* plants lacking the malate valve enzyme NADP-malate dehydrogenase. *J Exp Bot.* 63(3):1445-59.

Hendriks JHM, Kolbe A, Gibon Y, Stitt M, Geigenberger P (2003) ADP-glucose pyrophosphorylase is activated by posttranslational redox-modification in response to light and to sugars in leaves of *Arabidopsis* and other plant species. *Plant Physiol.* 133(2):838-849.

Ikegami A, Yoshimura N, Motohashi K, Takahashi S, Romano PGN, Hisabori T, Takamiya K, Masuda T (2007) The CHLI1 subunit of *Arabidopsis thaliana* magnesium chelatase is a target protein of the chloroplast thioredoxin. *J Biol Chem.* 282(27):19282-91.

Johnson GN (2011) Physiology of PSI cyclic electron transport in higher plants. *Biochim Biophys Acta.* 1807(3):384-9.

REFERENCES

Juric S, Hazler-Pilepic K, Tomasic A, Lepedus H, Jelicic B, Puthiyaveetil S, Bionda T, Vojta L, Allen JF, Schleiff E, Fulgosi H (2009) Tethering of ferredoxin:NADP⁺ oxidoreductase to thylakoid membranes is mediated by novel chloroplast protein TROL. *Plant J.* 60(5):783-94.

Kangasjärvi S, Lepistö A, Hännikäinen K, Piippo M, Luomala EM, Aro EM, Rintamäki E (2008) Diverse roles for chloroplast stromal and thylakoid-bound ascorbate peroxidases in plant stress responses. *Biochem J.* 412(2):275-85.

Koßmann J, Sonnewald U, Willmitzer L (1994) Reduction of the chloroplastic fructose-1,6-bisphosphatase in transgenic potato plants impairs photosynthesis and plant growth. *Plant J.* 6(5):637-50.

Kirchsteiger K, Pulido P, González M, Cejudo FJ (2009) NADPH thioredoxin reductase C controls the redox status of chloroplast 2-Cys peroxiredoxins in *Arabidopsis thaliana*. *Mol Plant.* 2(2):298-307.

Laugier E, Tarrago L, Courteille A, Innocenti G, Eymery F, Rumeau D, Issakidis-Bourguet E, Rey P (2013) Involvement of thioredoxin y2 in the preservation of leaf methionine sulfoxide reductase capacity and growth under high light. *Plant Cell Environ.* 36(3):670-82.

Lee Y, Kim S, Lazar P, Moon JC, Hwang S, Thangapandian S, Shon Y, Lee KO, Lee SY, Lee KW (2012) Comparative molecular modeling study of *Arabidopsis* NADPH-dependent thioredoxin reductase and its hybrid protein. *Plos One.* 7(9):e46279.

Lepistö A, Kangasjärvi S, Luomala EM, Brader G, Sipari N, Keränen M, Keinänen M, Rintamäki E (2009) Chloroplast NADPH-thioredoxin reductase interacts with photoperiodic development in *Arabidopsis*. *Plant Physiol.* 149(3):1261-76.

Lepistö A, Pakula E, Toivola J, Krieger-Liszakay A, Vignols F, Rintamäki E (2013) Deletion of chloroplast NADPH-dependent thioredoxin reductase results in inability to regulate starch synthesis and causes stunted growth under short-day photoperiods. *J Exp Bot.* 64(12):3843-54.

Lichter A and Häberlein I (1998) A light-dependent redox signal participates in the regulation of ammonia fixation in chloroplasts of higher plants – ferredoxin:glutamate synthase is a thioredoxin-dependent enzyme. *J Plant Physiol.* 153(1-2):83-90.

Lintala M, Allahverdiyeva Y, Kidron H, Piippo M, Battchikova N, Suorsa M, Rintamäki Eevi, Salminen TA, Aro EM, Mulo P (2007) Structural and functional characterization of ferredoxin-

REFERENCES

NADP⁺-oxidoreductase using knock-out mutants of *Arabidopsis*. *Plant Cell Environ.* 49(6):1041-1052.

Liu YJ, Norberg FEB, Szilágyi A, De Paepe R, Akerlund HE, Rasmusson AG (2008) The mitochondrial external NADPH dehydrogenase modulates the leaf NADPH/NADP⁺ ratio in transgenic *Nicotiana sylvestris*. *Plant Cell Physiol.* 49(2):251-63.

Livingston AK, Cruz JA, Kohzuma K, Dhingra A, Kramer DM (2010) An *Arabidopsis* mutant with high cyclic electron flow around photosystem I (*hcef*) involving the NADPH dehydrogenase complex. *Plant Cell.* 22(1):221-33.

Luo T, Fan T, Liu Y, Rothbart M, Yu J, Zhou S, Grimm B, Luo M (2012) Thioredoxin redox regulates ATPase activity of magnesium chelatase CHLI subunit and modulates redox-mediated signalling in tetrapyrrole biosynthesis and homeostasis of reactive oxygen species in pea plants. *Plant Physiol.* 159(1):118-30.

Meyer Y, Belin C, Delorme-Hinoux V, Reichheld JP, Riondet C (2012) Thioredoxin and glutaredoxin systems in plants: Molecular mechanisms, crosstalks, and functional significance. *Antioxid Redox Signal.* 17(8):1124-60.

Michalska J, Zauber H, Buchanan BB, Cejudo FJ, Geigenberger P (2009) NTRC links built-in thioredoxin to light and sucrose in regulating starch synthesis in chloroplasts and amyloplasts. *Proc Natl Acad Sci U S A.* 106(24):9908-13.

Michelet L, Zaffagnini M, Morisse S, Sparla F, Pérez-Pérez ME, Francia F, Danon A, Marchand CH, Fermani S, Trost P, Lemaire SD (2013) Redox regulation of the Calvin-Benson cycle: something old, something new. *Front Plant Sci.* 4:470.

Mikkelsen R, Mutenda KE, Mant A, Schürmann P, Blennow A (2005) α -glucan, water dikinase (GWD): A plastidic enzyme with redox-regulated and coordinated catalytic activity and binding affinity. *Proc Natl Acad Sci USA.* 102(5): 1785-90.

Montrichard F, Alkhalfioui F, Yano H, Vensel WH, Hurkman WJ, Buchanan BB (2009) Thioredoxin targets in plants: The first 30 years. *J Proteomics.* 72(3):452-74.

Motohashi K, Kondoh A, Stumpp MT, Hisabori T (2001) Comprehensive survey of proteins targeted by chloroplast thioredoxin. *Proc Natl Acad Sci USA.* 98(20):11224-9.

REFERENCES

Müller-Röber BT, Kossmann J, Hannah LC, Willmitzer L, Sonnewald U (1990) One of two different ADP-glucose pyrophosphorylase genes from potato responds strongly to elevated levels of sucrose. *Mol Gen Genet.* 224(1):136-46.

Née G, Zaffagnini M, Trost P, Issakidis-Bourguet E (2009) Redox regulation of chloroplastic glucose-6-phosphate dehydrogenase: a new role for f-type thioredoxin. *FEBS Lett.* 583(17):2827-32.

Neuhaus HE and Stitt M (1990) Control analysis of photosynthate partitioning. *Planta.* 182: 445-454.

Nielsen TH, Krapp A, Röper-Schwarz U, Stitt M (1998) The sugar-mediated regulation of genes encoding the small subunit of Rubisco and the regulatory subunit of ADP glucose pyrophosphorylase is modified by phosphate and nitrogen. *Plant Cell Environ.* 21(5): 443-454.

Nikkanen L and Rintamäki E (2014) Thioredoxin-dependent regulatory networks in chloroplasts under fluctuating light conditions. *Philos Trans R Soc Lond B Biol Sci.* 369(1640):20130224.

Noctor G, Lelarge-Trouverie C, Mhamdi A (2014) The metabolomics of oxidative stress. *Phytochemistry.* pii: S0031-9422(14)00365-3. doi: 10.1016/j.phytochem.2014.09.002. [Epub ahead of print]

Osuna D, Usadel B, Morcuende R, Gibon Y, Bläsing OE, Höhne M, Günter M, Kamlage B, Trethewey R, Scheible W-R, Stitt M (2007) Temporal responses of transcripts, enzyme activities and metabolites after adding sucrose to carbon-deprived *Arabidopsis* seedlings. *Plant J.* 49(3):463-91.

Perez-Ruiz JM and Cejudo FJ (2009) A proposed reaction mechanism for rice NADPH thioredoxin reductase C, an enzyme with protein disulfide reductase activity. *FEBS Lett.* 583(9):1399-402.

Perez-Ruiz JM, Guinea M, Puerto-Galán L, Cejudo FJ (2014) NADPH thioredoxin reductase c is involved in redox regulation of the Mg-chelatase I subunit in *Arabidopsis thaliana* chloroplasts. *Mol Plant.* 7(7):1252-5.

REFERENCES

Perez-Ruiz JM, Spinola MC, Kirchsteiger K, Moreno J, Sahrawy M, Cejudo FJ (2006) Rice NTRC is a high-efficiency redox system for chloroplast protection against oxidative damage. *Plant Cell*. 18(9):2356-68.

Pulido P, Spínola MC, Kirchsteiger K, Guinea M, Pascual MB, Sahrawy M, Sandalio LM, Dietz KJ, González M, Cejudo FJ (2010) Functional analysis of the pathways for 2-Cys peroxiredoxin reduction in *Arabidopsis thaliana* chloroplasts. *J Exp Bot*. 61(14):4043-54.

Rasmusson AG and Wallström SV (2010) Involvement of mitochondria in the control of plant cell NAD(P)H reduction levels. *Biochem Soc Trans*. 38(2):661-6.

Reichheld JP, Meyer E, Khafif M, Bonnard G, Meyer Y (2005) AtNTRB is the major mitochondrial thioredoxin reductase in *Arabidopsis thaliana*. *FEBS Lett*. 579(2):337-42.

Rey P, Sanz-Barrio R, Innocenti G, Ksas B, Courteille A, Rumeau D, Issakidis-Bourguet E, Farran I (2013) Overexpression of plastidial thioredoxins f and m differentially alters photosynthetic activity and response to oxidative stress in tobacco plants. *Front Plant Sci*. 4:390.

Richter AS, Peter E, Rothbart M, Schlicke H, Toivola J, Rintamäki E, Grimm B (2013) Posttranslational influence of NADPH-dependent thioredoxin reductase C on enzymes in tetrapyrrol synthesis. *Plant Physiol*. 162(1):63-73.

Sanz-Barrio R, Corral-Martinez P, Ancin M, Segui-Simarro JM, Farran I (2013) Overexpression of plastidial thioredoxin f leads to enhanced starch accumulation in tobacco leaves. *Plant Biotechnol J*. 11(5):618-27.

Sasaki Y, Kozaki A, Hatano M (1997) Link between light and fatty acid synthesis: Thioredoxin-linked reductive activation of plastidic acetyl-CoA carboxylase. *Proc Natl Acad Sci USA*. 94(20):11096-101.

Scheibe R, Backhausen JE, Emmerlich V, Holtgrefe S (2005) Strategies to maintain redox homeostasis during photosynthesis under changing conditions. *J Exp Bot*. 56(416):1481-9.

Scheibe R and Dietz KJ (2011) Reduction-oxidation network for flexible adjustment of cellular metabolism in photoautotrophic cells. *Plant Cell Environ*. 35(2):202-16.

REFERENCES

Scheible WR, Gonzales-Fontes A, Lauerer M, Müller-Röber B, Caboche M, Stitt M (1997) Nitrate Acts as a Signal to Induce Organic Acid Metabolism and Repress Starch Metabolism in Tobacco. *Plant Cell*. 9(5):783-98.

Schmitz J, Heinrichs L, Scossa F, Fernie AR, Oelze ML, Dietz KJ, Rothbart M, Grimm B, Flügge UI, Häusler RE (2014) The essential role of sugar metabolism in the acclimation response of *Arabidopsis thaliana* to high light intensities. *J Exp Bot*. 65(6):1619-36.

Schürmann P and Buchanan BB (2008) The ferredoxin/thioredoxin system of oxygenic photosynthesis. *Antioxid Redox Signal*. 10(7):1235-74.

Serrato AJ, Pérez-Ruiz JM, Spínola MC, Cejudo FJ (2004) A novel NADPH thioredoxin reductase, localized in the chloroplast, which deficiency causes hypersensitivity to abiotic stress in *Arabidopsis thaliana*. *J Biol Chem*. 279(42):43821-7.

Serrato AJ, Yubero-Serrano EM, Sandalio LM, Munoz-Blanco J, Chueca A, Caballero JL, Sahrawy M (2009) cpFBPaseII, a novel redox-independent chloroplastic isoform of fructose-1,6-bisphosphatase. *Plant Cell Environ*. 32(7):811-27.

Seung D, Thalmann M, Sparla F, Abou Hachem M, Lee SK, Issakidis-Bourguet E, Svensson B, Zeeman SC, Santelia D (2013) *Arabidopsis thaliana* AMY3 is a unique redox-regulated chloroplastic α -amylase. *J Biol Chem*. 288(47):33620-33.

Silver DM, Silva LP, Issakidis-Bourguet E, Glaring MA, Schriemer DC, Moorhead GBG (2013) Insight into the redox regulation of the phosphoglucan phosphatase SEX4 involved in starch degradation. *FEBS J*. 280(2):538-48.

Sokolov LN, Dejardin A, Kleczkowski LA (1998) Sugars and light/dark exposure trigger differential regulation of ADP-glucose pyrophosphorylase genes in *Arabidopsis thaliana* (thale cress). *Biochem J*. 336 (Pt 3):681-7.

Sowokinos JR and Preiss J (1982) Pyrophosphorylases in *Solanum tuberosum*: III. Purification, physical, and catalytical properties of ADPglucose pyrophosphorylase in potatoes. *Plant Physiol*. 69(6):1459-66.

Stengel A, Benz P, Soll J, Böltter B (2008) TIC62 redox-regulated translocon composition and dynamics. *J Biol Chem*. 283(11):6656-67.

REFERENCES

Stitt M, Lunn J, Usadel B (2010) Arabidopsis and primary photosynthetic metabolism - more than the icing on the cake. *Plant J.* 61(6):1067-91.

Stitt M and Zeeman SC (2012) Starch turnover: pathways, regulation and role in growth. *Curr Opin Plant Biol.* 15(3):282-92.

Suorsa M, Järvi S, Grieco M, Nurmi M, Pietrzykowska M, Rantala M, Kangasjärvi S, Paakkari V, Tikkanen M, Jansson S, Aro EM (2012) PROTON GRADIENT REGULATION5 is essential for proper acclimation of *Arabidopsis* photosystem I to naturally and artificially fluctuating light conditions. *Plant Cell.* 24(7):2934-48.

Tiessen A, Hendriks JH, Stitt M, Branscheid A, Gibon Y, Farré EM, Geigenberger P (2002) Starch synthesis in potato tubers is regulated by post-translational redox modification of ADP-glucose pyrophosphorylase: a novel regulatory mechanism linking starch synthesis to the sucrose supply. *Plant Cell.* 14(9):2191-213.

Tikkanen M, Mekala NR, Aro EM (2014) Photosystem II photoinhibition-repair cycle protects photosystem I from irreversible damage. *Biochim Biophys Acta.* 1837(1):210-5.

Toivola J, Nikkanen L, Dahlström KM, Salminen TA, Lepistö A, Vignols F, Rintamäki E (2013) Overexpression of chloroplast NADPH-dependent thioredoxin reductase in *Arabidopsis* enhances leaf growth and elucidates *in vivo* function of reductase and thioreductase domains. *Front Plant Sci.* 4:389.

Usadel B, Bläsing OE, Gibon Y, Retzlaff K, Höhne M, Günther M, Stitt M (2008) Global transcript levels respond to small changes of the carbon status during progressive exhaustion of carbohydrates in *Arabidopsis* rosettes. *Plant Physiol.* 146(4):1834-61.

Valerio C, Costa A, Marri L, Issakidis-Bourguet E, Pupillo P, Trost P, Sparla F (2011) Thioredoxin-regulated β -amylase (BAM1) triggers diurnal starch degradation in guard cells, and in mesophyll cells under osmotic stress. *J Exp Bot.* 62(2):545-55.

Ventriglia T, Kuhn ML, Ruiz MT, Ribeiro-Pedro M, Valverde F, Ballicora MA, Preiss J, Romero JM (2008) Two *Arabidopsis* ADP-glucose pyrophosphorylase large subunits (APL1 and APL2) are catalytic. *Plant Physiol.* 148(1):65-6.

Vojta L, Horvat L, Fulgosi H (2012) Balancing chloroplast redox status – regulation of FNR binding and release. *Periodicum biologorum.* 114(1):25-31.

REFERENCES

Wakao S and Benning C (2005) Genome-wide analysis of glucose-6-phosphate dehydrogenases in *Arabidopsis*. *Plant J.* 41(2):243-56.

Wang P, Liu J, Liu B, Feng D, Da Q, Wang P, Shu S, Su J, Zhang Y, Wang J, Wang HB (2013) Evidence for a role of chloroplastic m-type thioredoxins in the biogenesis of photosystem II in *Arabidopsis*. *Plant Physiol.* 163(4):1710-28.

Zeeman SC, Smith SM, Smith AM (2007) The diurnal metabolism of leaf starch. *Biochem J.* 401(1):13-28.

Curriculum vitae

Personal data

Name	Ina Thormählen
Date of birth	26.05.1981
Place of birth	Hamburg
Nationality	German
Email	thormaehlen@bio.lmu.de

Research experience

Since 2/2010	Ph.D. thesis project: Faculty of Biology (Botany), Ludwig Maximilians University Munich, Germany; Plant Metabolism group of Prof. Dr. Peter Geigenberger
3/2011 – 4/2011	Collaboration project: Institut de Biologie des Plantes, UMR CNRS 8618, Université Paris-Sud, France; Signalisation Redox group of Dr. Emmanuelle Issakidis-Bourguet
2/2009 – 11/2009	Diploma thesis project: Max Planck Institute of Molecular Plant Physiology, Potsdam-Golm, Germany; Energy Metabolism group of Prof. Dr. Joost T. van Dongen
9/2008 – 10/2008	Undergraduate internship: Max Planck Institute of Molecular Plant Physiology, Potsdam-Golm, Germany; Project Photobioreactor Design for <i>Chlamydomonas</i> Cultivation of Dr. Jens Rupprecht
6/2008 – 7/2008	Undergraduate project: Abisko Scientific Research Station, Abisko, Sweden; Plant Physiology group of Prof. Dr. Christine Stöhr

Teaching experience

Conference presentations

1/2014 JST/CREST International Symposium on Productivity Improvement of Plants – From Model to Crop Plants, Nara, Japan

10/2012 XV. Annual Meeting of the International Society of Endocytobiology – German Section, Munich, Germany

Research publications

Thormählen I, Meitzel T, Groysman J, Öchsner AB, von Roepenack-Lahaye E, Belén Naranjo, Cejudo FJ, Geigenberger P (2014) Interaction between thioredoxin f1 and NADPH-dependent thioredoxin reductase C regulates photosynthetic metabolism and plant growth. *Manuscript submitted (Plant Cell)*.

Rojas-González JA, Soto-Suárez M, García-Díaz Á, Romero-Puertas MC, Sandalio LM, Mérida Á, Thormählen I, Geigenberger P, Serrato AJ, Sahrawy M (2014) Disruption of both chloroplastic and cytosolic FBPases genes results in dwarf phenotype and important starch and metabolite changes in *Arabidopsis thaliana*. *Manuscript submitted, first revision (revision-major) (J Exp Bot)*.

Lintala M, Schuck N, Thormählen I, Jungfer A, Weber KL, Weber AP, Geigenberger P, Soll J, Böltner B, Mulo P (2014) *Arabidopsis tic62 trol* mutant lacking thylakoid-bound ferredoxin-NADP⁺ oxidoreductase shows distinct metabolic phenotype. *Mol Plant*. 7(1):45-57.

Thormählen I, Ruber J, von Roepenack-Lahaye E, Ehrlich SM, Massot V, Hümmel C, Tezycka J, Issakidis-Bourguet E, Geigenberger P (2013) Inactivation of thioredoxin f1 leads to decreased light activation of ADP-glucose pyrophosphorylase and altered diurnal starch turnover in leaves of *Arabidopsis* plants. *Plant Cell Environ.* 36(1):16-29.

CURRICULUM VITAE

De Dios Barajas-López J, Tezycka J, Travaglia CN, Serrato AJ, Chueca A, Thormählen I, Geigenberger P, Sahrawy M (2012) Expression of the chloroplast thioredoxins f and m is linked to short-term changes in the sugar and thiol status in leaves of *Pisum sativum*. *J Exp Bot.* 63(13):4887-900.

Schwachtje J, Karojet S, Thormählen I, Bernholz C, Kunz S, Brouwer S, Schwochow M, Köhl K, van Dongen JT (2011) A naturally associated rhizobacterium of *Arabidopsis thaliana* induces a starvation-like transcriptional response while promoting growth. *PLoS One.* 6(12):e29382.

Academic education

10/2004 – 12/2009 Biology (Diploma); Ernst Moritz Arndt University of Greifswald, Germany

10/2003 – 9/2004 Environmental sciences; Leuphana University of Lüneburg, Germany

Acknowledgement

First of all, I'd like to thank Peter Geigenberger for providing me with this interesting and fruitful Ph.D. project, but also for being a trusting and human supervisor, being both demanding and encouraging during the entire process of this scientific work.

Moreover, I need to thank the complete working group (including former and present colleagues and friends) for the funny, kind and supporting atmosphere in the lab and office, and for the manifold occasions spent together, e.g. playing soccer on the pitch, shipping on the river Isar, celebrating the Bavarian culture at the Wiesn and Christkindlmarkt, smoking cigarettes in Paris, running through the Olympia park, or sliding down the snowy mountains. Many thanks for this exceptional time! I'm already looking forward completing this list of events with milking cows in Norway.

Let me also take the opportunity to thank our cooperation partners Bettina Böltner, Edda von Roepenack-Lahaye, Emmanuelle Issakidis-Bourguet, Francisco Javier Cejudo, Mariam Sahrawy, and Tobias Meitzel for their productive and inspiring collaboration.

The undergraduate students, supervised during their study projects, I wish to thank as well, since they have been of great help in progressing the present work. Many thanks to Alexandra Bianca Öchsner, Ana Luz Rodriguez Muslera, Joachim Ruber, Melanie Verena Paul, Stella Schieferstein, Tobias Dombrowski, and especially Julia Groysman!

My previous supervisors, Axel Tiessen, Christine Stöhr, Jens Rupprecht, Jens Schwachtje, and Joost T. van Dongen, I greatly appreciated their teaching me basic scientific skills and making me find my way to the right direction.

Last, but of course not least, I'm grateful for the tremendous support and belief in me of my family and friends throughout the years.

Finally, this "book" is dedicated to my grandmother Lissy!